Student Theses and Dissertations

1979

Analysis and Synthesis of the Dynamic Response of Retinal Neurons

Scott E. Brodie

Analysis and Synthesis of the Dynamic Response of Retinal Neurons

A thesis submitted to the Faculty of The Rockefeller University

in partial fulfillment of the requirements

for the degree of Doctor of Philosophy

by

Scott E. Brodie, B.A., M.A.

April, 1979

The Rockefeller University

New York, New York

To H. K. Hartline

on the fiftieth anniversary of his first recordings

from the optic nerve of the horseshoe crab, Limulus.

Preface

It has been a rare privilege to participate in the research
described in this thesis. I must thank first my advisors,
Professors Bruce Knight and Floyd Ratliff. Bruce Knight first
drew my attention to the dynamics of retinal neurons, and much of
the work presented here derives from his original and penetrating
suggestions. Floyd Ratliff provided constant encouragement and
support, and much sound advice. I am grateful to him also for
the relaxed atmosphere and warm welcome which permeate his
laboratory.

The Wiener-Hopf treatment in chapter VII is due to
Professor Lawrence Sirovich, and is included here with his kind
permission. I also wish to acknowledge his collaboration on the
experiments described in chapter VIII. I thank Professors
Robert Shapley and Ehud Kaplan for sharing generously their
experience with the retinas of both Limulus and cat. I thank also
Professor James Gordon, who graciously assisted with the photo-
graphs which appear in Appendix A, and Fred Dodge, with whom I
had many important critical discussions. Professor H.K. Hartline
provided much-appreciated comment and perspective.

Norman Milkman designed and maintained much of the electronic
equipment used in this work. He also wrote the prototype for
the computer programs for stimulus control and data acquisition.

Summary.

The theory of linear systems analysis is developed
in a form directly applicable to the treatment of the Limulus
retina. The dynamics of the retina may conveniently be
characterized by means of a spatiotemporal transfer function,
which summarizes the response of the system to moving sinus-
oidal gratings ("analysis"). The response of the retina to
an arbitrary stimulus may then be calculated by addition
of the response to suitably weighted sinusoidal stimuli
("synthesis").

Responses were obtained from the in-situ retina by
means of extracellular recording of impulse activity in single
optic nerve fibers. Test ommatidia were chosen in the
interior of the retina, to avoid asymmetries introduced by
the edge of the retina. Stimuli which varied in both space
and time were produced under computer control on the screen
of a display oscilloscope, and were conveyed to the Limulus
eye by means of a fiber-optic taper. Transfer functions
were measured using counterphase modulation of cosine gratings
according to a sum-of-sinusoids temporal signal, a procedure
equivalent to the use of moving gratings, for ommatidia
with symmetrical receptive fields. By means of these
transfer functions, the responses of the Limulus eye to

visual stimuli moving at various velocities were predicted
in a parameter-free Fourier synthesis calculation. There
was good agreement between these predictions and the
measured responses to these stimuli.

A quantitative model for the dynamic, integrative action
of the Limulus retina is developed, based on the original
formulation for the steady state given by the Hartline-
Ratliff equations. The model comprises an excitatory generator
potential, and dynamic processes of self and lateral inhibition.
An explicit expression for the spatiotemporal transfer function
is obtained in terms of transfer functions for the generator
potential, self-inhibitory, and lateral-inhibitory transductions,
and spatial transforms of the lateral inhibitory kernel and
the point-spread characteristic of the experimental and physio-
logical optics. Explicit functional forms for these
component transductions are adopted. The parameters which
occur in these expressions serve to incorporate information
about the subcellular physiology of retinal neurons into the
quantitative description of the function of the retina as a
whole. Procedures are described for the estimation of these
parameters from empirical transfer function data.

Transfer functions calculated from the model on the basis
of parameters obtained with these procedures show good agreement

with the corresponding empirical transfer functions. The parameter values obtained in this way are, in general, quite consistent with the results of many more direct (and frequently more invasive) measurements reported in the literature. In particular, the inhibitory kernel, as determined from our transfer function measurements, shows a small crater in the vicinity of the test-ommatidium.

The dynamical model can be used to describe the response of the retina in the vicinity of its boundary, as well as in the interior. An analysis, based on the "Wiener-Hopf technique," is given for the response of peripheral retinal neurons. The predictions derived from this theory were compared with experiment through the use of illumination patterns in which one half of the retina was kept in darkness, while the remaining half was presented with a moving stimulus. This procedure permitted the calibration of model transfer functions by means of methods appropriate only for interior ommatidia, while simulating the neural environment at the edge of a homogeneous retina. Significant differences between the responses to stimuli which moved toward and away from the simulated edge were observed experimentally, in good agreement with the predictions of the theory. Similar behavior was also observed at the actual anatomical boundary of the eye.

The extension of these linear methods to the description of the dynamic response of X ganglion cells in the cat retina is discussed. Preliminary experiments suggest that, contrary to speculation in the literature, the responses of these cells cannot be predicted quantitatively by purely linear synthesis calculations.

TABLE OF CONTENTS

Bibliographic Note

Much of the material presented in this thesis has been published elsewhere, or has been submitted for publication. The following tabulation indicates the correspondence between the chapters of this thesis and the literature.

Brodie, Knight, and Ratliff, 1978a: Chapters II,III,IV; Appendix A,
C (Harmonic Analysis)

Brodie, Knight, and Ratliff, 1978b: Chapters V,VI; Appendix E

Brodie, 1979: Appendix B

Sirovich, Brodie, and Knight, 1979: Chapter VIII

Knight, Brodie, and Sirovich, 1979: Appendix C (Ouput Variables)

Chapter VII and Appendix D constitute a revised exposition of part of the theory presented in Sirovich, 1979.

"It's a poor sort of memory that only works backwards"

L. Carroll, 1871

"It may be said, therefore, that an explanation is not
fully adequate unless its explanans, if taken account
of in time, could have served as a basis for predicting
the phenomenon under consideration."

C.G. Hempel and
P. Oppenheim, 1948

I. Introduction.

This dissertation describes the results of quanti-
tative studies of the dynamic response of retinal neurons
by means of the techniques of linear systems analysis.
The retinal neurons were generally those of the lateral
eye of the horseshoe crab Limulus polyphemus; some brief
results concerning extensions of the work to the verte-
brate retina were also obtained. The reasons for the
undertaking of this project are explained below.

The single nerve cell, or neuron, has been recognized
since the early part of this century as the fundamental
structural and functional unit of the nervous system. Since
that time, a great majority of the efforts of neuro-
physiologists have been directed toward the elucidation of
the subcellular mechanisms of the function of single neurons
(or single synapses). This reductionist approach to neuro-
physiology has been very fruitful, leading to the identi-
fication of ionic currents and voltage-dependent conduct-
ances as the basis for the propagated action potentials
by which neural information is transmitted over long dis-
tances, and to the characterization of the neurotransmitters

and receptors which mediate synaptic communication between neurons.

On the other hand, this concentration on the microscopic aspects of neural function has, to some extent, diverted attention away from the study of the nervous system on any larger scale. This tendency to identify "neurophysiology" with the "physiology of single neurons" has fostered the relative neglect of the function of the larger assemblies of neurons, the so-called "neural networks," which underly the integrative action of the nervous system. It is the purpose of this dissertation to illustrate by example the feasibility and practical utility of the study of neurophysiology at the level of a neural network comprising many hundreds of interacting neurons. Thus, we will take as primitive the response characteristics of single neurons, and attempt to describe in quantitative terms the response of such neurons as a function of their inclusion in a network of interacting nerve cells.

The potential value of such a program may be illustrated by analogy with state-of-the art computers. The celebrated "Cray-1" machine, though built from standard, off-the-shelf integrated circuits (with modest specifications

comparable or inferior to those of integrated circuits used in competitive equipment), is generally conceded to be the most powerful "number cruncher" currently available (Metz, 1978). Thus a hypothetical "computer physiologist" who examined only the function of single integrated circuits, or the chemistry of the semiconductors which they contain, would be at a loss to explain the superior performance of the Cray-1. Only investigation of the organization of the basic circuits into larger sub-assemblies would elucidate the basis of the differences between the various machines.

Systems Analysis.

The study of large numbers of interacting neurons requires the use of more abstract techniques than are appropriate for the study of subcellular physiology. We thus choose to view a neural network primarily as a device which converts an appropriate stimulus into a measurable response. To characterize this system, we employ a body of general methods for the study of input-output relations known as "systems analysis." These methods here have as their first objective the "identification" of the system under study. By this is meant the presentation to the system

of an ensemble of test stimuli so chosen that the
responses which they generate can serve to distinguish
between the system under study and other comparable systems.
For example, such studies can serve to rule out conjectured
models for a system, by demonstrating a stimulus to which
the system and the model respond differently. Such a
program can be applied to a biological neural network on
two levels: first, to characterize the generic response
of the network under study (for example "the response" to
a light flash of a given type of retinal neuron), and
second, to characterize the response of a particular
specimen at hand as distinguished from that of other specimens
of the same type of network. The variability between
specimens of many biological systems is sufficiently large
that characterizations at this second level are necessary
whenever a quantitative treatment of the network's behavior
is sought.

The characterization of a system is generally sum-
marized by a tabulation, in some compact form, of the depend-
ence of suitable response attributes on the various parameters
of the chosen stimulus ensemble. While such a tabulation
will serve at the very least as a convenient label for the

system (hence the term "identification"), in favorable cases
it will actually embody enough information about the system to
enable the prediction of the response of the system to many
stimuli not present in the original testing ensemble. This
ability to predict the results of hypothetical experiments
is a great asset in the study of physiological systems, and
often helps prevent the fruitless expenditure of limited
experimental resources. Such a characterization can thus
represent an extremely powerful description of the function
of a physiological system.

The two phases of such a program may be referred to by the
terms "analysis" and "synthesis," drawn from the usage of
classical Greek geometry. Thus, analysis consists of the
elucidation of the system's response characteristics by the
study of responses to carefully chosen stimuli. Synthesis is
the process of reassembling the information gained in the analysis
phase to construct the response to an arbitrary stimulus. The
benefits of such a program are not confined to the development
of a method of response prediction. The information obtained
in the analysis procedure, and confirmed in the synthesis
calculation as a valid summary of the system's response
repertoire, can be of great value in the resolution of
questions about the physiological processes which underly
the system's macroscopic response.

Linear and Nonlinear Systems.

In practice, it is often possible to simplify the systems-analytic treatment of a system by incorporating into the procedure as much prior knowledge of the response characteristics of the system as possible. The foremost example of such a simplification occurs in the case of a "linear system" (that is, a system whose response to the sum of two stimuli is given by the sum of its responses to each stimulus presented separately). In this case, the ensemble of stimuli used for analysis may be reduced to a "basis" set of stimuli from which all other stimuli of interest may be constructed by addition.

Indeed, the linear formulation is so useful that non-linear systems are often treated by attempting to find a good linear approximation to which may be added such nonliner corrections as are necessary. In favorable cases these corrections may be small or few in number. The first few correction terms may also contain useful information about the system even if the subsequent corrections are not negligible.

The Retina.

Retinas, the neural networks in the eyes of vertebrates and

invertebrates which mediate the conversion of incident light into neural information, constitute an ideal class of biological system for the application of the techniques of systems analysis. The inputs (light) are well defined and easily manipulated in the laboratory. The outputs are readily accessible through the techniques of electrophysiology. Furthermore, the retinas of both vertebrates and invertebrates are systems of intrinsic interest, with an internal complexity well matched to the present level of theoretical investigations. Finally, the vertebrate retina in particular is actually a portion of the brain, and thus may serve as an instructive model system on the way toward an understanding of more complex and less accessible brain structures.

Nevertheless, there has been surprisingly little work done toward the full quantitative systems-analytic treatment of the retina. This record in part reflects the historical emphasis on the part of vision scientists on the difficult problems of the vertebrate retina in preference to the simpler retinas of many invertebrates. As a result of this trend, most investigators have proceeded only as far as the analysis portion of the program suggested above. A few of the more prominent studies are described below.

Perhaps the earliest quantitative treatment of the response of retinal neurons along the lines described above was the pioneering analysis of lateral inhibition in the _Limulus_ retina by Hartline and Ratliff (1957, 1958). By means of a set of simultaneous piecewise-linear equations, they were able to predict steady-state impulse rates in small sets of interacting ommatidia.

Another important early contribution was the detailed description of the responses of cat retinal ganglion cells to moving bar and disc stimuli by Rodieck and Stone (1965a). They were further able to map the receptive fields of ganglion cells by means of small spots (which were either moved or flashed to elicit neural responses), and to show that these receptive field properties could account, in a schematic way, for the various stereotyped responses they had observed (Rodieck and Stone, 1965b). In a subsequent paper, Rodieck outlined a linear convolution algorithm for the calculation of the responses to moving patterns, based on nominal receptive field properties (Rodieck, 1965). This study thus constitutes an example of systems analysis at the level of generic responses, as opposed to the characterization of a particular specimen.

Stimuli which varied sinusoidally in time were used
for the study of the vertebrate retina by Hughes and Maffei
(1966). They obtained amplitude and phase data for the
response of cat ganglion cells to flickering spots of light
They found that the response amplitude typically increased
only as the 0.75 power of the stimulus contrast, but that,
at least for low-frequency stimuli, harmonic distortion of
the responses to sinusoidal stimuli was rather small. They
did not attempt any synthesis calculations.

The _Limulus_ retina was a subject of another study
at the "generic" level by Lange and his colleagues at about

the same time (Lange,1965; Lange, Hartline, and Ratliff,
1966). This study used a calibrated model of the dynamics
of a generic Limulus ommatidium to predict the time
course of neural responses to stationary spot stimuli.
Pinter(1966) studied the time course of the Limulus
ommatidial generator potential in response to sinusoidal
and flashing stimuli. He was able to demonstrate excellent
quantitative agreement between the frequency response
(that is, the transfer function) of the generator potential
and the Fourier transform of the impulse response (see
chapter II for the theory of this relationship). He also
showed that the amplitude of the generator potential
response to sinusoidal stimulation scales linearly with
the stimulus modulation depth up to virtually 100% modulation
Though this study concerned only the first stage of the
Limulus visual transduction, it clearly demonstrated the
benefits of performing both analysis and synthesis
experiments on the same preparation.

The full power of linear transfer function methods
was soon brought to bear on the dynamics of the Limulus
retina. Ratliff, Knight, and Graham (1969) examined
the role of inhibitory dynamics on the response of the
retina to large flickering stimuli. They were thus able

to explain, in generic terms, the enhancement of the
response to flickering stimuli by lateral inhibition seen
previously in "small spot-large spot" experiments
(Ratliff, Knight, Toyoda, and Hartline, 1967). Sub-
sequently, Knight, Toyoda, and Dodge (1970) obtained direct
transfer function measurements for the processes of
excitation, self-inhibition, and lateral inhibition in
the Limulus eye. The generic parameter values from these
measurements, together with the steady-state measurements
of the inhibitory coupling constants which describe
the spatial organization of lateral inhibition (Barlow,
1967, 1969) allowed them to successfully predict the
results of a small spot-large spot experiment.

Other investigators continued to pursue more compli-
cated visual systems. Spekreijse (1969), studying recti-
fication in the goldfish retina, described a procedure
by which auxilliary, high-frequency signals superimposed
on sinusoidal stimuli could serve to "linearize" the
response of highly nonlinear systems. He was able to apply
the techniques toward an analysis of retinal ganglion cell
responses, but did not attempt any synthesis calculations.

Maffei and his colleagues continued their work on cat retinal
ganglion cells (Maffei, 1968; Maffei and Cervetto, 1968; Maffei
et al., 1970). They measured transfer functions for stimuli
localized in various portions of a cat retinal ganglion
cell's receptive field, and, in a sort of synthesis
experiment, were able to predict by linear summation the
responses to composite stimuli. (Ratliff, Knight, and
Milkman (1970) also reported similar results in the Limulus
retina.)

The entire "oculomotor system" of the fly (that is, the
transduction from visual stimuli to flight movements) was
studied throughout the 1970's by Reichardt and Poggio (for a
recent review, see Reichardt and Poggio, 1976; Poggio and
Reichardt, 1976), who have used nonlinear methods to analyze
the basic nature of the neural computations made by the flying
insect. A somewhat more formal approach was taken by
Marmarelis and Naka (1972, 1973a,b,c). Rather than attempt to
ignore the nonlinearities in the vertebrate retina (in
their case, that of the catfish), they implemented the very
general program of Wiener (1958) for the description of
a nonlinear system in terms of a series of orthogonal
functionals. They determined these functionals, which
thus serve to identify the system, by means of cross-
correlations between a Gaussian white-noise stimulus and the
response generated by this noise stimulus (Lee and
Schetzen, 1961). In practice, only the first- and second-

order functionals were measured. These were then used in a synthesis calculation to "predict" the response of the retinal neurons to the same white-noise stimulus which had been used to measure the functionals in the first place. Though this program was thus somewhat circular, the calculations did describe the strong rectification of these cells with considerable accuracy. This work prompted a great many efforts to apply the Wiener methods to a large variety of nonlinear systems, ranging from the growth of slime mold spore stalks to the effect of seismic vibrations on tall buildings (see McCann and Marmarelis, 1975).

One final piece of the Limulus story was added by Ratliff et al. (1974), who showed that the phase of the lateral inhibitory interaction in this retina is independent of the distance between interacting ommatidia, while the amplitudes scale by a real constant. They also presented a synthesis calculation, in which they were able to predict the response to stationary, square-wave modulated spots of light (either excitatory or inhibitory to the test-ommatidium) by means of sinusoidal-stimulus transfer function measurements. On the basis of the framework summarized by Knight (1973a), Leung and Freeman (1977) presented a plot of a (somewhat idealized) spatiotemporal transfer function for the Limulus retina, and predicted the response of the retina to the sudden onset of a cosine grating stimulus. They presented no experimental data. Though their study used only generic transfer function

parameters, and ignored the effect of the finite resolution of the _Limulus_ optics, it represents the closest anticipation of the present investigation.

Recently, Victor and Knight (1979) have developed useful frequency-domain analogues of the Wiener treatment for the study of nonlinear systems. (See also Victor, Shapley, and Knight, 1977; Victor, 1979a,b.) These techniques employ a sum-of-sinusoids stimulus instead of the white-noise stimuli suggested by Wiener. _A fortiori_, these methods also yield an efficient description of linear systems as a special case; in this way they have been employed extensively below.

Thus, though there have been many partial results towards systems-analytic characterizations of vertebrate and invertebrate retinas, the complete description of such a system, including the rigorous test of synthesis of its response to a nontrivial stimulus, other than that used for analysis,has not previously been accomplished. Such a characterization, for the _Limulus_ retina, is the principal objective of this dissertation.

The basic linear theory used for the analysis and synthesis of the response of the retina is developed in chapter II. Experimental methods, and the results thereby

obtained are described in chapters III and IV. A linear
model for the <u>Limulus</u> retina compatible with these data
is presented in chapter V; the quantitative calibration
of this model on the basis of transfer function data is
described in chapter VI. This model not only summarizes
the empirical transfer function data, but allows additional
applications on the basis of its functional form. Such
an application, to the response of neurons near the edge
of the retina, is presented in chapters VII and VIII.
A brief discussion of these results is given in chapter IX,
which is followed by a few tentative remarks concerning
the extension of the methods of this study to the
vertebrate retina (chapter X). Several subjects whose
treatment would divert the reader's attention from the main
exposition are treated in the appendices.

"Linear operations are common in physics - commoner
indeed in physics than in nature ..."

N. Wiener, 1933

II. Model-Free Linear Theory.

In this section we develop the theoretical basis for
our analysis of the response of the <u>Limulus</u> retina. We begin
with a very general discussion of linear systems analysis,
and then specialize this treatment for application to the
present measurements. We first make three fundamental assump-
tions about the system under study, which we may refer to as
<u>stationarity</u>, <u>linearity</u>, and <u>continuity</u>.

By stationarity, we refer to the assumption that the
properties of the system are stable with respect to time.
In other words, we require that the system give the same
response each time it is presented with the same stimulus. If
we denote the stimulus as a function of time by $S(t)$, and the
corresponding response by $R(t)$, and use an arrow ($\rightarrow$) to denote
the action of the system under study, we may express the
stationarity condition as

$$S(t) \rightarrow R(t) \text{ implies } S(t-\tau) \rightarrow R(t-\tau) \qquad (2.1)$$

where τ is any constant shift in time. Of course, as nearly
every biological system ages, and most neurophysiological
preparations deteriorate, this assumption is necessarily an
approximation.

Linearity refers to the assumption that the system obeys the superposition rule, that the response to a sum of inputs is the sum of the responses to the inputs taken separately. In symbols,

$$S_1(t) \rightarrow R_1(t) \ , \ S_2(t) \rightarrow R_2(t) \text{ implies} \qquad (2.2)$$
$$S_1(t) + S_2(t) \rightarrow R_1(t) + R_2(t) \ .$$

This is a very strong assumption, whose consequences will be vigorously exploited below. Many biological systems operate in a nearly linear manner when presented with stimuli which consist of small fluctuations about a steady mean value, but frequently saturate when presented with very strongly modulated stimuli.

The assumption of continuity states that small changes in the stimulus presented to the system produce only small changes in the response. This is a mild assumption for most systems in the middle of their operating range but it often does not hold for systems at the extremes of their range.[*] The effect of this assumption is to justify various mathematical manipulations below. For example, if x is some parameter and $S_x(t)$ varies smoothly with x, then the continuity assumption allows us to assert the following continuous analogue of equation (2.2):

$$S_x(t) \rightarrow R_x(t) \text{ implies} \int S_x(t)dx \rightarrow \int R_x(t)dx \ . \qquad (2.3)$$

---

[*] Consider, for example, the load of straw-camel's back system.

The assumptions of linearity and continuity together imply "weighted" versions of equations (2.2) and (2.3):

$$S_1(t) \rightarrow R_1(t) \ , \ S_2(t) \rightarrow R_2(t) \text{ implies}$$

$$aS_1(t) + bS_2(t) \rightarrow aR_1(t) + bR_2(t) \ ,$$

(2.2')

$$S_x(t) \rightarrow R_x(t) \text{ implies } \int a(x)S_x(t)dx \rightarrow \int a(x)R_x(t)dx \ , \quad (2.3')$$

where a,b are numbers, and a(x) is a function of x.

In general, a stationary, linear, continuous system (a "linear system," for short) can be completely characterized in several equivalent ways.

One such characterization consists of measuring the system's response to an "impulse," a stimulus of finite strength delivered within an arbitrarily short time. We will denote such a stimulus as a Dirac delta-function, $\delta(t)$. The response to such an impulse delivered at time $t = 0$ will be called the "impulse response," denoted $I(t)$. The impulse response provides a complete characterization of a linear system by virtue of the following identity, which constitutes a fundamental property of the delta-function:

$$S(t) = \int S(u)\delta(t-u)du \ .$$

(2.4)

This expresses an arbitrary stimulus $S(t)$ as a weighted combination of impulses occuring at different times; the

weighting function is simply the stimulus function itself.
The stationarity assumption implies that the response to
the stimulus $\delta(t-u)$ is $I(t-u)$; we may now apply (2.3') to conclude

$$S(t) \rightarrow R(t) = \int S(u) \cdot I(t-u) du \ . \qquad (2.5)$$

This is a formula for the response of the system to an
arbitrary stimulus S, given in terms of the impulse response I.

An alternative characterization of a linear system can be
obtained from (2.5) by considering the response of the system
to a sinusoidal input. We may greatly simplify the calcul-
ations by adopting the complex-exponential notation for sinus-
oidal functions; we thus identify cos ωt with the real part of the
complex exponential $e^{i\omega t}$ = cos ωt + i sin ωt. In general, any complex
quantity which appears below is to be interpreted as representing its
real part. With this convention, we choose for our stimulus
$S(t) = e^{i\omega t}$, a sinusoid of angular frequency ω. According to
equation (2.5), for this stimulus, we obtain the response

$$R(t) = \int e^{i\omega u} I(t-u) du \qquad (2.6)$$

$$= \int e^{i\omega(t-u)} I(u) du = \left(\int e^{-i\omega u} I(u) du \right) \cdot e^{i\omega t} \ .$$

(Here, the step from the first line to the second follows from a
standard change of variable (v=t-u;u=t-v;du=-dv):

$$\int_{-\infty}^{\infty} e^{i\omega u} I(t-u) du = \int_{+\infty}^{-\infty} e^{i\omega(t-v)} I(v)(-dv) = \int_{-\infty}^{+\infty} e^{i\omega(t-v)} I(v) dv \ .$$

Note the limits of integration at each step.)

Thus, the response of a linear system to a sinusoidal input $S(t) = e^{i\omega t}$ is a sinusoid of the same frequency, multiplied by some (complex) number which depends on the frequency, ω, and upon the impulse response, I, of the system. We refer to this coefficient (considered as a function of ω) as the "transfer function" of the system, and denote it by $F(\omega)$. We then have

$$R(t) = F(\omega) \cdot e^{i\omega t}, \tag{2.6'}$$

where

$$F(\omega) = \int e^{-i\omega t} I(t)dt. \tag{2.7}$$

That is, $F(\omega)$ is the Fourier transform of the impulse response, $I(t)$

The transfer function $F(\omega)$ provides a complete characterization of a linear system as a consequence of the following Fourier inversion formula:

$$S(t) = \frac{1}{2\pi} \int e^{i\omega t} \tilde{S}(\omega)d\omega , \tag{2.8}$$

where

$$\tilde{S}(\omega) \equiv \int e^{-i\omega t} S(t)dt . \tag{2.9}$$

This expresses an aribtrary stimulus $S(t)$ as a weighted sum of sinusoids $e^{i\omega t}$; the weighting function $\tilde{S}(\omega)$ is the Fourier transform of the stimulus. Applying (2.3') and (2.6') to (2.8)

yields

$$R(t) = \frac{1}{2\pi}\int e^{i\omega t} \cdot F(\omega) \cdot \tilde{S}(\omega)d\omega \ . \qquad (2.10)$$

This is an expression for the response of the system to an arbitrary stimulus $S(t)$ in terms of the transfer function $F(\omega)$. The response is the inverse Fourier transform of the product of the transfer function of the system and the Fourier transform $\tilde{S}(\omega)$ of the arbitrary stimulus $S(t)$.

It is appropriate to note here that while these two mathematical characterizations of a linear system are informationally equivalent, and each can be readily obtained from the other (by (2.7) and its Fourier inversion formula), the transfer function is often the more suitable characterization for direct laboratory measurement. This is because an impulse stimulus, though of finite total strength, has extremely large intensity (even in a laboratory realization of the theoretical infinite intensity). Such large signals may easily drive the system out of its linear range, or even damage it irreversibly (consider, for example, the study of a skin pressure receptor; in this case, an impulse takes the form of a sharp blow). Even when an impulse stimulus might not saturate the system, it may be difficult or impossible to provide a satisfactory impulse stimulus, especially if one studies a transduction whose only accessible input is the output of another transduction. In such a case, sinusoidal inputs are readily obtained, but impulses are unavailable.

We now proceed to formulate the analysis given above
in terms appropriate to our particular experimental situation.
We introduce coordinates on the Limulus lateral eye, with
the x-axis horizontal, the y-axis vertical, and the origin
centered on the test-ommatidium (the ommatidium whose eccentric
cell action-potentials are being recorded.) We assume that the eye
extends indefinitely far on either side of the test ommatidium.   A
completely general stimulus takes the form $S = S(x,y,t)$;
for computational convenience, we restrict all further dis-
cussion to stimuli which depend only on x and t, that is to
stimuli which, at any time t, are constant along each vertical
line. This reduces our problem to one dimension of time, and
one of space. To further facilitate the analysis, we ignore
the discrete structure of the Limulus eye, and assume instead
that it is made of a continuum of photosensitive elements,
each possessing the same dynamical properties as the test-
ommatidium (Kirschfeld and Reichardt, 1964). The ommatidia
are sufficiently numerous and homogeneneous that, in practice,
this approximation is innocuous. Our final specialization is
to restrict our calculations to predictions of the response to
arbitrary intensity patterns which move at a uniform speed across
the eye. While the Fourier methods outlined above are per-
fectly adequate to predict the response to an arbitrary time-
varying stimulus, the restriction to stimuli of the form
$S(x,t) = S(x-vt)$ (where $S(x)$ is some spatial pattern of
illumination, and v is the drift velocity) greatly facilitates
the calculation of the necessary Fourier transforms. Such

stimuli, with $S(x)$ arbitrary, and v at our disposal, are
sufficiently general to provide a rigorous test of the
adequacy of our characterization of the response of the eye.

This characterization is given in terms of a spatio-
temporal transfer function, which generalizes the temporal
transfer function of (2.7), above. We consider the response
as a function of space and time, $R = R(x,t)$, and ask what
is the response to a travelling spatial sinusoid $S(x,t) = e^{i(\xi x+\omega t)}$.
(We may put this expression in the form $S(x-vt)$ by writing
$e^{i(\xi x+\omega t)} = e^{i\xi(x+\frac{\omega}{\xi}t)} = e^{i\xi(x-vt)}$, where $v = -\frac{\omega}{\xi}$; this is
the equation of a sinusoid of spatial frequency ξ moving at the
speed $v = \omega/\xi$.) In addition to our previous assumptions,
we now also assume that the response of the eye is invariant under
translation (change of origin). This is the analogue for space
of the stationarity assumption in time. With this assumption,
an argument strictly analagous to that given above implies
that the response $R(x,t)$ to a sinusoidal input $S(x,t) = e^{i(\xi x+\omega t)}$
is again a sinusoidal function of space and time, with the
same spatial frequency ξ and the same temporal frequency ω.
In other words, we have the input-output relation

$$S(x,t) = e^{i(\xi x+\omega t)} \text{ implies } R(x,t) = F(\xi,\omega) \cdot e^{i(\xi x+\omega t)} \quad (2.11)$$

where

$$F(\xi,\omega) = \int\int e^{-i(\xi x + \omega t)} I(x,t) dx dt \qquad (2.12)$$

is a (complex) number depending on ξ and ω, given by the spatio-temporal Fourier transform of $I(x,t)$, the response of the system to a spatio-temporal impulse (a vertical line at $x = 0$ flashed at the instant $t = 0$).

We now fit the pieces together to calculate the response of the system to an arbitrary moving pattern. We first obtain the Fourier transform of the spatial pattern of the stimulus $S(x,t) = S(x-vt)$:

$$\tilde{S}(\xi) = \int e^{-i\xi x} S(x) dx. \qquad (2.13)$$

We also note the corresponding inversion formula:

$$S(u) = \frac{1}{2\pi} \int e^{+i\xi u} \tilde{S}(\xi) d\xi. \qquad (2.14)$$

Taking $u = x-vt$, we obtain a Fourier representation for the stimulus:

$$S(x-vt) = \frac{1}{2\pi} \int e^{i(\xi x - \xi vt)} \tilde{S}(\xi) d\xi = \frac{1}{2\pi} \int e^{i(\xi x + \omega t)} \tilde{S}(\xi) d\xi , \qquad (2.15)$$

where $\omega = \omega(\xi) = -\xi v$.

Applying (2.3') to (2.11) and (2.15) gives the final input-output

relation:

$$S(x-vt) \rightarrow R(x,t) = \frac{1}{2\pi} \int e^{i(\xi x + \omega t)} \cdot F(\xi, \omega) \cdot \tilde{S}(\xi) d\xi$$

$$= \frac{1}{2\pi} \int e^{i(\xi x - \xi vt)} \cdot F(\xi, -\xi v) \tilde{S}(\xi) d\xi$$

$$= \frac{1}{2\pi v} \int e^{i(\frac{-\omega}{v} x + \omega t)} F(\frac{-\omega}{v}, \omega) \tilde{S}(\frac{-\omega}{v}) d\omega \qquad (2.16)$$

Equations (2.11), (2.13), and (2.16) define a complete program for the characterization of our system: the transfer function $F(\xi, \omega)$ may be obtained by measurement of the responses of the system to sinusoidal stimuli. Given $F(\xi, \omega)$, the response to an arbitrary moving stimulus $S(x-vt)$ may be obtained by taking the Fourier transform of the stimulus spatial pattern, multiplying by the transfer function, and taking the inverse Fourier transform. In this way, knowledge of the transfer function $F(\xi, \omega)$ serves to completely characterize the system.

It is useful to assume that, in addition to being homogeneous (spatially invariant), the eye under study is isotropic, in the sense that the eye is indifferent to reflections about the test-ommatidium (x=0). This is equivalent to the assertion that the impulse response function possesses the symmetry $I(-x,t) = I(x,t)$. This symmetry induces certain useful symmetries in $F(\xi, \omega)$. For example we have, from (2.12) that

$$F(-\xi, \omega) = \int\int e^{-i(-\xi x + \omega t)} I(x,t) dx dt$$

$$= \int\int e^{-i(\xi(-x) + \omega t)} I(x,t) dx dt$$

$$= \int\int e^{-i(\xi u + \omega t)} I(-u,t) du dt$$

$$= \int\int e^{-i(\xi u + \omega t)} I(u,t) du dt = F(\xi, \omega). \qquad (2.17)$$

Futhermore, since $I(x,t)$ is real,

$$F(-\xi,-\omega) = \iint e^{-i(-\xi x-\omega t)}I(x,t)dxdt$$

$$= \iint \overline{e^{-i(\xi x+\omega t)}}I(x,t)dxdt$$

$$= \overline{\iint e^{i(\xi x+\omega t)}I(x,t)dxdt}$$

$$= \overline{F(\xi,\omega)} \ , \qquad\qquad (2.18)$$

where the horizontal bars indicate complex conjugates.

Together (2.17) and (2.18) imply

$$F(\xi,-\omega) = \overline{F(\xi,\omega)}. \qquad\qquad (2.19)$$

The symmetry (2.17) allows an important experimental simplification. We have:

$$e^{i(\xi x+\omega t)} \rightarrow F(\xi,\omega)e^{i(\xi x+\omega t)}$$

$$\qquad\qquad\qquad\qquad\qquad\qquad (*)$$

$$e^{i(-\xi x+\omega t)} \rightarrow F(-\xi,\omega)e^{i(-\xi x+\omega t)} = F(\xi,\omega)e^{i(-\xi x+\omega t)} \ .$$

Since

$$e^{i(\xi x+\omega t)} + e^{i(-\xi x+\omega t)} = e^{i\omega t}(e^{i\xi x}+e^{-i\xi x}) = e^{i\omega t}2\cos \xi x,$$

if we add the inputs and outputs in (*) and divide by 2, we obtain

$$S(x,t) = e^{i\omega t} \cdot \cos\xi x + F(\xi,\omega)e^{i\omega t}\cos x = R(x,t) . \quad (2.20)$$

Examining the output at x = 0 (the test-ommatidium), we have

$$S(x,t) = e^{i\omega t}\cos\xi x + R(t) \equiv R(0,t) = F(\xi,\omega)e^{i\omega t} . \quad (2.11')$$

The implication of this equation is that we may determine the transfer function $F(\xi,\omega)$ by examining the response of the eye the stationary counterphase grating stimulus $e^{i\omega t} \cdot \cos\xi x$, instead of the drifting sinusoidal grating stimulus $e^{i(\xi x+\omega t)}$. The counterphase stimulus consists of a sinusoidal grating in space, placed with a peak centered over the test-ommatidium, modulated by multiplication by a time-varying sinusoidal signal. Such a stimulus is especially well suited for experimental use (see below.

Again, by restricting our attention to the output at the test-ommatidium, we obtain an analogous version of equation (2.16)[*]:

$$S(x-vt) + R(t) \equiv R(0,t) = \frac{1}{2\pi}\int e^{i\omega t}F(\xi,\omega)\tilde{S}(\xi)d\xi.$$

$$= \frac{1}{2\pi}\int e^{-i\xi vt}F(\xi, -\xi v)\tilde{S}(\xi)d\xi$$

$$= \frac{1}{2\pi v} \int e^{i\omega t}F(\frac{-\omega}{v},\omega)\tilde{S}(\frac{-\omega}{v})d\omega . \quad (2.16')$$

The assumption of linearity is also useful for reasons of experimental convenience. For example, it is unnecessary to present the stimuli of equation (2.11') one at a time. Instead, we may form the linear combination stimulus $S(x,t) = \Sigma_n c_n e^{i\omega_n t}\cos\xi x$, where the c_n are constants at our disposal and the ω_n are the temporal frequencies at which $F(\xi,\omega)$.

---

*   It should be noted that if both the transfer function

measurement and the synthesis calculation are restricted to

a test-ommatidium at the origin (as in equations (2.11') and

(2.16'), then the assumption that the retina is invariant under

spatial translation may be dropped.   This is discussed more

fully in chapter VIII.

is sought. By (2.2'), we have, for this stimulus,

$$S(x,t) = (\sum_n c_n e^{i\omega_n t}) \cdot \cos\xi x \rightarrow R(t) = \sum_n c_n F(\xi,\omega_n)e^{i\omega_n t} \quad . \quad (2.21)$$

For the fixed spatial frequency ξ, the transfer function can
easily be recovered from this composite response with the aid
of Fourier methods (see below). Indeed, the frequencies ω_n
can be so chosen that all the second harmonics are distinct
from the input frequencies. With such a choice of the ω_n,
the (presumably negligible) response detected at second harmonic
frequencies can be used as a simple monitor of the linearity
of the system (Victor et al., 1977; Victor, 1979b; Victor
and Knight, 1979). Such a choice of test stimulus has
two advantages in the present situation. First,

it substantially reduces the data acquisition time necessary
to characterize the system response over the grid of spatio-
temporal frequency points. Second, because such a stimulus
contains modulation over a substantial range of temporal
frequencies, it prevents the occurence of "phase locking,"
a distinctly non-linear phenomenon which affects many neural
encoders driven predominantly at a single frequency (Knight,
1972a). By choosing the weighting coefficients c_n roughly
reciprocal to the anticipated magnitude $|F(\xi,\omega_n)|$ of the trans-
fer function at each frequency ω_n, one produces a response
with roughly equal output power at each frequency ω_n.
Under such circumstances, phase locking becomes exceedingly
unlikely. Furthermore, this procedure optimizes the signal-to-
noise ratio for all the frequencies in the stimulus.

We note that this linear analysis applies, strictly speaking, only to the variations of the various functions about their mean level (light intensity, on input; and impulse rate, on output). This restriction is necessary, in part, because our experimental variables do not take on negative values. Furthermore, when considered as a function of absolute stimulus intensity, the response of most sensory transducers, including the Limulus eye, is decidedly nonlinear, and exhibits a nearly logarithmic response to time-independent stimuli which vary over many orders of magnitude (Stevens, 1975).

Finally, over periods comparable to our experimental trials many sensory transducers, including the Limulus eye, show considerable fatigue or adaptation, in violation of our assumption of stationarity. Such systems may be treated by linear methods only in terms of their fluctuations about a mean operating level which has been adjusted to include the effects of short-term adaptation. Thus, for the present study, in order to compare responses with linear predictions, the mean level and adaptation rate were measured, subtracted from the output signal, and then added back to the results of the linear calculation. The correction for adaptation rate was, in general, practically negligible. We made no attempt to predict the mean output levels.[*]

---

[*] In the Limulus visual system, the use of signals consisting of perturbations about a mean level also allows us to ignore in the analysis the phenomenon of inhibitory thresholds (Hartline and Ratliff, 1957), a decidedly nonlinear effect. See also below.

"You'll be catching a crab directly"

L. Carroll, 1871

III. Methods

Stimulus.

Patterns of light, varying in space and time, were formed on the screen of a large oscilloscope (Hewlett-Packard Model 1321A High Speed Graphic Display; phosphor P31) using analog voltages produced by a system of circuits designed for this purpose (Shapley and Rossetto, 1976), and digital-to-analog converters (DAC's) controlled by a PDP 11/45 computer. This time-varying pattern was then imaged by a high-quality camera lens (Nikon Nikkor f/1.2, focal length 55 mm) onto the flat surface of a fiber-optic taper, which was glued to the cornea of a _Limulus_ eye. This fiber-optic device, supplied according to our specifications by Walter P. Siegmund of the American Optical Co., Southbridge, Mass., conveyed the visual stimulus to the curved array of _Limulus_ photoreceptors. The details of the optical system are discussed in Appendix A. The overall effect of this optical system was to convert a pattern 15 cm wide and 2 cm high on the oscilloscope face to a stimulus 1 cm wide and 0.13 cm high on the corneal surface. The height of the image, roughly $\frac{1}{4}$ of the height of the eye, was chosen as a compromise between the theoretically desirable goal of illuminating the entire eye, and the need to illuminate a sufficiently narrow band to get an acceptably high impulse rate. (Larger stimuli produce low impulse rates by producing more lateral inhibition, and by spreading the same photon flux over a greater number of ommatidia).

For all stimuli produced, a high-frequency triangle-wave was applied to the Y-input of the display oscilloscope; the X-input was driven with a sawtooth waveform generated by the computer, and the Z-input (intensity) was driven by computer-generated signals synchronized to the X-input sawtooth. This arrangement produced a rectangle of light on the screen, whose intensity varied with horizontal position and time, but whose intensity was independent of vertical position. Three types of stimuli were used: a "set-up" stimulus to align the stimlus coordinates with the test-ommatidium, an "analysis" stimlus for measuring the spatio-temporal transfer function, and a "synthesis" stimulus which consisted of a uniformly drifting pattern of illumination.

The "set-up" stimulus consisted of a single bright vertical line at x = 0 surrounded by a uniform dim background; this stimulus did not vary with time. This pattern was manually moved across the face of the oscillo-scope until the bright line was centered on the test-ommatidium, as indicated by monitoring its impulse-train discharge. This adjustment was generally reproducible to within ±.004 eye-widths,[*] and proved more than adequate

---

[*] In our experimental apparatus, the width of the <u>Limulus</u> eye under study is the most natural unit for the horizontal coordinate. For a typical eye, this may be converted as follows: 1.0 eye-widths = 1.0 cm = 40 ommatidial diameters (in the horizontal direction). The conversion to visual angle (in the horizontal direction) is somewhat complicated, because even though the ommatidia are rather evenly spaced, their optical axes diverge non-uniformly. Thus, in the center of the eye, an ommatidium sub-tends approximately 6° of visual angle, but the whole eye (40 ommatidia in width) only covers a total visual angle of approximately 200°.

for the purposes of these experiments.

The "analysis" stimulus was produced by using for the Z-input of the display oscilloscope a signal which consisted of a constant offset plus the analog product of three computer-generated signals: a constant voltage (to control the total contrast), a "temporal modulation" signal whose value was changed before each sweep of the X-input sawtooth (each sweep lasted .01536 s; this yielded a temporal sampling rate of 65.1 Hz), and a "spatial modulation" signal, a rapid sinusoidal modulation synchronized to the X-input sawtooth so as to produce a cos ξx spatial pattern. (This is shown schematically as a block diagram in Figure 3-1.) The X-sawtooth was obtained by rapidly producing 256 successive equally-spaced voltage values with a DAC. This provided a spatial sampling mesh of 256 points/eye-width (which corresponds to eight points per cycle at the highest spatial frequency used). The temporal modulation signal was a sum of eight sinusoids with frequencies 0.1, 0.233, 0.5, 1.033, 2.1, 4.233, 8.5, and 17.033 Hz.[*] The relative amplitudes of these components were 60, 50, 45, 30, 15, 10, 20, and 40, respectively.

The "synthesis" stimulus was generated in a similar manner, by holding the "temporal modulation" signal constant, and by producing the spatial modulation by sending to the DAC successive numbers from a list of intensities which described the arbitrary spatial pattern, synchronized to the X-sawtooth. By progressive shifts of the phase of the intensity list with respect to the sawtooth, the pattern was made to drift across the screen at any desired rate.

By reversal of the order in which the X-sawtooth voltages were read out by the DAC, it was possible to reflect the synthesis stimulus about

---

[*] $(2^{n+1} - 1)/30$, in Hz.
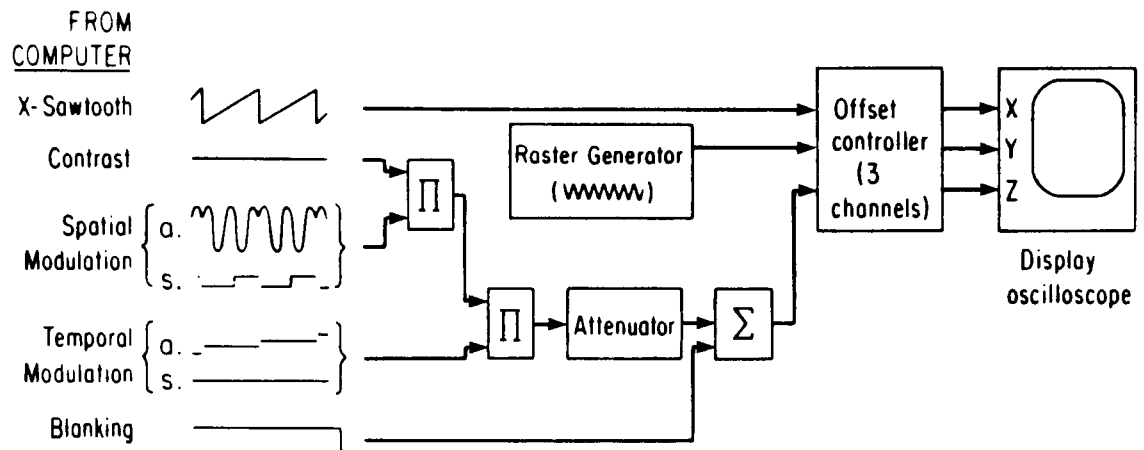
Figure 3-1. Block-diagram of spatio-temporal stimulus generation. Π indicates analog multipliers, Σ indicates analog summer. The raster generator produces a free-running 100 KHz triangle wave for the Y-axis. The attenuator is a voltage divider, set by hand to adjust overall contrast level. The offset controller adds analog signals to manually adjusted constant voltages. Three channels are provided: x and y offset moves the stimulus origin on the oscilloscope face; z offset adjusts mean illumination level. Two cycles of computer-generated input are shown at left (a. denotes analysis episodes, s. denotes synthesis episodes). Note spatial and temporal modulation are synchronized to X-sawtooth. Constant "contrast" voltage allows computer control of contrast level. "Blanking" signal darkens oscilloscope between experimental episodes.

the test-ommatidium , in order to verify our assumptions concerning the symmetry of the eye, and also to check the accuracy of the alignment of the stimulus origin with the test-ommatidium. For the synthesis stimuli, spatial resolution was upgraded to 512 points/eye-width, at the expense of lowering the sweep rate to 39.1 Hz. (For comparison, the comparable temporal resolution for commercial television is 30 Hz in the U.S., 25 Hz in Europe; movies are typically shown at a frame rate of 24 Hz.) Spatial patterns were fixed at 2.0 eye-widths in length, and were presented in a periodic fashion through a "window" one eye-width wide, so that at high drift velocities, the pattern was seen several times during the course of an experimental episode.

The response of the display oscilloscope to these analogue control signals was verified with a silicon photocell. At typical mean operating levels, the luminance of the oscilloscope varied linearly with the control voltage up to a modulation depth of approximately 40% contrast;[*] experiments were performed at a maximum contrast not exceeding 35%. The mean luminance of the stimulus as measured at the face of the oscilloscope screen with a Spectra brightness spot meter (Photo Research Corp.) was approximately 20 cd/m^2. The illuminance produced behind the spherical surface of the

---

[*] $\text{contrast} = \dfrac{(\text{maximum luminance}) - (\text{minimum luminance})}{(\text{maximum luminance}) + (\text{minimum luminance})}$

fiber-optic taper was approximately 9 lumens/m^2, as measured with a UDT model 40a photometer. This illuminance is roughly equivalent to a photon flux (λ = 555 nm) of 3.7 x 10^{16} photons/m^2/s at the front of the layer of glue between the fiber-optic taper and the cornea. The absorbance of the glue is presumably negligible. However, the absorbance of the cornea and crystalline cones is significant, and is highly variable between Limulus specimens. Thus, these numbers should be taken only as a rough estimate of the photon flux incident on the retina itself.

The Biological Preparation.

Adult horseshoe crabs (Figure 3-2), 15-20 cm
in diameter, were obtained from Gulf Specimens Inc.,
Panacea, Fla. The animals were kept in filtered artificial
sea-water at 10° C. They were generally used within six weeks
of delivery, during which time they were not fed. Animals
selected for use had "clear" eyes, with no perceptible
abrasion of the cornea, and in an informal "neurological exam"
they demonstrated brisk, vigorous flexion of the hinge muscle
after noxious stimulation of the gill. In general, the speed
and strength of the hinge muscle reflex appeared to correlate
well with the health of the retina.

Recordings of neural activity were made using an
in situ preparation (Corning et al. 1965; Biederman-Thorson
and Thorson, 1971; Adolph, 1971; Kaplan and Barlow, 1975).
In brief, the animal was secured to a wooden board on top
of a manipulator which allowed the animal to be rotated and
tilted. The gills were placed on a paper towel moistened
with the sea water in which the animal had been
living. The animals were always capable of vigorous motion
when removed from the apparatus, often after as long as 18
hours. A surgical trephine was used to cut a hole 2 cm in
diameter in the carapace, about 3 cm anterior to the animal's
right eye, above the optic nerve.[*] The nerve was transected,

---

[*]   A count of the resulting discs indicates that over 140
dissections on over 120 Limulus specimens were performed during
the course of this work.
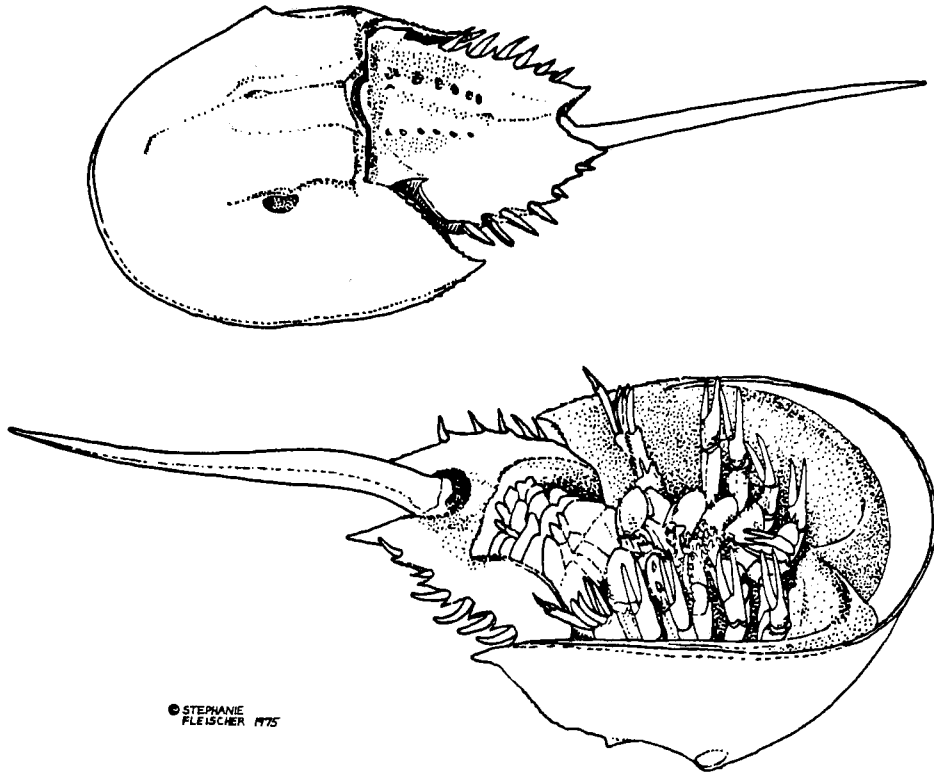
Figure 3-2. _Limulus_ _polyphemus_. Top, dorsal view;
Bottom, ventral view. (Drawing © Stephanie Fleischer, 1975)

dissected free, and pulled into a small recording chamber, which was then screwed into the carapace. The chamber was filled with sea water, and the nerve dissected with glass needles until a strand which contained a single functioning axon was obtained (Hartline and Graham, 1932). This strand was laid on a cotton wick-silver/silver chloride electrode. The signal from the electrode was amplified and filtered by a differential amplifier, and monitored via oscilloscope and loudspeaker. In order to ensure the symmetry of the retina about the test-ommatidium, only optic nerve fibers from ommatidia located near the center of the eye (away from the edges of the retina) were used.

The temperature of the crab was measured by means of a thermistor probe (Yellow Springs Instruments Co., Yellow Springs, Ohio) inserted in a hole placed medial to the animal's left eye. The animal's temperature was controlled by coupling it to a constant-temperature circulator (Lauda Instruments Division, Brinkmann Instruments, Inc. Westbury, N.Y.) with a modified ice-bag. Eye temperature was held at 22° C, and typically varied less than 0.5° C over the course of a 10-hour experiment. This elevated temperature was chosen because it raises the mean impulse rate (Adolph, 1973) and enhances the response to flickering light (see Appendix B).

Data Acquisition.

The amplified signal from the wick electrode was converted to a train of uniform pulses by a discriminator. These pulses served as input to the PDP 11/45 computer, which recorded the successive intervals between impulses in a file on magnetic disk for later analysis. Resolution was 10^{-4}s, and the same clock was used to time impulse arrivals as was used to generate the time-varying stimuli. The uniform pulses were also used to drive a "hyperbolic sweep" monitor, which gave a visual indication of instantaneous rate. (This device employed a new digital design by M. Rossetto, and replaced the analog circuit of MacNichol and Jacobs, 1955).

Protocol.

The experimental schedule consisted of 60s periods of illumination in alternation with 90s periods of darkness. This episode pattern was designed to maintain the eye in a uniform state of light-adaptation, over the duration of the experiment, as estimated by the total number of neural impulses produced in each episode. Successive episodes alternated between the analysis stimulus (a sinusoidal grating in space modulated temporally by a sum-of-sinusoids signal) and the synthesis stimulus (a pattern of light drifting across the eye at a constant speed). A stimulus cycle consisted of 16 episodes: analysis episodes at each of eight spatial fre-quencies (1/10, 1,2,4,8,16,20, and 32 cycles/eye-width) interleaved with two presentations of the synthesis stimulus

at each of four drift velocities, one presentation in each direction.

These stimulus cycles (which lasted 40 minutes) were repeated indefinitely until the nerve fiber ceased conducting impulses. Experiments typically lasted at least six hours, and occasionally as long as 10 hours. Nerve conduction failures were as a rule the result of the drying out of the exposed portion of the optic nerve; activity was readily obtained from more proximal portions of the nerve. We are thus confident that the retina did not significantly deteriorate over the course of an experiment.

Computations.

All computations were based on data from the last 50s of each 60s episode, well after the initial on-transient had decayed. The spatio-temporal transfer function $F(\xi,\omega)$ was obtained from the analysis episodes by means of a least-squares fitting algorithm, as described in Appendix C. This procedure is equivalent to ordinary discrete Fourier analysis of binned (histogram) data, with arbitrarily narrow bins; equivalently, it yields the spectrum of the impulse train interpreted as a series of δ-functions. The algorithm is particularly suited to the handling of pooled data from episodes with identical stimuli.

For each spatial frequency, the algorithm determines real numbers r_n so that the function $f(t) = \Sigma r_n f_n(t)$ best

approximates the population response r(t) (in a certain least-squares sense - see Appendix C), where the f_n's are the functions 1, $t-t_m$ (t_m is the midpoint of the data collection period), $\sin \omega_m t$, $\cos \omega_m t$, $\sin 2\omega_m t$, and $\cos 2\omega_m t$ (where the ω_m's are the input frequencies). The coefficient of the function 1 gives the mean impulse rate over the episode; the coefficient of the function $t-t_m$ (the "ramp slope") describes the slow decay of the impulse rate over the course of an episode. As described above, these parameters are ignored in the remaining analysis, but are added back to the Fourier synthesis at the end of the calculation. The coefficients of the $\sin \omega_m t$ and $\cos \omega_m t$ terms determine the value of $F(\xi,\omega_m)$ (where ξ is the spatial frequency of the stimulus which produced the particular data being analyzed): the amplitude of $F(\xi,\omega_m)$ is the square-root of the sum of the squares of these two coefficients, while the tangent of the phase of $F(\xi,\omega_m)$ is given by their quotient. The coefficients of $\sin 2\omega_m t$ and $\cos 2\omega_m t$ measure nonlinearities in the response of the system.
The entire set of coefficients was determined for the pooled data from all the analysis episodes at each spatial frequency.

The phase information for the transfer-function at each spatio-temporal frequency pair (ξ_n,ω_m) was obtained, as described above, by taking the arctangent of a quotient;

the computer expressed these results as real numbers between
$-\pi$ and π. These phase data were individually adjusted by subtraction of a
multiple of 2π so as to obtain continuous phase curves. Thus,
values of $F(\xi,\omega)$, as amplitude and phase, were obtained at the
64 spatio-temporal frequency points corresponding to all the
possible combinations of the 8 spatial and 8 temporal frequencies
present in the analysis stimuli. In order to estimate $F(\xi,\omega)$
for (ξ,ω) between the points of the input lattice, a two-
dimensional cubic spline was used. For this purpose, the
transfer function data were expressed in terms of two separate
real functions (log amplitude, and phase) of the variables
$\log \xi$ and $\log \omega$. The complex transfer function $F(\xi,\omega)$ was
then reconstructed from the amplitude and phase.

In order to avoid artifacts due to abrupt frequency
cut-offs, the transfer-function was extrapolated beyond the
spatio-temporal frequency lattice at which it had been measured.
The extrapolation to high spatial frequency extended the observed
attenuation of amplitude seen at spatial frequencies above 20
cycles/eye-width; for each spatial frequency, the amplitude
was fixed as a small constant multiple of the amplitude observed
at the highest spatial frequency where measurements were made.
Phases were extrapolated by setting them equal to the phases
measured at the highest spatial frequency used. The Fourier
syntheses were insensitive to the details of these high-
frequency extrapolations. It was unnecessary to extrapolate

to low spatial frequency, as the data extended down to 0.1
cycles/eye-width. The high temporal frequency extrapolations
were provided as approximate continuations of the typically
observed high-frequency roll-off in amplitude and phase.

For the extrapolation to low temporal frequencies, the
low frequency transfer-function measurements of Biederman-
Thorson and Thorson (1971) were used as a guide. Under
experimental conditions quite similar to ours, they measured
temporal transfer functions from 0.4 Hz down to 0.004 Hz.
In this regime they found that the transfer function could
be expressed as $F(\omega) = K \cdot (i\omega)^p$ where p is a real exponent
between 0.18 to 0.27 (mean 0.23), and K
is a real constant of proportionality. For simplicity we
adopted the exponent p = 0.25, and extrapolated the transfer
functions accordingly, fixing the proportionality constant
by the amplitude observed at the lowest frequency where measure-
ments were available (0.1 Hz), and extrapolating the phase to the
low frequency phase lead of $\pi/8$ radians implied by the exponent p=¼
While the very low frequency features of the Fourier syntheses
were not insensitive to the details of the low temporal
frequency extrapolation, this parameter-free procedure pro-
duced no systematic discrepancies between experiment and pre-
diction in the very low frequency range.

The synthesis episodes were treated differently. Data from episodes with identical stimuli were averaged together on a mesh of 1024 equally-spaced points covering the 50-second episode length. The resultant mean individaul rate response function, $\sigma(t)$ was plotted on a digital plotter (Cal Comp 565) for later comparison with the Fourier synthesis (see Appendix C).

The synthesis stimuli were presented in two directions at each velocity. As these pairs of stimuli consisted of reflections of each other about the test-ommatidium, they served to verify our assumptions about the symmetry of the inhibitory fields, and to verify the accurate placement of the stimulus origin so as to coincide with the test-ommatidium. In all cases the responses to the two mirror-image stimuli appeared nearly identical (see Results, below). This observation permitted us to further increase the signal-to-noise ratio by averaging together all the synthesis episodes at each velocity, thus combining the response to each synthesis stimulus with the response to its mirror image.

The Fourier synthesis computations were done in Fortran complex arithmetic with the Fast Fourier Transform algorithm (FFT) on a mesh of 1024 equally-spaced points covering the response to one full period of the periodic synthesis stimulus. (Thus, for rapidly-drifting patterns, each experimental record provided several repetitions of the response to the moving stimulus. Except for any slow drift in mean impulse rate, these repetitions should, in principle, be identical.) The translation of the synthesis formula (2.16') (derived above in terms of Fourier integrals) into a form suitable for use with the (discrete) FFT is essentially straightforward. The computation consisted

of filling an array with the transform of the stimulus pattern (obtained either analytically or by FFT), multiplying by the transfer function, and inverting by FFT.[*] The time-stationary (periodic) portion of the response was then available as the real part of this result. The mean impulse rate and "ramp" (describing the slow drift of the impulse rate over the course of an episode) were added to the periodic response, and the sum was plotted in a form compatible with the plots of the averaged synthesis episodes for direct visual comparison. This calculation was repeated for each stimulus drift velocity.

It should be emphasized that this entire calculation, from the measurements of the transfer function to the calculation of the Fourier synthesis prediction, allowed no adjustment of free parameters. The prediction is explicitly and unambiguously determined by the measured transfer function, mean impulse rate, and ramp slope.

---

[*] Because of the phenomenon of "aliasing," the discrete Fourier transform (on which the FFT algorithm is based) may be interpreted equivalently as operating either on the array of frequencies $0, \xi, 2\xi, \ldots, (2^N-1)\xi$, or on the array $0, \xi, 2\xi, \ldots, 2^{N-1}\xi, -(2^{N-1}-1)\xi, -(2^{N-1}-2)\xi, \ldots, -2\xi, -\xi$. For our purposes, the second interpretation is the correct one, because the power in the negative-frequency components greatly exceeds that in the positive high-frequency components, due to the high-frequency cut-off of both the stimulus ($\tilde{S}(\xi)$) and the transfer function ($F(\xi, -\xi\nu)$). The transfer function for negative frequencies is obtained from the symmetry relations (2.17-19).

"Just the place for a Snark! I have said it twice:
     That alone should encourage the crew.
 Just the place for a Snark! I have said it thrice:
     What I tell you three times is true."

L. Carroll, 1876

IV. Results.

The outcome of the analysis portion of the protocol
is depicted in Figures 4-1 and 4-2. Figure 4-1 shows the mean
individual   rate function $\sigma(t)$ for the response to a
typical analysis episode. It is important to note that, not-
withstanding its noisy appearance, such a record is in fact
a definite response to a fixed temporal signal, albeit a
harmonically rich signal. In Figure 4-2, the marked dependence
of the response on the spatial frequency of the analysis
stimulus is illustrated. At low spatial frequencies, a
moderate response to the temporal modulation of the stimulus
is observed. As the spatial frequency is increased, an increase
in the response to flicker is apparent. The peak sensitivity is
approximately four cycles/eye-width. At higher spatial fre-
quencies, the response decreases, until at 32 cycles/eye-
width it is essentially undetectable. It may be noted that,
as all the analysis episodes share a common temporal modulation
signal, the records at different spatial frequencies show
corresponding features at corresponding time-points.

These effects are specified quantitatively in Figure 4-3
which shows the full spatio-temporal transfer-function derived
from the same preparation as in Figure 4-2. Though the general
trend of the curves agrees with the description above, the
following features should be noted. The relative sensitivity
of the eye to sine-wave gratings of differing spatial frequency
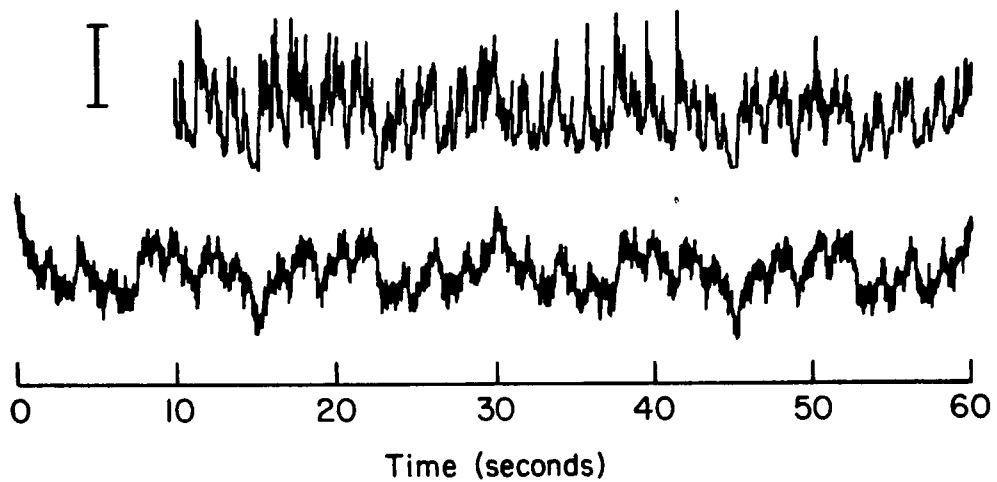
Figure 4-1. Response of test-ommatidium to temporally modulated sine-wave grating. The bottom record shows the sum-of-sinusoids temporal signal used to modulate a sinusoidal grating stimulus over each 60-second episode. The top record shows the mean individual rate response ($\sigma(t)$) obtained from 14 repetitions of such an analysis stimulus, with a spatial frequency of 4 cycles/eye-width. The data from the first ten seconds of each episode were discarded to avoid the effect of the initial on-transient. Scale marker: 10 impulses/sec.
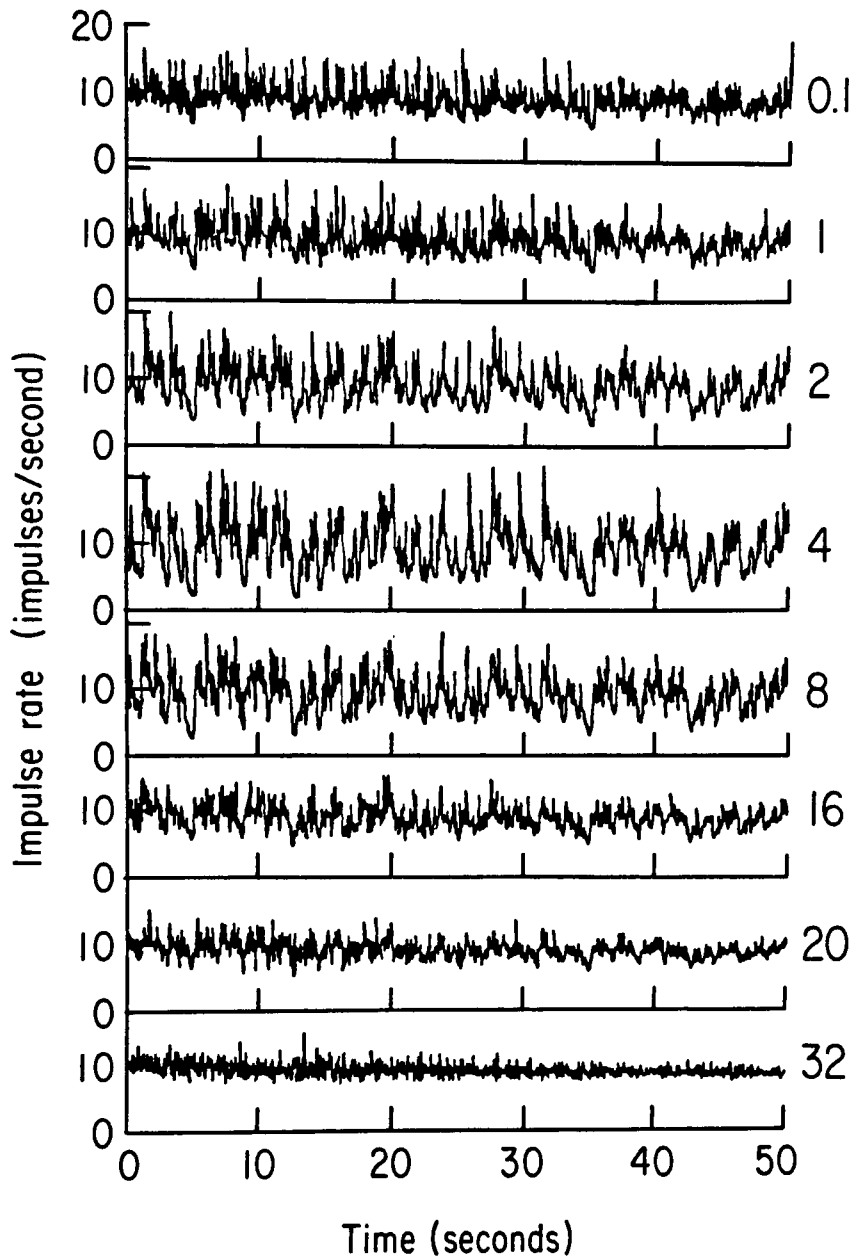
Figure 4-2. Effect of spatial frequency on response to temporally modulated sine-wave gratings. Each record is the average of 14 episodes. The stimulus consisted of a sinusoidal grating (spatial frequencies shown at right) placed with a peak centered over the test-ommatidium, modulated according to the temporal signal shown in Figure 4-1. The records show the response to the last 50 seconds of each analysis stimulus.

Figure 4-3. Spatio-temporal transfer functions for the preparation of Figure 4-2 (a) Plots (log amplitude vs. log frequency) of the fractional modulation of the mean impulse density r(t) for each spatial frequency. The points indicated (O) were obtained from experimental measurements; the remaining portions of the curves were extrapolated as described in the text. (This preparation produced no detectable response at 32 cycles/eye-width (see Fig. 4-2). As a curve for this spatial frequency was needed for computational purposes, it was extrapolated by setting the amplitude at 32 cycles/eye-width equal to 10% of the amplitude measured at 20 cycles/eye-width.) (b) Phase vs. log frequency is indicated (modulo 2π) on a separate axis for each spatial frequency. The curves were extrapolated in the same regions as the amplitudes, above. (c) The transfer function amplitudes for the same preparation, in terms of the mean individual rate function $\sigma(t)$, obtained by multiplying the transfer function in (a) by the transfer function $|B(\omega,\nu)|^2$ (see text). The small undulations of the amplitude curves ((a) and (c)) at low frequency are artifacts of the extrapolation procedure.
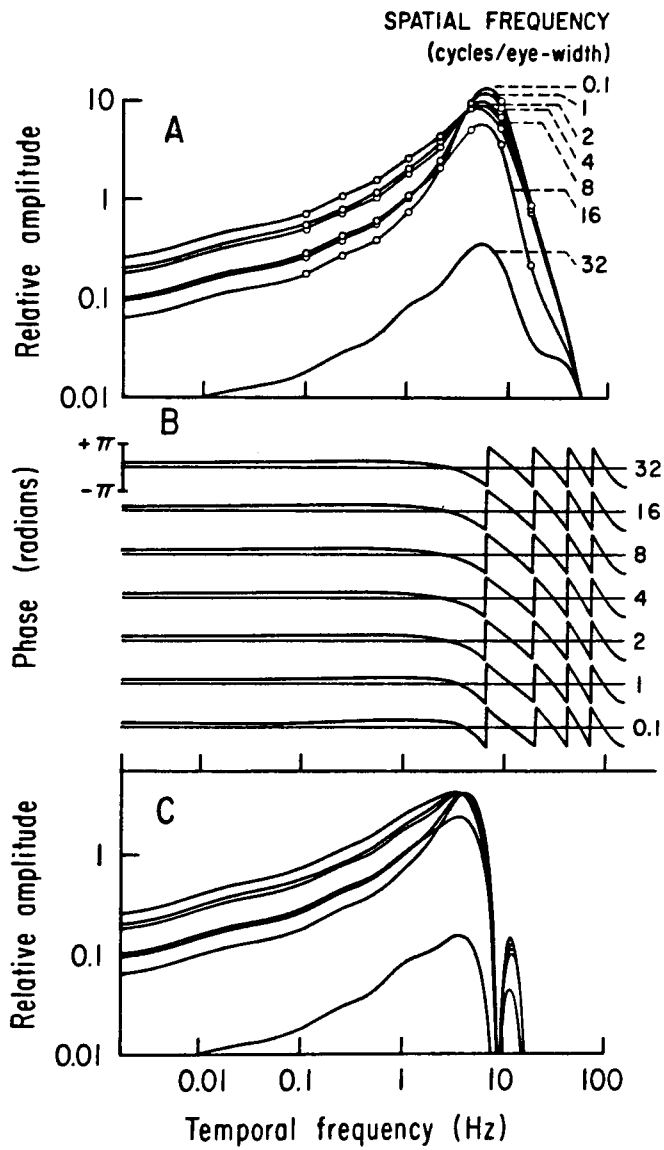
Figure 4-3

depends strongly on temporal frequency. Thus at low temporal frequency, the response is greatest at intermediate spatial frequency, falling off gently at low spatial frequency, and sharply at high spatial frequency. At intermediate temporal frequency, the eye is most responsive at <u>low</u> spatial frequency, with response decreasing monotonically with increasing spatial frequency. At high temporal frequency, there is little dependence on spatial frequency, except for the ultimate high-frequency cutoff. These findings may be considered the analog, with sine-wave gratings, of the more familiar "small spot-large spot" experiments (Ratliff et al., 1967; Ratliff et al., 1969; Knight et al., 1970).

The spatial dependence of the phase of the transfer function is more subtle, with detail concentrated at the lower temporal frequencies. The low-frequency phase lead is slightly greater at low spatial frequencies and persists to higher temporal frequencies. Once it starts, however, the rate of increase of the phase lag with temporal frequency is greater at low spatial frequency, so that there is little difference in the phase lags seen at all spatial frequencies at high temporal frequency.

It is appropriate to discuss here the precision of the transfer function measurements. As a rule, the complex transfer

function values for any spatiotemporal frequency pair (ξ,ω) obtained in successive experimental cycles form a cluster of points on the complex plane whose size is independent of the frequency pair (ξ,ω). Thus, the precision of these measurements is not well described in terms of the logarithmic coordinates of the Bode plots (log amplitude vs. log frequency; phase vs. log frequency). For example, as the amplitude of the response decreases, the uncertainty of the phase grows markedly as the data points approach the origin of the complex plane, but the uncertainty of the transfer function value is really no greater than that for large responses. In practice the variance of our transfer function measurements is typically such that "error bars" would be entirely covered by the dots in Figures such as 4-3, except at high frequencies where the response is greatly attenuated. The full implications of the transfer function measurements are discussed at greater length in chapter VI.

The Fourier syntheses of responses to moving stimuli were computed in terms of a mean individual rate output variable, as discussed in Appendix C. For this purpose, the transfer function amplitudes (measured initialy in terms of the population firing rate, $r(t)$) were multiplied by the factor $|B(\omega,\nu)|^{2}$.[*] The resultant amplitudes

---

[*] $B(\omega,\nu) \equiv (1-e^{i\omega/\nu})/(i\omega/\nu)$, where ν is the mean impulse rate. See Appendix C.

are shown in Figure 4-3C. The effect of this operation is mainly to attenuate the response at frequencies above the mean impulse rate. The phases are, of course, unchanged.

Typical averaged responses from the synthesis portion of the protocol are shown at the top of Figure 4-4. For the experiment shown, the synthesis stimulus consisted of a square-wave of spatial frequency 0.5 cycles/eye-width, which was moved slowly across the eye. Because the stimulus was viewed by the animal through an effective "window" one eye-width across, the stimulus had the appearance of a "step" of light intensity advancing across the screen. As the records from such mirror-image presentation of the stimulus are, in general, nearly identical, we have deemed it appropriate to average together all such responses. Such an averaged response is shown in the bottom of Figure 4-4; the improvement in signal-to-noise ratio is evident. The features seen in this record, while to some extent dependent on the drift velocity of the stimulus (here, 0.06 eye-widths/s), are common to such step-responses (see below). Of particular interest are the antici-patory "Mach bands"[1] of excitation or inhibition that precede

---

[1]Strictly speaking, the term "Mach band" refers to the psycho-physical maximum or minimum seen in a static stimulus pattern consisting of a gradient of intensity between two uniform areas of different intensity (see Ratliff, 1965). We generalize the use of the term here to include the maxima and minima in neural responses to stepwise changes in intensity.
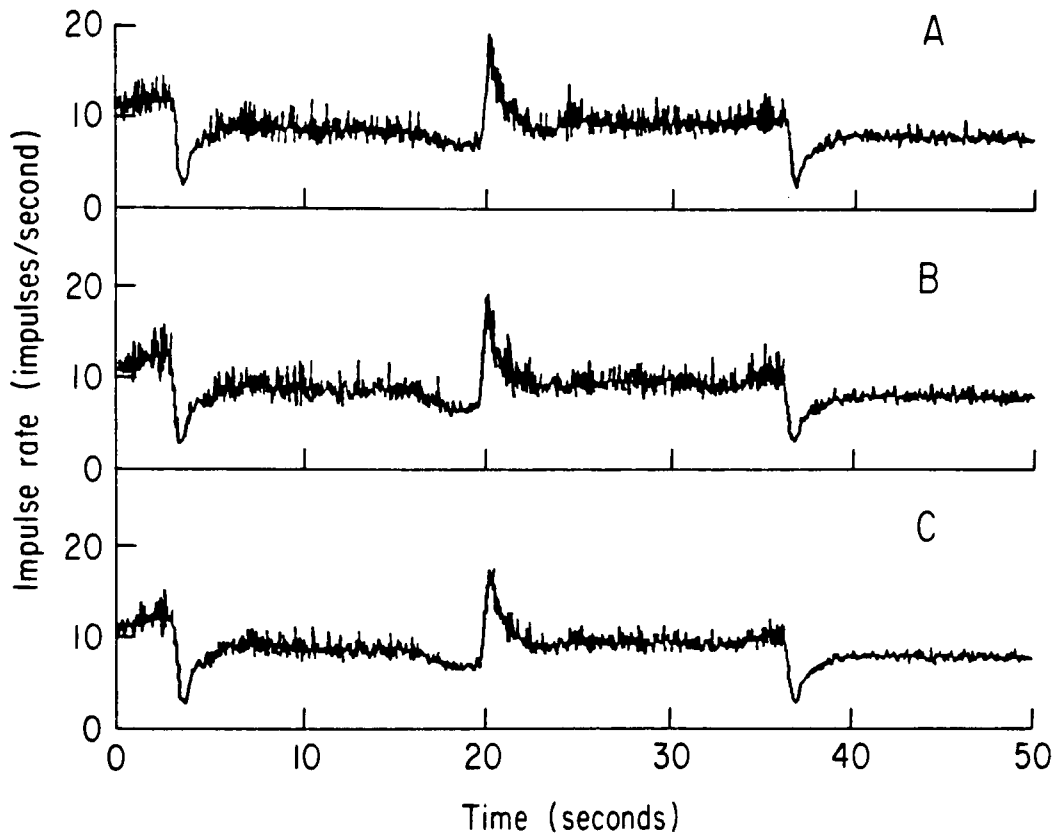
Figure 4-4. Comparison of the response to mirror-image stimuli. The top two records show the mean individual rate response ($\sigma(t)$) obtained from 14 presentations of a drifting edge stimulus moving with drift velocity +0.06 eye-widths/s (a) or -0.06 eye-widths/s (b). The record (c) is the averaged response of all 28 episodes. The preparation is the same as used in Figures 4-2 and 4-3.

the crossing of the test-ommatidium by the moving edge.
The crossing itself is seen as a clear on- or off-transient,
which then decays, sometimes with a small overshoot, as
here. In the intervals between the step-transients, the
impulse rate settles to a steady state value. This value
is nearly the same, regardless of whether the steady state
is a response to the bright or dim region of the step-pattern
stimulus.

Ommatidia near the perimeter of the eye necessarily
possess asymmetrical inhibitory fields, and thus fail to demon-
strate the type of symmetry depicted in Figure 4-4. (An
example of the behavior of such a neuron is given in Figure 8-8.)
For this reason, ommatidia near the boundary of the retina were
scrupulously avoided in the experimental studies described in
this chapter and in chapter VI. Accordingly, all responses
to mirror-image stimuli obtained in these experiments have been
averaged together to optimize the signal-to-noise ratio of
the response records. The dynamics of peripheral ommatidia
are discussed extensively in chapters VII and VIII.

The records from synthesis episodes at four different
drift velocities are shown in Figure 4-5. The responses show
a marked dependence on the drift velocity of the stimulus.
At very low speeds the step in light intensity takes a significant
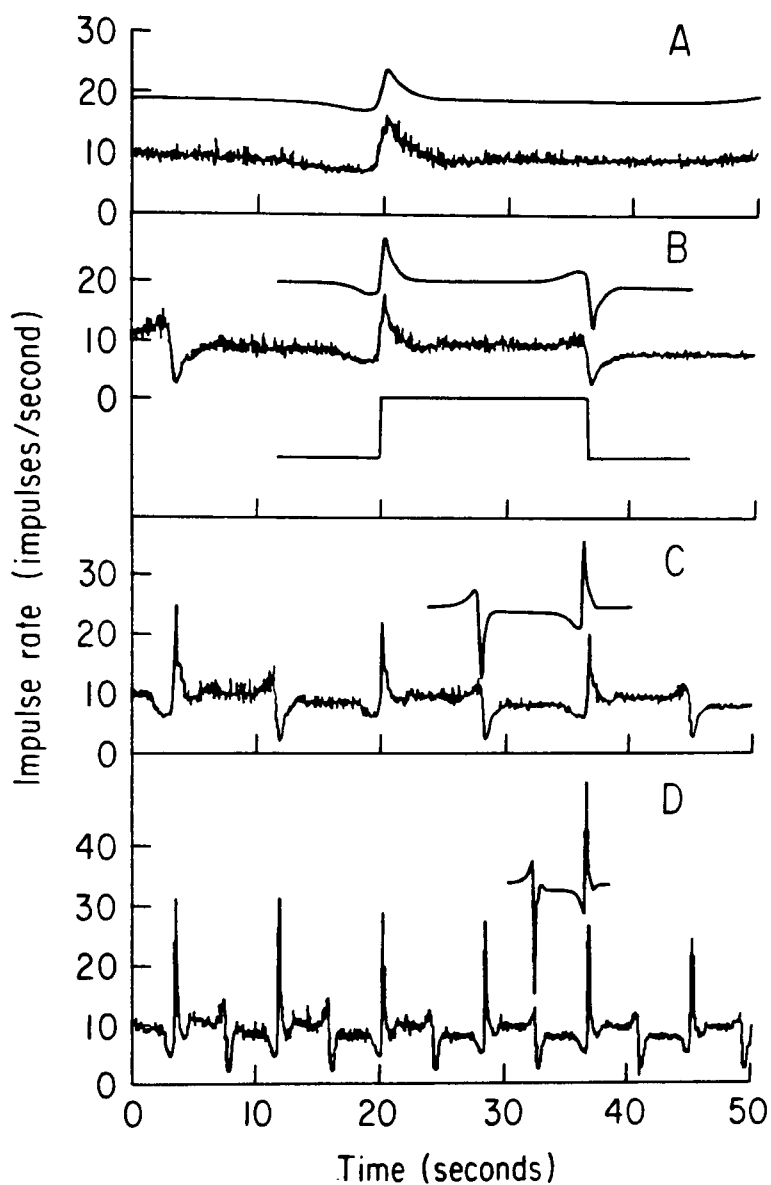
Figure 4-5. Fourier-synthesis of step-transient responses.
The figure shows the observed averaged response ($\sigma(t)$) to
drifting steps of light intensity (same preparation as Figs.
4-2,3,4). Drift velocities were (a) 0.03, (b)0.06,
(c) 0.12, and (d) 0.24 eye-width/s. The episodes at the
slowest speed provided only one on-transient; the others
provided at least one full cycle of the stimulus. The curves offset
immediately above the observed records are the predictions,
for one cycle of the stimulus, of the Fourier synthesis
procedure described in the text, applied to the spatio-
temporal transfer function shown in Figure 4-3. The intensity
of the stimulus at the test-ommatidium is shown for one stimulus
cycle in (b).

time to cross the test-ommatidium, and there is only a modest transient response to the step-stimulus. This transient decays monotonically to a steady response. As the velocity is increased, the transient responses increase dramatically. The unit is momentarily driven at over three times its average impulse rate. The inhibitory precursors are somewhat strengthened, but, of course, occupy a shorter interval of time. Immediately after the on-transient responses, the impulse rate falls rapidly, overshooting the subsequent steady response to the bright portion of the step. At high velocity, the off-transients, which would have to extend to "negative" impulse rates to mirror the observed on-transients, are severely truncated.

The predictions of the Fourier synthesis procedure (using the transfer-function data from Figure 4-3, parts b and c) are shown above the experimental records. The agreement between the Fourier predictions and the experimental records is, on the whole, excellent. The linear theory successfully predicts the form and height of the step-transients (a sensitive function of drift velocity), and the width and strength of the Mach bands. The limited dependence of the "steady state" response on the intensity of the illumination between step-transients is also correctly predicted by the Fourier synthesis calculation.

The synthesis shows only a few systematic discrepancies from the actual responses. The slight overshoot of the response at intermediate velocities is somewhat underestimated, and the sculpturing of the on-transient at the lowest velocity is slightly distorted. The biggest discrepancy is the truncation of the off-transients at high drift rates.

This highly non-linear phenomenon is beyond the scope of our linear theory. The truncation also produces secondary effects, such as the absence of overshoot after high speed off-transients, which likewise are not predicted by the Fourier synthesis (Figure 4-6)

We have obtained results comparable to those shown above on several other preparations. Further evidence of the extent to which our transfer function measurements characterize the response of a Limulus eye to moving stimuli is presented below.

Figures 4-7 and 4-8 show the results of an analysis-synthesis experiment performed on a Limulus with weak and sluggish reflexes; this specimen would not have been used had a healthier one been available. The transfer function shows better optical resolution than that of Figure 4-3, with a readily measurable response at 32 cycles/eye-width, but very little dependence on spatial frequency. This apparent lack of lateral inhibition is confirmed by the synthesis records, which show virtually no Mach band effects at all. Nonetheless, the agreement between the Fourier synthesis and the experimental records is striking, at velocities ranging over an order of magnitude. It thus appears that our transfer-function measurements even describe accurately the dynamics of a somewhat pathological eye.

We have also performed syntheses of the response to drifting patterns other than steps. Figures 4-9 and 4-10 show the
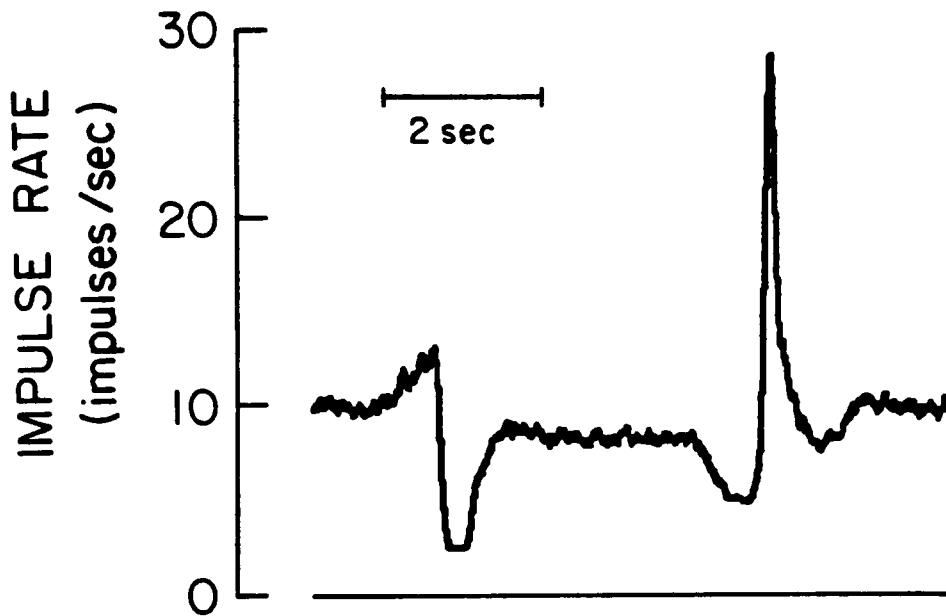
Figure 4-6. Secondary effects of truncation of off-transient response to rapidly moving stimulus. Data of Figure 4-5d (averaged within episodes, as well as between successive episodes) are redrawn on a larger scale.
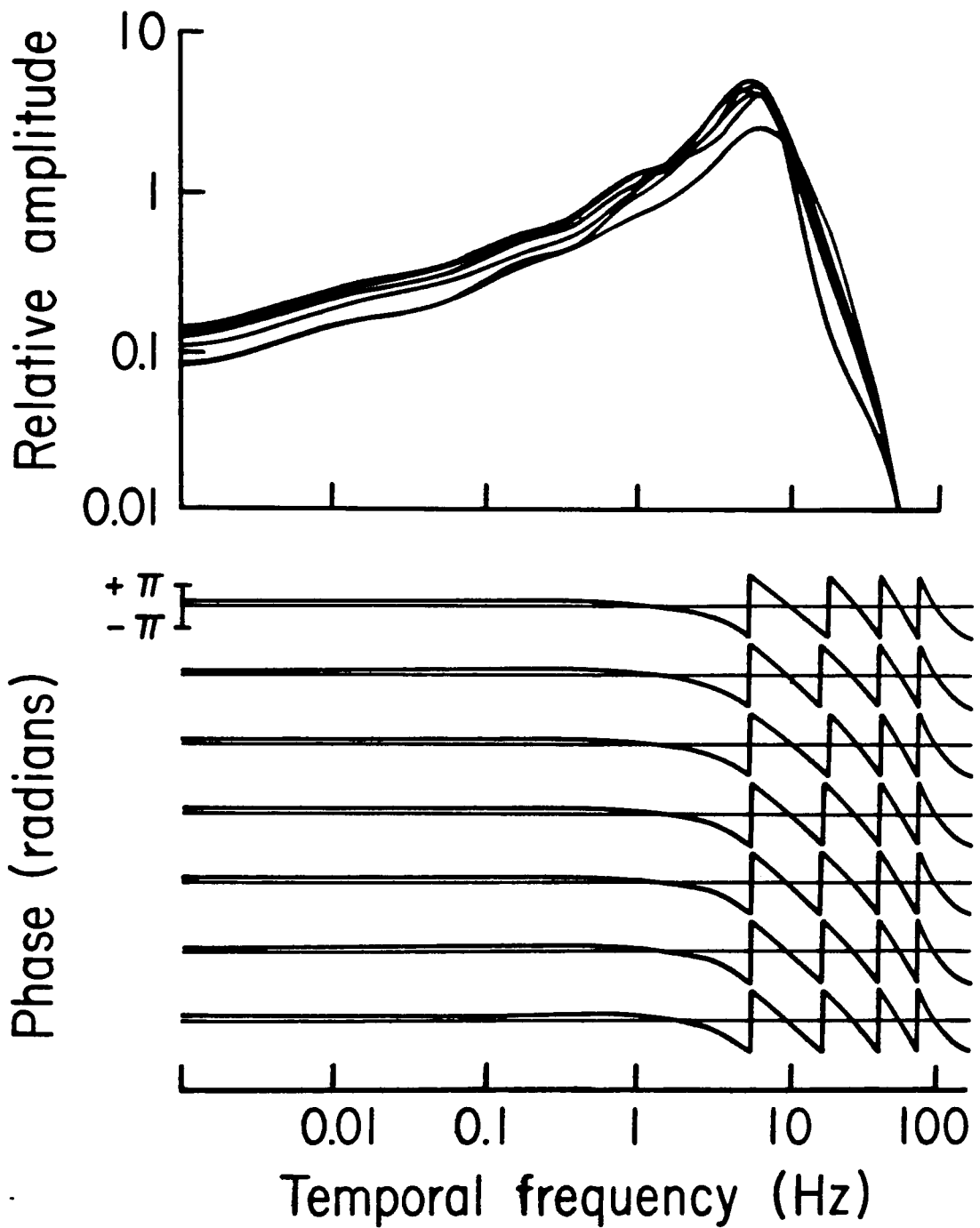
Figure 4-7. Transfer function for a "sick" Limulus. Bode
plots of measured spatio-temporal transfer function, plotted
as in Figure 4-3 At the peak, amplitudes decrease mono-
tonically with increasing spatial frequency.
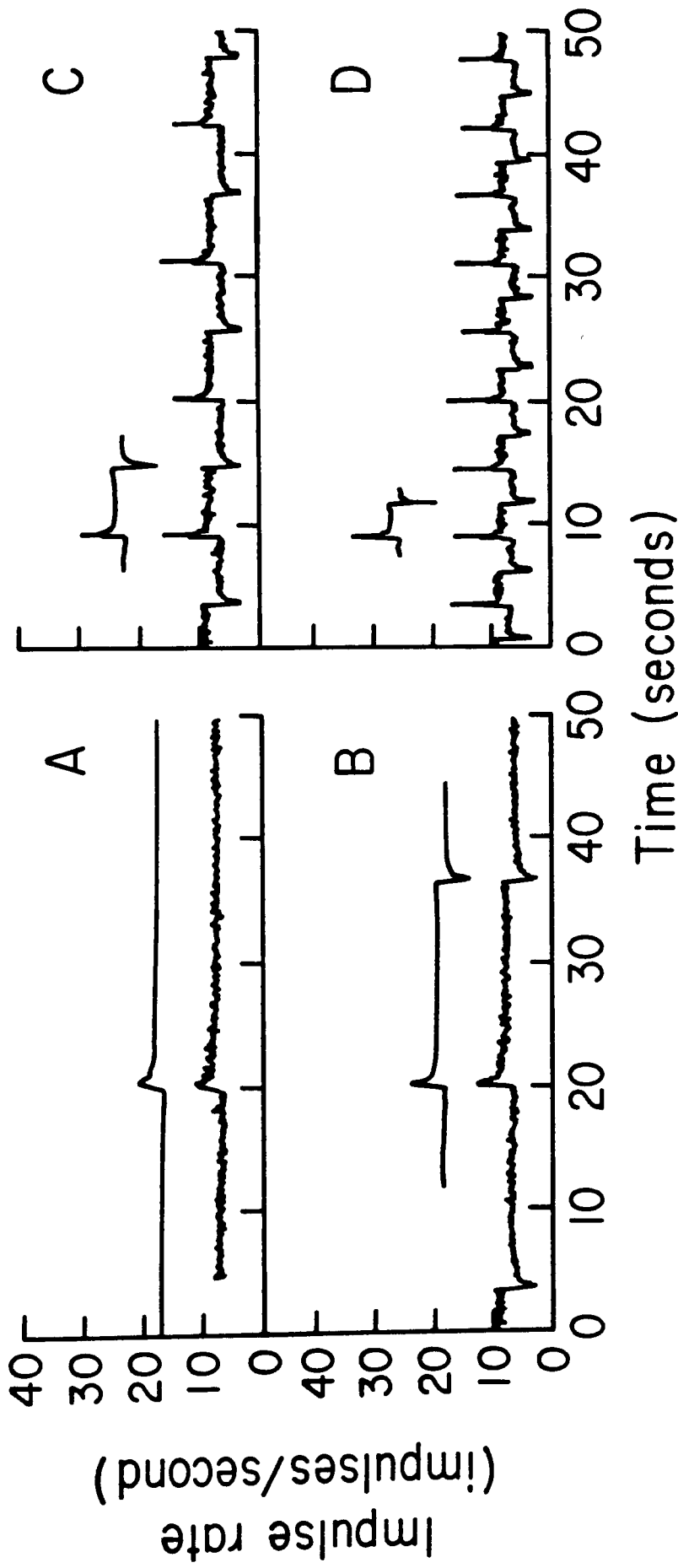
Figure 4-8. Fourier syntheses for "sick" Limulus (same preparation as Fig. 4-7). Predicted and measured responses (averages of 8 episodes) to drifting step stimuli are plotted as in Figure 4-5. Drift velocities were (a) 0.03, (b) 0.06, (c) 0.18, and (d) 0.36 eye-widths/sec.

results of a synthesis of the response to the "step-complement" stimulus of Ratliff and Sirovich (1978). This stimulus, which is composed of a sinusoid of the lowest possible frequency (0.5 cycles/eye-width) plus a fast exponential decay superposed on a step, is designed to resemble the step stimulus as little as possible, yet produce similar visual responses. Even though the stimulus possesses no sharp dicontinuities, the response clearly resembles the typical response to true drifting steps, especially at low velocities. At higher speeds, the eye readily perceives the 0.5 cycles/eye-width sinusoid. All of these responses, up to a velocity of 0.8 eye-widths/s, are well predicted by the Fourier synthesis. With the measured spatio-temporal transfer function, we can perform a Fourier synthesis to predict the response of this preparation to a true step stimulus, such as the one used for the experiments of Figures 4-5 and 4-8. These predictions are shown in Figure 4-11, for comparison with the response to the step-complement stimulus.

As a final test of the ability of our procedure to handle "arbitrary" stimuli, we produced a visual stimulus whose light-intensity profile resembles a row of buildings. The results of an experiment using this stimulus are shown in Figures 4-12 and 4-13. The agreement between the predicted and measured responses is again excellent.

.
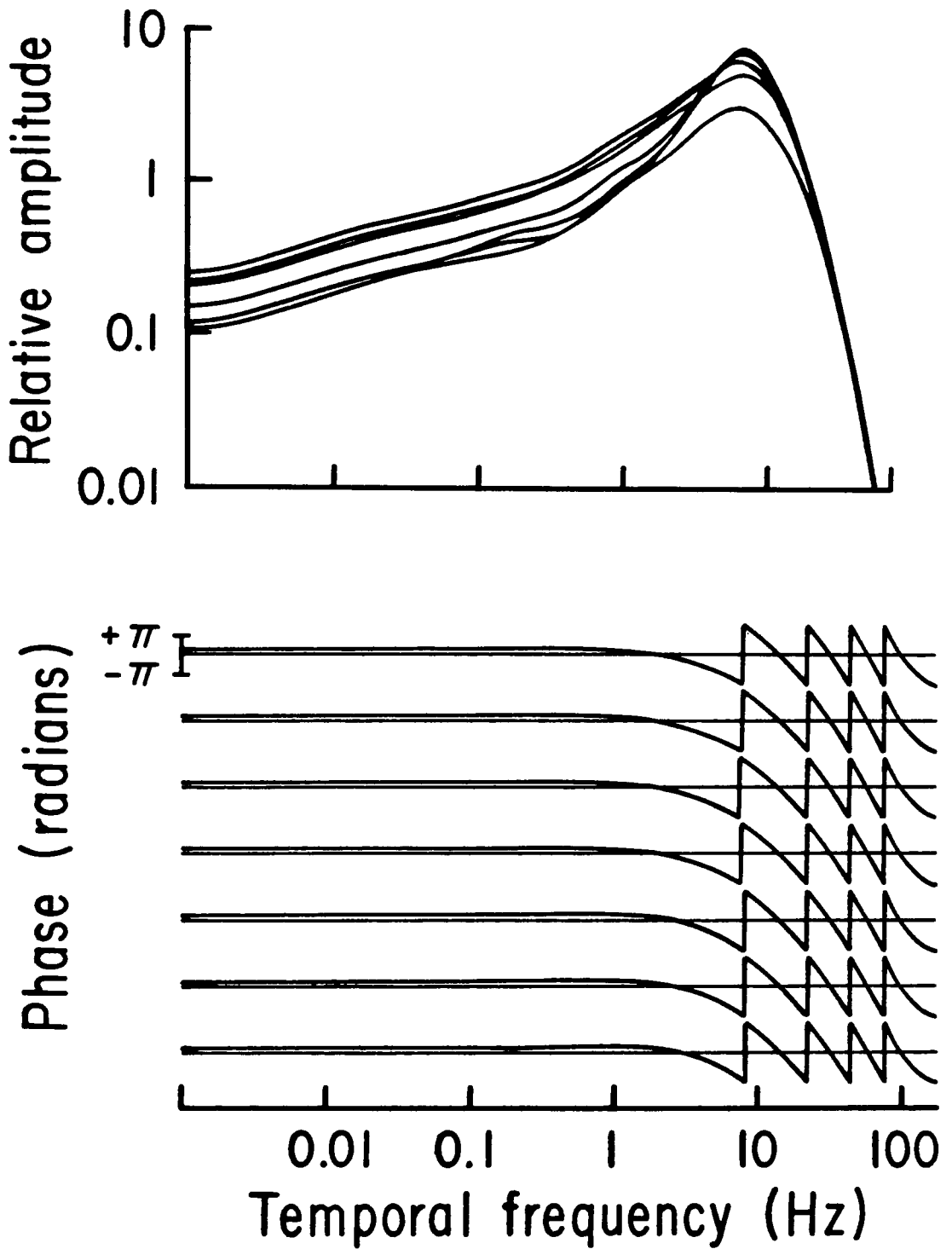
Figure 4-9. Transfer function for experiment of Figure 4-10. At peak, amplitudes decrease monotonically with increasing spatial frequency.

Figure 4-10. Predicted and measured responses to moving "step-complement" stimulus. One cycle of the stimulus is reproduced as bottom record in (a). Drift velocities were (a) 0.06, (b) 0.20, (c) 0.40, and (d) 0.80 eye-widths/sec. Measured responses are the average of 12 episodes.
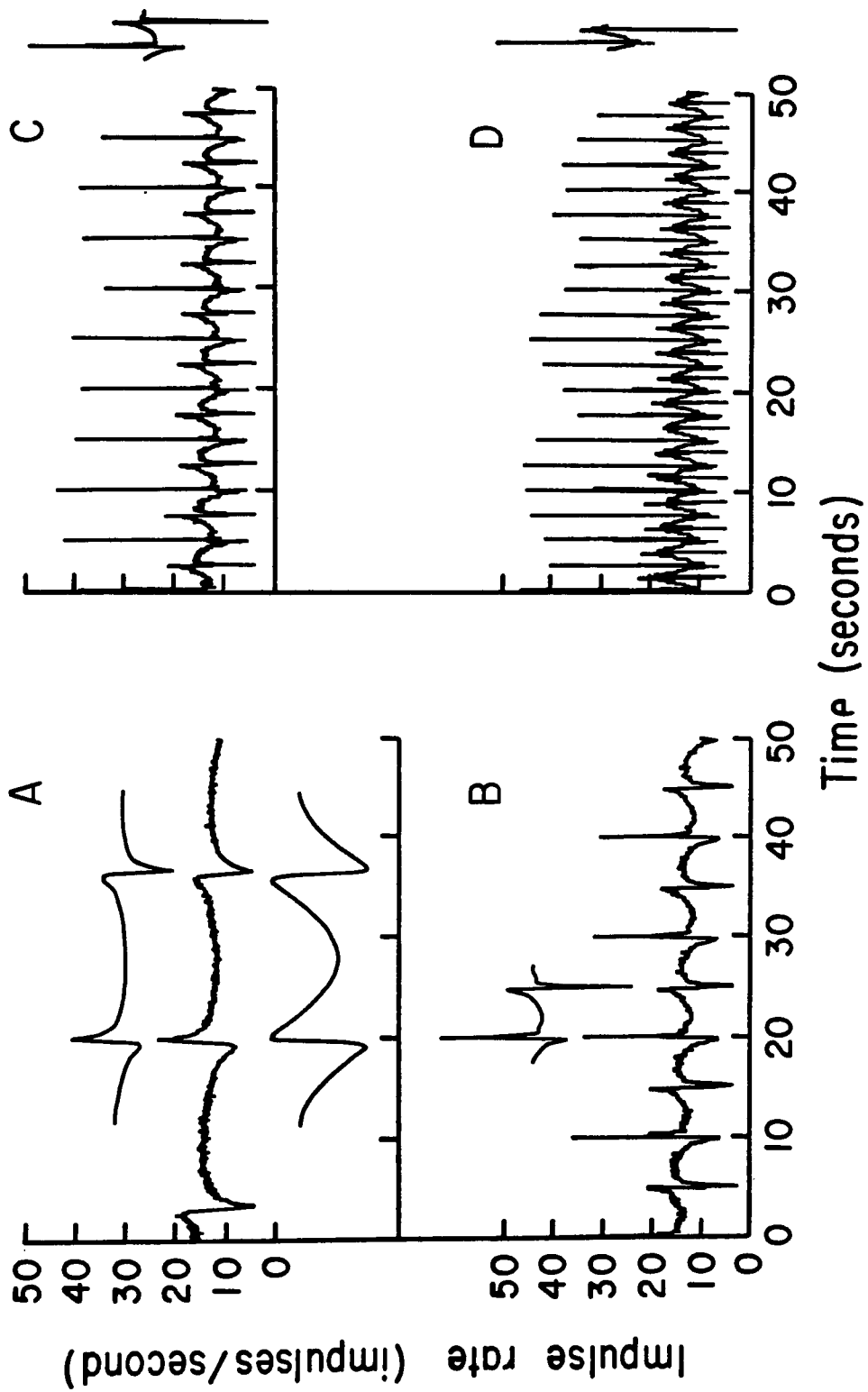
Figure 4-10
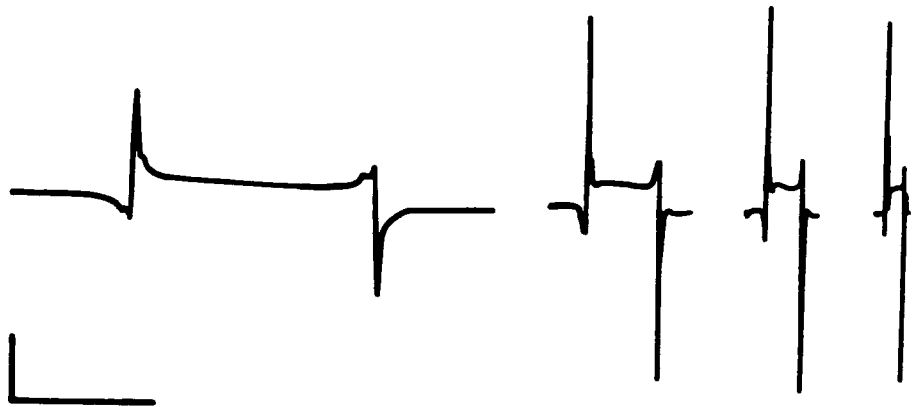
Figure 4-11. Predicted step-responses for preparation
of Figures 4-9 and 4-10. Drift velocities, from left to
right: 0.06, 0.20, 0.40, 0.80 eye-widths/sec. Scale
marker: horizontal, 10 sec; vertical 10 impulses/sec.
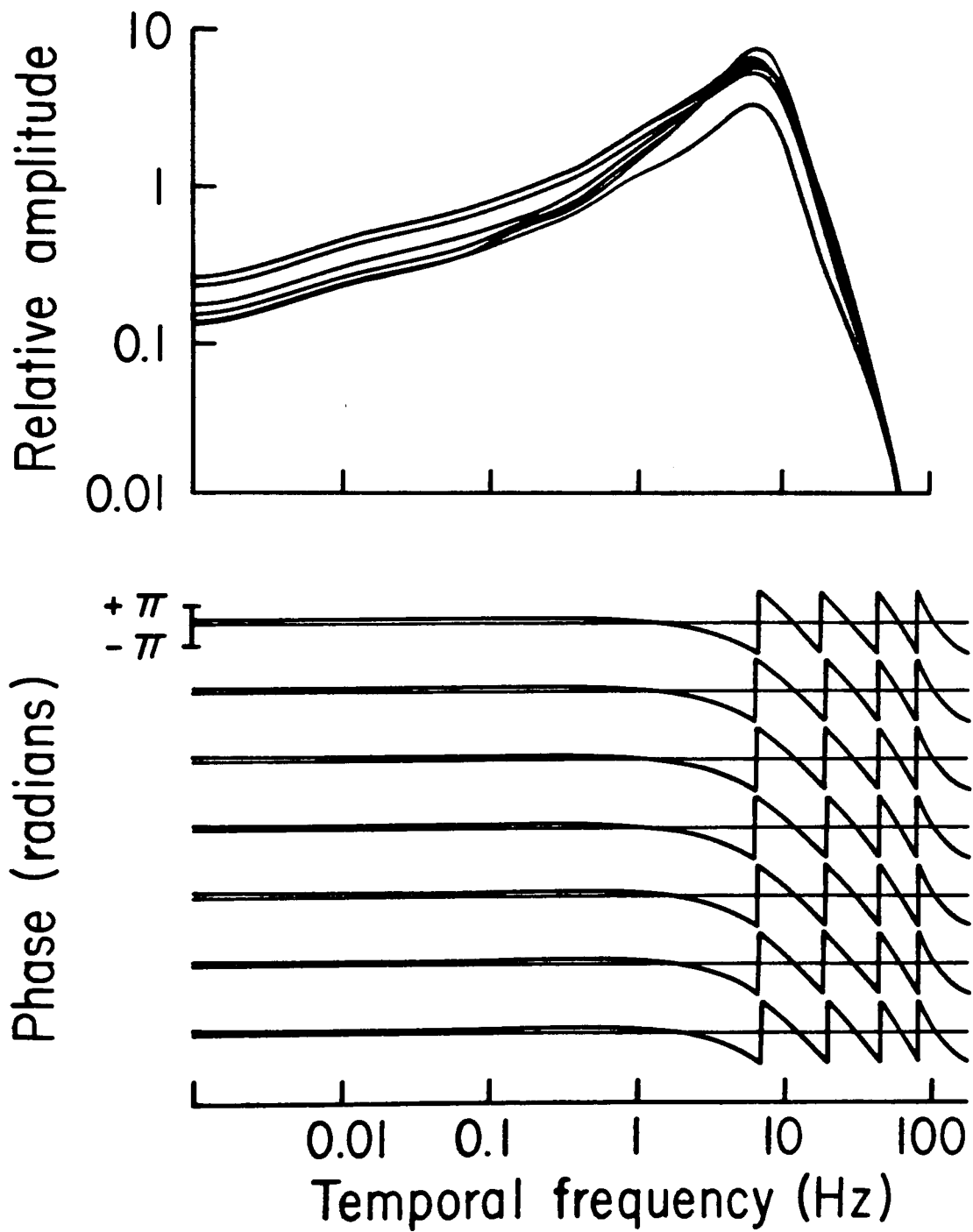
Figure 4-12. Transfer function for experiment of Figure 4-13

Figure 4-13. Predicted and measured responses to moving "arbitrary" stimulus. One cycle of the stimulus is reproduced as bottom record in (b). Drift velocities were (a) 0.03, (b) 0.06, (c) 0.12 and (d) 0.24 eye-widths/sec. Measured responses are the average of 22 episodes.
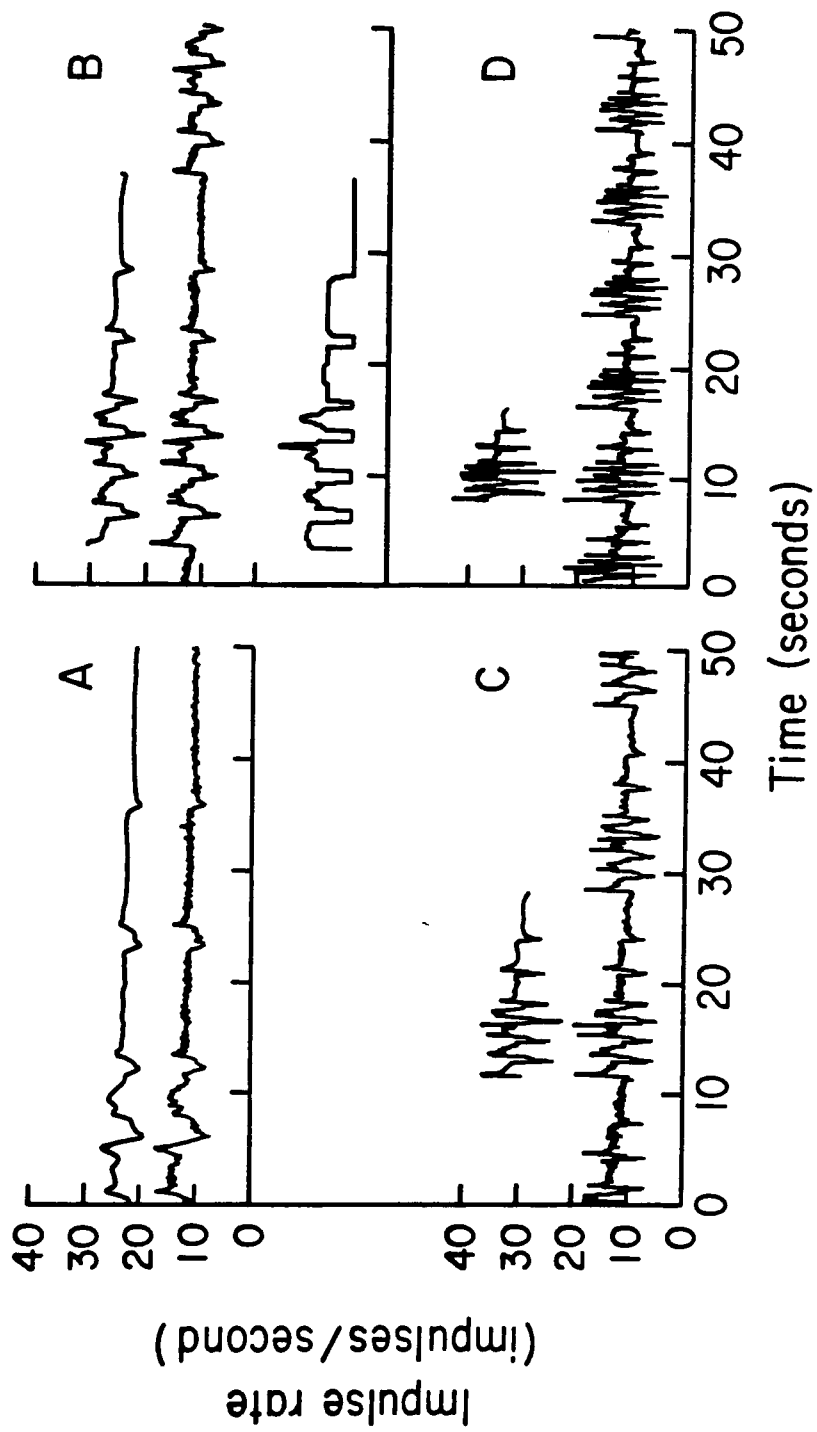
Figure 4-13

Discussion.

The extensive agreement between the measured responses to moving stimuli and the predictions of our Fourier-synthetic calculations demonstrates the essential validity of our program of linear systems analysis. Though the major assumption of linearity is known to hold for many aspects of the Limulus visual transduction, especially in the vicinity of a fixed operating point, there are important known exceptions, such as the dependence of inhibitory coupling on excitation levels, and the existence of inhibitory thresholds. Our results confirm that, in spite of these potential complications, the Limulus system responds with linear behavior well beyond the range of small perturbations.

The only striking nonlinear effect demonstrated in our study is the truncation of off-transients corresponding to the limitation of the pulse-coding scheme. Our data appear to be consistent with the hypothesis that, under the conditions of widespread illumination and moderate impulse rate, the effective threshold for lateral inhibition (at least for inhibitory transients) is the absolute threshold: the absence of impulses in the inhibiting units.

"Mathematics are a species of Frenchman; if you say
something to them, they translate it into their own
language and presto! it is something entirely different."

attributed to Goethe

V. The Hartline-Ratliff Model for the Limulus Lateral Eye.

It has been shown in the preceding chapters that the

response of the Limulus lateral eye to arbitrary time-varying

patterns of illumination is well predicted by the methods

of linear systems analysis. In the course of such a treat-

ment, the dynamic properties of the eye are incorporated

into the eye's spatiotemporal transfer function. It follows

that much of what can be learned of the eye's physiological

properties through examination of its responses to light

may be deduced from careful analysis of the measured transfer

function.

The methods of systems analysis are indifferent to the

nature of the processes which underly the relations between

stimulus and response - it is precisely this independence

of mechanism which gives these methods their great generality.

In order to draw physiological conclusions from systems-

analytic data, it is necessary to interpret the data by

comparison with more direct studies of the underlying

physiology. For example, it is reasonable to ascribe a

feature of a measured transfer function to a certain physio-

logical process only after the existence of the process has

been suggested by independent investigations. However, in

the context of a model suggested by such studies, the systems-analytic data can constitute significant evidence for the evaluation of physiological hypotheses.

The present chapter presents such a model for the Limulus retina, based on the results of numerous investigations of the physiological processes which form the basis of the Limulus visual response. (For reviews, see Graham and Ratliff, 1974; Ratliff, 1974). In the context of this model, most statements concerning the physiology of the retina can be expressed in terms of the various parameters which occur in the model. In the subsequent chapter, these parameters are determined by means of various deductions from the properties of the measured spatiotemporal transfer function.

Excitation.

As a general rule, singly-illuminated retinal neurons in the Limulus eye show an increase in impulse activity in response to stimulation by light. Thus, the basic action of light on these cells is termed "excitation." The degree of excitation of a retinal neuron depends, in general, on attributes of both the stimulus (such as intensity, wavelength, and

duration) and the neuron itself (such as its state of
light- or dark-adaption). Within limits, these factors
can be varied in such a way as to compensate for each other,
and thus leave the neural response invariant (Hartline,
1934; Graham and Hartline, 1935; Hartline and McDonald,
1947). This so-called "univariance" of the response of
a single photoreceptor was greatly clarified with the advent
of intracellular microelectrode recordings from the Limulus
retina (Hartline, Wagner, and MacNichol, 1952). With these
intracellular techniques it was demonstrated that the
impulse activity which is recorded in the fibers of the optic
nerve is generated in the so-called "eccentric cell" found
within each ommatidium (Fig. 5-1). Furthermore, it was
found that the membrane potential of the eccentric cell
serves as an intermediate variable between the early photo-
chemical processes associated with the absorption of light,
and the subsequent generation of neural impulses (MacNichol,
1956; Fuortes, 1959). Thus, incident light causes a
depolarization of the eccentric cell membrane. This
depolarization, or a comparable depolarization produced
by the direct intracellular injection of current, induces
the production of a train of action potentials by the
eccentric cell.
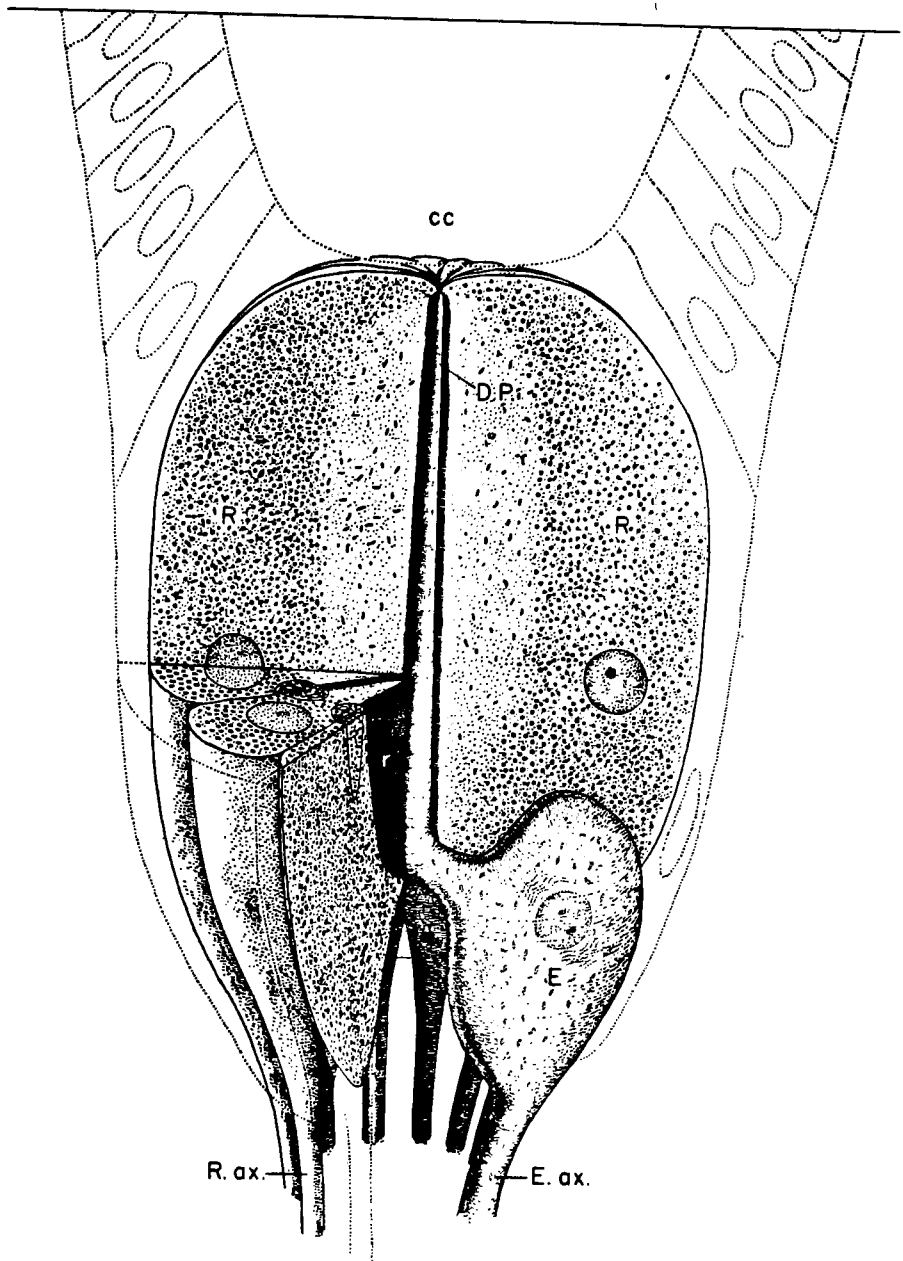
Figure 5-1. Diagrammatic drawing of Limulus ommatidium in
cutaway view. CC, crystalline cone; R, retinular cells;
r, rhabdom; R. ax., retinular cell axon; E, eccentric cell;
DP, eccentric cell dendrite ("distal process"); E. ax., eccentric
cell axon. (after B. Tagawa)

The experimental separation of the excitatory process
into two sequential transductions allows the use of a
simple modelling strategy, as follows: We treat the trans-
duction from incident light to eccentric cell depolarization
(the "generator potential") as a single, self-contained
"front end" process, which will be further characterized
only in phenomenological terms. Such characterization
will be based on more detailed studies of the phototrans-
duction process, but need not consider the great body of
information available concerning this major problem of
sensory physiology. Similarly, we treat the transduction
from membrane potential to neural impulse activity (the
"encoder") as an isolated process, to be described in
quantitative, but abstract terms based on more detailed
studies of encoder neurophysiology. These detailed
descriptions of the generator potential and encoder trans-
ductions are given later in this chapter.

Lateral inhibition.

The second major factor in the response of the Limulus
retina to light is a reciprocal interaction between nearby
ommatidia such that impulse activity in any unit tends to

suppress impulse activity in neighboring units. This
so-called "lateral inhibition" accounts for a great deal
of the continued interest in the Limulus retina as a model
system in neurophysiology. It may be shown by surgical
means that this interaction is mediated by a "lateral
plexus" of axon collateral brances (Fig. 5-2) which inter-
connects the ommatidia just deep to the origins of the
eccentric cell axons (Hartline, Wagner, and Ratliff, 1956).
Intracellular recording reveals the inhibitory effect as
a hyperpolarization of the eccentric cell membrane potential
in response to either orthodromic or antidromic impulse
activity in neighboring ommatidia (Tomita, 1958; Purple
and Dodge, 1965). Many details of the biophysics and
neruochemistry of this "inhibitory post-synaptic potential"
have been worked out by subsequent investigators, but these
mechanistic considerations are of mostly incidental interest
for the development below. We will be content with a
quantitative description of the behavior of the lateral
inhibitory transduction.

Such a description, for the steady-state, was first
given by Hartline and Ratliff (1957, 1958) in the form
of a system of simultaneous, piecewise-linear equations
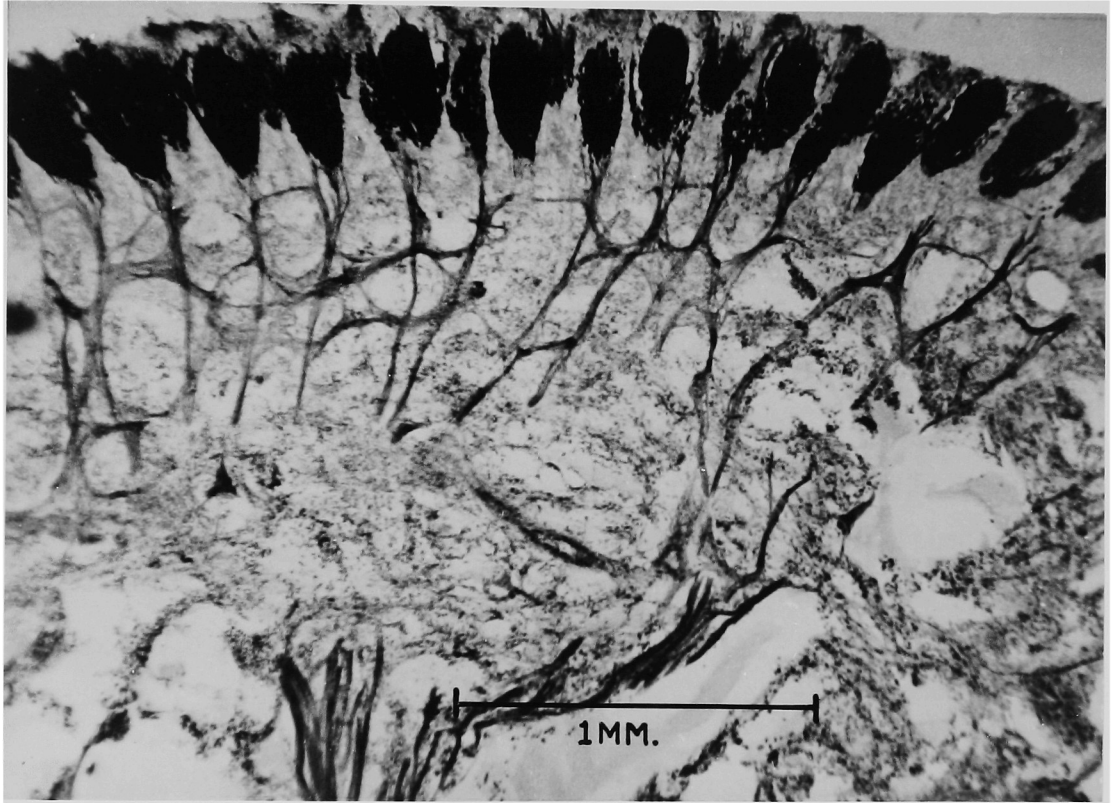
Figure 5-2. Photomicrograph of <u>Limulus</u> lateral eye section, perpendicular to the cornea. (Samuel's silver stain.) Light enters from top of figure. Heavily stained ovals at top are the ommatidia. Irregular network of fibers connecting nerve bundles just deep to the ommatidia constitutes the lateral plexus. Fibers coalesce at bottom to form the optic nerve. (Photomicrograph by W.H. Miller, from Hartline et al., 1956).

for the impulse rates of several interacting ommatidia:

$$r_m = e_m - \sum_{n \neq m} k_{m \leftarrow n} \cdot (r_n - t_{m \leftarrow n})_+ \quad . \tag{5.1}$$

Here r_m is the response of the m'th ommatidium, e_m is the excitation of the m'th ommatidium (that is, the rate it exhibits under the given stimuli in the absence of lateral inhibition), $k_{m \leftarrow n}$ is a coupling constant for the inhibitory effect of the n'th ommatidium on the m'th ommatidium, $t_{m \leftarrow n}$ is a threshold for this inhibitory effect, and the notation $(\ )_+$ indicates the piecewise-linear operator such that $(x)_+ = x$, for $x \geq 0$, and $(x)_+ = 0$, for $x < 0$. Equations (5.1) express the "recurrent" nature of the inhibition, and the fact that the inhibition is a function of the response of the inhibiting units, rather than merely a function of their state excitation. The matrix of steady-state inhibitory coefficients $k_{m \leftarrow n}$ was measured by Barlow (1967,1969), and found to be nearly translation-invariant over the eye. Subsequently, equation (4.1) was modified (Lange, 1965; Barlow and Lange, 1974) to include a dependence of the inhibitory coupling on the excitation level of the inhibited ommatidia; this refinement does not appear to be relevant to the experimental regimes considered here, and will be ignored.

Self-inhibition.

The absence of a "diagonal" term in equation (5.1)
reflects the impossibility, in practice, of separating
excitatory and inhibitory influences within a single
ommatidium on the basis of   steady-state responses.
Nevertheless, once time-dependent responses are considered,
a notion of "self-inhibition" (the tendency of a neural
impulse to suppress subsequent impulse activity in the same
neuron, for any given pattern of stimulation) may be
entertained. Such a process was detected in the Limulus
ommatidium following stimulation by intracellular injection
of current (Stevens, 1964) or by light (Purple, 1964;
Dodge, 1969). We can incorporate self-inhibition into the
Hartline-Ratliff equations (5.1) by setting $e_m = \varepsilon_m - K_s r_m$:

$$r_m = \varepsilon_m - K_s r_m - \sum_{n \neq m} k_{m \leftarrow n} \cdot (r_n - t_{m \leftarrow n})_+ \quad , \qquad (5.2)$$

where ε_m is the "pure" excitation of the m'th ommatidium,
and K_s is the self-inhibitory coupling constant. A block
diagram of the information flow described by equation (5.2)
is shown in Figure 5-3.
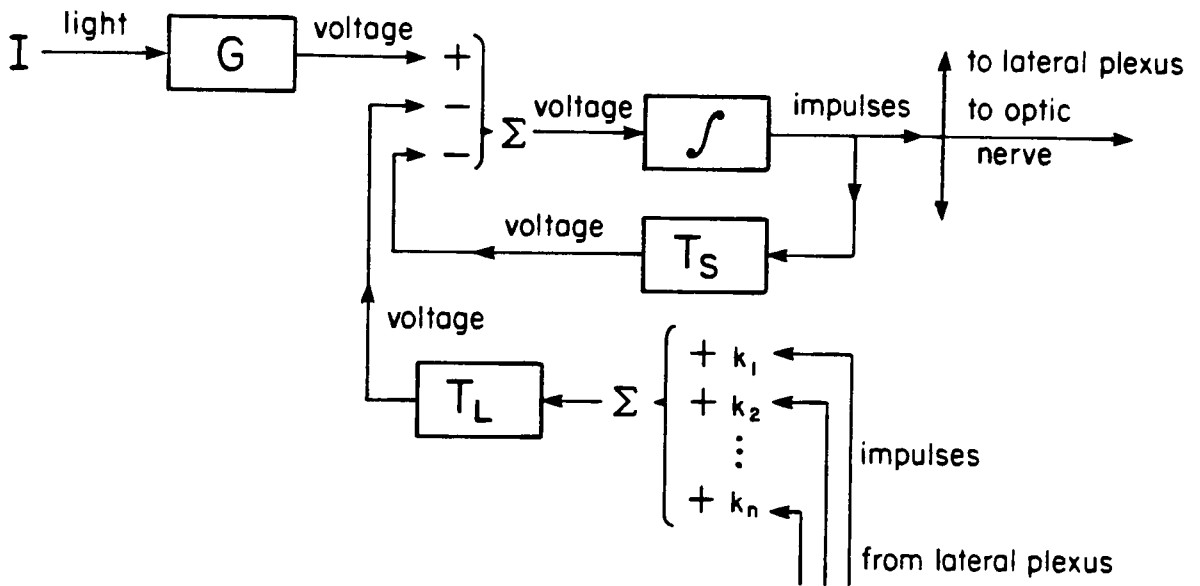
Figure 5-3. Block-diagram of the Limulus retina. G denotes transduction from light to generator potential, $\int$ denotes the impulse generating mechanism, T_S denotes the self-inhibitory transduction, T_L denotes the lateral-inhibitory transductions. Σ denotes summing points, where effects combine linearly, with signs as indicated.

The time-dependent Hartline-Ratliff equations.

The neural organization depicted schematically in Figure 5-3, unlike the system of equations (5.2), applies equally well to the time-dependent operation of the retina as to the steady state. In order to obtain a set of dynamical equations, we adopt the following conventions: First, in recognition of the fact that the self-inhibitory process is not experimentally separable from the mechanism of impulse generation, we combine the self-inhibitory feedback loop and the impulse generator into a single transduction, which we will refer to as the "encoder" (Fig. 5-4). Second, we restrict attention to stimuli which cause all the ommatidia to fire impulses at a rate which fluctuates about some mean operating level. As a rule, this operating level will be such that all the ommatidia fire at a rate above their inhibitory thresholds.[*] In this regime, it is convenient to define the input and output variables of the visual transduction as follows: The input

---

[*] The inhibitory threshold for very large numbers of interacting ommatidia appears to be essentially zero; see chapter IV, and Barlow and Fraioli (1978). We ignore the occasional off-transient which may momentarily silence a few retinal neurons.
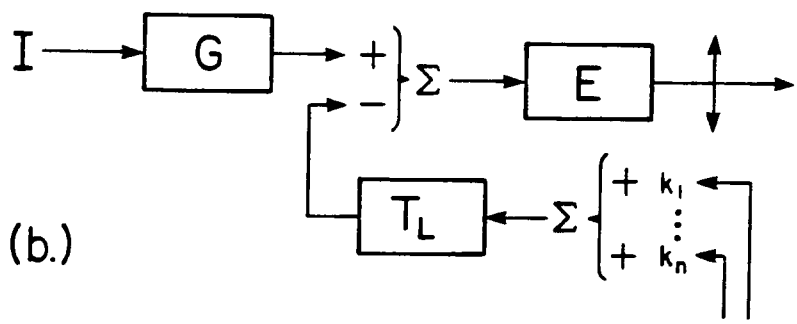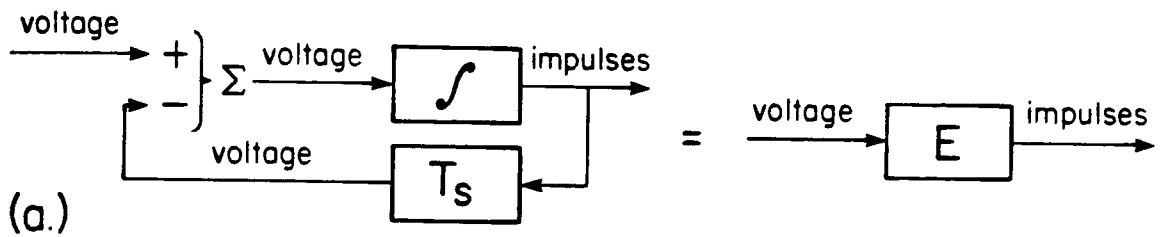
Figure 5-4. (z) Incorporation of the self-inhibitory feedback loop and impulse-generating mechanism into a single encoder transduction, E. (b) Simplified block-diagram of Limulus retina.

variable is taken to be the deviation of the stimulus
light intensity from its average value over the course
of a stimulus episode. Likewise, the output variable is
taken to be the deviation of the impulse rate of the various
ommatidia from their mean rate over the course of the
episode. With these conventions, we may ignore the threshold
terms in the Hartline-Ratliff equations (Ratliff et al., 1974).

We now redefine the coupling coefficients in the
Hartline-Ratliff equations so as to incorporate the dynamic
aspects of the neural interactions which they represent.
This is most simply accomplished by considering responses
to signals which vary sinusoidally in time (Knight et al.,
1970; Knight, 1973a). By virtue of the linearity of the
Limulus eye, each portion of the visual transduction
(generator potential, encoder, lateral inhibition) responds
to a sinusoidal input with a sinusoidal output, according
to its own transfer function. We represent the sinusoidal
signals as (the real parts of) complex exponentials, and
treat each stage of the visual transduction in turn. First,
we consider the excitatory component of the generator potential:

$$\varepsilon_m(t) = G(\omega)I_m e^{i\omega t} \quad , \tag{5.3}$$

where $G(\omega)$ is the light-to-generator-potential transfer function, and $I_m e^{i\omega t}$ is the illumination incident on the m'th ommatidium. The net intracellular potential V_m is the sum of this excitation and the total lateral inhibition:

$$V_m(t) = \varepsilon_m(t) - T_L(\omega) \cdot \sum_{n \neq m} k_{m \leftarrow n} \, r_n(t) \quad . \qquad (5.4)$$

Here, $V_m(t)$ and $r_n(t)$ are functions of time proportional to $e^{i\omega t}$. The equation (5.4) has been written so as to incorporate the remarkable experimental observation of Ratliff et al. (1974) that all the inhibitory interactions within the eye show the same temporal transfer function for lateral inhibition, which is here denoted $T_L(\omega)$. For example, there is no significant phase lag associated with the distance between interacting ommatidia. The matrix of inhibitory coefficients $k_{m \leftarrow n}$ is presumed to be the same as that which describes the inhibitory coupling in the steady state.

Finally, the impulse-train output is related to the net potential V_m according to the formula:

$$r_m(t) = E(\omega)V_m(t) \quad , \qquad (5.5)$$

where $E(\omega)$ is the transfer function of the encoder, which comprises both impulse generation and self-inhibition.

Since in our experiments, the intracellular potential V_m is not accessible to direct measurment, it is convenient to express this potential in units of the steady-state impulse rate which it would produce in the m'th ommatidium. With this choice of units for V_m, we may treat the encoder transfer function $E(\omega)$ as a dimensionless quantity. Equations (5.3-5.5) can be combined to obtain a dynamic equation analogous to the static equations (5.1, 5.2):

$$r_m(t) = E(\omega) \left[G(\omega) \cdot I_m e^{i\omega t} - T_L(\omega) \cdot \sum_{n \neq m} k_{m \leftarrow n} r_n(t) \right] \quad (5.6)$$

The relation (6) is an explicit inhomogeneous set of simultaneous linear equations which may be solved for the $r_m(t)$ in terms of the stimulus pattern I_m. For our purposes, however, it is more convenient to work instead with a continuous version of this system (Kirschfeld and Reichardt, 1964). To this end, we restrict our attention to stimuli which vary in space only along the x-axis (and thus at any time t are constant along vertical lines), and assume that each ommatidium in a given vertical column responds in the same way to such a stimulus. (This last assumption is made only for reasons of computational convenience; a more detailed treatment is discussed in Appendix E.) We may now replace the discrete

index m with the continuous variable x, the horizontal
coordinate along the eye. With this notation, equation (6)
may be replaced by a corresponding integral equation:

$$r(x,t) = E(\omega) \left[G(\omega)I(x)e^{i\omega t} - T_L(\omega)\int k(x-u)r(u,t)du \right], \quad (5.7)$$

where we have incorporated the experimental observation that,
at least away from the edges of the eye, the inhibitory
coupling between two (vertical strips of) ommatidia depends - to a good
approximation - only on the distance between them (Barlow. 1969).
In other words, the inhibitory kernel takes the translation-
invariant form k(x,u) = k(x-u).[*]

To obtain the spatio-temporal transfer function from
equation (5.7),we take as input a sinusoidal grating $I(x) = e^{i\xi x}$.
The response to such a sinusoidal input must be a sinusoidal
signal of the form $r(x,t) = F(\xi,\omega)e^{i(\xi x+\omega t)}$, where $F(\xi,\omega)$ is,
by definition, the spatio-temporal transfer function of the

---

[*]   More generally, if $S(x,t) \to R(x,t)$, and $\tilde{S}(x,\omega)$ and $\tilde{R}(x,\omega)$
denote Fourier transforms of the stimulus and response, respectively,
we have
$$\tilde{R}(x,\omega) = E(\omega)\left[G(\omega)\tilde{S}(x,\omega) - T_L(\omega)\int k(x-u)\tilde{R}(u,\omega)du\right] ,$$
which follows from (5.7) by Fourier transformation and appli-
cation of the superposition principle.

system. We have

$$F(\xi,\omega)e^{i(\xi x+\omega t)} = E(\omega)\left[G(\omega)e^{i(\xi x+\omega t)}\right.$$

$$\left. - T_L(\omega)\int k(x-u)\, F(\xi,\omega)e^{i(\xi u+\omega t)}du\right]$$

$$= e^{i(\xi x+\omega t)}E(\omega)\left[G(\omega) - T_L(\omega)F(\xi,\omega)\int k(u)e^{-i\xi u}du\right]$$

$$= e^{i(\xi x+\omega t)}E(\omega)\left[G(\omega) - T_L(\omega)F(\xi,\omega)\tilde{k}(\xi)\right], \quad (5.8)$$

where $\tilde{k}(\xi) = \int k(u)e^{-i\xi u}du$ is the Fourier transform of the
inhibitory kernel. Equation (5.8) may be solved readily for
$F(\xi,\omega)$, yielding the expression:

$$F(\xi,\omega) = \frac{E(\omega)G(\omega)}{1+E(\omega)T_L(\omega)\tilde{k}(\xi)}. \quad (5.9)$$

It is necessary to make one correction to the idealized
transfer function of equation (5.9) to account for the limited
resolving power of the _Limulus_ optics. The derivation above
assumes that the eye is, in effect, a perfect continuum of visual
receptors, each excited only by illumination at exactly one
x-coordinate. The effect of our imperfect stimulus optics
and the finite size of the ommatidial light-collectors may be
accounted for by convolving the stimulus with an effective
"point spread function," $P(x)$, and using this degraded stimulus
as the input $I(x)$ in equation (5.7). The equivalent correction

in the frequency domain is the multiplication of the spatio-temporal transfer function by the Fourier transform of the point-spread function, which we denote by $\tilde{P}(\xi)$.[*] We thus obtain the final form:

$$F(\xi,\omega) = \frac{\tilde{P}(\xi)E(\omega)G(\omega)}{1+E(\omega)T_L(\omega)\tilde{k}(\xi)} . \tag{5.10}$$

The model of the Limulus visual system summarized by equation (5.10) is based, in essence, on the notion of recurrent mutual lateral inhibitory interaction first described in the original Hartline-Ratliff equations. Accordingly, we will refer to equation (5.10) as the Hartline-Ratliff model for the Limulus spatio-temporal transfer function.

We now consider in turn the various transductions $\tilde{P},E,G,T_L$, and $\tilde{k}$, which enter into the Hartline-Ratliff model transfer function (5.10). For each transduction, we obtain an explicit expression for the corresponding transfer function, in terms of parameters describing more basic aspects of the underlying physiology. Numerical values for these parameters are obtained in the next chapter.

* In the field of optics, the function $\tilde{P}(\xi)$ is known as the (spatial) "modulation transfer function."

We begin with $G(\omega)$, the transfer function from light
to generator potential. This transduction may be studied
directly in excised preparations by impaling the Limulus
eccentric cell with a micro-electrode and measuring the changes
in intracellular potential induced by flickering light
(Purple, 1964; Pinter, 1966; Dodge et al., 1968; Knight et al.,
1970). Data obtained in this way have been well accounted for by the
"adapting-bump model" (Rushton, 1961; Dodge et al., 1968; Knight, 1973c;
Wong, 1977; Wong and Knight, 1979; Wong et al., 1979). This model is
motivated by the observation that, at low light levels, the generator
potential is clearly resolved into a sequence of small discrete depolar-
izations ("bumps") which increase in frequency, but which decrease in
size ("adapt") as the incident illumination increases. On
the basis of a few statistical and physiological assumptions,
these considerations lead to an explicit form for the generator
potential transfer function:

$$G(\omega) = e^{-i\omega t_{\ell}} \cdot \left(\frac{1}{1+it_d\omega}\right)^{n_d} \cdot \left(\frac{1}{1+it_b\omega}\right)^{n_b} \cdot \left(1-\frac{R}{1+t_a\omega}\right) \cdot \left(\frac{it_a\omega}{1+it_a\omega}\right)^{p}. \quad (5.11)$$

The factor $e^{-i\omega t_{\ell}}$ is a pure phase lag introduced by the finite
delay ("latency") between the absorption of incident photons
and the occurrence of the bumps they produce; t_{ℓ} is the mean
delay. The next factor $1/(1+it_d\omega)^{n_d}$ describes the effect of

stochastic variation of this latency interval about its mean. Here, the distribution of latencies is approximated by a gamma-density with parameters t_d and n_d. This corresponds, in the frequency domain, to the factor indicated (Wong, 1977). The third factor $1/(1+it_b\omega)^{n_b}$ expresses the dependence of the transfer function on the bump shape, which is modelled as a gamma-density with parameters t_b and n_b.

The last two factors in equation (5.11) describe the light-adaptation of the generator potential. As may be seen from direct measurements of the light-to-generator potential transduction (for example, Dodge, et. al., 1968), this adaptation occurs on two different time scales. At very low frequencies, the dynamics show a frequency response proportional to $(i\omega)^p$ (Biederman-Thorson and Thorson, 1971; Thorson and Biederman-Thorson, 1974). At higher frequencies, there is a stronger dependence on frequency, which we have modelled, after the "minimal model" of Knight (1973c), as a high-pass filter $(1-R/(1+it_a\omega))$. Here, t_a is a time-constant which specifies the frequency region over which this adaptation effect occurs, and R describes the magnitude of the adaptation effect in this frequency region. We have adopted the form $\left[it_a\omega/(1+it_a\omega)\right]^p$ to describe the very-low-frequency adaptation effect in such a way as to make a gradual transition to unity, centered around

the characteristic frequency $\omega = 1/t_a$.[*]

   We consider next $E(\omega)$, the transfer function for the encoder, which includes the impulse-generating mechanism and a self-inhibitory feedback loop. The precise form of this function depends on the choice made for the variable which describes the output of the encoder. For reasons of simplicity and compatibility with experimental data, we shall use the "population firing rate" function, $r(t)$, as described in Appendix C. Such encoders have been described in great detail (Knight et al, 1970; Barbi et al., 1975; Fohlmeister et al., 1977a), but for our purposes, a simplified model will suffice. First, we assume that the impulse-generating mechanism is adequately described as a simple "integrate-and-fire" device, which produces a nerve impulse whenever the running integral of the input voltage reaches a criterion value; the integral is reset to zero after each impulse is

---

[*]   The transfer function (5.11) has been written so as to correspond to the response generated by "normalized" bumps. As we have no method for direct calculation of the actual bump size, we have retained this form in the model calculations below, and allowed for a scaling of the overall response amplitude as a free parameter, which has been fixed for each preparation, where necessary, by the peak height of a Fourier synthesis calculation at one stimulus velocity. For most purposes, discussed below, only ratios of transfer function values are required, and the scaling of the transfer function may be ignored.

fired. An important property of such an encoder is that, if

the population rate r(t) is taken as the output variable,

then the encoder produces an output which is a perfect replica

of the input (Knight, 1972a). In other words, the transfer

function of the impulse-generator is the constant 1.

The transfer function $T_s(\omega)$ for the self-inhibitory

transduction cannot be measured directly, but it may be deduced

from measurements of the self-inhibitory impulse-response seen

in the intracellular potential following the occurrence of a

neural impulse (Purple, 1964; Stevens, 1964; Dodge, 1969).

This inhibitory transient may be modeled accurately as a single

exponential decay of the form $\kappa e^{-t/\tau}$, where κ describes the

strength of the self-inhibitory effect, and τ is the time

constant for the decay. This impulse response corresponds to

the transfer function

$$T_s(\omega) = \frac{\kappa}{1+i\tau\omega} \ .$$
(5.12)

Note that in equation (5.12) we have incorporated the self-

inhibitory coefficient κ into the function T_s.

In a neural encoder with self-inhibition, the inhibitory

transients occur as discrete events, phased to the occurrence

of impulses in the encoder output. This discrete aspect of the

inhibitory process is reflected in subtle features of the corre-

sponding transfer function for the encoder (Knight et al., 1970;

Shapley, 1971). As these features occur mainly at frequencies greater than the mean impulse rate, we may safely ignore them in our analysis. With this simplification, we may regard the encoder as an ordinary (continuous variable) linear system with feedback (Fig. 5-4a). We thus immediately obtain the relation

$$E(\omega) = 1 - E(\omega) \cdot T_s(\omega). \tag{5.13}$$

Solving for $E(\omega)$ yields

$$E(\omega) = \frac{1}{1+T_s(\omega)} = \frac{1}{1 + \frac{\kappa}{1+i\tau\omega}} = 1 - \frac{\frac{\kappa}{1+\kappa}}{1+i\frac{\tau}{1+\kappa}\omega} \quad . \tag{5.14}$$

This result is strictly equivalent to the approximation of Shapley (1971) (who obtained it as a limiting case of a more elaborate treatment), and is closely related to the model of Stevens (1964).

We next turn our attention to $T_L(\omega)$, the transfer function for the lateral-inhibitory transduction from impulse rate (in the population of inhibiting ommatidia) to inhibitory post-synaptic potential (in the test-ommatidium). This transfer function, like T_s, cannot be measured directly, but it can be determined by two indirect methods, both of which rely on antidromic stimulation of neighboring ommatidia as a source of inhibition on the test-ommatidium (Knight et al, 1970). Transfer functions can be measured for the voltage-to-impulse

rate transduction in the test-ommatidium by passing current through an intracellular microelectrode, and then for the transduction from the (antidromic) impulse rate in the inhibiting units to the reduction of impulse rate in the test-ommatidium. The quotient of these two transfer functions yields the transfer function $T_L(\omega)$. Alternatively, one can hyperpolarize the cell to prevent it from firing impulses, and measure the responses of the intracellular potential to antidromic stimulation of neighboring ommatidia, either to brief bursts or to impulse trains with sinusoidally modulated impulse rate. In such hyperpolarized cells, the impulse response to a short burst of antidromic impulses in the neighboring units is well predicted by the inverse Fourier transform of the transfer function describing the response of the same cell to inhibition from sinusoidally modulated antidromic stimulation of neighboring cells. There is satisfactory agreement between the transfer function measured indirectly as a quotient (with the cell operating at its normal resting potential) and the direct transfer function measurement on the same cell, hyperpolarized.

The lateral inhibitory impulse response typically takes a biphasic form, with a small excitatory effect preceding the main inhibitory hyperpolarization (Knight et al., 1970). We may model this waveform as a combination of four exponential decays. Such a model yields the following expression

for the lateral-inhibitory transduction, $T_L(\omega)$:

$$T_L(\omega) = \frac{1}{1-C} \cdot \left[\frac{1}{1+i\tau_1\omega} \cdot \frac{1}{1+i\tau_2\omega} - \frac{C}{1+i\tau_3\omega} \right] \cdot \frac{1}{1+i\tau_4\omega} \cdot \qquad (5.15)$$

Here, τ_1, τ_2, τ_3 and τ_4 are time-constants chosen to fit the inhibitory impulse-response, and C describes the relative strength of the brief excitatory feature of the impulse response. The transfer function here is normalized to unity at $\omega = 0$. (The strength of lateral inhibition will be reflected in the inhibitory kernel: see below.)

The remaining transfer functions $\tilde{k}(\xi)$ and $\tilde{P}(\xi)$ depend only on spatial frequency. The two-dimensional inhibitory kernel $k(x,y)$ has been studied extensively, generally by making measurements of inhibitory coupling coefficients in the steady state as a function of distance along the retina (Barlow, 1967, 1969; Johnston and Wachtel, 1976). The data may be summarized as a difference of two-dimensional Gaussian distributions:

$$k(x,y) \propto e^{-(x^2+\frac{y^2}{\eta^2})/a^2} - D \cdot e^{-(x^2+\frac{y^2}{\zeta^2})/b^2} \qquad (5.16)$$

Here, the main inhibitory feature has a Gaussian distribution whose width is determined by the parameter a, with iso-inhibitory contours whose shape is governed by the parameter η. Barlow's data suggested a small "crater" in the inhibitory kernel, which is similarly described by the second term in

equation (5.16). In our one-dimensional situation, we may
replace this formula with a simpler form:

$$k(x) = N \cdot \left[Ae^{-x^2/a^2} - Be^{-x^2/b^2} \right], \qquad (5.17)$$

where N is a normalization constant, and the coefficients A
and B describe the relative strength of the crater (see
Appendix). We may fix the constant N by stipulating that

$$\int_{-\infty}^{\infty} k(x)dx = K \qquad (5.18)$$

In the case where the stimulus illuminates the entire vertical
extent of the eye, K is equal to the total inhibition exerted
by the entire eye on any one ommatidium. If the stimulus does
not cover the entire eye, K is the total inhibitory strength
of the portion of the eye which is illuminated. From equations
(5.17) and (5.18) we have

$$K = N \cdot (Aa\sqrt{\pi} - Bb\sqrt{\pi}), \quad \text{or} \qquad (5.19)$$

$$k(x) = \frac{K}{(Aa-Bb)\sqrt{\pi}} (Ae^{-x^2/a^2} - Be^{-x^2/b^2}) . \qquad (5.20)$$

Taking the Fourier transform of (20) yields the effective
1-dimensional transfer function $\tilde{k}(\xi)$:

$$\tilde{k}(\xi) = \int k(x)e^{-i\xi x}dx = \frac{K}{(Aa-Bb)} (Aae^{-\xi^2 a^2/4} - Bbe^{-\xi^2 b^2/4}). \qquad (5.21)$$

We note that $\tilde{k}(0) = K$, as required by equation (5.18).

The point-spread function P(x) describes the distribution on the retina of the image of a "point" stimulus (here, a vertical line). For convenience, we model this function as a normalized Gaussian distribution. This model yields the transfer function

$$\tilde{P}(\xi) = \int_{\infty}^{\infty} P(x)e^{-i\xi x}dx = e^{-\xi^2 s^2/4} , \qquad (5.22)$$

where s is a parameter describing the width of the point spread function. Specifically, s is the distance from the center of the image of a point light source to the position where the intensity of the image drops to 1/e of its intensity at the center.

A summary of the equations of the Hartline-Ratliff model appears in Table I. This description of the dynamics of the Limulus lateral eye contains some twenty nominal parameters. These are constrained, not only to model the overall spatio-temporal transfer function, but also to model each component transduction so as to agree, within reasonable limits, with direct measurements of the corresponding physiological process. For comparison, it may be noted that the empirical spatio-temporal transfer functions, with which the model calculations are to be compared, are obtained by interpolation from 128 independent measurements (amplitude and phase at 64 spatio-temporal frequency pairs).

"The fusion plasma requires a temperature of 500 million
degrees, but I forget whether that's Centigrade or Absolute"

anonymous.

VI.   <u>Calibration of the Hartline-Ratliff Model</u>.

In this chapter, we complete the systems-analytic
program described above, by demonstrating how the empirical
spatiotemporal transfer function can be related to the
physiology of the <u>Limulus</u> retina by means of the Hartline-
Ratliff model of the previous chapter.

<u>Experimental Methods</u>.

The spatiotemporal transfer function $F(\xi,\omega)$ was measured
as described in chapter III. However, in order to optimize
the signal-to-noise ratio of the transfer function measure-
ments, in several experiments the experimental protocol was
modified by dropping the moving-pattern "synthesis" episodes
from the stimulus sequence. This allowed the acquisition
of twice as many responses to the "analysis" stimuli within
the finite lifetime of the preparation. For one experiment,
the analysis patterns were presented in an orientation
rotated 90° from the (usual) horizontal, in order to measure
the distribution of the lateral-inhibitory coupling constants
in the vertical direction.

Calculations based on the measured transfer functions
were implemented with the cubic spline interpolations described
in chapter III. Model-based calculations were implemented
with a library of FORTRAN-IV complex arithmetic subroutines.

Results.

The results of a typical analysis experiment are shown in
Figure 6-1. We note the following features: the transfer
function shows a marked attenuation of the response to flicker-
ing light at very high spatial frequency. Careful inspection
of the data indicates that this high-frequency cut-off
affects the response equally at all temporal frequencies; the
amplitude is diminished with little change in phase. The
behavior at low spatial frequency is more complex, and depends on
temporal frequency. At low temporal frequencies, the response
to flicker is diminished at low spatial frequency. Conversely,
at intermediate temporal frequency, the response to flicker
at low spatial frequency is enhanced, as compared to the response
at intermediate spatial frequency. At high temporal frequency,
there is little dependence on spatial frequency in the low-to-
moderate range. The net result is an effective narrowing
at low spatial frequency of the "tuning" of the transfer function
to a band of intermediate temporal frequency (Ratliff et al,
1967; Ratliff et al., 1969). The general features of the
dependence on temporal frequency are a sharp cut-off at high
frequency and a broader attenuation of the response to low
frequency flicker. Under our conditions, the peak response is
at approximately 6 Hz. This is somewhat higher than has been
reported previously (Knight et al., 1970), and may reflect the
elevated temperature of our preparation (see Appendix B).
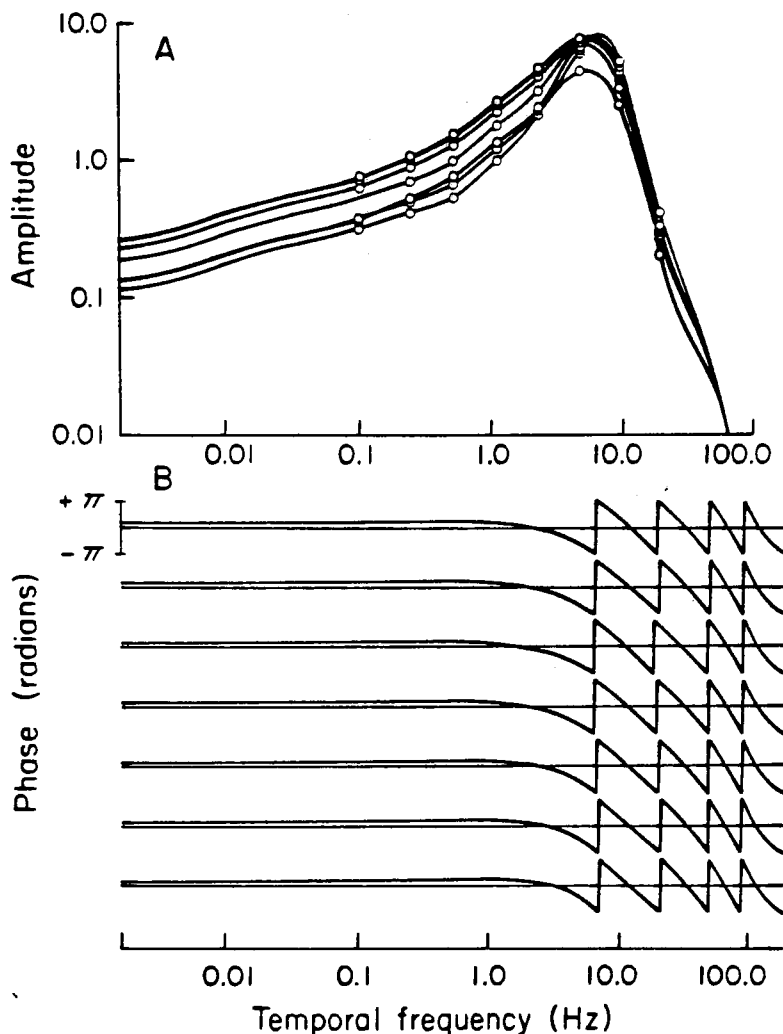
Figure 6-1. Spatiotemporal transfer function for the Limulus lateral eye   Bode plots (log amplitude vs. log frequency; phase vs. log frequency)of measured response at seven spatial frequencies (0.1, 1,2, 4, 8, 16, and 32 cycles/eye-width). (a) The amplitude curves are superimposed on one set of axes for comparison (at the peak, near 6 Hz, the amplitudes decrease monotonically with increasing spatial frequency).   Data points indicated (O) are direct measurements; the remainder of the curves are interpolated and extrapolated as described in chapter III.   Small undulations of the amplitude curves at low frequency are an artifact of the extrapolation pro-cedure.   (b) Phase curves are shown on separate axes, modulo 2π; they are extrapolated at the same frequencies as the amplitudes, above. Spatial frequencies increase from bottom to top.

These features may be interpreted as follows: The cut-off at high spatial frequency, which effects all temporal frequencies equally, is presumably due to the degradation of the sinusoidal grating stimulus by the point-spread characteristic of the system optics. At such high spatial frequencies, lateral inhibition is cancelled out (see below); thus, the only effect of the optical system is to average the sine-wave grating stimulus so as to reduce its effective contrast at the test-ommatidium, reducing the response amplitude equally at all temporal frequencies. The tuning of the frequency response at lower spatial frequencies is presumed to be a consequence of lateral inhibition. The nature of the transition from attenuation (at low temporal frequencies) to enhancement (at intermediate temporal frequencies) to little effect (at high temporal frequencies) is a function of the temporal properties of the lateral inhibitory transduction, T_L. The lateral inhibition increasingly lags in phase with increasing temporal frequency, until, at about 6 Hz, the phase lags by one-half cycle, and the inhibition appears as excitation (Ratliff, et al., 1970). The general high temporal frequency cut-off and low frequency attenuation reflect the temporal structure of the generator potential transduction G. The low-frequency structure is the result of the "adaptation" process, while the high-frequency structure depends mainly on the "bump shape."

Determination of Parameters

Point-spread.

We begin with the attenuation at high spatial frequency. In this regime, the stimulus grating oscillates several times over distances in which the inhibitory kernel presumably varies only slightly. As a result of the linearity of the system, this results in effective cancellation of the time-varying component of the inhibitory action of the retina on the test-ommatidium. We therefore may ascribe any dependence of the transfer function on spatial frequency in this regime to the effect of the point-spread transfer function, $\tilde{P}(\xi)$. Since this function enters the full spatio-temporal transfer function only as a real multiplicative factor, we expect this effect to operate equally at all temporal frequencies, and to produce no phase shift. Hence, for ξ large, the expression (10) reduces to the simpler approximate form

$$F(\xi,\omega) = \tilde{P}(\xi) \cdot E(\omega)G(\omega), \qquad (\xi \text{ large}). \qquad (6.1)$$

Thus (at high spatial frequencies) for fixed temporal frequency, the transfer function is directly proportional to the point-spread function $\tilde{P}(\xi)$. Accordingly, we may determine the point-spread parameter s in equation (5.22) by plotting, for any fixed temporal frequency ω, the quantity $\log|F(\xi,\omega)|$ versus ξ^2; the slope of this line is proportional to s^2. The internal

consistency of this determination may be assessed by comparing
the s-parameter values derived from data obtained from the same
preparation at several different temporal frequencies. Such an
analysis of the high spatial frequency cut-off is shown in
Figure 6-2. For the preparation of Figure 6-1, we obtain the
point-spread parameter value s = 0.0083 eye-widths. In general,
the observed point-spread parameter values are comparable to the
radius of a <u>Limulus</u> ommatidium (0.0125 eye-widths), and are thus
in good agreement with the estimate of the effective optical
point-spread obtained in Appendix A by direct inspection of the
crystalline cones.

<u>Lateral Inhibitory Kernel</u>.

According to our model, the remainder of the dependence
of the spatio-temporal transfer function on spatial frequency
is due to the structure of the inhibitory kernel k(x), as
reflected in its Fourier transform $\tilde{k}(\xi)$. In order to determine
this function from the experimental data, we have found it
expedient to work with plots of the locus, on the complex plane,
of $1/F(\xi,\omega)$ as a function of spatial frequency (ξ), with temporal
frequency (ω) fixed. From equation (5.10) we have

$$\frac{1}{F(\xi,\omega)} = \left[\frac{1}{\tilde{P}(\xi)} \cdot \frac{1}{E(\omega)G(\omega)} + \frac{\tilde{k}(\xi)}{\tilde{P}(\xi)} \cdot \frac{T_L(\omega)}{G(\omega)} \right] \qquad . \qquad (6.2)$$
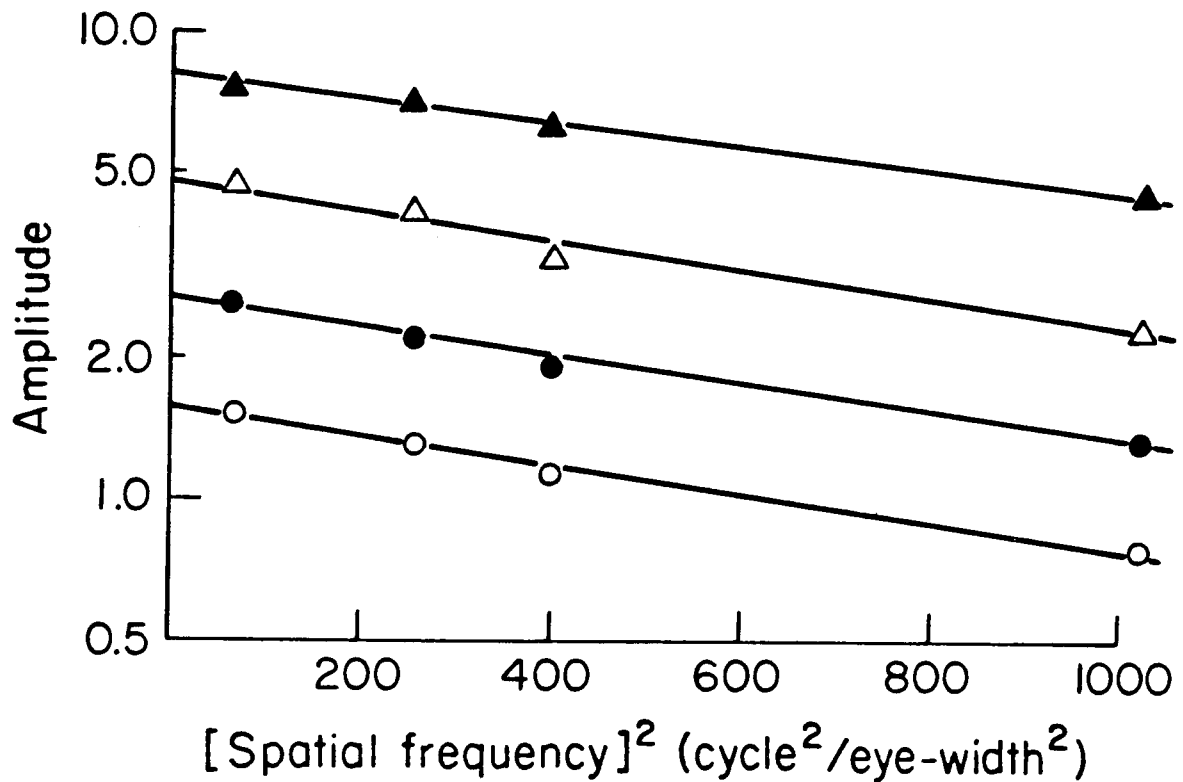
Figure 6-2. Estimation of the point-spread parameter s. For each fixed temporal frequency ω, $\log|F(\xi,\omega)|$ is plotted vs. ξ^2, the square of the spatial frequency. At high spatial frequency, slope of this locus is $s^2/4$ (see text). Data from the preparation of Figure 6-2. Temporal frequencies were 0.5 Hz (O), 1.03 Hz (●), 2.1 Hz (△) and 4.23 Hz (▲). Values for the parameter s were 0.0085, 0.0085, 0.0085, and 0.0078 eye-widths, respectively (mean 0.0083 eye-widths).

This function has an extremely convenient form: it is a sum of two terms, each of which is a (complex) function of temporal frequency multiplied by a real function of spatial frequency. For fixed ω, we may regard the complex numbers $1/E(\omega)G(\omega)$ and $T_L(\omega)/G(\omega)$ as fixed vectors in the complex plane. As ξ varies, this "reciprocal locus" (6.2) traces out a weighted sum of these two vectors (Fig. 6-3). Interpretation of these loci is considerably simplified by the fact that the spatial transfer functions $\tilde{P}(\xi)$ and $\tilde{k}(\xi)$ vary strongly with ξ in different regions of spatial frequency. Thus, for low and intermediate values of ξ, where $\tilde{k}$ is of interest, the function $\tilde{P}(\xi)$ is nearly constant; conversely, at high spatial frequency, where $\tilde{P}$ shows structure of interest, $\tilde{k}$ has essentially fallen to zero. Thus, the reciprocal loci have

a basic V-shaped form, first moving toward the origin along a vector parallel to $T_L(\omega)/G(\omega)$, then moving away from the origin along the vector $1/E(\omega) \cdot G(\omega)$. This separation of the scales of the functions $\tilde{P}(\xi)$ and $\tilde{k}(\xi)$ corresponds to the fact that the point-spread function $P(x)$ is considerably narrower than the narrowest feature of the inhibitory kernel $k(x)$.

We may further isolate the role of the inhibitory kernel by multiplying equation (6.2) by the point-spread transfer function $\tilde{P}(\xi)$:

$$\frac{\tilde{P}(\xi)}{F(\xi,\omega)} = \left[\frac{1}{E(\omega)G(\omega)} + \tilde{k}(\xi) \cdot \frac{T_L(\omega)}{G(\omega)} \right] \quad . \qquad (6.3)$$
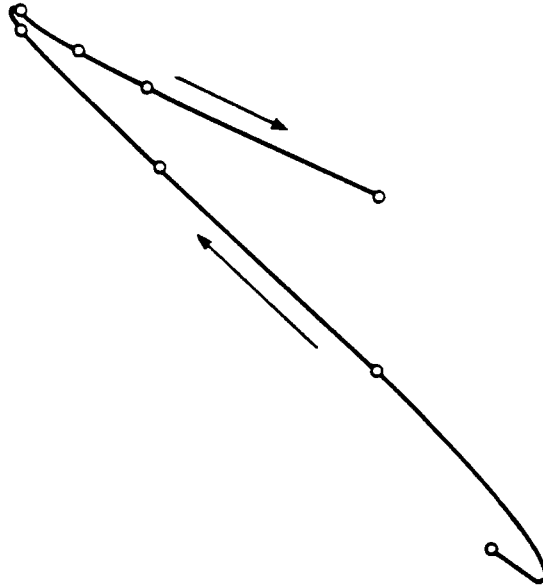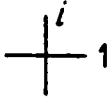
Figure 6-3. Reciprocal locus. The locus of the reciprocal of

the measured spatio-temporal transfer function is plotted on

the complex plane as a function of spatial frequency, with

temporal frequency held fixed.   Data from Figure 6-3, with

temporal frequency held at 1.03 Hz.   Points at which measure-

ments were made are indicated (O).   The arrows indicate

the direction of increasing spatial frequency along the locus

The loop at the low frequency end of the locus is an artifact

of the spline interpolation procedure used to generate the

curve.

The quantity on the left of this equation may be thought of as the reciprocal of the spatio-temporal transfer function, "corrected" for the effect of the point-spread function. If we now hold ω fixed and plot on the complex plane the locus of equation (6.3) as a function of ξ, we obtain a corrected reciprocal locus, which traverses a line parallel to the vector $T_L(\omega)/G(\omega)$, according to the function $\tilde{k}(\xi)$ (Fig. 6-4). We may fix an origin for the quantity $\tilde{k}$ on this locus by considering the limit of high spatial frequency. In this limit, $\tilde{k}(\omega)$ approaches zero, as described above, and we have the asymptotic result

$$\frac{\tilde{P}(\xi)}{F(\xi,\omega)} = \frac{1}{E(\omega)G(\omega)} \quad , \qquad (\xi \text{ large}). \qquad (6.4)$$

Equivalently, we may fix this reference point as the intersection of the high frequency asymptote of the reciprocal locus (equation (6.2)) with the low-frequency arm of the locus. This point presumably describes the phase of the system's response in the complete absence of lateral inhibition (Fig. 6-4).

Once this reference point is located on the corrected reciprocal locus, we may then directly measure the signed distances of the points $\tilde{P}(\xi)/F(\xi,\omega)$ of the locus from this origin. These distances, as a function of ξ, are proportional to $\tilde{k}(\xi)$, the Fourier transform of the inhibitory kernel.
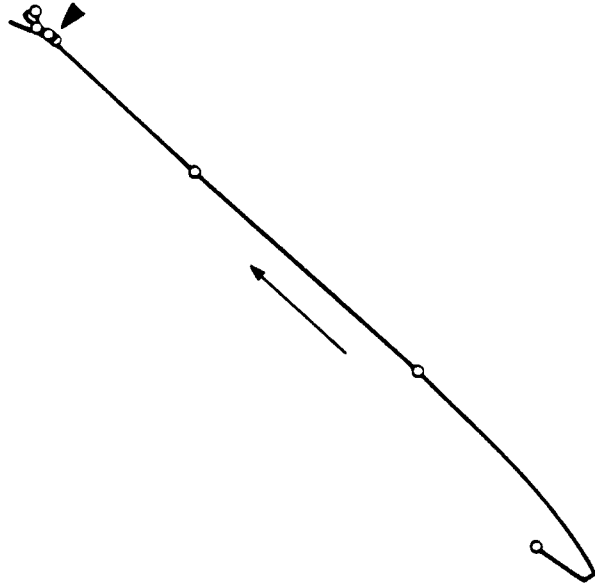
Figure 6-4.   Corrected reciprocal locus. The locus of the

product of the reciprocal of the measured transfer function

(data of Fig. 6-1, 1.03 Hz) and the estimated point-spread

transfer function (eq. (5.22), s-parameter determined from

data of Fig. 6-2) is plotted as a function of spatial fre-

quency, with temporal frequency held fixed. Points at which

measurements were made are indicated (O); the point of

origin for the measurement of the inhibitory kernel transform

$\tilde{k}(\xi)$ is indicated by the large arrowhead. Arrow indicates

direction of increasing spatial frequency. The short straight

line which points toward the origin is an artifact of a small

disparity between the spline interpolation of the transfer

function and the point-spread correction based on equation (5.22)

Typical results of this procedure are shown in Figures 6-5 and 6-6. The measured values for $\tilde{k}(\xi)$ have been interpolated linearly. Though the data are somewhat noisy at high spatial frequency, where the attenuation of the response reduces the signal-to-noise ratio, the basic form of the function is clear. The transform $\tilde{k}$ falls rapidly from its inital value, overshoots the origin, where $\tilde{k} = 0$, and, at high spatial frequency, slowly returns to zero from below. This overshoot corresponds to the slight offset of the vertex of the V-shaped reciprocal locus to the opposite side of the high-frequency asymptote from the low-frequency end of the locus (Fig. 6-3). This overshoot may be considered as evidence, in the spatial frequency domain, for a small "crater" in the inhibitory kernel $k(x)$* In essence, at intermediate spatial frequency, the broad inhibitory portion of the kernel is cancelled by the oscillation of the grating stimulus, but the narrower, oppositely-signed component can still resolve the grating, and results in a reversal in the sign of the time-dependent inhibitory effect. This qualitative indication of the presence of a crater in the inhibitory kernel represents an important advantage of sinusoidal gratings over single bars of

---

* Such an overshoot can also correspond to a slight flattening of the peak of the inhibitory kernel, rather than an actual crater, depending on the strength of the overshoot. In general, the overshoot corresponds to a crater whenever $\int_0^\infty \xi^2 \tilde{k}(\xi) d\xi < 0$.
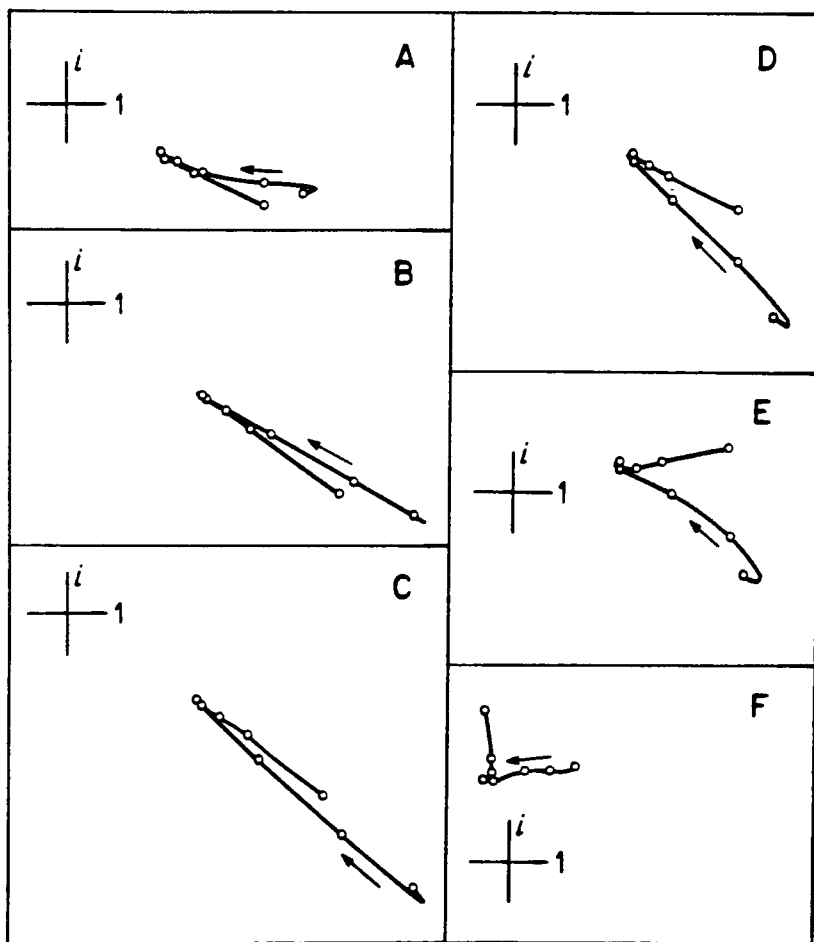
Figure 6-5. Reciprocal loci, as in Figure 6-3, are plotted for six temporal frequencies: (a) 0.1 Hz, (b) 0.23 Hz, (c) 0.5 Hz, (d) 1.03 Hz, (e) 2.1 Hz, and (f) 4.23 Hz. The loci have been magnified by factors of 1,2,3,4,6, and 8, respectively. Arrows indicate direction of increasing spatial frequency.
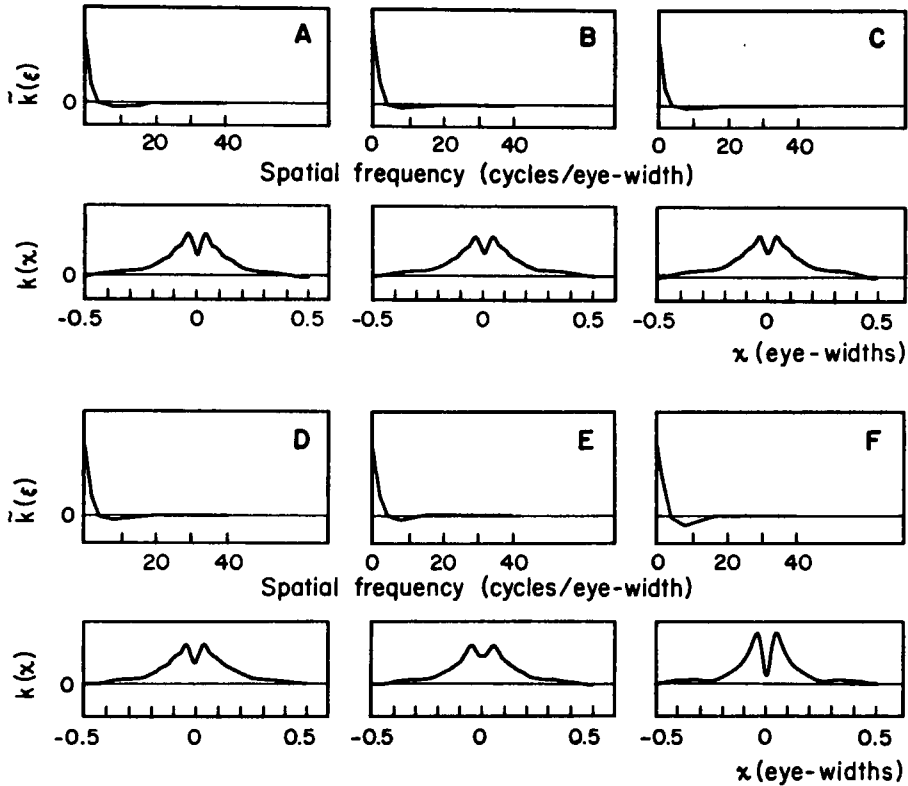
Figure 6-6. Inhibitory kernel measurements. For each of six temporal frequencies, the inhibitory transfer function $\tilde{k}(\xi)$ and the corresponding inhibitory kernel $k(x)$ are shown. Inhibitory transfer functions obtained from measurements of corrected reciprocal loci, as in Figure 6-4; each inhibitory kernel is the inverse Fourier transform of the corresponding inhibitory transfer function. Data from Figure 6-1; temporal frequencies are (a) 0.1 Hz, (b) 0.23 Hz, (c) 0.5 Hz, (d) 1.03 Hz, (e) 2.1 Hz, (f) 4.23 Hz.

varying width as a test-stimulus for the analysis of the spatial organization of such a system. The inhibitory kernel k(x) may be obtained from these data by taking the inverse Fourier transform of the measured function $\tilde{k}(\xi)$ (Fig. 6-6). In both the space and spatial frequency domains, there is essential agreement between the inhibitory kernel measurements at the different temporal frequencies. This verifies the internal consistency of these measurements, and the applicability of the Hartline-Ratliff model (eq. 5.10).

The inhibitory kernel data at the various temporal frequencies were averaged together (Fig. 6-7). This averaged kernel was then fitted by eye with a difference of two Gaussian distributions, according to equation (5.20). The parameters of this model kernel specify the geometry of the inhibitory field. For the preparation of Figure 6-1, we obtained the following values: A = 2.06, a = 0.17 eye-widths; B = 1.2, b = 0.025 eye-widths. Similar data obtained in this way from several preparations all strongly imply the existence of a small crater in the inhibitory kernel.

This fitting procedure was also used for one experiment in which the usual stimulus was rotated 90°, so as to produce a vertical band of light whose intensity varied sinusoidally as as a function of the vertical coordinate, y. The inhibitory kernel in the vertical direction was found to be similar to that in the horizontal direction, with a large Gaussian inhibitory lobe, and a small crater surrounding the test-ommatidium. (Parameters A = 3.7, a = 0.09 eye-widths, B = 0.9, b = 0.02 eye-widths.)

Inhomogeneities in the retina.

In a small number of instances, the reciprocal loci (plots on the complex plane of $1/F(\xi,\omega)$ as a function of ξ, with ω held fixed) did not conform to the pattern described above. Instead of a V-shaped locus with the two straight arms predicted by the Hartline-Ratliff model, these units produced reciprocal loci whose low-frequency arms were bent into circular arcs (Fig. 6-8). This discrepancy could not be accounted for by the experimental uncertainly of the transfer function measurements. Fortunately, it was possible to approximate the curves with straight lines sufficiently well to permit the estimation of the inhibitory kernel in the usual way (see below). We offer the following analysis as a likely explanation of the disparity between these units and the Hartline-Ratliff model:

Suppose that the test-ommatidium is dynamically distinct from the other ommatidia of the eye (assumed to be dynamically identical), with one or more of its temporal transfer functions $G'(\omega)$, $E'(\omega)$, and $T'_L(\omega)$ unequal to the corresponding transfer functions $G(\omega)$, $E(\omega)$, and $T_L(\omega)$ common to the rest of the ommatidia.[*] Indeed, we may even allow variation among

---

[*] Under our conventions for the normalization of the transfer function, an optical defect which obscures only the test ommatidium may be incorporated into this formalism as a real scalar which multiplies the transfer function $G'(\omega)$.
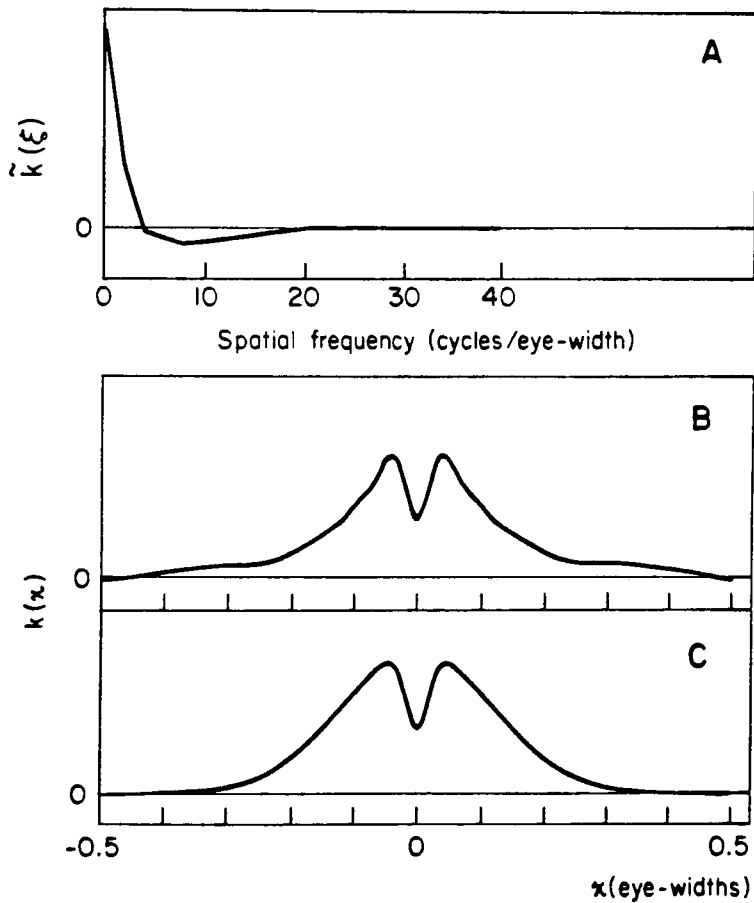
Figure 6-7.(a) Averaged inhibitory transfer function, from data
of Figure 6-6. (b) Averaged inhibitory kernel, obtained as
inverse Fourier transform of (a). (c) Model inhibitory kernel
(eq. (5.20), fitted by eye to measured kernel of (b).
Parameters are A = 2.06 a = 0.17 eye-widths, B = 1.2,
b = 0.025 eye-widths.

Figure 6-8. Curved reciprocal loci. Loci are plotted as in

Figure 6-3. Temporal frequencies: (a) 1.0 Hz, (b) 2.0 Hz,

(c) 3.0 Hz, (d) 4.0 Hz. (The loci have been plotted at

temporal frequencies other than those used in the analysis

stimuli in order to avoid the artifactual loops at the low

(spatial) frequency ends of the loci due to the spline inter-

polation procedure used to generate the curves.) The loci

have been magnified by factors of 2,5,5, and 10, respectively.

Arrows indicate direction of increasing spatial frequency.

Approximate centers of curvature of low-frequency arms of

the loci are indicated by (⊕). True circular areas centered

about these points have been drawn as thinner lines superimposed

on the reciprocal loci; they are nearly obscured by the

coincident arcs of the experimental loci. Data from preparation

of Figure 4-3.
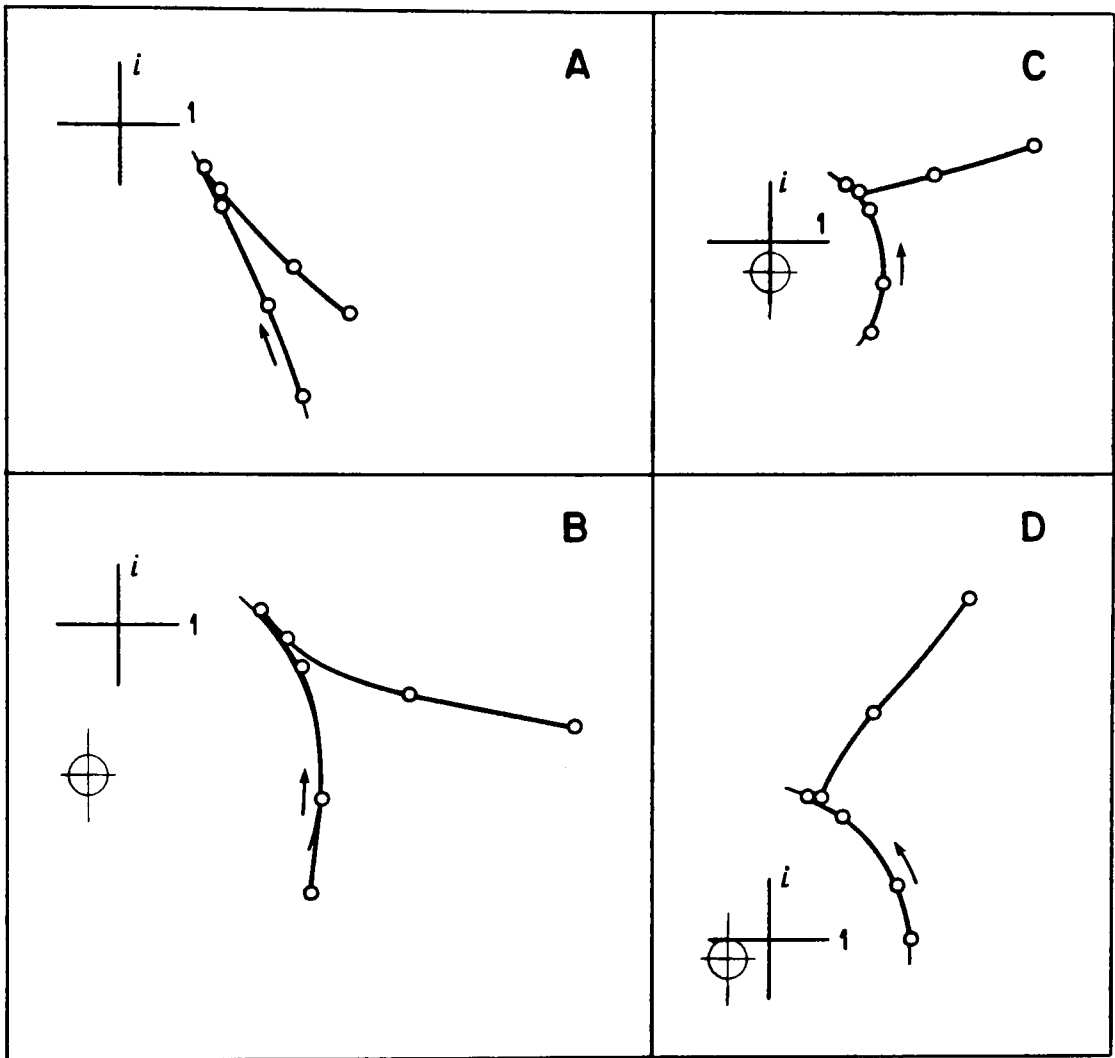
Figure 6-8

inhibiting units, so long as their summed response may be
approximated by that of a homogeneous retina. Further, the
total inhibitory strength K' of the inhibition exerted on
the test-ommatidium may differ from the total inhibitory
strength K for the rest of the retina, but we suppose
there is no further disparity between the inhibitory kernels
of the test-ommatidium and the rest of the eye. Since
the response of the inhibiting population is scarcely
altered by varying the small contribution of the test-
ommatidium, we may write the following modified Hartline-
Ratliff equation for the response of this distinguished
unit:

$$R(0,t) = E'(\omega)\left[G'(\omega)S(0,t) - T'_L(\omega)\int k'(x-y)R(y,t)dy\right] \quad , \quad (6.5)$$

where the stimulus is $S(x,t) = e^{i(\xi x + \omega t)}$, and the primes
denote functions pertaining to the test-ommatidium, located
at x = 0. Then the response of the test-ommatidium is
given by $R(0,t) = F'(\xi,\omega)S(0,t)$, while the response elsewhere
is given by $R(x,t) = F(\xi,\omega)S(x,t)$, where $F(\xi,\omega)$ is given
by equation (5.9) (we ignore the point-spread function as
it has no effect on the low-frequency arcs of the reciprocal
locus - see above). Substituting these relations into (6.5)

yields

$$F'(\xi,\omega) = E'(\omega)\left[G'(\omega) - T_L'(\omega) \cdot \tilde{k}'(\xi) \cdot \frac{E(\omega)G(\omega)}{1+E(\omega)T_L(\omega)\tilde{k}(\xi)}\right] \tag{6.6}$$

This may be rearranged to yield

$$\frac{1}{F'} = \frac{1+E\ T_L\tilde{k}}{E'\left[G'(1+E\cdot T_L\tilde{k})-T_L'\tilde{k}'EG\right]} \quad . \tag{6.7}$$

By virtue of equation (5.9), division of numerator and denominator by EG gives

$$\frac{1}{F'} = \frac{1/F}{E'G'\ \frac{1}{F} - E'T_L'\tilde{k}'} \quad . \tag{6.8}$$

Furthermore, since $\tilde{k}' = \frac{K'}{K} \tilde{k}$, rearrangement of (5.9) gives

$$E'T_L\tilde{k}' = \frac{E'T_L'K'}{E\ T_LK} \left(EG\frac{1}{F} - 1\right) \ , \tag{6.9}$$

whence

$$\frac{1}{F'} = \frac{1/F}{\left(E'G'-EG \cdot \dfrac{E'T_L'K'}{E\ T_LK}\right) \dfrac{1}{F} + \dfrac{E'T_L'K'}{E\ T_LK}}$$

$$= \frac{1/F}{E'G'\left(1 - \dfrac{GK'T_L'}{G'KT_L}\right) \dfrac{1}{F} + \dfrac{E'T_L'K'}{E\ T_LK}} \quad . \tag{6.10}$$

For fixed ω, this equation has the form of a so-called "fractional linear transformation" of the complex variable $1/F$ into the variable $1/F'$. Since the locus of the variable $1/F$ is a straight line, its image under the fractional linear transformation will, in general, be an arc of a circle (see Rudin, 1974, p298).

The complicated form of the coefficients in (6.10) probably precludes separate evaluation of all the primed and unprimed quantities in it, except perhaps in favorable special cases. Nevertheless, this analysis is useful by virtue of its contrapositive. Thus (except in the unlikely event that $GK'T_L' = G'KT_L$, and the coefficient of $1/F$ in the denominator of (6.10) vanishes) the various inhomogeneities considered above may be virtually ruled out for any preparation whose reciprocal loci conform to the predictions of the Hartline-Ratliff model, and show no curvature.

Total Inhibitory Strength.

The total inhibitory strength K is best determined at very low temporal frequencies, where there is no significant phase lag between excitation and inhibition, and where we may treat the response amplitude as a simple scalar sum of excitation and inhibition. As ω approaches zero, we obtain the following limiting form for equation (5.10)

$$F(\xi,\omega) = \frac{\tilde{P}(\xi)\cdot(1-R)\cdot(i\omega)^p\cdot(\frac{1}{1+\kappa})}{1+\tilde{k}(\xi)/(1+\kappa)}, \qquad (\omega \text{ small}) .$$

(6.11

Because the scales of $\tilde{P}(\xi)$ and $\tilde{k}(\xi)$ are well-separated (see above), we may ignore the point-spread function $\tilde{P}(\xi)$ for low and moderate spatial frequencies, where $\tilde{P}(\xi) \cong 1$. With this approximation, we may attribute all of the dependence of the response amplitude in this regime of spatial frequency to the effect of lateral inhibition. The total extent of this dependence directly reflects the total inhibitory strength K, as follows: We define ξ_0 as that spatial frequency at which the inhibitory transfer function $\tilde{k}(\xi)$ first crosses the ξ-axis (Fig.6-9). At this spatial frequency, the effect of the crater in the inhibitory kernel exactly cancels the effect of the main inhibitory part of the kernel, and the test-ommatidium sees no time-dependent inhibition: thus,

$$F(\xi_0,\omega) = (1-R) \cdot (i\omega)^P \cdot (\frac{1}{1+\kappa}), \qquad (\omega \text{ small}). \qquad (6.12)$$

On the other hand, we have $\tilde{k}(0) = K$, whence

$$F(0,\omega) = \frac{(1-R)(i\omega)^P(\frac{1}{1+\kappa})}{1+K/(1+\kappa)}, \qquad (\omega \text{ small}). \qquad (6.13)$$

We thus obtain the following expression for the (observable) quotient $Q_0 = F(\xi_0,\omega)/F(0,\omega)$:

$$Q_0 = \frac{(1-R)(i\omega)^P(\frac{1}{1+\kappa})}{(1-R)(i\omega)^P(\frac{1}{1+\kappa})/(1+\frac{K}{1+\kappa})} = 1 + \frac{K}{1+\kappa}, \qquad (6.14)$$
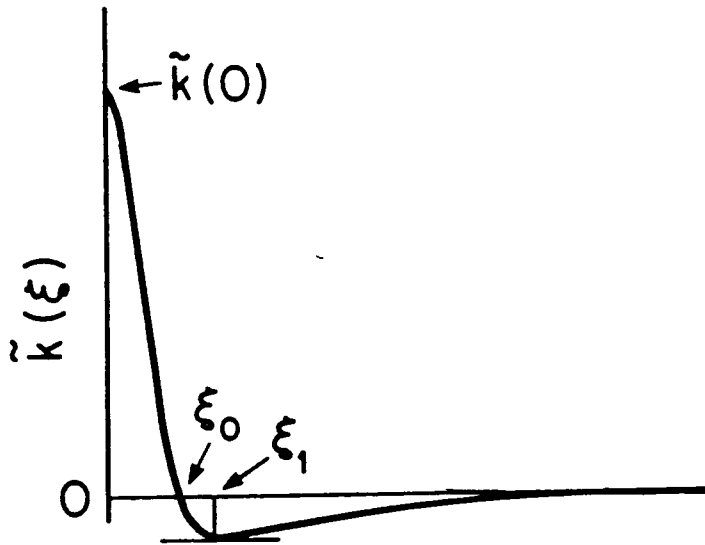
Figure 6-9. Determination of total inhibitory strength.
Characteristic spatial frequencies ξ_0 and ξ_1 are defined from the
measured spatial inhibitory transfer function $\tilde{k}(\xi)$ as shown.
The parameter θ is determined as the ratio $-\tilde{k}(\xi_1)/\tilde{k}(0)$. For the
data of Figure 6-1, this procedure produced quotients $Q_0 = 2.545$,
$Q_1 = 2.63$ ($\theta = .069$), yielding estimates of $\frac{K}{1+K} = 1.545$ and
1.380, respectively (see text).

or

$$\frac{K}{1+\kappa} = Q_0 - 1. \qquad (6.15)$$

Alternatively, we may define ξ_1 as that spatial frequency at which the inhibitory transfer function $\tilde{k}(\xi)$ takes on its most negative value (Fig.6-9). Near this spatial frequency (for low temporal frequency), the effect of the lateral ("inhibitory") interaction is to <u>enhance</u> the response of the test-ommatidium; at $\xi = \xi_1$, the response is maximal. If we set $\tilde{k}(\xi_1) = -\theta\tilde{k}(0) = -\theta\cdot K$, we have

$$F(\xi_1,\omega) = \frac{(1-R)\cdot(i\omega)^P\cdot(\frac{1}{1+\kappa})}{1-\frac{\theta K}{1+\kappa}} , \quad (\omega \text{ small}) \qquad (6.16)$$

We may thus form the (observable) quotient $Q_1 = F(\xi_1,\omega)/F(0,\omega)$:

$$Q_1 = \frac{(1-R)(i\omega)^P\cdot(\frac{1}{1+\kappa})/(1-\frac{\theta K}{1+\kappa})}{(1-R)(i\omega)^P\cdot(\frac{1}{1+\kappa})/(1+\frac{K}{1+\kappa})} = \frac{1+\frac{K}{1+\kappa}}{1-\frac{\theta K}{1+\kappa}} , \qquad (6.17)$$

or

$$\frac{K}{1+\kappa} = \frac{Q_1-1}{1+\theta\cdot Q_1} . \qquad (6.18)$$

These two estimates depend on observation of somewhat different features of the low frequency transfer function, and provide a check on each other. For the preparation of Figure 6-1, we obtained the values $Q_0 = 2.545$, $Q_1 = 2.63$ ($\theta = 0.069$), yielding estimates of $\frac{K}{1+\kappa} = 1.545$ and 1.380, respectively. (Our model transfer function (Fig. 6.11) was calculated with $\frac{K}{1+\kappa} = 1.3$, which fit the data slightly better.) The occurrence of the quotient

K/(1+κ) on the left of equations (6.15) and (6.18) reflects the fact that the lateral inhibitory transduction follows the encoder transduction, and cannot be studied in isolation by our methods.

The transfer functions which remain to be determined are those that depend only on temporal frequency: $E(\omega)$, $G(\omega)$, and $T_L(\omega)$. These functions determine the directions and lengths of the "arms" of the reciprocal loci at the different temporal frequencies (Fig. 6-5),   but because they occur as products or quotients in equation (6.3) it is difficult to extract the model parameters for these functions directly from measurements of these loci, as was done for the spatial transfer functions. Instead, we have found it convenient to adjust these parameters so as to match the Bode plots of the complete spatio-temporal transfer function (Fig.6-10); the reciprocal loci calculated for the model transfer function then serve to check the accuracy of the model. Below, we discuss the extent to which the individual parameters can be associated with specific features of the measured transfer function.

Figure 6-10. Estimation of temporal transfer function parameters.
The features indicated depend most strongly on particular
transfer function parameters, as shown, and were used to fit
these parameters, as discussed in the text. (a) High-frequency
cut-off determines generator potential time-constants t_d and t_b.
(b) Steepness of phase-lag determines exponents n_d and n_f; low-
frequency phase lead determines time-constant t_ℓ. (c) Frequency
range of adaptation effect determines time-constant t_a.
(d) Magnitude of adaptation effect determines adaptation
coefficient R. (e) Low spatial frequency tuning amplitude peak
and phase dependence fitted by strength κ and time-constant τ

for encoder transfer function $E(\omega)$. (f) Lateral inhibitory
transfer function $T_L(\omega)$ adjusted to fit fine structure of
spatial dependence at intermediate temporal frequencies.
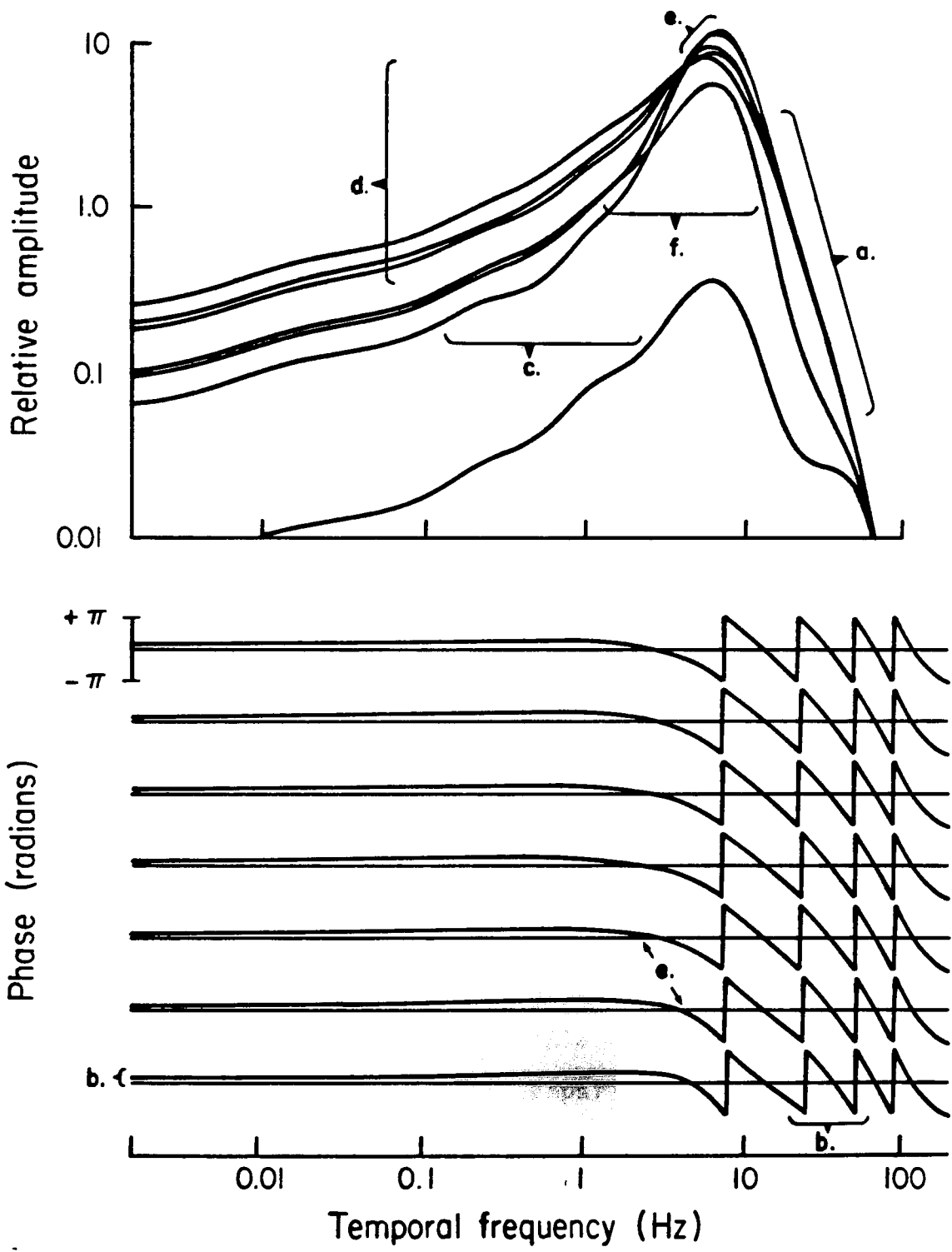
Figure 6-10

Generator Potential.

We begin with the generator potential transfer function $G(\omega)$ (eq. (5.11). The most prominent feature of the generator potential transfer function is the severe cut-off at high frequencies. This is a consequence of the two factors of the form $(\frac{1}{1+i\omega t})^n$. In general, such a factor produces a severe attenuation at frequencies exceeding $2\pi/nt$. Thus, the time-constants in these factors can be estimated by noting the frequency at which the high-frequency cut-off begins. In practice, the two factors of this form are not separable in terms of their effect on the overall transfer function. However, they have been independently measured in excised preparations by Wong, who measured the intracellular voltage directly by means of intra-cellular micro-electrodes (Wong, 1977; Wong and Knight, 1979; Wong et al., 1979). Such measurements provide starting points for estimates of the parameters for our data. For example, Wong's values for t_d, the time constant for dispersion of bump latencies, were approximately one-half of his values for t_b, the time constant for the bump shape; we have preserved this relationship in our choice of parameters to describe the preparation of Figure 6-1: $t_d = 0.0091$ sec, $t_b = 0.019$ sec.

The exponents n_d and n_b control the steepness of the high-frequency amplitude cut-off (as opposed to the frequency at which it occurs), and also the rate of increase of the high-frequency phase lag of the generator potential transfer function with increasing frequency. For our data, the phase effect proved very dramatic, and unambiguously required that $n_d + n_b = 8$. (As further information about these parameters was lacking, we set $n_d = n_b$ in all our parameter sets - see Table II.) This choice of exponents is consistent with Wong's more direct measurements. The time constant t_ℓ, the mean latency of the voltage bumps, produces a small adjustment in the phase of the response, with no effect on amplitude. For the data of Figure 6-1, we used $t_\ell = 0.023$ sec.

Adaptation Parameters.

We consider next those parameters of the generator potential transfer function which describe the adaptation process. For the exponent in the factor $\left[it_a \omega / (1 + it_a \omega) \right]^p$, we chose the value $p = 0.25$, as suggested by the measurements of low-frequency transfer function data by Biederman-Thorson and Thorson (1971). This choice of exponent is consistent with our measurements below 1 Hz, and, as described in the preceding chapters, it correctly accounts for the response of the eye to slowly-moving stimuli. The adaptation time-constant t_a determines the frequency above which adapation ceases to significantly affect the response of the eye, it may be estimated from the position

(relative to the frequency axis) of the increasing portion of the amplitude data (see Fig.6-10). For the data of Figure 6-1, the value $t_a = 0.020$ sec was chosen.

There remains to be determined the parameter R in the factor $(1 - \frac{R}{1+it_a\omega})$, which governs the magnitude of the adaptation effect. In the absence of lateral inhibition, the effect of this factor cannot be formally distinguished from the effect of self-inhibition, which is described by a factor of similar form. On the other hand, unlike light-adaptation, self-inhibition modifies the effect of lateral inhibition. This allows the independent determination of the parameters of self-inhibition (see below). Once these are estimated, the parameter R may then be adjusted to account for the residual attenuation of the response at low frequencies. (The ratio of the response at low frequencies to that at intermediate frequencies is proportional to 1 - R.) For the preparation of Figure 6-1, this procedure resulted in the value R = 0.89.

Lateral inhibition.

The lateral inhibition transfer function $T_L(\omega)$ is described by four time constants and the ratio of the initial excitatory component to the main inhibitory component (eq. (5.15)) This transfer function controls the transition from attenuation to enhancement of the response to low-spatial-frequency gratings as temporal frequency increases; it also controls the high-

frequency cut-off of lateral inhibition, which sets in at somewhat lower frequencies than the cut-off of the generator potential. The calculated transfer function is most sensitive to these parameters in the region of the "inversion" of the sign of the lateral "inhibitory" interaction (see Fig. 6-10), though it is difficult to systematically describe the effects of the individual time-constants. For the data of Figure 6-1 the best fit was obtained with the magnitude C of the excitatory component set equal to zero; the corresponding time-constant τ_3 becomes undefined. The other time-constants, which then become formally equivalent, were given values of 0.0415, 0.0415, and 0.010 seconds.

Self-inhibition.

The effects of self-inhibition are contained in the transfer function of the encoder mechanism, $E(\omega)$. This transfer function occurs twice in the Hartline-Ratliff model (eq. (5-10): in the numerator, where it describes a high-pass characteristic of the excitatory process, and in the denominator, where it represents a similar feature of the lateral-inhibitory process. As mentioned above, it is difficult to separate the effect of self-inhibition on the excitatory process from that of light-adaptation, though direct measurements of self-inhibition suggest it is a much slower process. We therefore relied mostly on the modulation of lateral inhibition by self-inhibition to determine the self-inhibitory parameters.

It may be recalled that the ratio $K/(1+\kappa)$ was directly determined from the transfer function data at low frequency. With this parameter regarded as fixed, the effect of self-inhibition is to adjust the magnitude of the "inhibitory" tuning effect seen in the intermediate temporal frequency range at low spatial frequencies.[*] Thus, the size of this tuning peak effectively fixes the strength of self-inhibition. For the data of Figure 6-1 the value $\kappa = 1.0$ was obtained. The time-constant τ was then selected to best fit the overall width of the transfer-function peaks. For the data of Figure 6-1 the value $\tau = 0.125$ sec was chosen. This confirms our assumptions that self-inhbition is considerably slower than light-adaptation ($t_a = 0.020$ sec). After the parameters for self-inhibition were estimated, the adaptation parameters were readjusted as described above. No further improvement in the fit of the model was obtained by further iterating the procedure.

---

*This may be demonstrated as follows: As above, define ξ_0 such that $\tilde{k}(\xi_0) = 0$, and set $Q_0 = F(\xi_0,0)/F(0,0) = 1 + \frac{K}{1+\kappa}$ (eq. (6.14)). We regard Q_0, and hence $K/(1+\kappa)$ as known. Define ω_p as the frequency such that $|F(0,\omega_p)|$ is maximal, and set $W = F(0,\omega_p)/F(\xi_0,\omega_p)$. W is very nearly real, and measures the magnitude of the tuning effect. As we may safely assume that $E(\omega_p) \doteq 1$, we have $F(0,\omega_p) = G(\omega_p)/(1 + KT_L(\omega_p))$, and $F(\xi_0,\omega_p) = G(\omega_p)$. This yields $W = 1/(1 + KT_L(\omega_p)) = 1/(1 + (1 + \kappa)(Q_0-1)T_L(\omega_p))$. As Q_0 and T_L have been determined, we now fit W by adjusting κ. (Here, $T_L(\omega_p)$ is a complex number whose phase is typically such that increasing κ actually increases $|W|$.)

The model transfer function.

Once all these parameters have been estimated, the
complete model transfer function can be compared with the
data in several ways. A Bode plot of the Hartline-Ratliff
transfer function is shown in Figure 6-11; it is to be compared di-
rectly with Figure 6-1. All of the qualitative features dis-
cussed above are well modeled, as are most of the quantitative
features. The reciprocal loci offer another comparison between
the model and the data: Figure 6-12 shows the locus for a temporal
frequency of 1.03 Hz, and should be compared with Figure 6-3
Loci for several temporal frequencies are shown in Figure 6-13
(compare with Fig. 6-5). The reciprocal loci are well modeled
over a broad range of temporal frequencies. The parameters for
the transfer function of Figure 6-1, are summarized
in Table II.

An alternative strategy for evaluating the accuracy
of the Hartline-Ratliff model is to use the empirical and model
transfer functions to produce Fourier syntheses of the response
of the eye to a moving stimulus, as described in preceding
sections. As was shown in chapter IV, such predictions are in
general extremely accurate, and can be taken as a characterization
of the eye, even when such moving stimuli were not included in the
experimental protocol. Predictions for the response to a square-
wave stimulus moving at several different velocities are shown in
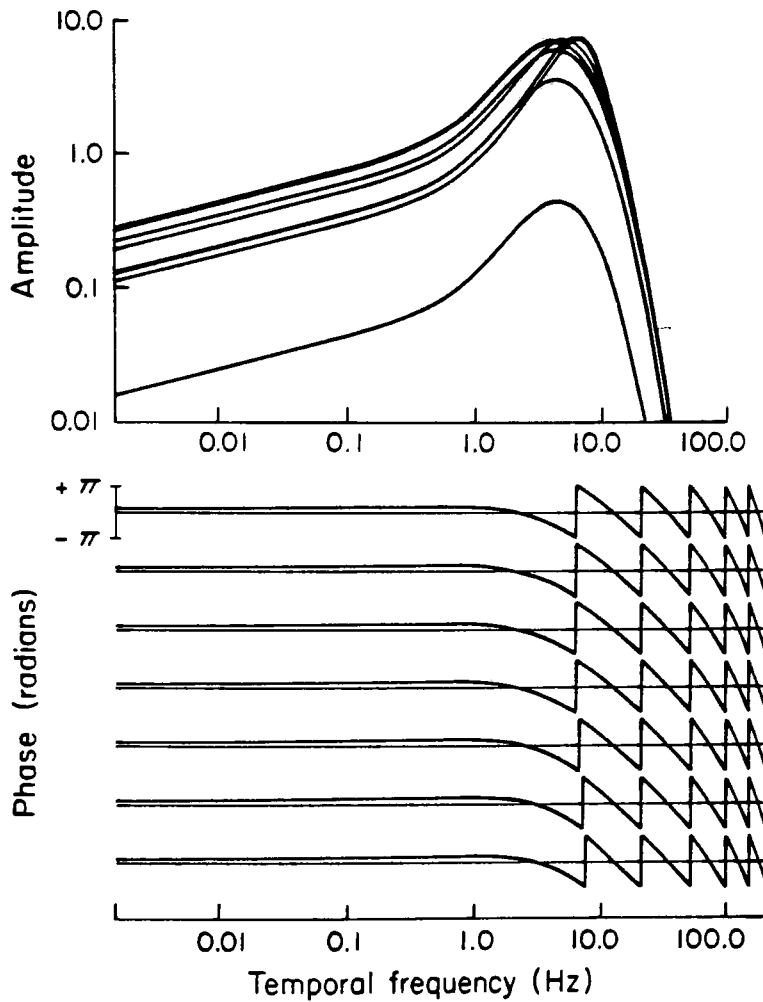
Figure 6-11. Hartline-Ratliff model spatiotemporal transfer function for the Limulus lateral eye. Bode plots (as in Fig.6-1)of predicted response at seven spatial frequencies. Curves are obtained from the equations given in the text (see Table I), with parameters chosen to fit empirical transfer function of Figure 6-1 (see Table II).
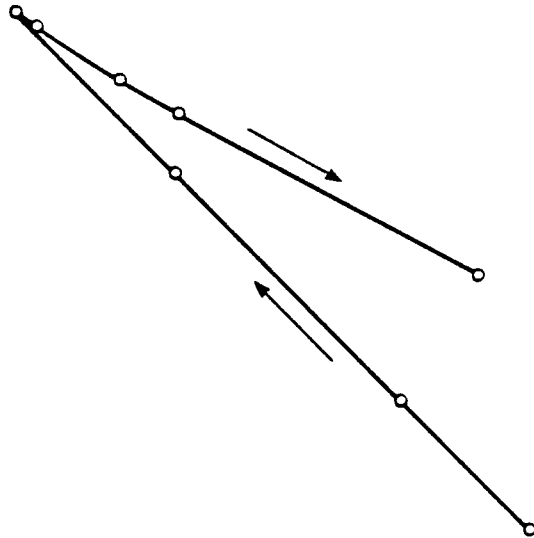
Figure 6-12. Reciprocal locus for temporal transfer frequency
of 1.03 Hz, as predicted by Hartline-Ratliff model, with
parameters as in Figure 6-11. Compare with Figure 6-3.
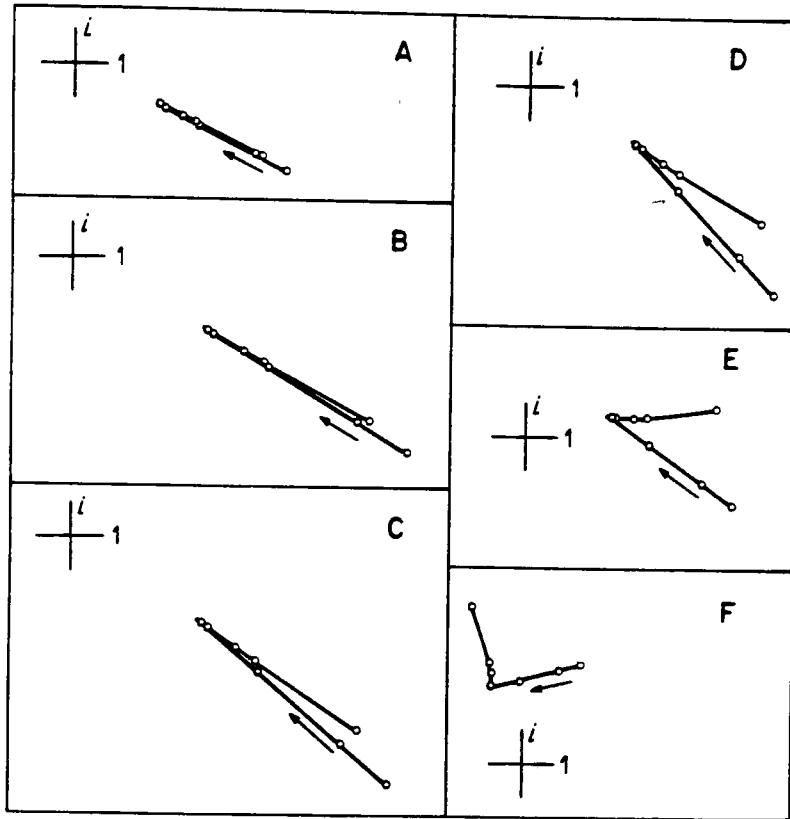
Figure 6-13. Reciprocal loci for six temporal frequencies,
as predicted by Hartline-Ratliff model, with parameters as
in Figure 6-11 (Table II). Compare with Figure 6-5. Temporal
frequencies are (a) 0.1 Hz, (b) 0.23 Hz, (c) 0.5 Hz,
(d) 1.03 Hz, (e) 2.1 Hz, (f) 4.23 Hz. Loci are magnified
by relative factors of 1,2,3,4,6, and 8, respectively.
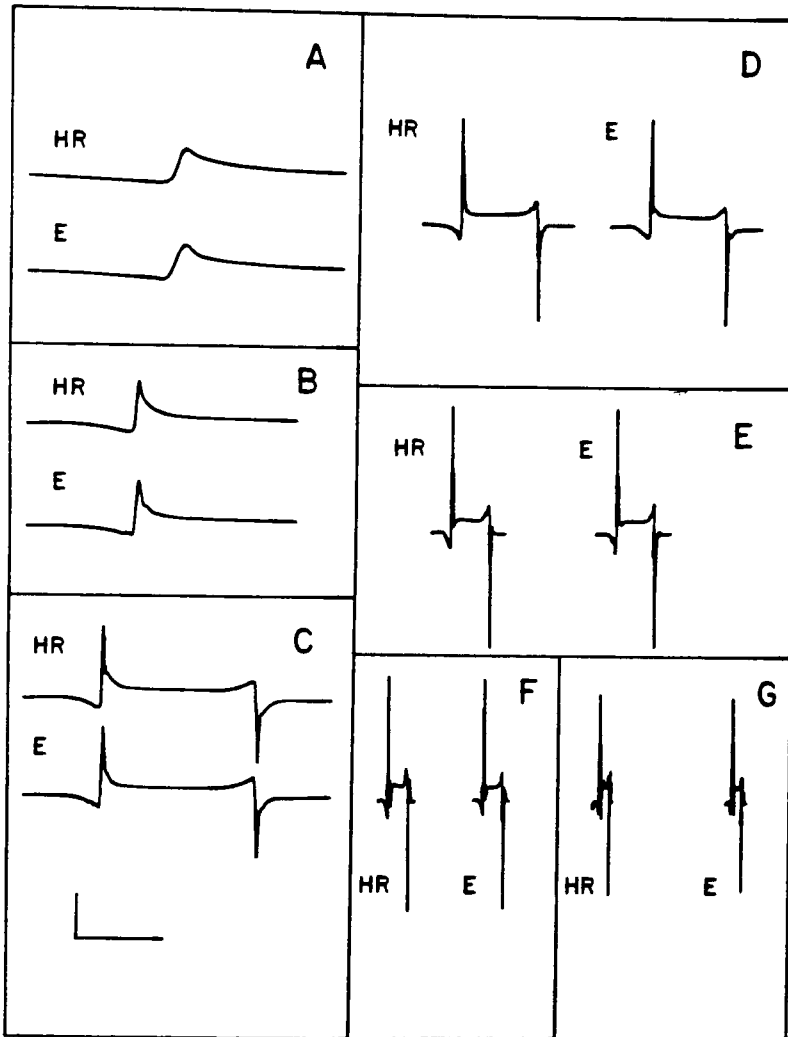
Figure 6-14. Fourier synthesis of the response to a moving square-wave stimulus at several velocities. For each velocity, E denotes response calculated from empirically measured transfer function (Fig. 6-1), and HR denotes response calculated from Hartline-Ratliff model transfer function, with parameters as in Table II (Fig. 6-11). Drift velocities (a) 0.01, (b) 0.03, (c) 0.06, (d) 0.12, (e) 0.24, (f) 0.48, (g) 0.96 eye-widths/sec. Scale marker: horizontal, 10 sec; vertical, 10 impulses/sec.

Figure 6-14. There is excellent agreement between the predictions
derived from the measured transfer function and the Hartline-
Ratliff model. The few small discrepancies are comparable
to those typically seen between actual measured responses to
moving stimuli and the Fourier synthesis predictions of these
responses from measured transfer function data.

A complete linear systems-analysis treatment of the
Limulus eye is represented in Figures 6-15 and 6-16. A comparison
is shown of measured responses to moving square-wave stimuli,
Fourier synthesis predictions obtained from an empirically meas-
ured transfer function, and a transfer function calculated from
the Hartline-Ratliff model (parameters are given in Table II).

The principal features of these square-wave responses
may be readily interpreted in terms of the Hartline-Ratliff
model. At low velocities, lateral inhibition precedes the
arrival of the step at the test-ommatidium, resulting in an
anticipatory "Mach band" in the impulse rate, just before the
on-transient. Also, at low drift velocities, the on-transient
itself is much attenuated. This is due to the predominance of
low-frequency components (to which the eye is relatively insensi-
tive) in the low-velocity stimuli. This predominance is further
enhanced by the optical point-spread effect, which filters out
the high (spatial) frequency components from the moving
stimuli. At higher velocities, the on-transient becomes very
pronounced as the stimulus contains greater spectral power at
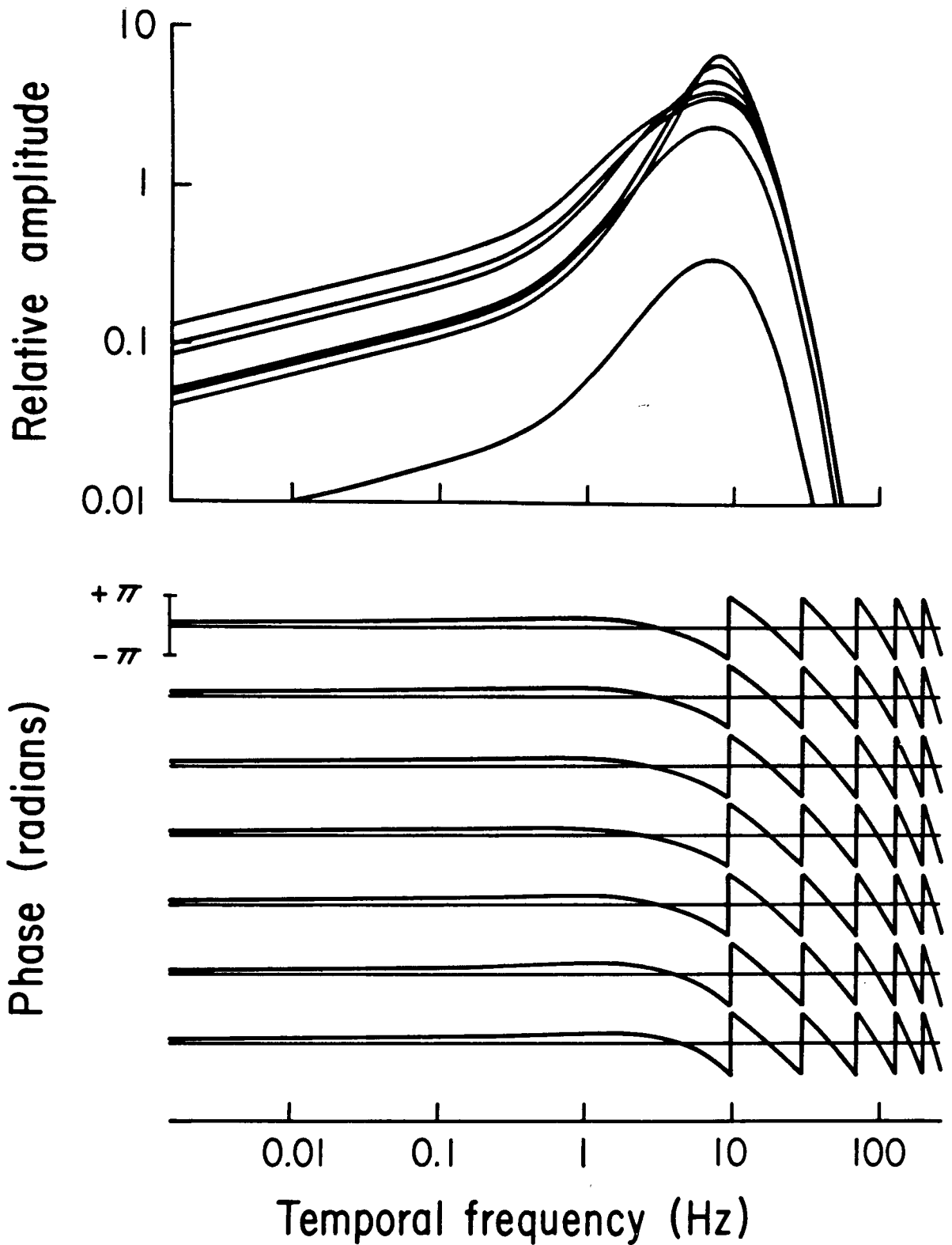
Figure 6-15. Hartline-Ratliff model spatio-temporal transfer function with parameters chosen to fit preparation of Figure 4-3.

Figure 6-16. Fourier synthesis of response to moving square wave stimuli: comparison of predictions derived from empirical and model transfer functions with measured response. Predicted response records denoted by (E), empirical transfer function (Figure 4-3), and (HR), model transfer function (Figure 6-15). Drift velocities: (a) 0.03, (b) 0.06, (c) 0.12, (d) 0.24 eye-widths/sec. Measured response records from Figure 4-5.
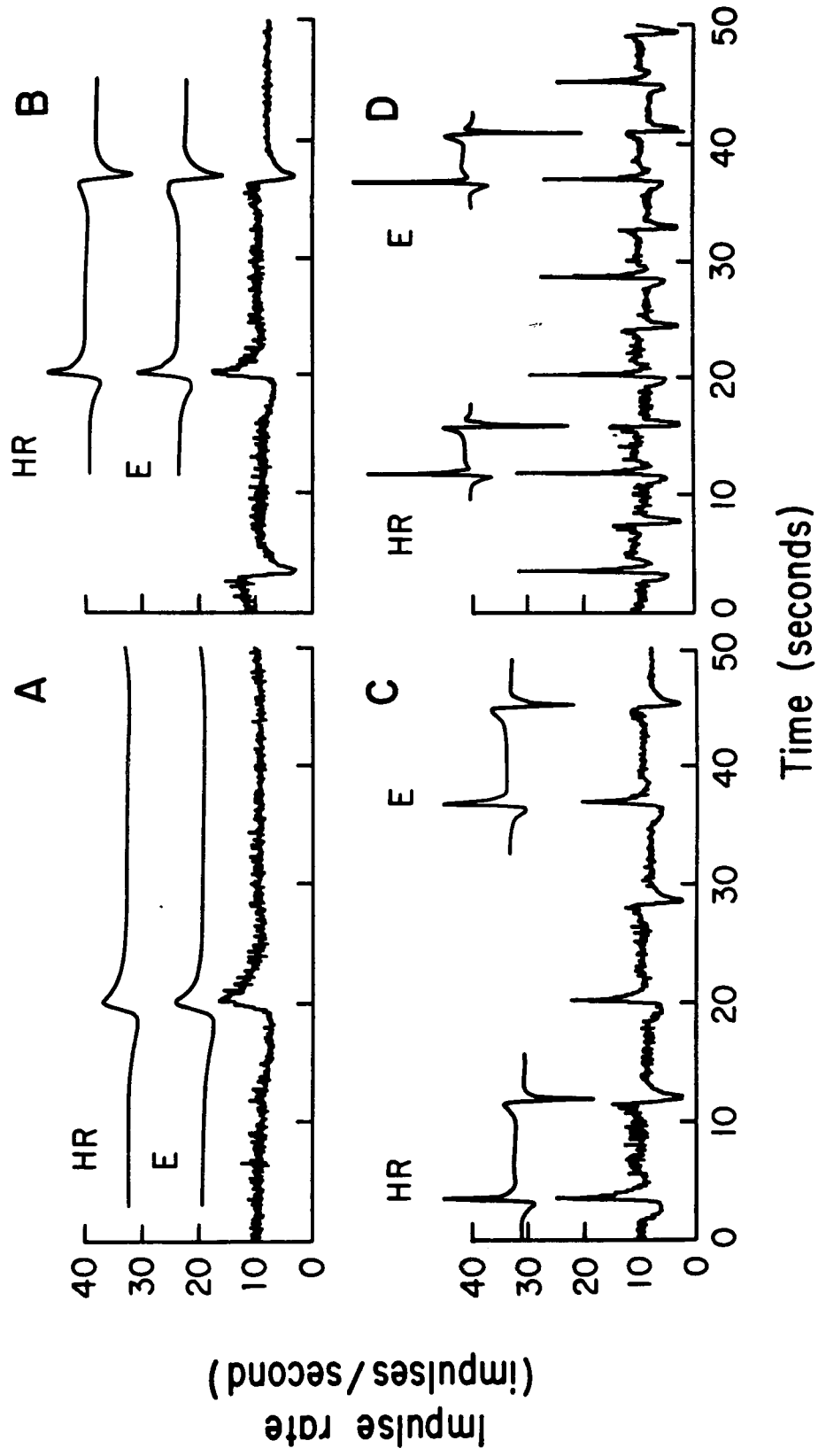
Figure 6-16

frequencies near the peak of the spatio-temporal transfer
function. Due to the nature of a step-transient stimulus,
the on-transient of the response remains large even at very
great velocities.[*]

Discussion.

        The data presented above clearly demonstrate the adequacy
of the Hartline-Ratliff model to explain the dynamic properties
of the Limulus lateral eye, at least those properties concerned
with its responses to small and moderate changes in light
intensity around a mean operating level. Conversely, the success
of this analytic program demonstrates the suitability of our
analysis stimuli, which consist of sinusoidal gratings in space
modulated according to a sum-of-sinusoids signal in time,
for the characterization of this sensory transducer.

---

[*]   It should be noted that the computations of Knight (1973a),
similar to those shown in Figure 6-4, contain a systematic error in
velocity. Due to a programming error, the velocities given in
Knight's Figure 38 should be multiplied by 2π. Those calculations
did not allow for the point-spread effect. The model transfer function
used for the calculations was based on parameters for excised eyes
at room temperature (Knight, Toyoda, and Dodge, 1970). Our heated,
intact preparations show a considerably faster response (see Appendix E);
we calculate that , in our preparations, only steps moving at speeds
of at least 1 eye-width/sec will produce responses with little or
no inhibitory "Mach band" precursor (see chapter VIII).

While the overall performance of the model is excellent, we have avoided attempting to assess the goodness-of-fit in quantitative terms, as there is no well-established estimator of the "distance" between two spatio-temporal transfer functions. Nevertheless, we can state that, except as noted below, the parameters given above are "correct" to within a few percent, in the sense that alteration of any individual parameter by more than that amount produces a demonstrably inferior fit of the model transfer function to the data. We have also considered the possibility of trade-offs between certain parameters (such as those of light-adaptation and self-inhibition). While such trade-offs do occur, the fits obtained with the parameters given above are in general at least as good as those obtained with alternative choices.

Our characterization of the point-spread phenomenon is simple and reliable. The measurements of the inhibitory kernel are more complex. This determination depends strongly on the phase information at high spatial frequency, in order to determine a reference point for the measurement of $\tilde{k}$ from the corrected reciprocal locus. Such phase data are least reliable at these high spatial frequencies, because the point-spread effect substantially attenuates the response to the high-frequency gratings. Nonetheless, at least for data taken below 5 Hz, the consistency of the measurements is very good. (At higher frequencies, there is sufficient noise in the phase

data to render impossible measurements of the inhibitory kernel from data at these frequencies.) Our estimates of the size and strength of the main inhibitory lobe of the kernel are strongly confirmed by the Fourier synthesis calculation at low velocity, which are very sensitive to this feature. While the data consistently indicate, by the characteristic offset of the vertex of the reciprocal locus, the presence of a small crater in the inhibitory kernel, our estimates of its width and strength are somewhat crude (see Appendix E).

The bump-shape parameters of the generator potential transfer function are strongly reflected in the high-frequency amplitude and phase data, and are therefore reliably determined, at least to the extent that they are in principle separable from one another. The strength and time-constant for light adaptation are also well determined. It is not possible to model the data in such a way that adaptation and self-inhibition have similar time-constants, or are combined into a single process

The parameters for the temporal structure of lateral inhibition are buried rather deeply in the model. In particular, the structure constant describing the strength of the initial excitatory feature has little effect on the computed transfer functions; most of the effective delay of the inhibitory transient is accounted for by the three low-pass filter stages. Nonetheless, even those slight variations among the time constants which preserve their sum, but which alter the fastest time constant, result in considerable worsening of the fit of the model to the peaks in the transfer function data.

The determination of the strength of the self-inhibitory process is quite straightforward, and the parameter is thus fixed with considerable accuracy. The time-constant is less strongly reflected in the computations, and is thus less rigidly determined. It may also be noted that we have determined the effective parameters of the combined effect of self-inhibitory transients and the encoder transduction. Thus, our values for these parameters are, to some extent, also a function of our choice of encoder model (see Appendix E).

The Fourier synthesis comparisons further enhance our confidence in the model. However, in general, they are less sensitive to the choice of parameters than are the Bode plots or reciprocal loci, because they constitute, in effect, averages over a large number of spatio-temporal frequencies.

Our choice for the parameters of the Hartline-Ratliff model may be compared with those determined by more direct means in other studies (see Appendix E). In general, the agreement is very good, considering our indirect methods, and the elevated temperature of our preparation, which considerably "speeds up" the time scale of the eye. Comparison of our measurements of the inhibitory kernel with other measurements is rather complex, and is discussed separately (Appendix E).

We thus conclude that the spatio-temporal transfer function provides a convenient and concise characterization of the dynamics of the _Limulus_ retina. This characterization can be readily interpreted in terms of component processes of the visual transduction, and quantitative descriptions of these component transductions can be obtained from the transfer function data. The Hartline-Ratliff model summarizes this analysis, and provides good quantitative predictions of the integrated response of the eye.

"There is something fascinating about science. One gets such wholesale returns of conjecture out of such a trifling investment of fact."

Mark Twain, 1883

VII. Wiener Hopf theory

The theory and experiments of the previous chapters have been predicated on the assumption that the Limulus retina constitutes a homogeneous neural network, in which all the neurons are dynamically equivalent. While this treatment is adequate for neurons located well within the interior of the eye, it clearly does not apply to neurons in the vicinity of the eye's boundary. Such neurons must necessarily possess asymmetrical inhibitory fields, and should therefore be dynamically distinguishable from neurons in the interior. This chapter describes an extension of the linear analysis presented above to include the case of a test ommatidium located at or near the boundary of an otherwise homogeneous neural network. The predictions derived from this analysis are compared with appropriate experiments in the subsequent chapter.

Consider first the homogeneous infinite one-dimensional neural network treated in previous chapters. In order to introduce a boundary into this system, we simply remove that portion of the neural network lying to the left side of the origin. This results in a semi-infinite system of identical neurons, each of which interacts with its neighbors in the same fashion as in the full infinite network, except that those neurons immediately to the right of the boundary now receive no lateral

inhibition from the "missing" portion of the network. Likewise, any inhibitory effects formerly exerted by neurons which lie to the right of the origin on those to the left are simply lost. In other words, we assume that the neural network is abruptly truncated at the origin, with no alteration of the basic pattern of neural connectivity in the vicinity of the boundary.

In preparation for the modelling of the response of the truncated network, it is instructive to rewrite the time-dependent Hartline-Ratliff equation (Eq.(5.7)) for the full eye as follows:

$$\tilde{R}(x,\omega) = E(\omega) \left[G(\omega) \cdot P(x)*\tilde{S}(x,\omega) - T_L(\omega) \int_{-\infty}^{\infty} \tilde{k}(x-y)\tilde{R}(y,\omega)dy \right]. \quad (7.1)$$

Here, $\tilde{S}(x,\omega)$ is the Fourier transform in time of the stimulus $S(x,t)$, $\tilde{R}(x,\omega)$ is the temporal transform of the response. The transfer functions for the encoder, generator potential, and lateral inhibitory transductions are denoted by $E(\omega)$, $G(\omega)$, and $T_L(\omega)$, respectively. $P(x)$ denotes the optical point spread function (in the spatial domain), and the $*$ indicates a convolution with respect to space. In the last term, which represents the spatial summation of lateral inhibition, k denotes the lateral inhibitory kernel, and the spatial convolution has been written out to emphasize the infinite limits of integration appropriate to the treatment of the full eye.

We may separate the underlying physiology, which is complicated, from the mathematical structure of equation (7.1), which

is simple, by introducing the following definitions:

$$\tilde{Q}(x,\omega) \equiv E(\omega) \cdot G(\omega) : P(x) * \tilde{S}(x,\omega) \tag{7.2}$$

$$S(\omega) \equiv E(\omega) \cdot T_L(\omega) \tag{7.3}$$

With this notation, eq (7.1) becomes simply

$$\tilde{R}(x,\omega) = \tilde{Q}(x,\omega) - S(\omega) \int_{-\infty}^{\infty} \tilde{k}(x-y)\tilde{R}(y,\omega)dy \tag{7.4}$$

This equation is readily solved by Fourier transformation with respect to space*:

$$\tilde{R}(\xi,\omega) = \tilde{Q}(\xi,\omega) - S(\omega)\cdot\tilde{k}(\xi)\cdot \tilde{R}(\xi,\omega),$$

or

$$\tilde{R}(\xi,\omega) = \tilde{Q}(\xi,\omega) \quad \frac{1}{1+S(\omega)\tilde{k}(\xi)} \quad . \tag{7.5}$$

In this last form, the quantity $\tilde{Q}$ can be regarded as a generalized input to an abstract feedback system characterized by the transfer function $1/[1+S(\omega)\tilde{k}(\xi)]$. Equivalently, this transfer function can be regarded as the Fourier transform in space and time of the response of the abstract system to a delta-function input. From this point of view, the factor $1/[1+S(\omega)\tilde{k}(\xi)]$ can be considered as the "solution operator" for the full eye problem.

---

*Functions which have been Fourier transformed with respect to both space and time will be indicated by the use of the frequency domain argument variables ξ and ω.

It follows immediately from the remarks above that the Hartline-Ratliff equations for the truncated retina (analogous to equations (7.1) and (7.4)) may be obtained by simply modifying the limits of integration in the lateral inhibitory terms to reflect the truncated array of inhibiting neurons:

$$\tilde{R}(x,\omega) = E(\omega) \left[G(\omega) \cdot P(x) * \tilde{S}(x,\omega) \right.$$

$$\left. - T_L(\omega) \int_0^\infty k(x-y) \tilde{R}(y,\omega) dy \right], \quad x \geq 0$$

(7.6)

or

$$\tilde{R}(x,\omega) = \tilde{Q}(x,\omega) - S(\omega) \int_0^\infty k(x-y) \tilde{R}(y,\omega) dy, \quad x \geq 0. \tag{7.7}$$

These equations are valid only for $x \geq 0$, as the response R is undefined for $x \leq 0$, where the neural network has been removed.

Equation (7.7) cannot be solved by direct application of the Fourier transform, because the inhibitory term is no longer a convolution integral. However, under suitable hypotheses on the functions $\tilde{Q}$ and k, the equation can be solved by means of the so-called Wiener-Hopf technique (Wiener and Hopf, 1931; Noble, 1958). This solution (Sirovich, 1979) is presented below, for the special case of uniformly moving stimuli.

For such a moving stimulus $S(x,t) = S(x-vt)$, the "effective stimulus" at the retina is again given by a simple convolution: $P(x)*S(x,t) = (P*S)(x-vt)$. This has the Fourier transform in time

$$(P*S)\widetilde{\ }(x,\omega) = \int(P*S)(x-vt)e^{-i\omega t}dt$$

$$= \frac{1}{v}\, e^{-i\frac{\omega}{v}x} \cdot \tilde{P}(\frac{-\omega}{v}) \cdot \tilde{S}(\frac{-\omega}{v})\ . \qquad (7.8)$$

In this equation, only the factor $e^{-i\frac{\omega}{v}x}$ depends on space (which is the variable of integration in equation (7.7)). We may thus further simplify the problem at hand by setting

$$\tilde{Q}(x,\omega) = \tilde{P}(\omega) \cdot e^{-i\frac{\omega}{v}x}\ , \qquad (7.9)$$

whence

$$\tilde{P}(\omega) = \frac{1}{v}\, E(\omega)G(\omega)\tilde{P}(\frac{-\omega}{v})\tilde{S}(\frac{-\omega}{v}) \qquad (7.10)$$

It then follows from the linearity of the integral operator that if $\tilde{\phi}(x,\omega)$ satisfies the equation

$$\tilde{\phi}(x,\omega) = e^{-i\frac{\omega}{v}x} - S(\omega)\int_0^\infty k(x-y)\tilde{\phi}(y,\omega)dy\ , \quad x\geq 0\ , \qquad (7.11)$$

then the solution $\tilde{R}(x,\omega)$ to the original equation (7.7) is given by the product

$$\tilde{R}(x,\omega) = \tilde{P}(\omega) \cdot \tilde{\phi}(x,\omega)\ . \qquad (7.12)$$

Thus $\tilde{\Phi}(x,\omega)$ serves as the solution operator for the response of the truncated neural network to moving stimuli. Accordingly, we now direct our attention the the solution of equation (7.11).

In order to apply the Wiener-Höpf technique to equation (7.11), we first extend the domain of $\tilde{\Phi}(x,\omega)$ by setting

$$\tilde{\Phi}(x,\omega) = 0 \ , \ x<0 \tag{7.13}$$

Similarly, we define

$$-\tilde{\Theta}(x,\omega) = \begin{cases} e^{-i\frac{\omega}{v}x} - S(\omega)\int_0^\infty k(x-y)\tilde{\Phi}(y,\omega)dy, & x\leq 0 \\ 0 \ , & x>0 \ . \end{cases} \tag{7.14}$$

Combining these definitions with equations (7.11), we obtain

$$\tilde{\Phi}(x,\omega) = e^{-i\frac{\omega}{v}x} + \tilde{\Theta}(x,\omega) - S(\omega)\int_{-\infty}^\infty k(x-y)\tilde{\Phi}(y,\omega)dy \ , \ -\infty<x<\infty \ . \tag{7.15}$$

This equation is valid for all real x, and, by virtue of equation (7.13), contains a convolution integral which runs over the full real line. Fourier transformation of (7.15) with respect to space now yields

$$\tilde{\Phi}(\xi,\omega) = 2\pi\delta(\xi-(\frac{-\omega}{v})) + \tilde{\Theta}(\xi,\omega) - S(\omega)k(\xi)\tilde{\Phi}(\xi,\omega) \ . \tag{7.16}$$

We thus convert the intractable integral equation (7.11) into a single functional equation which contains two unknown, albeit

related, functions $\tilde{\Phi}$ and $\tilde{\Theta}$. Fortunately, these functions, by virtue of their definitions as Fourier transforms, possess analyticity properties which enable the solution of the equation. We have

$$\breve{\Phi}(\xi,\omega) = \int_0^\infty e^{-i\xi\omega}\ \tilde{\Phi}(x,\omega)dx$$

and   (7.17)

$$\breve{\Theta}(\xi,\omega) = \int_{-\infty}^0 e^{-i\xi\omega}\ \tilde{\Theta}(x,\omega)dx \quad .$$

It follows from the analyticity of the complex exponential function that $\breve{\Phi}(\xi,\omega)$ and $\breve{\Theta}(\xi,\omega)$ are analytic functions of the complex variable ξ wherever the corresponding integrals in (7.17) are convergent. Thus, under the assumption that $\tilde{\Phi}(x,\omega)$ is as integrable function of x, it follows that $\breve{\Phi}(\xi,\omega)$ is analytic for $Im(\xi) \leq 0$. Since the response must be finite, and must fall to zero roughly as fast as the inhibitory kernel, this integrability assumption thus follows from the underlying physiology. As for $\tilde{\Theta}$, it follows from equation (7.14) that, since k(x) is an integrable function (the total inhibitory strength is finite), $\tilde{\Theta}(x,\omega)$ is likewise integrable (the exponential term is no problem), whence $\breve{\Theta}(\xi,\omega)$ is analytic for $Im(\xi) > 0$. In order to help keep track of these facts, we will henceforth label functions which are analytic in the

upper half plane by a superscript plus sign ($^+$), and will label functions analytic in the lower half plane by a superscript minus sign ($^-$).

The formula (7.17) also provides a useful estimate of the growth of $\tilde{\Phi}(\xi,\omega)$ as $|\xi| \to \infty$. Integration by parts yields

$$\tilde{\Phi}(\xi,\omega) = \tilde{\Phi}(x,\omega) \left. \frac{e^{-i\xi\omega}}{-i\xi} \right]_0^\infty - \int_0^\infty \frac{e^{-i\xi\omega}}{-i\xi} \frac{\partial}{\partial x} \tilde{\Phi}(x,\omega)dx \ .$$

For $\text{Im}(\xi)<0$, the first term is convergent. As for the second term the Riemann-Lebesgue lemma asserts that it is of order smaller than $\frac{1}{\xi}$.* We may thus conclude that, as $|\xi| \to \infty$,

$$\tilde{\Phi}^-(\xi,\omega) = \frac{\tilde{\Phi}(x=0,\omega)}{i\xi} + o(\tfrac{1}{\xi}) \quad , \quad \text{Im}(\xi) \leq 0 \quad . \tag{7.18}$$

Likewise, for $\tilde{\Theta}^+$, we obtain, for $|\xi| \to \infty$

$$\tilde{\Theta}^+(\xi,\omega) = \frac{\tilde{\Theta}(x=0,\omega)}{i\xi} + o(\tfrac{1}{\xi}) \quad , \quad \text{Im}(\xi) > 0 \quad . \tag{7.19}$$

In the same spirit, we may represent the delta function in equation (7.16) in the following form:

---

*The Riemann-Lebesgue lemma (Katznelson, 1968, p.123; Sirovich, 1971, pp.63-64) states that if $\tilde{f}(\xi)$ is the Fourier transform of an integrable function f, then $\lim_{\xi \to \infty} \tilde{f}(\xi)=0$.

$$2\pi\delta(\xi-(\tfrac{-\omega}{v})) = \tfrac{1}{i}(\frac{1}{\xi-(\tfrac{-\omega}{v})-i\epsilon} - \frac{1}{\xi-(\tfrac{-\omega}{v})+i\epsilon}) \quad . \ *$$

(7.20)

Insertion of this relation into equation (7.16) yields

$$\tilde{\Phi}^-(\xi,\omega)(1+S(\omega)\tilde{k}(\xi)) - \tfrac{1}{i}(\frac{1}{\xi-(\tfrac{-\omega}{v})-i\epsilon})^- = \tfrac{-1}{i}(\frac{1}{\xi-(\tfrac{-\omega}{v})+i\epsilon})^+ + \tilde{\Theta}(\xi,\omega)^+$$

(7.21)

Now, suppose that $1 + S(\omega)\tilde{k}(\xi)$ is in fact a rational function of ξ (that is, a quotient of polynomials in ξ). In this case, we could set

$$1 + S(\omega)\tilde{k}(\xi) = \frac{Y^-(\xi,\omega)}{Z(\xi,\omega)} \quad , \qquad (7.22)$$

where Y^- is analytic in the lower half-plane, with a pole of finite order at infinity, and $Z(\xi,\omega) = \Pi_j(\xi-\lambda_j)$, where the λ_j are the locations of those poles of $1+S(\omega)\tilde{k}(\xi)$ which lie in the lower half-plane. We could then rearrange equation (7.21) so as to segregate the various terms according to their regions of analyticity:

$$\tilde{\Phi}(\xi,\omega) \cdot Y^-(\xi,\omega) - Z(\xi,\omega) \cdot \tfrac{1}{i}(\frac{1}{\xi-(\tfrac{-\omega}{v})-i\epsilon})^-$$

$$= Z(\xi,\omega)(\tfrac{-1}{i})(\frac{1}{\xi-(\tfrac{-\omega}{v})+i\epsilon})^+ + Z(\xi,\omega)\tilde{\Theta}^+(\xi,\omega) \quad . \qquad (7.23)$$

---

* This represents the delta function in the sense that an integral along the real line may be evaluated by closing a contour in either half plane and applying the Cauchy integral formula.

Since $Z(\xi,\omega)$ is a polynomial, the left-hand side of this equation is analytic in the lower half-plane, while the right-hand side is analytic in the upper half-plane. Thus, either side of equation (7.23) in fact represents a function which is analytic in the entire complex plane. Furthermore, the fact that $Y^-(\xi,\omega)$ has a pole of finite order at infinity, taken together with the estimates of (7.18) and (7.19) implies that this entire function itself has a pole of finite order at infinity. It then follows from a well-known theorem in the theory of functions of a complex variable[*] that the entire function represented by (7.23) must be a polynomial. This polynomial may in general be determined by careful examination of the structure of equation (7.23), from which the solution operator $\Phi^-(\xi,\omega)$ may then easily be recovered. This line of reasoning constitutes the method of Wiener and Hopf for the solution of the integral equation (7.11).

The difference-of-Gaussians form for the lateral inhibitory kernel used in the preceding chapters is not particularly well suited for this treatment, as it possesses an essential singularity, rather than a pole of finite order, at infinity. Though an exact (if tedious) Wiener-Hopf treatment is possible for this kernel, we have found it convenient to adopt a different functional form to represent the inhibitory kernel data. A suitable choice is the rational expression

$$\tilde{k}(\xi) = \frac{N(\xi^2)}{D(\xi^2)} , \qquad (7.24)$$

---

[*]Liouville's theorem: A bounded function analytic on the whole complex plane is constant (Rudin, 1974, p.228; Noble, 1958, p.6)

where N and D are polynomials with real coefficients. In general, one may choose D to have leading coefficient equal to one. This form reflects the fact that the kernel k(x) must be a real-valued, even function of x. Finally, the Riemann-Lebesgue lemma requires that the degree of N be less than the degree of D. (We will denote by M the degree of D in ξ^2; thus D is of degree 2M in ξ.) The specific polynomials adopted for the representation of our Limulus data will be discussed later.

By virtue of equation (7.24), we have

$$1 + S(\omega)\tilde{k}(\xi) = \frac{D(\xi^2)+S(\omega)N(\xi^2)}{D(\xi^2)} . \tag{7.25}$$

In order to accomplish the factorization indicated in equation (7.22), we set

$$D(\xi^2) + S(\omega)N(\xi^2) = \prod_{\ell=1}^{M} (\xi^2-\mu_\ell^2(\omega)) \tag{7.26}$$

and (7.27)

$$D(\xi^2) = \prod_{m=1}^{M} (\xi^2-\lambda_m^2) .$$

If we assume that the retina is a stable dynamic system (a reasonable assumption for our experiments, but see also Barlow and Fraioli (1978)), then it follows from a consideration of equation (7.5) that for real ω, none of the roots μ_ℓ lie on the real line (see Sirovich, 1979). Since the left hand side of equation (7.25) is known to be nonsingular for real ξ, it

follows that none of the roots λ_m lie on the real line either.
Thus we may fix the choice of roots in equations (7.26, 7.27)
by adopting the convention that the roots μ_ℓ, λ_m lie in the
upper half-plane. Then

$$Z(\xi,\omega) = \prod_{m=1}^{M}(\xi+\lambda_m) \ ,$$

and

$$Y^-(\xi,\omega) = \prod_{\ell=1}^{M}(\xi^2-\mu_\ell^2(\omega))\Big/\prod_{m=1}^{M}(\xi-\lambda_m) \ ,$$

and equation (7.23) becomes

$$\tilde{\Phi}^-(\xi,\omega) \cdot \frac{\prod\limits^{M}(\xi^2-\mu_\ell^2(\omega))}{\prod\limits^{M}(\xi-\lambda_m)} - \prod^{M}(\xi+\lambda_m) \cdot \frac{1}{i}(\frac{1}{\xi-(\frac{-\omega}{v})-i\varepsilon})^-$$

$$= \prod^{M}(\xi+\lambda_m)(\frac{-1}{i})(\frac{1}{\xi-(\frac{-\omega}{v})+i\varepsilon})^+ + \prod^{M}(\xi+\lambda_m) \cdot \tilde{\Theta}^+(\xi,\omega) \ . \tag{7.28}$$

As described above, we now observe that the left hand side of
this equation is analytic in the lower half-plane, while the
right hand side is analytic in the upper half-plane.
Since the two forms agree on the real axis, they must
therefore be analytic continuations of each other. Thus
the two sides of equation (7.28) represent a single
function $f(\xi,\omega)$ which is analytic on the entire complex
ξ-plane. Indeed since both $\tilde{\Phi}^-(\xi,\omega)$ and $\theta^+(\xi,\omega)$ are of
order $1/\xi$ as $\xi\to\infty$, every term in (7.28) is of order ξ^{M-1}
as $\xi\to\infty$. It follows, as indicated above, that

$$f(\xi,\omega) = \sum_{n=0}^{M-1} a_n(\omega)\xi^n \, , \tag{7.29}$$

where the coefficients $a_n(\omega)$ are functions ω which are yet to be determined.

To this end, we equate the left hand side of (7.28) with the right hand side of (7.29), and solve for the solution operator $\tilde{\Phi}^-(\xi,\omega)$:

$$\tilde{\Phi}^-(\xi,\omega) = \frac{\prod\limits_{m}^{M}(\xi-\lambda_m)}{\prod\limits_{\ell}^{M}(\xi^2-\mu_\ell^2(\omega))}\left[\sum_{n=0}^{M-1} a_n(\omega)\xi^n + \prod_{m}^{M}(\xi+\lambda_m)\ \frac{1}{i}\left(\frac{1}{\xi-(\frac{-\omega}{v})-i\varepsilon}\right)\right] . \tag{7.30}$$

We can now determine the a_n by observing that, since the left hand side of (7.30) is analytic in the lower half-plane, the apparent poles of the right hand side located at $\xi = -\mu_\ell(\omega)$ must, in fact, be cancelled by corresponding zeroes of the bracketed expression on the right side of (7.30). This condition can be expressed in two useful ways. First, we can write the bracketed expression in (7.30) over a common denominator, and then express the numerator in factored form. This yields

$$\tilde{\Phi}^-(\xi,\omega) = \frac{\prod_m^M (\xi-\lambda_m)}{\prod_\ell^M (\xi-\mu_\ell(\omega))(\xi+\mu_\ell(\omega))} \cdot \left[\frac{(1+ia_{M-1})\prod_\ell^M (\xi+\mu_\ell(\omega))}{i(\xi-(\frac{-\omega}{v})-i\varepsilon)}\right] ,$$

or

(7.31)

$$\tilde{\Phi}^-(\xi,\omega) = \frac{\prod_m^M (\xi-\lambda_m)}{\prod_\ell^M (\xi-\mu_\ell(\omega))} \cdot \frac{1+ia_{M-1}}{i(\xi-(\frac{-\omega}{v})-i\varepsilon)} . \tag{7.31}$$

Alternatively, we can equate the bracketed expression of (7.30) to zero for $\xi =-\mu_\ell(\omega)$, and then obtain a set of M simultaneous equations for the a_n:

$$\sum_{n=0}^{M-1} a_n \cdot (-\mu_\ell(\omega))^n = \frac{\prod_m^M (-\mu_\ell(\omega)+\lambda_m)}{i(\mu_\ell(\omega)+(\frac{-\omega}{v}))} , \quad \ell=1,2,\ldots,M . \tag{7.32}$$

Here we have set $\varepsilon= 0$, as we are interested in the algebraic, rather then the analytic structure of (7.32).

If we let ξ approach infinity in (7.31), and compare the result with (7.18), we find that

$$\tilde{\Phi}(x=0,\omega) = 1 + ia_{M-1}(\omega) , \tag{7.33}$$

whence

$$\tilde{\Phi}^-(\xi,\omega) = \frac{\tilde{\Phi}(x=0,\omega)}{i(\xi-(\frac{-\omega}{v})-i\epsilon)} \cdot \frac{\prod\limits_m^M(\xi-\lambda_m)}{\prod\limits_\ell^M(\xi-\mu_\ell(\omega))} . \tag{7.34}$$

Thus, the entire problem hinges on the determination of the coefficient $a_{M-1}(\omega)$ from (7.32). This calculation, which involves merely linear algebra, is taken up in appendix D. The result, which little reflects the algebra from which it derives, is

$$\tilde{\Phi}(x=0,\omega) = 1 + ia_{M-1}(\omega) = \prod\limits_j^M \frac{\frac{-\omega}{v} + \lambda_j}{\frac{-\omega}{v}+\mu_j(\omega)} . \tag{7.35}$$

It is instructive to compare this result with the analogous solution operator at x = 0 for the full eye. It is readily deduced from (7.5) that this is simply obtained from (7.25, 26, and 27) by identifying ξ with $-\frac{\omega}{v}$, and taking reciprocals:

$$\tilde{\Phi}(x=0,\omega)_{\text{full eye}} = \prod\limits_j^M \frac{(\frac{-\omega}{v})^2-\lambda_j^2}{(\frac{-\omega}{v})^2-\mu_j^2(\omega)} , \tag{7.36}$$

or $\tilde{\Phi}(x=0,\omega)_{truncated} = \tilde{\Phi}(x=0,\omega)_{full\ eye} \cdot \prod_j^M \dfrac{(\frac{-\omega}{v})-\mu_j(\omega)}{(\frac{-\omega}{v})-\lambda_j}$

$$(7.37)$$

We note that, unlike the result (7.35) for the truncated network, the full eye response is indifferent to the sign of v.

In practice, the responses in the time domain corresponding to these formulas for $\tilde{\Phi}(x=0,\omega)$ are calculated numerically by means of the Fast Fourier Transform algorithm. Nevertheless, it is useful to consider the form of the Fourier inversions in time. We have

$$\tilde{\Phi}(x=0,t) = \frac{1}{2\pi} \int_{-\infty}^{\infty} e^{+i\omega t} \tilde{\Phi}(x=0,\omega)d\omega , \qquad (7.38)$$

where either the truncated network result (7.35) or the full eye result (7.36) may be used for $\tilde{\Phi}$. For t<0, the integral may be evaluated by contour integration in the lower half of the complex ω-plane. In the full eye case, we may observe that, since the poles of $\tilde{\Phi}$ occur in both half planes, the response of the network anticipates the arrival of the stimulus at the origin. This phenomenon has been abundantly demonstrated in previous chapters.

On the other hand, in the case of the truncated network, we note that, whenever v is positive (that is, the stimulus moves from left to right, and approaches the origin from the inactive side of the network), the solution operator (7.35) has no poles in the lower half-plane, since the roots $\mu_j(\omega)$ have positive imaginary parts. Furthermore, it can be shown that the denominator of (7.35) has no branch points in the lower half-plane (Sirovich, 1979). It follows that, for v>0, the network produces a flat response until the stimulus arrives at the origin, at t=0. There are no Mach band procursors. This is precisely what is to be expected from the truncated network, which is inactive to the left of the origin. When v<0, the expression (7.35) has poles in the lower half-plane, and yields a non-zero anticipatory response.

Away from the origin, the full-eye response is simply a suitably retarded (or advanced) replay of the response produced at x=0:

$$\Phi(x,t) = \Phi(x=0, \ t-\frac{x}{v}) \ , \tag{7.39}$$

or

$$\tilde{\Phi}(x,\omega)_{full \ eye} = \tilde{\Phi}(x=0,\omega)_{full \ eye} \cdot e^{i(\frac{-\omega}{v})x} \ . \tag{7.40}$$

In order to obtain the response of the truncated network, away from the origin, we perform a Fourier inversion in space on the expression (7.34):

$$\tilde{\Phi}(x,\omega) = \frac{1}{2\pi} \int \frac{e^{+i\xi x}\ \tilde{\Phi}(x=0,\omega)}{i(\xi-(\frac{-\omega}{v})-i\varepsilon)}\ \frac{\prod_m^M(\xi-\lambda_m)}{\prod_\ell^M(\xi-\mu_\ell(\omega))}\ d\xi\ . \tag{7.41}$$

For x<0, this integral may be evaluated by means of contour integration in the lower half of the complex ξ-plane; we simply note that the roots $\mu_\ell(\omega)$ all lie in the upper half plane, so that $\tilde{\Phi}(x,\omega)$ vanishes for x<0. We thus recover the definition (7.13).

For x>0, we evaluate (7.41) by contour integration in the upper half-plane. Each factor in the denominator contributes a residue to the result:

$$\tilde{\Phi}(x,\omega) = \tilde{\Phi}(x=0,\omega)\ \cdot\left\{\prod_j^M \frac{\frac{-\omega}{v}-\lambda_j}{\frac{-\omega}{v}-\mu_j(\omega)}\ \cdot\ e^{i(\frac{-\omega}{v})x}\right. \tag{7.42}$$

$$\left.+\sum_j^M \frac{\prod_m(\mu_j(\omega)-\lambda_m)}{\prod_{\ell+j}(\mu_j(\omega)-\mu_\ell(\omega))}\ \frac{e^{i\mu_j(\omega)x}}{\mu_j(\omega)-(\frac{-\omega}{v})}\right\}\ .$$

In order to compare this result with the response of the full eye, we use (7.37) and (7.40) to obtain the equivalent form

$$\tilde{\Phi}(x,\omega)_{truncated} = \tilde{\Phi}(x,\omega)_{full\ eye} + \tilde{\Phi}(x=0,\omega)_{truncated} \cdot$$

$$\sum_{j}^{M} \frac{\Pi_m(\mu_j(\omega)-\lambda_m)}{\underset{\ell\neq j}{\Pi}(\mu_j(\omega)-\mu(\omega))} \cdot \frac{e^{i\mu_j(\omega)x}}{\mu_j(\omega)-(\frac{-\omega}{v})} \cdot \tag{7.43}$$

We observe that, since the $\mu_j(\omega)$ have positive imaginary parts, as x approaches infinity the second term in (7.43) approaches zero, and the response of the truncated network approaches that of the full eye. Thus, neurons well removed from the retinal boundary do indeed behave as if they were located in the midst of an infinite neural network.

In summary, the response of either the full eye or the truncated network may be computed by multiplying the Fourier transform of the stimulus pattern by a suitable "transfer function" (obtained by combining equations (7.10), (7.12) and either (7.40) or (7.43))

$$\tilde{R}(x,\omega) = \tilde{S}(\frac{-\omega}{v}) \cdot \frac{1}{v} E(\omega)G(\omega)P(\frac{-\omega}{v}) \cdot \tilde{\Phi}(x,\omega) \quad , \tag{7.44}$$

and then obtaining the Fourier inversion in time.

```
        I go past a stone
        by the road twice a day
        in my regular
              toing and froing.
        The sight of it tells me
        I'm over half way --
        whether I'm
              coming or going.
```

<div align="right">

("The Optimist's Obelisk")
Piet Hein, 1973
</div>

VIII. Comparison of the Wiener-Hopf theory with Experiment.

In this chapter we present the results of experiments which permit comparison of the quantitative predictions of the theory developed in the previous chapter with the measured responses of _Limulus_ retinal neurons. We begin by outlining the theoretical considerations on which the experimental designs were based.

The truncated neural network model treated in the last chapter does not lend itself to direct application to neurons located near the anatomical boundary of the _Limulus_ eye. The principal difficulty lies in the estimation of the model parameters which form the basis for the theoretical calculations. In general, we determine these parameters from a detailed analysis of the empirical spatiotemporal transfer function $F(\xi,\omega)$ of the neuron under study, as described in chapter VI. The empirical transfer function, in turn, is obtained from experiments which are based on the assumption that the test-ommatidium under investigation is located in the midst of a homogeneous, isotropic neural network.[*]

---

*   The two assumptions of homogeneity and isotropy play dif-
ferent roles in the theory. As far as the analysis-synthesis
experiments of the sort described in chapters III and IV are
concerned, the only consequence of the isotropy assumption is
that it allows the measurement of the transfer function
by means of counterphase modulated cosine grating stimuli.
Were this assumption to fail, the synthesis protocol
would continue to hold, provided that the responses to
counterphase modulated sine gratings (that is, sinusoidal
gratings placed with a zero-crossing aligned with the
test-ommatidium) were incorporated into the transfer
function. Furthermore, as far as measurements on a single
test ommatidium are concerned, the homogeneity assumption
plays no role at all: the sinusoidal gratings form a
suitable basis for the vector space of <u>stimuli</u>, and only
linearity of the eye, considered as a single-output system,
is necessary to justify the synthesis calculation.

On the other hand, both isotropy and homogeneity
assumptions are necessary for interpretation of the transfer
function measurements in terms of the Hartline-Ratliff model

as presented in chapter IV. The homogeneity assumption
is essential for the description of the summed lateral
inhibition   in terms of a convolution integral, which
permits subsequent factorization under Fourier trans-
formation . As for the isotropy assumption, it serves
only to assure that the inhibitory kernel transform
$\tilde{k}(\xi)$ is real-valued (for ξ-real). This fact is crucial
for the analysis of the reciprocal loci from which we
determined the shape of the inhibitory kernel. However,
should some strategy for the elucidation of k become
available which circumvents this restriction, the isotropy
assumption would no longer be necessary.

The term "isotropy" here refers to the symmetry of
our model one-dimensional retina about each ommatidium
(except near the boundaries of the eye). The two-dimensional
structure of the Limulus retina is not, in fact, strictly
isotropic (see chapter V); the retina does, however, possess
reflection symmetry in all directions about each ommatidium
(except those near the boundary of the eye).

(end of footnote)

Both of these assumptions fail unequivocally for neurons
near the boundary of the eye. Therefore, in order to
avoid this situation, we are forced to simulate, by
means of some experimental manipulation, the neural
environment at the edge of a truncated retina, in the
vicinity of an interior neuron, whose transfer function
parameters can be determined in the usual way. The
strategy of studying simulated network boundaries near
interior neurons has the additional advantage that any
edge effect so observed cannot be contaminated by the
action of any specialized network structure which may
exist in the vicinity of the actual boundary of the retina.

Two approaches for the isolation of an interior
ommatidium from that portion of the retina lying entirely
to one side of it may be considered: first, surgical disruption
of the lateral plexus, and second, modification of the light
stimuli falling on the retina. Though the separation
of the retina into two isolated halves by means of a
vertical cut through the cornea would be dramatic, this
strategy would be greatly complicated by bleeding
from the open circulation of the in-situ preparation,
and it is also incompatible with the use of our fiber-optic

taper stimulus system to measure a transfer function
on the intact retina before separating it into two halves.
Accordingly, we concentrated our efforts on the physiologi-
cal, as opposed to anatomical, isolation of one half of
the retina.

Such a stategy is made possible by the fact that,
except following prolonged dark adaptation, healthy
Limulus retinal neurons produce no neural impulse activity
in the absence of illumination ("spontaneous activity;" Kaplan
and Barlow, 1975). Since, so far as is known, all lateral
communication between ommatidia in the retina is initiated
by impulse activity in the inhibiting units, it follows that
a portion of the retina left in darkness is effectively
removed from communication with any portion of the retina
which is illuminated. In particular, neurons located
within an illuminated portion of the retina, but adjacent
to an area kept in darkness, should function dynamically
as if they were located near the origin of the truncated
model retina discussed in the previous chapter. Indeed,
such physiological isolation of part of the retina allows

the direct comparison of the response of the <u>same neuron</u>
to "full eye" stimuli (in which the neuron functions in
the midst of the fully illuminated, homogeneous retina)
and to "simulated edge" stimuli (in which the neuron
functions at the edge of the illuminated portion of the
retina) based on the same moving pattern stimulus. This
is precisely the comparison described in theory by the
two interpretations of equation (7.44) outlined in the
previous chapter. Thus, the simulated edge paradigm
allows direct comparison between theory and experiment,
as well as a straightforward evaluation of the magnitude
of the edge effects induced by the proximity of a retinal
neuron to the boundary of the retina.

A few comments on this program are in order. First, we
must carefully distinguish between the effects of nearby reti-
nal boundaries on the variation of the impulse rate from its
mean level, and the effect of boundaries on the impulse

rate itself. It is the former quantity which corresponds
to the variable R whose behavior is discussed in the previ-
ous chapter. The overall impulse rate, as discussed
in previous chapters, is a complicated nonlinear function
of the state of adaptation of the eye and the absolute
illumination level, as well as of the dynamic properties

of the retina itself. In the present situation, the mean
impulse rate is further modified by the steady-state
Mach band effects produced by real or simulated boundaries
in the retina (Barlow and Quarles, 1975). In the
experiments described below, these effects produced
a variation of between 5 and 10 percent (that is, less
than 1 impulse/second) in the mean impulse rate between
comparable episodes with "full eye" and "simulated edge"
illumination. This variation was considered sufficiently
small as to be ignorable, and all model calculations
were based on one steady-state impulse rate for each test-
ommatidium under all stimulus configurations.

Another subtle effect is the degradation of the sim-
ulated edge by the point-spread characteristic of the
stimulus optics, including the Limulus cornea and
crystalline cones. The point spread factor incorporated
into the Hartline-Ratliff model corrects for this effect
only as far as the moving stimulus pattern is concerned;
the model of the previous chapter makes no provision
for a blurring of the edge between the active and inactive
regions of the retina. Fortunately, as is demonstrated
in Appendix A, the Limulus optical system proved to be
of sufficiently high quality that this potential discrepancy

between our experiments and our theoretical model system
was likewise ignorable with apparent impunity. This
approximation was further justified by the relatively
high stimulus velocities used in our edge experiments.
At lower velocities, the point-spread effect becomes
much more significant (see chapter IV), but the dynamic
edge effects which are the concern of the present
chapter are greatly attenuated.

Finally, in the hope of demonstrating some similarity
between our model systems, both theoretical and experi-
mental, and the behavior of neurons near the real boundary
of the Limulus eye, we performed one experiment on a
test ommatidium located as near as possible to the anatomical
boundary of the eye.

Methods.

The experimental methods employed in these experiments were essentially those described in chapter III. A few changes in procedure are noted below.

Time-varying stimulus patterns were produced on a display oscilloscope under computer control and conveyed to the Limulus eye by lens and a fiber-optic taper. As a rule, two types of stimuli were presented in alternation: "analysis stimuli," which consisted of counter-phase modulated sinusoidal gratings, and "synthesis stimuli," in which spatial patterns moving at constant velocity were presented to the eye, in order to generate responses for comparison with the theoretical predictions. For all stimuli, the frame rate was 39.1 Hz, and the spatial resolution was 256 points/eye-width. For some episodes, the computer-generated blanking signal was used to darken one half of the display screen in order to generate edge-illumination of the test-ommatidium. This edge was placed approximately 0.05 eye-widths away from the nominal position of the test-ommatidium, in order to ensure its full illumination, despite the finite point-spread characteristic of the stimulus optics and small uncertainties in the alignment of the stimulus with the test-ommatidium.

In order to preserve the eye's state of light adapt-
ation, the experiments were scheduled with 60-second periods of
illumination in alternation with 90-second periods of darkness.
For those experiments performed on test ommatidia near
the center of the eye, episodes alternated between analysis
stimuli and synthesis stimuli. The successive analysis
episodes passed in turn through each of eight spatial fre-
quencies. Successive synthesis episodes presented the moving
stimulus in opposite directions, first in the "full-eye"
configuration, and then with simulated boundary illumination.
Stimulus velocities of 0.3, 0.5, 0.8, and 1.3 eye-widths/second
were used.

One potential problem with this protocol arises
because that half of the retina which is kept in darkness
during the "simulated edge" episodes receives 25% less total
illumination over the duration of the experiment than does
the other half, which is illuminated during every episode.
In principle, this difference could induce different states
of light-adaptation in the two halves of the retina. As
this possibility was effectively ruled out by comparison of

responses to mirror-image stimuli presented in the "full eye"
configuration (see Figure 8-6, below), it was deemed unnecessary
to compensate for this potential complication.

In addition to the simulated boundary experiments,
we also measured the responses to moving stimuli of ommatidia
as close as possible to the actual boundary of the <u>Limulus</u>
eye. As our optical system often couples imperfectly to such
extreme ommatidia, it was difficult to obtain adequate
impulse rates from many units at the extreme periphery.
In our most successful experiment of this type, we recorded
from an ommatidium located 3-4 ommatidial
diameters from the anterior border of the eye. This unit pro-
duced a mean impulse rate of ~7 impulses/second. For this
experiment, only moving pattern stimuli were used.
As this ommatidium was effectively at the boundary of the
eye, it was unnecessary to use a simulated edge
stimulus. Accordingly, in this experiment, the illumination
extended well beyond the natural border of the eye, and the
experimental protocol consisted of drifting patterns moving
at several velocities in opposite directions across the
boundary of the eye.

The "full eye" moving stimuli are shown in Figure 8-1
and may be expressed formally by

$$S_f(x,t) = M + H(\pm x - vt)e^{-(\pm x - vt)} , \qquad (8.1)$$

Figure 8-1. Comparison of full-eye and simulated-boundary stimuli.
(A): Full-eye stimulus, moving to the left. (B): Full-eye stimulus,
mirror image of (A). Step moves to right. (C): Formation of
edge stimulus, with step appearing "out of light." Stationary
step pattern, with left half of eye in darkness (bottom) is multi-
plied by moving stimulus as in (A) to produce simulated boundary
stimulus, top. (D): Formation of edge stimulus, with step appearing
"out of the dark." Stationary step pattern with left half of eye
in darkness (bottom) (as in (C)) is multiplied by moving stimulus
as in (B) to produce simulated boundary stimulus, top.
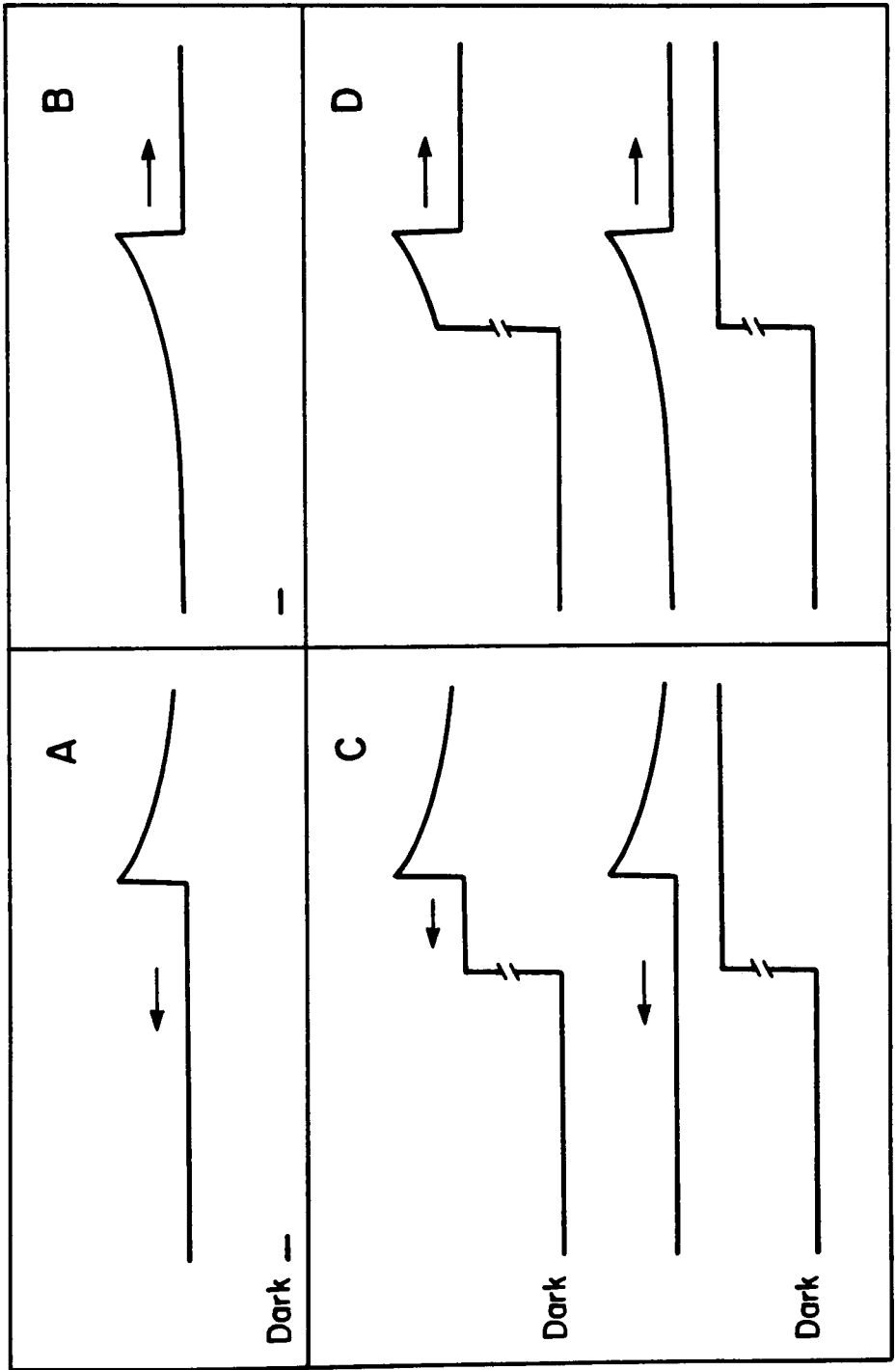
Figure 8-1

where M is a stimulus intensity offset. H, the Heaviside
function, is 0 for negative arguments, and 1 for positive
arguments. The stimuli were repeated every 4/v seconds;
this produced the appearance of an endless series of
step-transients followed by exponential decays, with each
decay 4 eye-widths in length. Simulated edge stimuli
were of the form

$$S_e(x,t) = H(x) \cdot S_f(x,t) \quad . \tag{8.2}$$

Thus the moving pattern either moved from the
periphery of the illuminated portion of the eye toward
the simulated edge (minus signs in eq. 8.1 ; Fig. 8-1C),
or appeared suddenly at the simulated edge and moved
through the illuminated portion of the eye toward the
periphery of the retina (plus signs in eq. 8.1; Fig. 8-1D).
The exponential form of these stimuli was chosen in order
to obtain a periodic stimulus with sharp "on-transients,"
but without sharp "off-transients." This choice minimized
the nonlinear truncation of transient responses to dark
stimulus features which took place with the more
symmetrical stimuli used in previous experiments (chapter IV),
and which we felt could only complicate our efforts to
detect border effects in the present experiments.

Except as described below, our procedure for
adjusting the parameters of the Hartline-Ratliff model
in order to match the empirical transfer function data
were the same as those presented in chapter IV.

The theory developed in the last chapter was
based on the functional form

$$\tilde{k}(\xi) = N(\xi^2)/D(\xi^2) \tag{7.24}$$

for the transform of the inhibitory kernel, where N and D
are polynomials with real coefficients, with deg (N)<deg(D) = M,
and D monic (that is, with leading coefficient equal to
one). To make this explicit, we attempted to fit our measure-
ments of $\tilde{k}(\xi)$ from the reciprocal loci to the form

$$\tilde{k}(\xi) = K \cdot \frac{a_2\xi^4 + a_1\xi^2 + a_0}{\xi^6 + b_2\xi^4 + b_1\xi^2 + a_0} \quad , \tag{8.3}$$

which constitutes the most general rational expression
of the desired type which can be determined from the
number of observations available. This determination
was made by substituting five experimentally observed

values for $k(\xi_n)/K$, together with the frequencies ξ_n into
(8.3), which results in a system of simultaneous linear
equations for the coefficients a_i, b_i.

In practice, this procedure frequently resulted in
polynomials N and D with nearly coincident positive real
roots. The slight disparity between these roots produced
an artifactual singularity in the function $\tilde{k}(\xi)$. This
phenomenon suggested that the polynomials in (8.3) were
unnecessarily general for the description of typical Limulus
inhibitory kernels. We therefore adopted instead a quotient
of quadratic and quartic polynomials:

$$\tilde{k}(\xi) = K \frac{a_1\xi^2 + a_0}{\xi^4 + b_1\xi^2 + a_0} = K \frac{1 - (\frac{\xi}{\alpha})^2}{(\frac{\xi}{\beta})^2 + 2(\frac{\xi}{\gamma})^2 + 1} \quad . \tag{8.4}$$

The first form in (8.4) meets the specifications given
above; the second form, in which the coefficients take on
units of spatial frequency, produces coefficients which
are more stable with respect to small perturbations in
in the data than those of the first form. Parameters for differ-
ence of Gaussian kernels equally compatible with the data were
also estimated (as described in chapter VI), to facilitate comparison

of these ommatidia with those studied previously. The
two forms for the inhibitory kernel are compared in
Figure 8-2; a comparison of an empirical transfer
function and a model transfer function including equation
(8.4) is shown in Figure 8-3. Parameters for the ommatidia
whose responses are discussed below are summarized in
Table II.

The roots $\mu_j(\omega)$ and λ_m in equations (7.36) and (7.37)
were calculated by means of the quadratic formula; the
Fourier syntheses were then calculated from equation (7.44)
by means of the Fast Fourier Transform on a mesh of
1024 points.
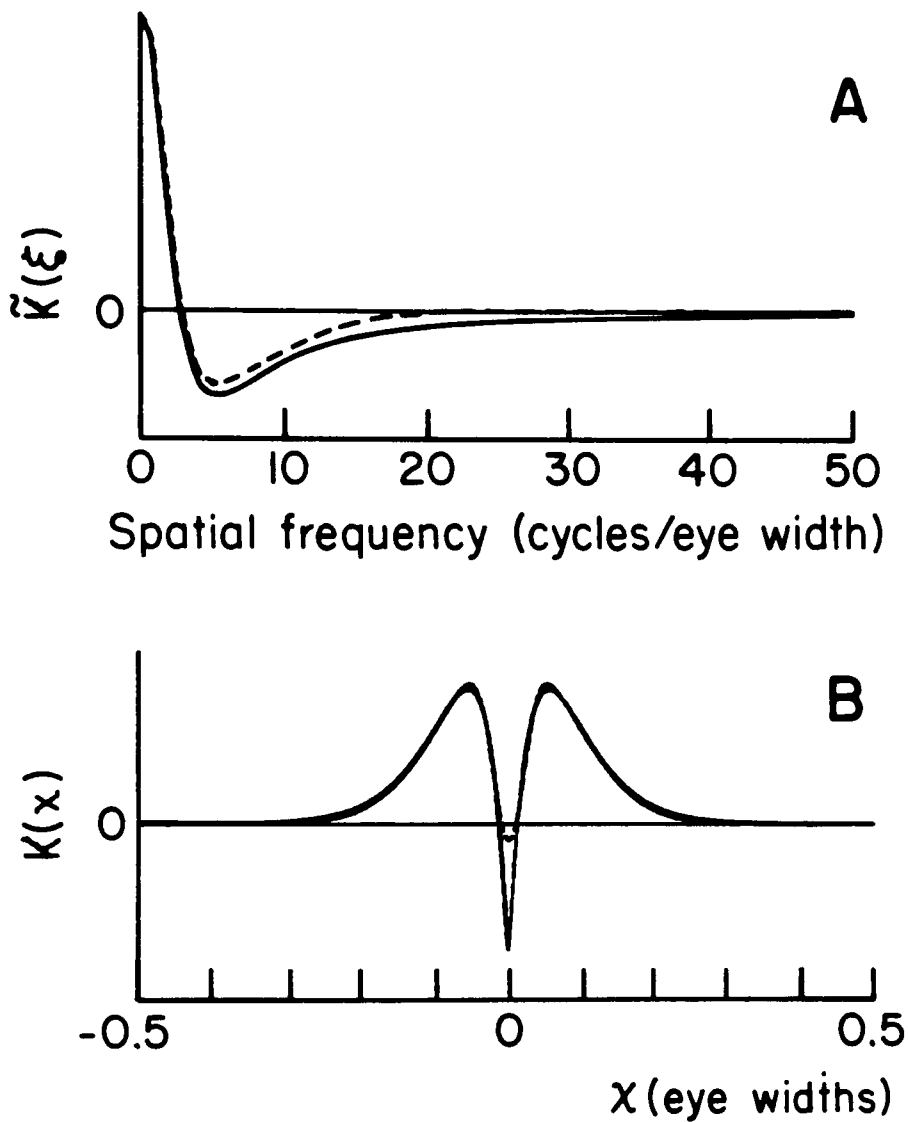
Figure 8-2. Comparison of model inhibitory kernels. Inhibitory
kernels with parameters determined to match the transfer function
of Figure 8-3 (see Table II) are shown in the frequency domain
(A) and spatial domain (B). Solid curves indicate quotient-of-
polynomials kernels (equation (8.4)); dashed curves indicate
corresponding difference-of-Gaussian kernels (equation (5.21)).
The small disparity between the frequency-domain kernels in (A)
corresponds to the singularity at the origin in the quotient-
of-polynomials kernel in (B), and is of no physiological significance.

Figure 8-3. Empirical and model transfer functions.

Left: Empirical spatiotemporal transfer function.

The dots indicate measured amplitude values. Spatial frequencies

(in cycles/eye-width) are indicated at left; near the peak

($\sim$4 Hz), the amplitudes decrease monotonically with increasing

spatial frequency. Phases are shown on separate axes for each

spatial frequency, modulo 2π. Spatial frequency increases from bottom

to top as indicated at right. Right: Hartline-Ratliff model trans-

fer function with parameters chosen to match the transfer function

at left. (For parameters, see Table II.) Near the peak, ampli-

tudes decrease monotonically with increasing spatial frequency.
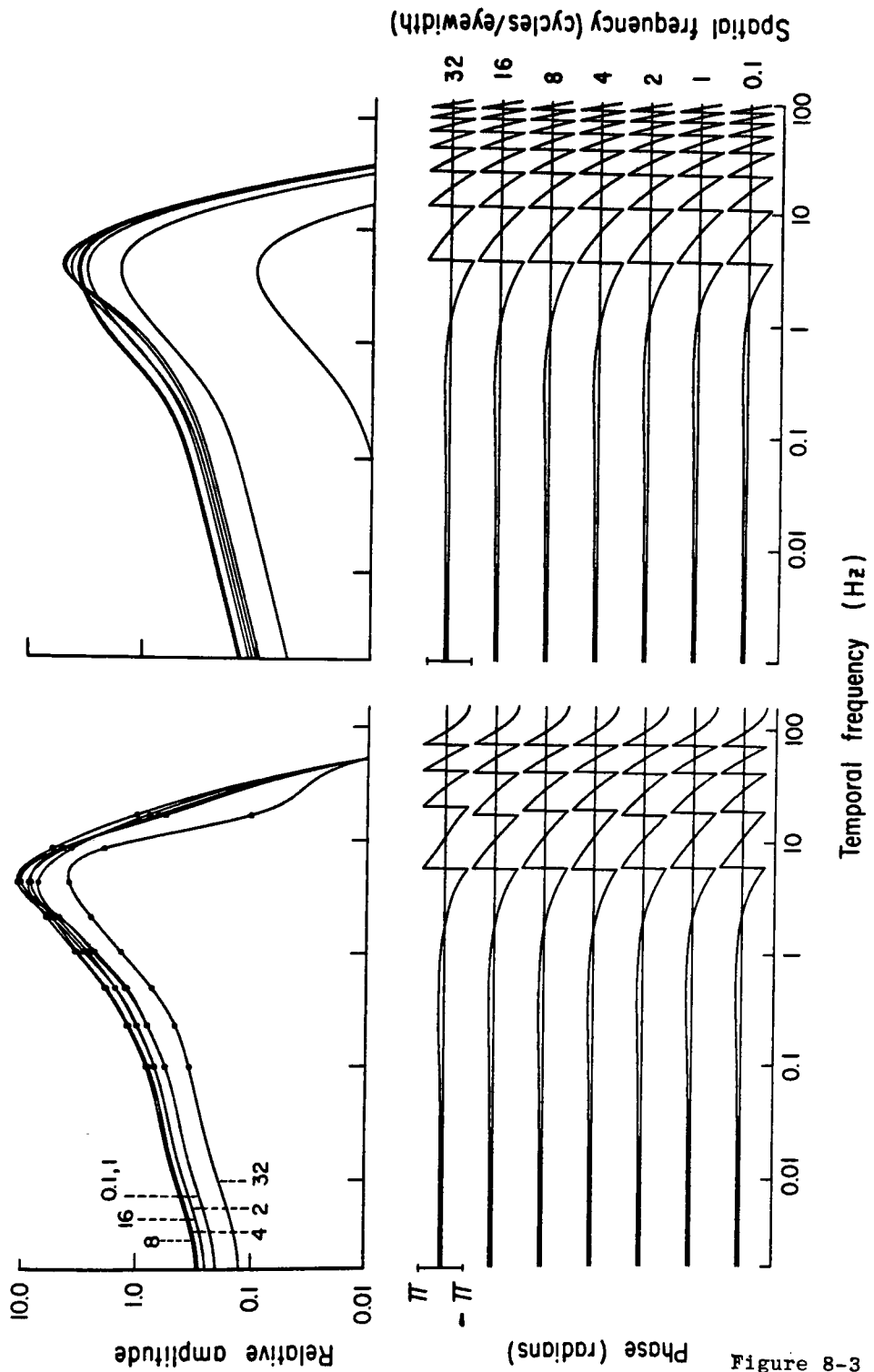
Figure 8-3

Results

       Predicted responses to moving stimuli which consist of step-transients followed by exponential decays (see Methods), are shown in Figure 8-4.   These records were calculated according to the theory outlined above, under the assumption that the test ommatidium is located exactly at the edge of the active neural network (x=0). The waveforms show a significant dependence on the velocity of the moving step.

       At low speed (0.3 eye-widths/second), the full-eye response shows a prominent anticipatory Mach band followed by a vigorous upstroke as the step crosses the test ommatidium Following this on-transient, there is a rapid return to a moderate impulse rate, with a marked "notch" in the response before the eye returns to its mean firing rate. The slow decline in the mean rate after transient activity associated with the step-crossing is due to both the exponential shape of the stimulus waveform and the dynamics of light-adaptation. The edge-illumination responses show marked differences from the full eye response. When the step appears "out of the dark," there is no Mach band preceding the on-transient, but the decay following the step-crossing closely resembles that seen for the full-eye case. Conversely, when the step appears from the illuminated side of the edge ("out of the light"), there is an anticipatory Mach band similar to that

<u>Figure 8-4</u>. Predicted edge and full-eye responses to moving stimuli,
based on the model transfer function of Figure 8-3. Responses were cal-
culated at four stimulus velocities, as shown at right. For each
velocity, the two records at left show the predicted response to
a simulated boundary stimulus, with the step coming "out of the
dark"; the middle two records show the predicted response to moving
steps for the full-eye stimulus; and the two records at right
show the predicted response to a simulated boundary stimulus, with
the step coming "out of the light." The scale markers at left
apply to the longer record of each pair, and represent 2.0 seconds. The
short vertical tick marks above the horizontal axes for these records
indicate the arrival of the moving step at the test ommatidium.
The longer records are plotted with horizontal scales proportional
to stimulus velocity, so that horizontal distance on these records
represents distance on the retina at the same scale for all velocities.
The shorter record of each pair depicts the response transient of
the corresponding long record, replotted on a uniform time scale
for all velocities. (The scale marker shown for 0.3 eye-width/
second also represents 2.0 seconds on all the short records.)
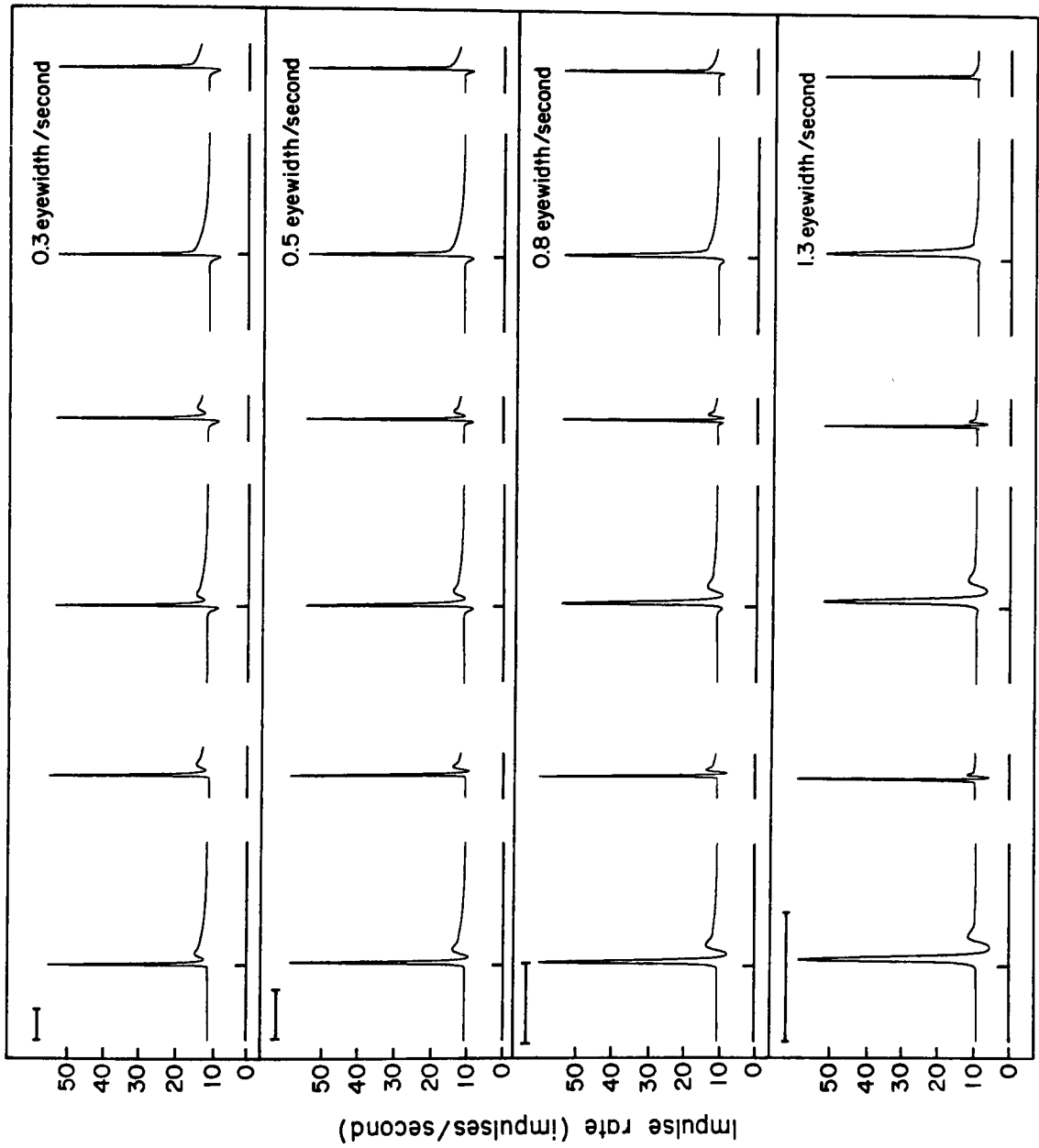
Figure 8-4

seen in the full-eye, but the decay following the on-transient lacks the notch seen in the full-eye response.

As the velocity is increased, two trends may be noted in the predicted response for full-eye illumination: First, the anticipatory Mach band becomes reduced in size, and second, the notch following the on-transient becomes much more prominent, as does the secondary maximum which follows it. Corresponding trends may readily be percieved in the responses under edge-illumination to steps moving in the appropriate direction: ʹout of the dark, ʹ the notch following the on-transient grows, while "out of the light," the anticipatory Mach band shrinks, as velocity is increased. It may also be noticed that at high velocities, a small notch appears following the transient in the "out of the light" direction. Finally, at high velocities, the height of the on-transient for the "out of the dark" stimulus becomes noticeably greater than that seen in either the full-eye or "out of the light" stimulus conditions.

The responses actually observed from the ommatidium whose dynamics are predicted in Figure 8-4 are shown in Figure 8-5. Direct superposition of the records shows that the agreement between predicted and observed responses is in general very good, though the precision of the agreement appears to be

Figure 8-5. Observed edge and full-eye responses to moving stimuli.
Measured responses to stimuli moving at four velocities are shown,
plotted in the same manner as the predictions of Figure 8-4.
Responses to steps moving "out of the dark" are shown at left;
responses to steps moving "out of the light" are shown at right.
Middle column records show the average of responses to steps moving
in both directions, with full-eye illumination (see Figure 8-6).
Each response is plotted (long records) on a uniform space scale
(time scale proportional to velocity; scale markers at left represent
2.0 seconds); the response transients (short records) are also
replotted on a uniform time scale (scale marker for 0.3 eye-width/
second represents 2.0 seconds for all short records). Short
vertical tick marks indicate arrival of moving step at test
ommatidium.
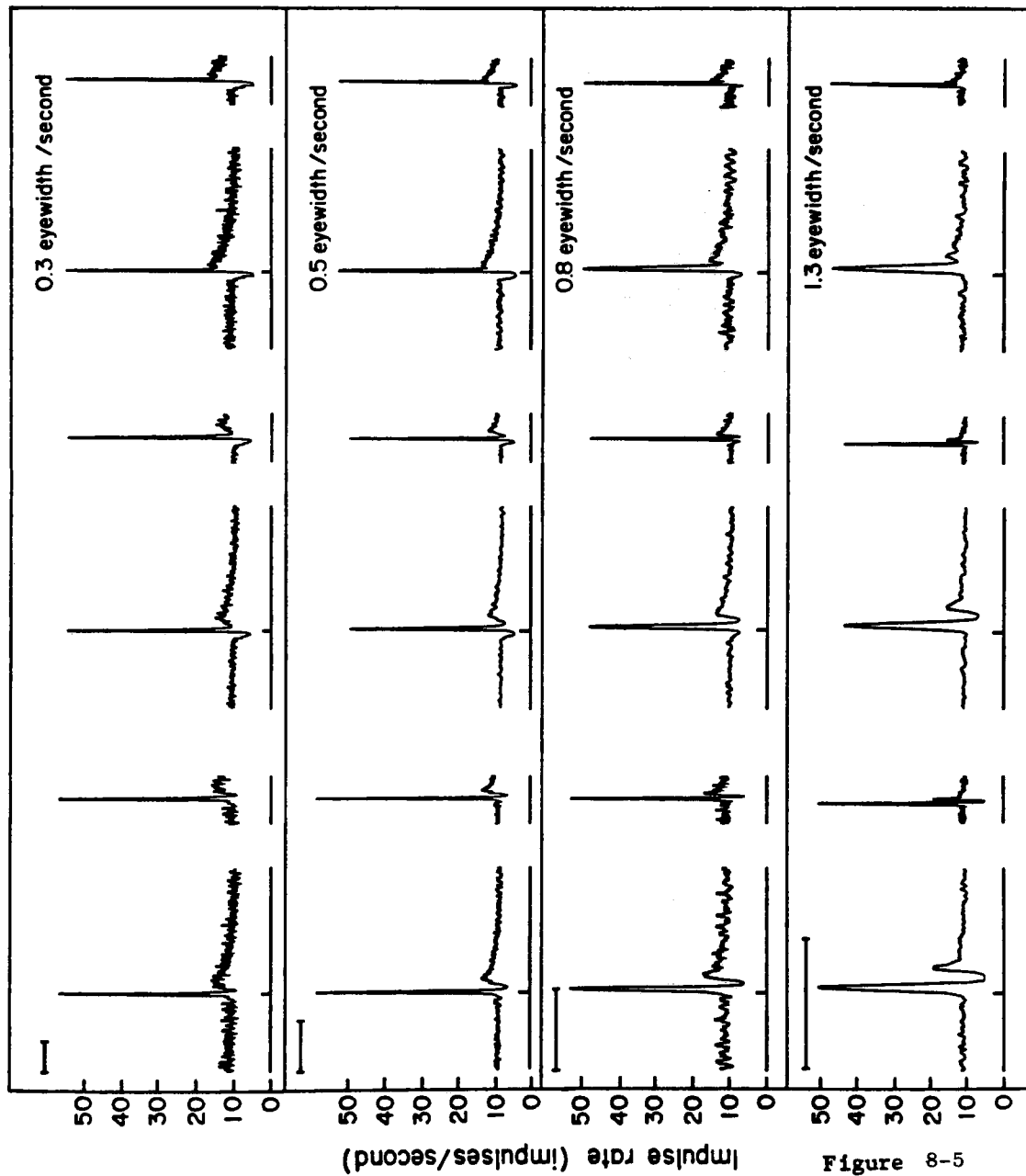
Figure 8-5

Figure 8-5

slightly less at the highest velocities. All of the quali-
tative features described above for the model records may
readily be seen in the actual responses. The predicted changes
in the response with increasing velocity are likewise evident.

It is instructive to compare these records with the
responses to full-eye illumination with step stimuli moving
in opposite directions (Fig.8-6). This serves as a control
against the possibility that the retina itself is asymmetrical,
or that the two portions of the eye are in a significantly
different state of light-adaptation. The observed simil-
arity of responses rules out such asymmetry as a contributing
factor to the effects documented in Figure 8-5. As in previous
chapters, we have exploited this symmetry by averaging responses
to mirror-image full-eye stimuli in all the other full-eye records

The difference between the peak height of the response
to step transients moving rapidly towards or away from the
simulated boundary of the neural network is clearly illustrated
in data from another Limulus preparation (Fig.8-7). For this
eye, the peak response to a step coming "out of the dark"
was nearly fifty percent greater than the response to a step
coming "out of the light." Similar responses have been
observed whenever we have presented these simulated edge-
stimuli to the Limulus retina.

In one experiment (see Methods) we attempted to measure
the responses to moving steps of an ommatidium as near as

Figure 8-6. Comparison of responses to mirror-image full-eye stimuli. Responses to steps moving in opposite directions across the full eye (see Figure 8-1, A,B) are shown for two stimulus velocities. Scale markers indicate 2.0 seconds; vertical tick marks indicate arrival of moving step at test ommatidium.
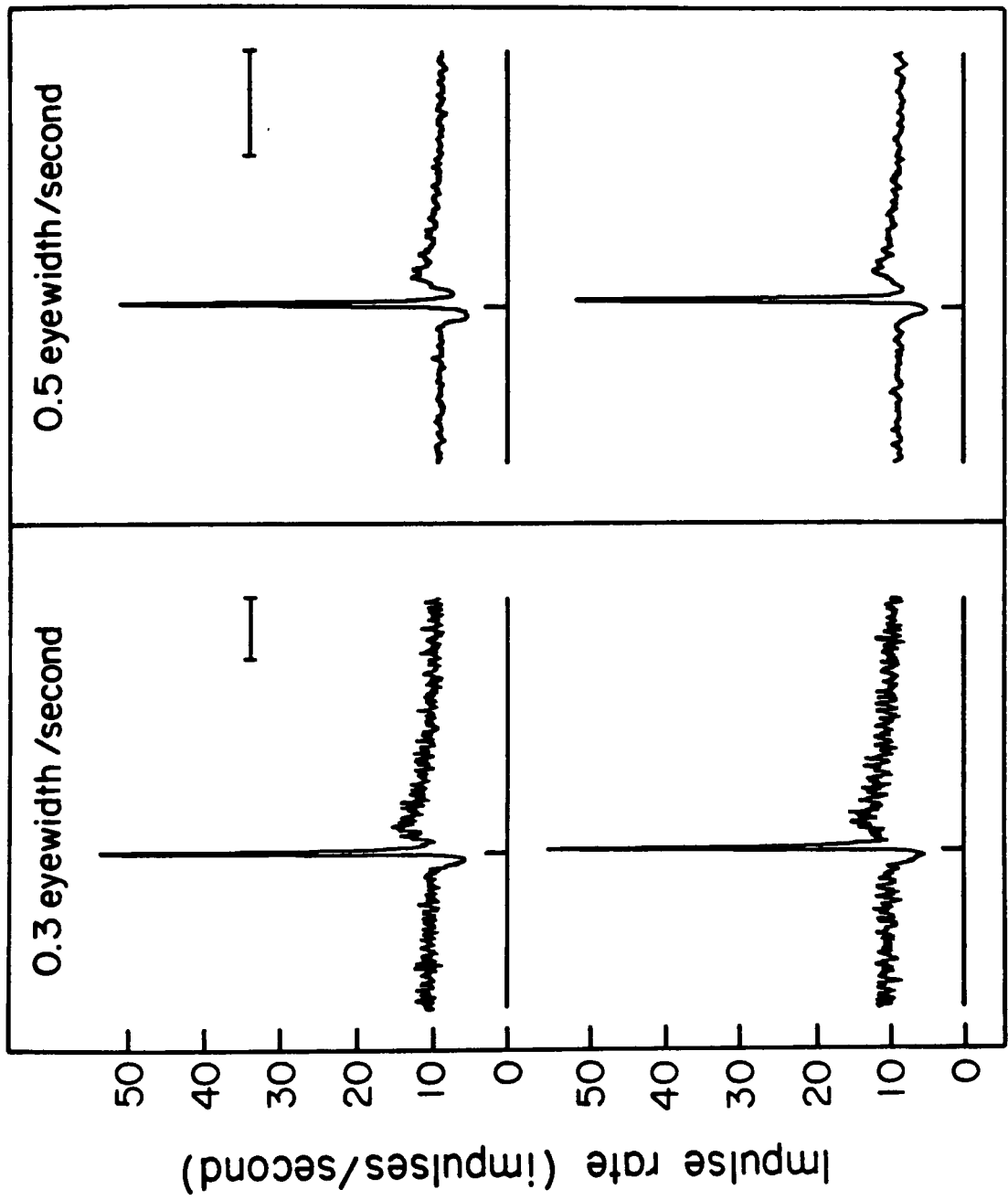
Figure 8-6

Figure 8-7. Effect of simulated boundary for high velocity stimuli.
Top row: observed responses to moving step stimuli, plotted as
in Figure 8-5. Bottom row: predicted responses; see Table II for
transfer function parameters. Records at left show response
to stimuli moving "out of the dark"; records at right show response
to stimuli moving "out of the light"; middle records show response
to full-eye stimuli. Scale marker represents 2.0 seconds (long
records). Short records show response transients, replotted for
comparison with Figure 8-5. (Short records are 3.08 seconds long.)
Tick marks indicate arrival of moving step at test ommatidium.
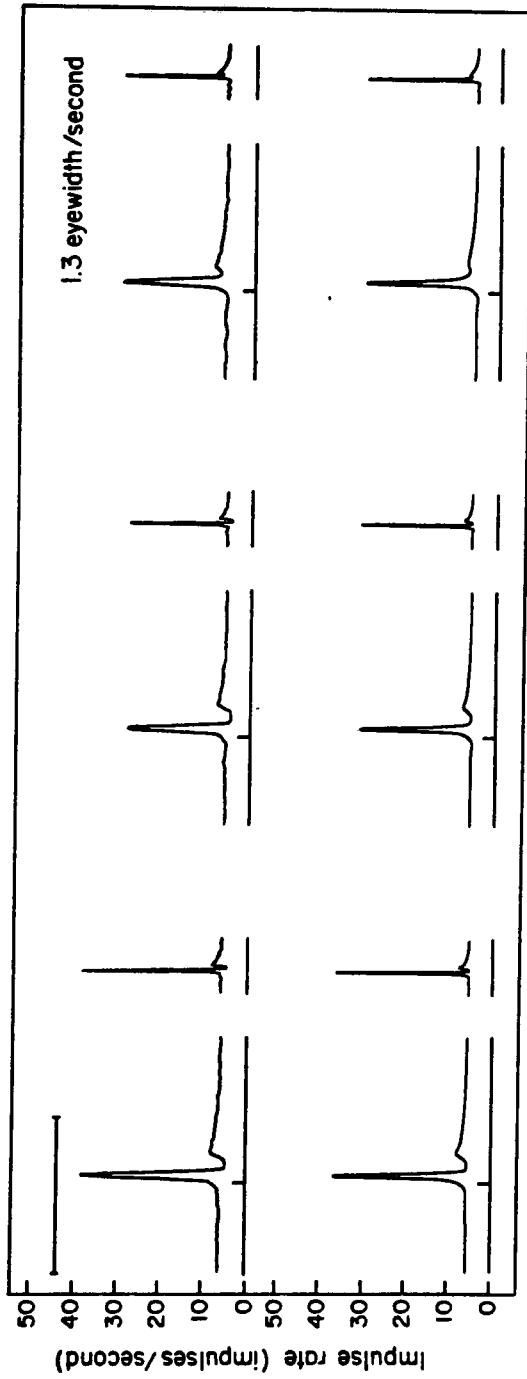
Figure 8-7

possible to the actual boundary of the Limulus retina. The

ommatidium selected for the experiment was within three or

four ommatidial diameters (~0.1 eye-widths) of the edge of

the eye. (This compares with a maximum displacement in the

simulated edge experiments of 0.05 eye-widths.) The results of this

experiment are shown in Figure 8-8. Though there is a slight

anticipatory Mach band seen at low velocities in the response

to a step which is nominally coming "out of the dark" (which

is presumably due to the slight displacement of the ommatidium

from the edge of the eye), the similarity between these records

and those recorded at simulated edges in the interior of the

neural network is unmistakeable: Steps coming "out of the

light" show prominent anticipatory Mach bands, and only

small notches in the response following the peak response

transient. Steps in the other direction produce little

anticipation, but show a marked interval of inhibition follow-

ing the peak transient response. The height of the peak

response to steps coming "out of the dark" is greater than that

of the response to steps moving in the other direction.

Our procedures for the measurement of an empirical

transfer function could not be applied to this edge ommatidium,

because of its demonstrably asymmetric inhibitory field. Thus,

in order to assess the compatibility of the responses from this

unit with the Wiener-Hopf treatment of the Hartline-Ratliff

model, we calibrate a set of model parameters

by comparison of the observed responses with the predictions of

model calculations, instead of by comparison of empirical and

Figure 8-8. Observed responses of an ommatidium near the boundary of the eye to moving stimuli. Measured responses to stimuli moving at three velocities are shown. Responses to stimuli moving from the periphery toward the interior of the eye (analagous to stimuli moving "out of the dark" in simulated edge experiments) are shown at left; responses to stimuli moving from the interior of the eye toward the periphery (analagous to stimuli moving "out of the light" in simulated edge experiments) are shown at right. Test ommatidium was approximately 0.1 eye-width (3-4 ommatidial diameters) from the anterior boundary of the eye. Long records are plotted on uniform space scale (time scale proportional to velocity; scale markers at left indicate 2.0 seconds). Short records show response transients replotted on uniform time scale (scale marker for 0.3 eye-width/second indicates 2.0 seconds for all short records).

Short vertical tick marks indicate arrival of moving step at test ommatidium.
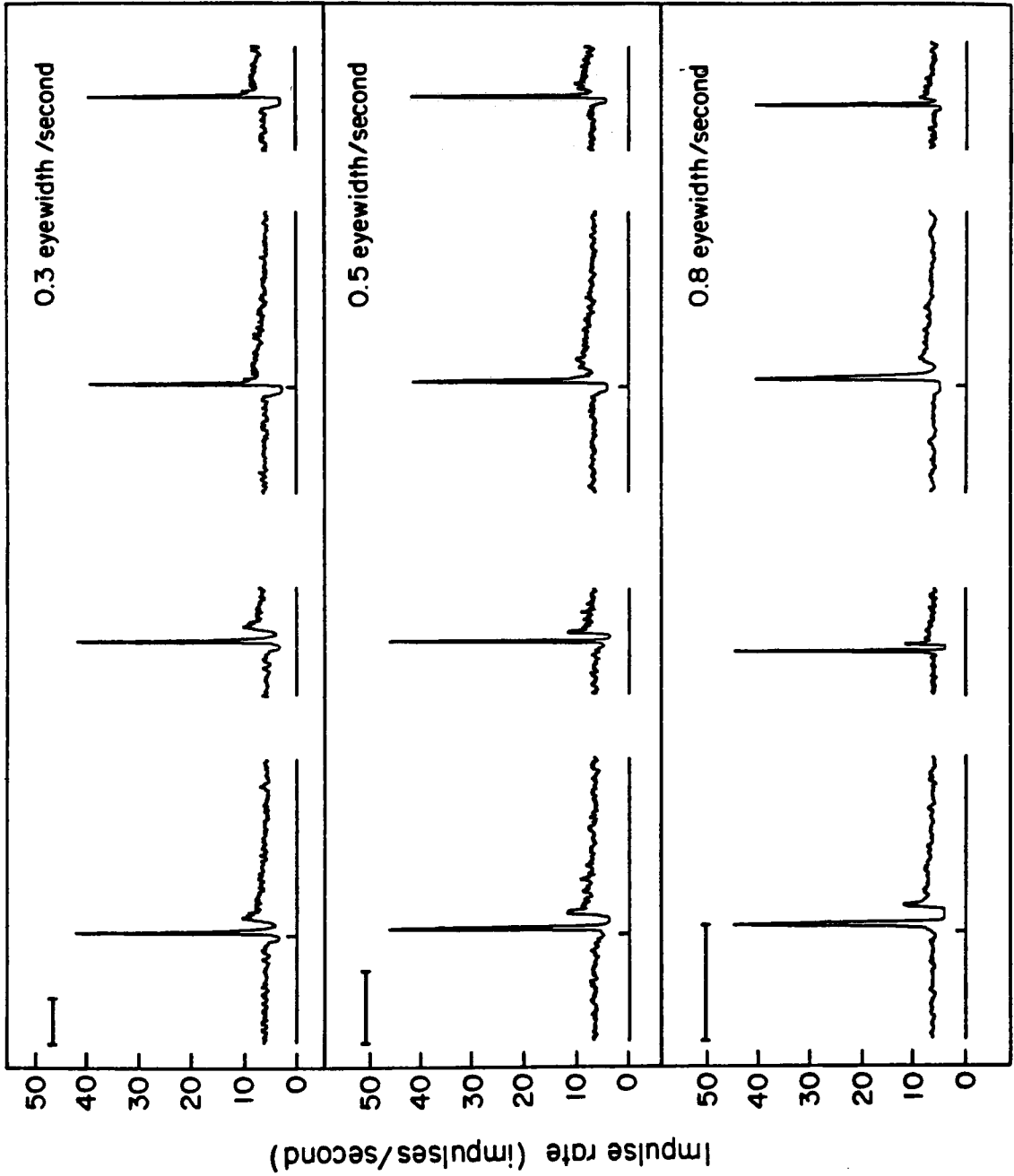
Figure 8-8

model transfer functions. The parameters for the model transfer

function used for the predictions in Figure 8-4 were used as a

starting point for the parameter search, and were modified only

as dictated by specific response features. In the final parameter

set (Table II), the generator potential parameters were adopted

without change. Small changes were required for most of the

parameters of the self- and lateral-inhibitory processes, but it

was necessary to increase the total lateral inhibitory strength

to several times its previous value. (The significance of this

observation is discussed below.) The results of this fitting

procedure are shown in Figure 8-9. These calculations included

provision for the finite distance between the test ommatidium and

the edge of the retina.

  Indeed, such calculations, which allow for the small

offset between the simulated boundary and test ommatidium (Fig. 8-10),

also account for the small notches in the response records follow-

ing the peak transient response to steps moving "out of the

light" in the experiment of Figure 8-4.

Discussion

  The agreement between the Wiener-Hopf calculations

and the observed responses of the Limulus retina to simulated

edge stimuli constitutes additional evidence of the adequacy

of the Hartline-Ratliff model for the quantitative description

of the dynamic response of the Limulus eye. In this chapter

we extend to nearly two orders of magnitude the range of

stimulus velocities over which the model appears valid. The

empirical transfer function measurements are not sufficiently

accurate at temporal frequencies which considerably exceed

the mean impulse rate to enable us to critically evaluate

the calibration of the model at velocities much greater

Figure 8-9. Calculated responses of ommatidium near the boundary
of the eye to moving stimuli. Estimated responses calculated
from model transfer function with parameters adjusted
for compatibility with measured responses of Figure 8-8.
(See Table II for parameter values.) Records at left show calculated
responses to stimuli moving from the periphery toward the interior
of the eye; records at right show calculated responses to stimuli
moving from the interior toward the periphery of the eye. Scale
markers at left indicate 2.0 seconds (long records); short records
show response transients replotted on uniform time scale (scale
marker for 0.3 eye-width/second indicates 2.0 seconds for all short
records). Tick marks indicate arrival of moving step at test
ommatidium.
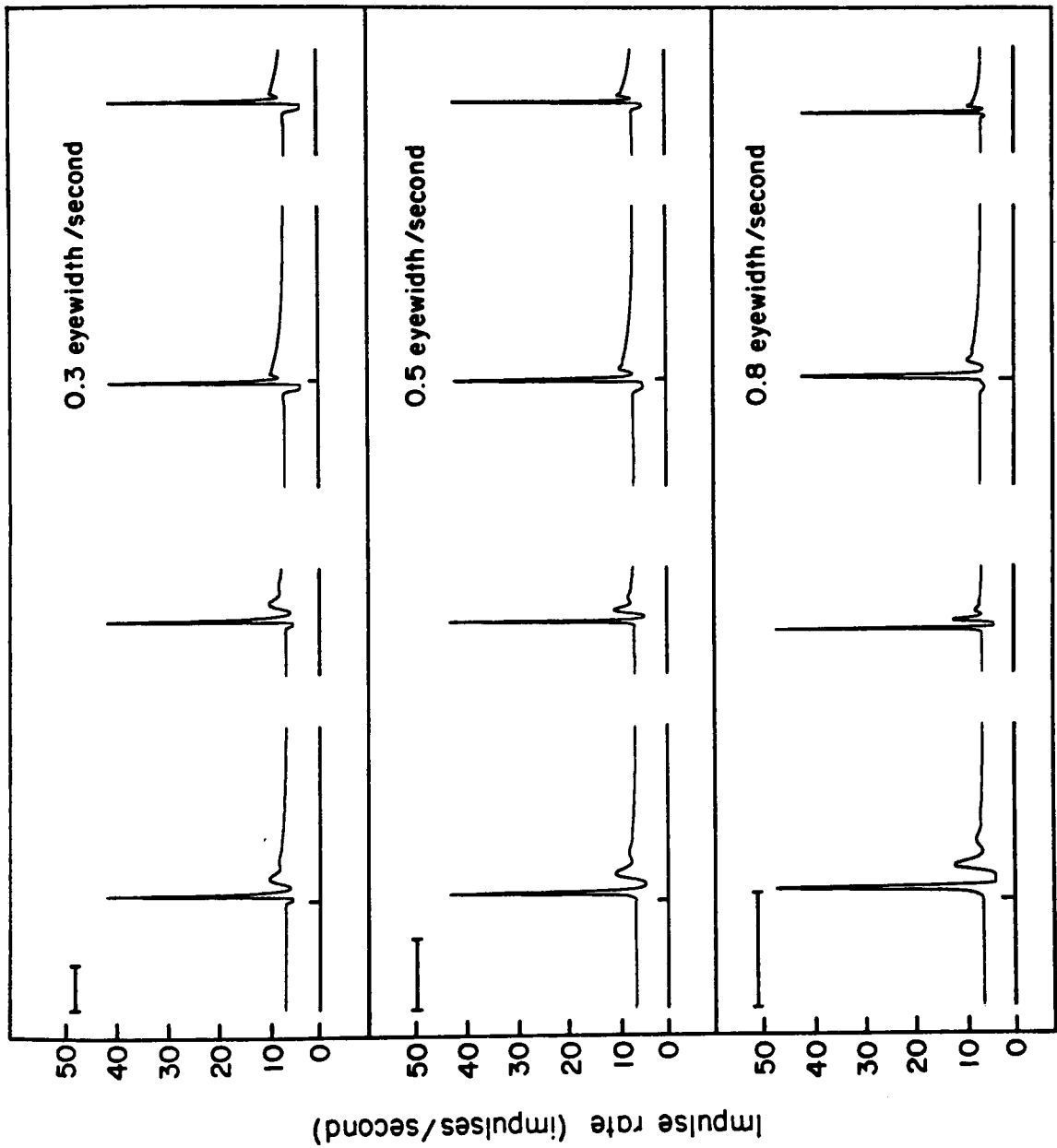
Figure 8-9

Figure 8-10. Predicted responses to moving stimuli, including small

offset between simulated edge and test ommatidium; preparation of

Figures 5 and 6. Offset was 0.05 eye-widths, or 2 ommatidial diameters.

Records at left simulate responses to stimuli coming "out of the dark,"

records at right for stimuli coming "out of the light." Scale

markers at left represent 2.0 seconds; tick marks indicate arrival

of moving step at test ommatidium.
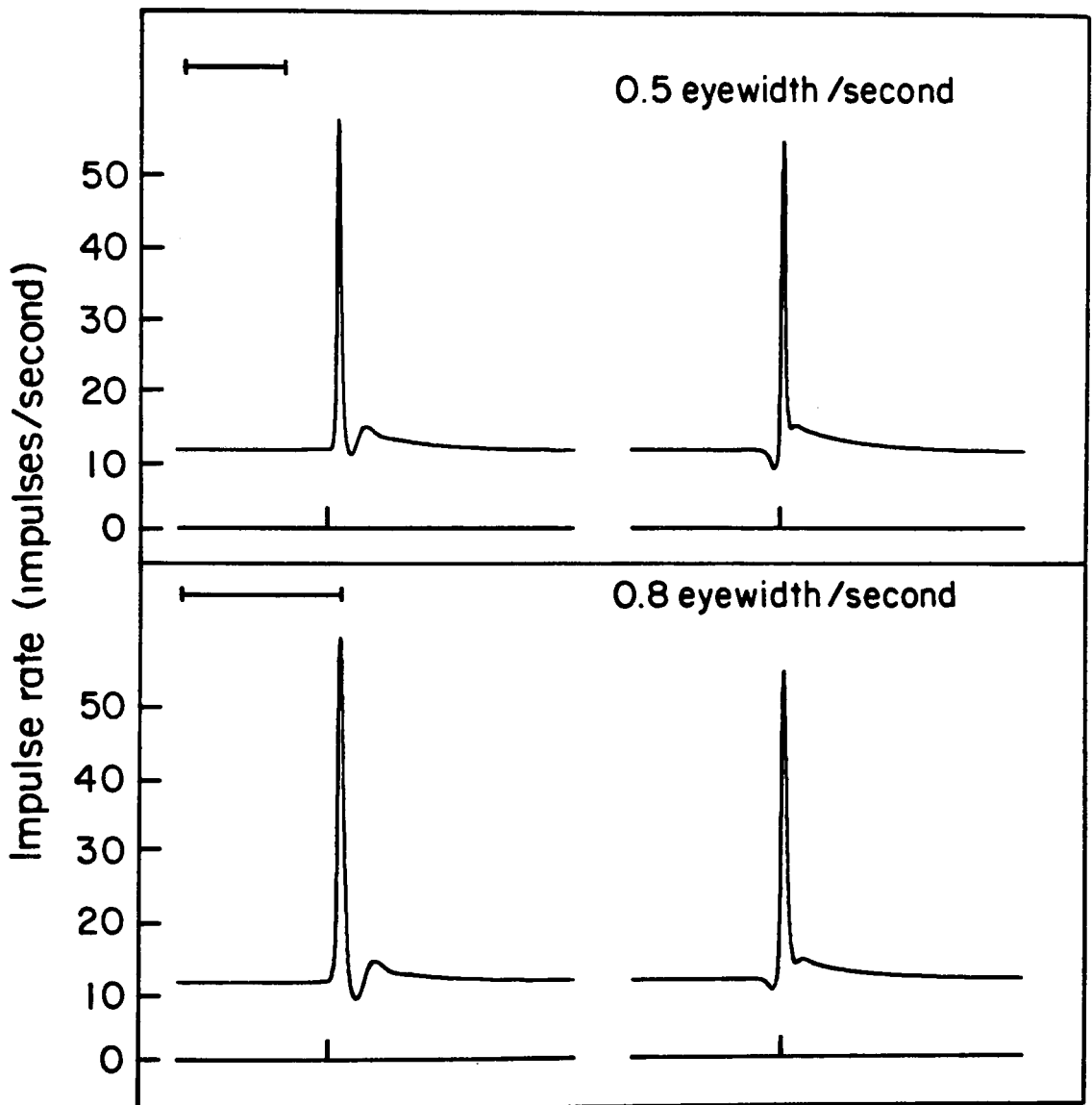
Figure 8-10

than those presented above. In any event, preliminary
experiments and model calculations suggest that there
are no further significant quantitative changes to be seen
in the retinal response at higher velocities.

Though the calculations described above model the
observed responses directly in terms of the analytic structure
of the Hartline-Ratliff model, it is nonetheless useful to
describe the responses to edge-stimuli in terms of the physio-
logical processes which underly the model. The large peak
response in the impulse rate results from the light-to-
generator potential transduction, followed by the encoder
transduction, which includes self-inhibition. As the step-
stimulus moves across the eye, this excitatory peak is
accompanied by zones of decreased neural response, as mediated
by the spatial and dynamic properties of the lateral-inhibitory
transduction. The shape of these moving "Mach bands" depends
on the stimulus velocity; at high speeds, the moving step
tends to "overrun" the lateral inhibition, so that the anticipatory
Mach band is much less pronounced than that following the
excitatory transient.

The effect of the simulated edge on these response features
is straightforward. In the "out of the light" configuration,
the test ommatidium shows an essentially typical full-eye
response so long as it remains ahead of the advancing edge.
Just after the step crosses the test-ommatidium, producing
the usual excitatory transient, it passes beyond the illuminated
portion of the eye. The test ommatidium is thus not in a

position to receive the burst of inhibitory impulses which
would follow in the full-eye setting. The impulse rate therefore
declines gradually, reflecting the intensity of the stimulus
and the dynamics of light-adaptation and self-inhibition.
At high speeds, the self-inhibitory process can produce a
small notch in the response following the on-transient (Figs. 8-4
and 8-7). Conversely, in the "out of the dark" configuration,
the test-ommatidium is the first unit in the retina to
be excited by the moving step. Thus, there is no anticipatory
Mach band whatever. Subsequently, as the step moves away from
the test ommatidium it is inhibited by the on-transient in
essentially the same fashion as in the full-eye situation.

At high speed, the height of the on-transient peak is
greater for steps moving "out of the dark" than for those
moving "out of the light." This is a manifestation
of the time scale of the lateral inhibitory transduction. At
high speeds for steps coming "out of the light" the inhibi-
tory effect on the test-ommatidium of the approaching on-
transient lasts sufficiently long to sum with the
excitatory transient when it arrives at the test-ommatidium
a few moments later; when the step approaches "out of the dark,"
there is no anticipatory inhibition, and the on-transient is
correspondingly greater in height.

A striking feature of the responses to high speed

stimuli is the presence of secondary maxima following the
excitatory on-transients, in the full-eye and "out of the dark"
stimulus conditions. The separation between the principal
excitatory peaks and these secondary maxima is constant when
the response records are plotted on a constant "space scale"
(Fig. 8-4,5). This implies that these secondary maxima are not
features of the intrinsic impulse response of the test-
ommatidium, but rather represent genuine disinhibition of the
test-ommatidium by the strong inhibitory Mach band following
the initial on-transient.

We have confirmed this description of the neural events
responsible for the observed responses to the extent that
variation of the model parameters corresponding to any partic-
ular physiological process produces the expected changes in
the predicted response. It should also be possible to obtain
more direct confirmation of this description by means of
physiological manipulation of the Limulus eye. For example,
many processes in the eye are highly sensitive to the temperature
of the preparation (see Appendix B). It is also possible to alter
the properties of the neural network by pharmacological means
(MacNichol and Benolken, 1956; Adolph, 1966 and 1976; Adolph and
Tuan, 1972). Differences between the neural properties of a "sick"
Limulus retina and those of healthy animals were shown in chapter IV
In all such instances, variations in retinal physiology should

produce analogous changes in both the empirical transfer function and the observed responses to moving stimuli, so that the former continue to predict the latter.

It is suggested above that the truncated homogeneous network embodied in the simulated edge experiments is a useful model for the naturally-occurring boundaries of real neural networks. The similarity between the observed responses near real and simulated edges in the Limulus retina suggests that this network may be an instance where such a model is valid. However, the data do not rule out various possibilities for the existence of modified network properties near the boundary of the Limulus retina. For example, the experiment on an ommatidium near the eye's actual boundary yielded a set of dynamical parameters within the normal range of our experience, with the notable exception of the total strength of lateral inhibition $(K/(1+K))$, which was roughly twice as large as we have ever measured for any ommatidium in the interior of a Limulus eye. This is consistent with unpublished observations of Dodge and Kaplan that the total inhibition converging on ommatidia at the bottom edge of the eye is equal to the total inhibition converging on ommatidia in the interior, despite the fact that these edge units lie entirely to one side of their inhibitory field. Such variation in the pattern of connectivity of the lateral plexus is presumably sufficiently gradual as to fit into the

framework of a nearly homogeneous structure.

We observe that the neural organization at a boundary distinguishes the direction of motion across it. The response of a stimulus crossing a boundary from the interior portion is clearly different from the response to oppositely directed movement. Thus boundary neurons could act as primitive directional motion detectors.

It has thus been demonstrated that the dynamic response of the Limulus retina at a simulated edge may be described quantitatively in terms of the same Hartline-Ratliff model as was developed to model the response of the full eye. This description is obtained by solving the Hartline-Ratliff equations on the half-line, instead of on the full line, by means of the Wiener-Hopf technique. The effect of the simulated edge configuration on the response of Limulus retinal neurons is significant. Responses measured near the physical boundary of the eye are qualitatively similar to those obtained at simulated edges in the interior. Such simple truncation of a homogeneous neural network may well serve as a model for edge effects at the boundaries of other neural networks.

'The time has come,' the Walrus said,
'To talk of many things ...'

L. Carroll, 1871

IX. Discussion

The apparent success of the empirical and theoretical
linear techniques presented above in the prediction of
the response of the _Limulus_ retina substantiates the
belief that this neural network operates as a linear
dynamical system, and that we have adequately identified
and characterized physiological component processes which
together constitute its visual response. It is important,
however, to recognize the limitations of this treatment,
and to indicate some of the phenomenology of _Limulus_
vision which it does not include.

Consider first the limitations of our empirical
transfer function measurements. These are based on a
stimulus whose highest frequency component lies near
17 Hz. While it is likely that no important physiological
process has gone undetected, the extrapolations to high
frequency performed above do not perfectly characterize
the system. For example we have occasionally found size-
able errors in the overall amplitude of the Fourier
synthesis predictions of the response to very rapidly
moving stimuli (with velocities of 1.8 eye-widths/second),

though the waveform shapes were generally accurate.
This scaling problem is presumably an artifact of the
procedures for extrapolation of the transfer function
beyond the frequencies at which it was measured. Should
such high-frequency behavior prove of interest, the
inclusion of suitable stimulus components in the analysis
stimuli would circumvent this problem. If necessary,
two or more sets of input frequencies could be used in
alternation to extend the range or resolution of the
transfer function measurements without compromising
the power at each stimulus frequency necessary for adequate
response measurements.

   At the other end of the spectrum is the dependence
of the response on the steady mean illumination level
about which the stimuli varied in time. Our stimulus
generation equipment did not allow for the systematic
study of this experimental variable. While it is likely
that large changes in the illumination level would produce
some changes in the model parameters with which we have
described the eye, the basic model would probably remain
valid. Of course at very low light levels, impulses
would become so rare as to call into question the entire

program of dynamic analysis. Indeed, the study of the
effects on vision of changes over many orders of magnitude
in mean illumination has long been a favorite subject in
the fields of visual psychophysics and neurophysiology.
However, it should be pointed out that such studies must
of necessity consider only steady-state responses, or
parametric changes in the dynamic response, as the dynamic
response of the retina is completely saturated by much
more modest changes in illumination, provided they occur
rapidly. Only by changing its "operating point" by means
of the relatively (and often absolutely) slow processes
of light and dark adaptation can the eye operate dynamically
over its fabled range of sensitivity. Even in an ordinarily
lighted scene, variation of one order of magnitude in the
reflected light intensity is extreme (comparable to the
contrast of black ink on white paper). Thus, the use of
relatively small variations of light intensity in the
above studies does not weigh strongly against their validity
as characterizations of the dynamics of the response of
the Limulus retina.

As was mentioned above, we have ignored a well-known
nonlinearity in the inhibitory coupling (Lange, 1965; Barlow

and Lange , 1974). This effect is manifest in the steady
state as the excitation level (that is, the uninhibited
response) of the unit being inhibited varies over tens
of impulses per second. While this effect would thus
be unimportant in the prediction of the Mach band
effects described above, it might still alter the inhibi-
tory coupling during the brief on-transients of the
response. The success of the linear model in predicting
the results of the simulated-edge experiments of Chapter
VIII, however, argues that the dependence of inhibitory
coupling on excitation does not occur on the brief time
scale of the observed on-transients. It remains possible
that this nonlinear effect can be observed dynamically,
but this would require very large variations in stimulus
intensity on an intermediate time scale.

Another failure of linearity in the Limulus eye
is a facilitation of lateral inhibitory transients by
preceding activity in the inhibiting ommatidia (Graham
et al., 1973). The repetitive nature of our stimuli
make the assessment of the role of this phenomenon in
the present experiments very difficult. Though the

experimental conditions used by Graham et al. differed

greatly from those employed here, it is still worth

mentioning that in their hands, a steady impulse rate

of 10 impulses/second in the inhibiting units sufficed

to evoke maximal facilitation. Thus it is possible

that our dynamic measurements reflect the properties

of inhibition in its fully facilitated operating regime,

which may well be a more normal physiological state

than the highly dark-adapted condition in which inhibi-

tory facilitation may be readily demonstrated.

One final question to be considered is the extent

to which the data given above are compatible with, or

rule out, alternatives to the Hartline-Ratliff model

of the Limulus retina. Actually, this question may be

considered on two levels: first, as it concerns the

general structure of the model (for example, as described

in Figure 5-3 or equation (5.7)), and second, as it

concerns the functional forms for the component trans-

ductions, and the values for the parameters (as presented

in chapters V and VI).

The data do appear to single out the Hartline-Ratliff

model in the following sense. First, as far as dynamic

responses of the retina are concerned, the model-free
considerations of chapters II and IV convincingly
demonstrate that only linear models of the retina need
be considered. Except for the final nonlinearity in-
herent in the process of encoding intracellular "slow"
potentials into impulse trains with modest mean impulse
rates (a somewhat trivial nonlinearity from the systems-
analytic point of view), any dynamic nonlinearities in
the retina are sufficiently subtle as to be safely
ignored, at least at the level of sophistication of our
present measurements. Second, as was described in
Chapter V, the component processes of light-induced
excitation (the generator potential), lateral inhibi-
tion, and self inhibition, and the algebraic summation
of these effects to produce a net intracellular potential
which in turn drives the impulse-generating mechanism
of the eccentric cell, have all been documented by direct
intracellular recording, and must therefore be included
in any prospective model of the Limulus retina. Thus
the Hartline-Ratliff model may be considered a minimal
model, relative to the known physiological repertoire
of the Limulus eye. The success of this model in the

various applications of Chapters VI and VIII suggests
that this minimal model is in fact adequate to predict
the responses of the system under widely varying condi-
tions. It is thus unlikely that a physiologic process
of any major significance has been omitted from the
Hartline-Ratliff model.

On the other hand, the functional forms and para-
meter values cannot be uniquely specified by these
experiments. Nevertheless, some of the information repre-
sented by these forms is of physiological significance.
For example, to our knowledge, these experiments repre-
sent the first determination of the inhibitory kernel
under dynamic conditions. Our finding of a "crater" in
the inhibitory kernel, by methods independent of those
used previously should help resolve a longstanding contro-
versy in the field concerning the existence of this feature.
We likewise are able to demonstrate the effective "delay"
of the lateral inhibitory process, and to fix, at least
in general terms, the high-pass and low-pass characteristics
of the light-to-generator potential transduction.

On the other hand, it remains possible that under
different experimental conditions, these functional forms
may be found inadequate. Alternative models of the

component transductions may eventually be devised which can describe aspects of retinal physiology not incorporated into our present formulation, particularly the dependence of the steady-state response parameters on illumination intensity.

In summary, we have pursued a program designed to relate the macroscopic response of the Limulus retina as a whole to the known physiological processes which have been shown elsewhere to underly the visual transduction at the cellular level. We thus obtain an empirical transfer function which sufficiently characterizes the eye to predict the response of interior neurons to a wide variety of arbitrary moving stimuli. This transfer function is then used to calibrate a quantitative model for the retina in terms of parameters which describe the microscopic component processes of the visual transduction. This calibrated model not only accounts for the response of neurons located in the interior of the retina, but also may be extended to predict the response of neurons located near the edge of the retina. We are thus able to describe the retina in quantitative terms from both a microscopic and macroscopic point of view, on the basis of purely noninvasive, macroscopic measurements which leave the retina functionally intact.

Of course, the <u>Limulus</u> retina has long been recognized as a particularly favorable system; it may never be possible to characterize such complicated neural networks as the vertebrate retina or cerebral cortex on the basis of a systems-analytic characterization of the output of a single representative neuron. Nevertheless, we submit that the present study may well serve as an example of the utility of the occasional suppression of our knowledge of subcellular neurophysiology in lieu of more comprehensive descriptions of the functioning of the many interacting neurons of complex neural networks.

"All right," said the Cat; and this time it vanished quite slowly, beginning with the end of the tail, and ending with the grin, which remained some time after the rest of it had gone.

L. Carroll, 1865

X. EPILOGUE - Applications to the Response Dynamics of Cat Retinal Ganglion Cells

The use of systems-analytic techniques for the characterization of the vertebrate retina was discussed briefly in Chapter I. Though the idea of applying formal linear or non-linear methods to vertebrate visual neurons has often preceded application to the simpler retinas of invertebrates, the full program of analysis and synthesis has only rarely been attempted. One system which appears susceptible to such a treatment is the X-type retinal ganglion cell of the cat   (Figure 10-1). In the few paragraphs below, some considerations arising from preliminary investigations of these neurons are discussed.

The ganglion cells of the vertebrate retina constitute the only output pathway from the retina to the brain, as well as the final site of neural integration within the retina, much like the eccentric cells in the eye of Limulus. The study of the dynamics of ganglion cells in the cat retina was greatly clarified by the separation of these cells by Enroth-Cugell and Robson (1966) and

Figure 10-1. Cat, anterolateral view. (After J. Tenniel;
see L. Carroll, 1865).

others (see Rowe and Stone, 1977) into classes with markedly

different properties of response dynamics and spatial summation:

"X cells" show predominantly first-order responses (that is,

responses which contain only those temporal frequency components

present in the stimulus) to counterphase-modulated

sinusoidal gratings; such gratings may be positioned in

such a way that a "null" response is obtained, a finding

taken to indicate linear spatial summation. In contrast,

"Y cells" show responses with major components at frequen-

cies double those present in the stimulus; these frequency-

doubled responses are insensitive to the position of the

grating stimulus. These distinctions are best made with

responses to gratings of the highest spatial frequency

which the ganglion cells can resolve (Hochstein and Shapley,

1976).

The Y-cells are evidently very nonlinear transducers,

and are thus not appropriate for a linear treatment such

as that given above for the Limulus retina. On the other

hand, the X cells appear to be likely candidates for such

a treatment, which might thus realize, in quantitative

terms, and for specific ganglion cells, a significant

improvement over the "generic" linear descriptions referred

to in chapter I.

It was decided to begin with the analysis and syn-
thesis of the response of the retina to purely temporal
signals (that is, to stationary bars or gratings modulated
in time), as most previous studies have concentrated on
only <u>analysis</u> of ganglion cell responses, or have skipped
immediately to moving stimuli, which vary in space as well as
in time. Thus, in any one experiment, one spatial pattern
was chosen and modulated with either a sum-of-sinusoids
signal, for analysis, or a simple square wave signal, to
generate responses for comparison with synthesis calcula-
tions. (On occasion, temporal signals in the form of
square waves with exponential decay were also employed
for synthesis episodes.) The contrast of the analysis
or synthesis stimulus was sometimes varied between runs
in order to examine the scaling of the response with
contrast, which provided a direct test of the superposi-
tion property.

Methods

The methods used in our laboratory for the extra-
cellular recording of dynamic responses from retinal
ganglion cells in the cat are described in detail else-

where (Hochstein and Shapley, 1976). Recordings were
made with tungsten-in-glass microelectrodes positioned
by stereotaxic means in the optic tract. The cats were
maintained under urethane anaesthesia. Stimuli were
produced as described in chapter III, but with a frame
rate of 250 Hz. First- and second-order response com-
ponents were determined from the impulse train data as
described in Appendix C. Contamination by response components
of order higher than two were suppressed by varying the phases of
the stimulus components, as described by Victor and Shapley (1979)
Square wave responses were displayed by means of histo-
grams synchronized to the stimulus period.

Results

For typical analysis stimuli (for example, a 1.0
cycle/degree grating modulated with a maximum contrast
of 50% about a mean luminance of approximately 10 cd/m^2)
frequency-doubled response components were in
general less than one-tenth as large as the corresponding
first-order responses. This suggests that the first-order
frequency response functions (such as those shown in Fig. 10-2)
may indeed provide a useful description of the dynamic response
of X cells under these conditions.
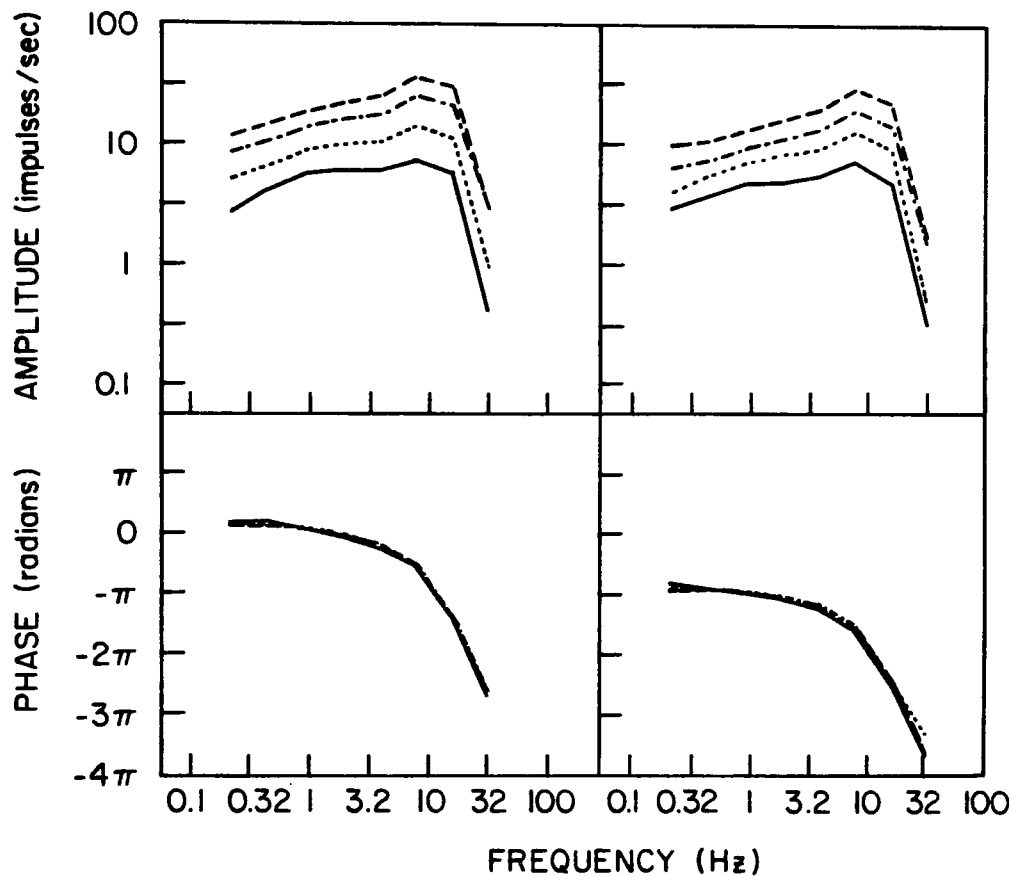
Figure 10-2. First-order frequency response functions for cat X cells. The analysis stimuli consisted of 1.0 cycle/degree sinusoidal gratings modulated according to a temporal signal composed of eight sinusoidal components of equal strength, with frequencies of 0.214, 0.458, 0.946, 1.923, 3.876, 7.782, 15.594, and 31.219 Hz. Stimulus gratings were positioned so as to evoke a maximal response. Data from two ganglion cells are shown, an "on-center" cell at left, and an "off-center" cell at right (note phase at low frequency). Response functions were measured at four contrast levels, with maximum contrast successively reduced by a factor of 2 between measurements. Amplitudes (top) decrease with decreasing contrast.

The scaling of these response functions with contrast,
however, differs from that expected of a linear system.

As the contrast is increased by three successive doublings,
the phases remain unchanged, and amplitudes increase by roughly
the same factor at each temporal frequency (as expected of a
linear system), but the increase in response amplitude is less
than the increase in stimulus contrast. For the "on-center"
X cell data shown at left in Figure 10-2, the response grows
by less than a factor of 5 in response to the eight-fold increase
in stimulus contrast. The "off-center" response shown at right
grows by less than a factor of 4 under the same conditions.
The scaling of these responses, while not precisely equal for the
successive doublings of stimulus contrast, conforms rather well
to a power-law relationship between the stimulus contrast and
the response amplitude. (The exponents are approximately 0.7
for the "on-center" cell at left, and 0.6 for the "off-center"
cell at right.) These results thus confirm and extend the
findings of Hughes and Maffei (1966), who reported similar
scaling of responses to sinusoidally modulated spot stimuli,
with power-law exponents which ranged from 0.68 to 0.78. [*]

---

[*]   Because the response of these cells does not scale
linearly with contrast, the quotient of the response and the
stimulus is no longer independent of contrast. Hence, the ratio
of the output to the input for the various sinusoidal signal

components no longer defines an unambiguous "transfer function" for the response of these cells. Thus, for the response functions shown in Figure 10-2,3, the amplitude curves represent merely the relative response amplitude, with no normalization for stimulus contrast. However, for the purposes of a synthesis calculation, some normalization procedure is necessary. For the synthesis experiment described below, responses to stimulus components were normalized as if the response of the system varied linearly with contrast.

(end of footnote)

Even greater deviations from the superposition principle can be demonstrated with coarser stimulus gratings (Fig. 10-3). The responses of this cell show considerable change in phase as the contrast is increased; the amplitudes no longer scale with contrast uniformly across temporal frequencies. Indeed, the cells whose responses are shown in Figure 10-2 appear to be exceptionally linear (Shapley and Victor, 1978).

A similar saturation was observed in an attempted synthesis calculation shown in Figures 10-4 and 10-5. The analysis stimuli were presented at only one contrast, and yielded the frequency response function shown in Figure 10-4. Two temporal synthesis signals, a square wave, and a square wave with exponential decay, were used. These synthesis stimuli were presented at maximum contrasts of one-half and one-fourth that of the analysis stimuli, and produced the responses shown in Figure 10-5. The modulation produced by the higher-contrast stimuli was greater than that produced by the same stimuli at one-half the contrast, but by much less than a factor of two. Similarly, the predictions of the linear synthesis calculation, which are based on the partially saturated response to the high-contrast analysis stimulus, considerably underestimate the size of the square-wave responses. It should also be noted that the linear synthesis seriously underestimates the magnitude of the high-frequency on-transient response components.
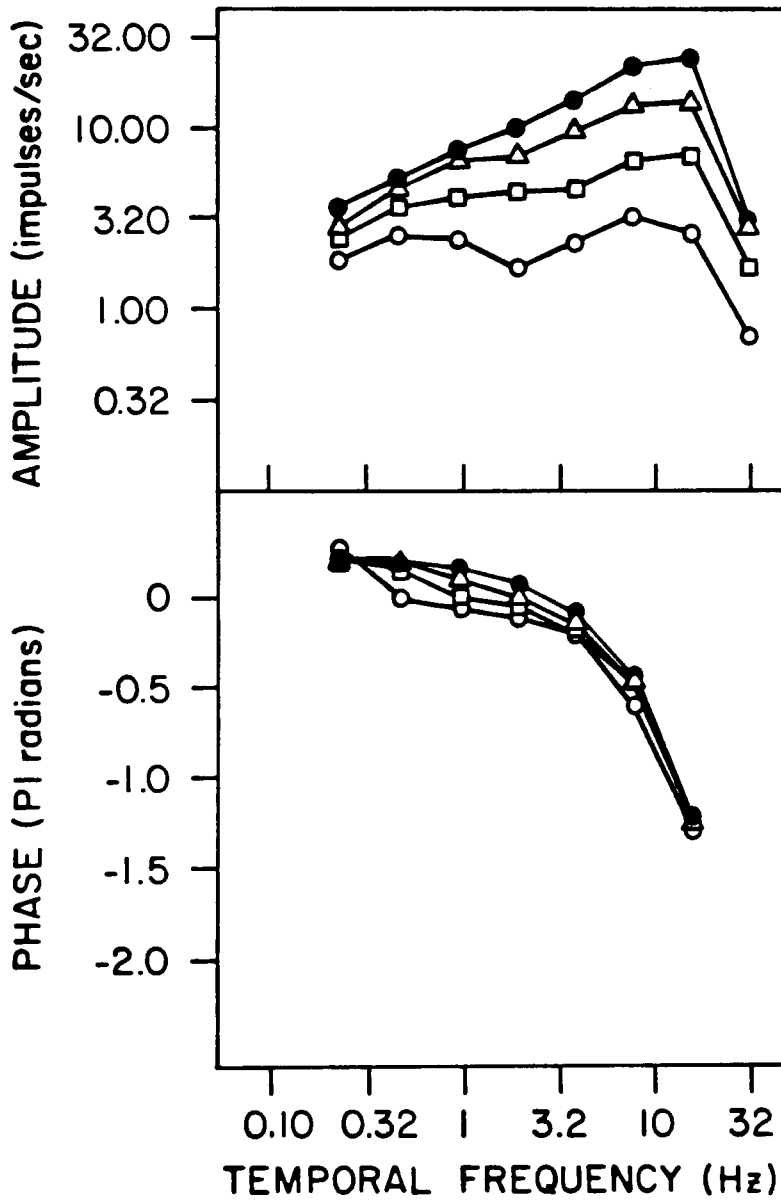
Figure 10-3. Frequency response function for cat X cells. Conditions were the same as in Figure 10-2, except that a sinusoidal grating stimulus of 0.2 cycles/degree spatial frequency was used (from Shapley and Victor, 1978).
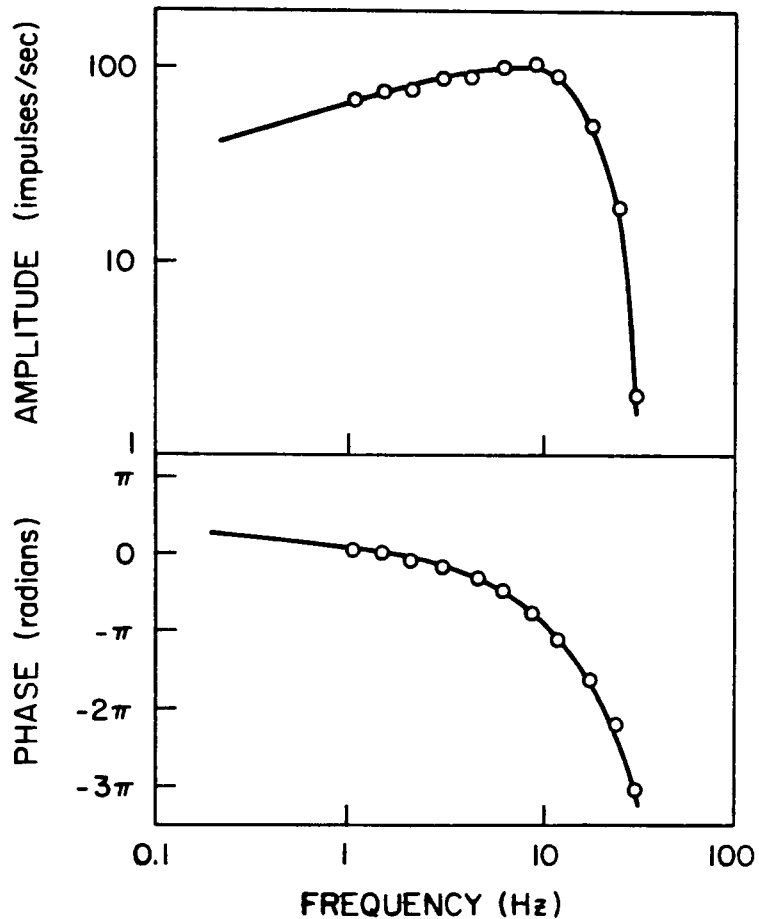
Figure 10-4. High-resolution frequency response function for synthesis experiment. The stimulus consisted fo a 1.0 degree wide bar modulated about the steady illumination level of the surrounding region. The bar was positioned for maximal response. The temporal signal for analysis consisted of 11 sinusoidal components of equal amplitude, with frequencies of 1.07, 1.50, 2.17, 3.08, 4.36, 6.44, 9.06, 12.12, 17.85, 25.12, and 31.16 Hz. Maximum contrast for all analysis episodes was 50%. The response function was extrapolated to low frequencies as shown for the purposes of the synthesis calculations shown in Figure 10-5.

Figure 10-5. Cat X cell synthesis experiment. The spatial

pattern was the same as used to obtain frequency response functions for

Figure 10-4. Temporal pattern was either a square wave (records

at left) or a square wave with exponential decay (records at

right; the time constant of the decay was equal to one-half the

repeat period of the stimulus). Maximum contrast of the

synthesis stimuli was either 25% (top row) or 12.5% (bottom

row). Histograms show observed responses; smooth curves show

predicted responses as calculated from equation (2.10), using

the response function of Figure 10-4.

Figure 10-5
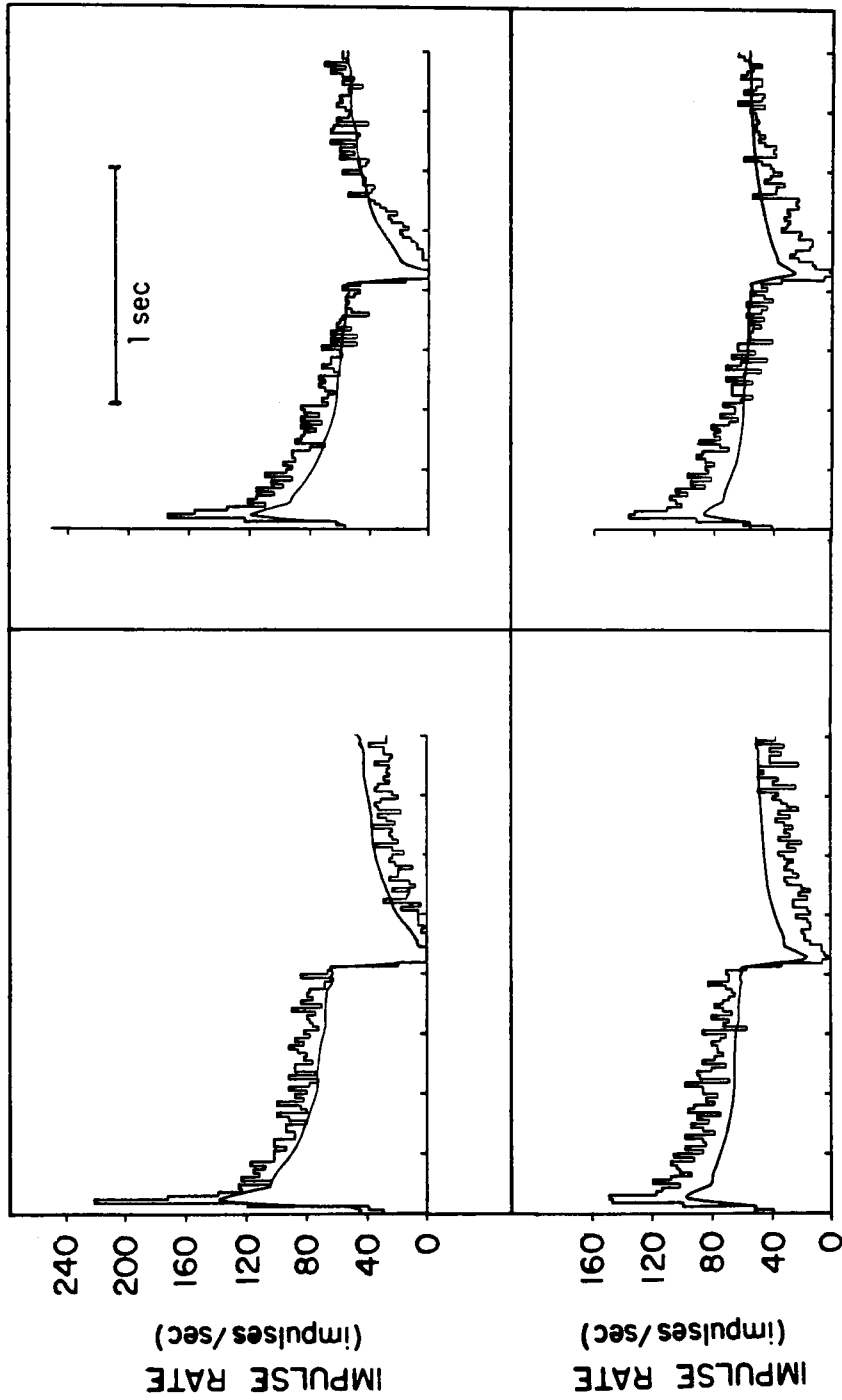
Discussion

The few results described above are of a preliminary nature. A complete characterization of the transfer characteristics of X cells will require systematic study of the effect of contrast and spatial pattern on the response measurements (see Shapley and Victor, 1978 for results in this direction). However, even the sparse results given here suggest that these ganglion cells function in an intriguing way: like linear systems, they produce sinusoidal responses to sinusoidal stimuli, but these responses do not scale linearly with stimulus contrast. Thus these cells appear to lie somewhere between the linear transducers treated above and the nonlinear systems usually encountered, such as rectifiers and power-law devices. In any event, it appears unlikely that these cells can be satisfactorily described for quantitative purposes by means of a single transfer-function, or any equivalent procedure couched in terms of impulse responses and convolutions. The development of a concise and effective formalism for the quantitative description of these ganglion cells thus remains an important problem for future work.

TABLE 1

Summary of Equations for the Hartline-Ratliff Model for the _Limulus_ Lateral Eye

Description	Equation #	Equation
Spatio-Temporal transfer function	(5.10)	$$F(\xi,\omega) = \frac{\tilde{P}(\xi)\cdot E(\omega)\cdot G(\omega)}{1+E(\omega)\cdot T_L(\omega)\cdot \tilde{k}(\xi)}$$
Generator Potential	(5.11)	$$G(\omega) = e^{-i\omega t}\ell\cdot\left(\frac{1}{1+it_d\omega}\right)^{n_d}\cdot\left(\frac{1}{1+it_b\omega}\right)^{n_b}\cdot\left(1-\frac{R}{1+it_a\omega}\right)\cdot\left(\frac{it_a\omega}{1+t_a\omega}\right)^p$$
Encoder	(5.14)	$$E(\omega) = \frac{1}{1+\dfrac{\kappa}{1+i\tau\omega}} = 1 - \frac{\kappa/(1+\kappa)}{1+\dfrac{\tau}{1+\kappa}\omega}$$
Lateral Inhibition	(5.15)	$$T_L(\omega) = \frac{1}{1-C}\cdot\left(\frac{1}{1+i\tau_1\omega}\cdot\frac{1}{1+i\tau_2\omega} - \frac{C}{1+i\tau_3\omega}\right)\cdot\frac{1}{1+i\tau_4\omega}$$
2-dimensional inhibitory kernel	(5.16)	$$k(x,y) \propto e^{-(x^2+\frac{y^2}{\eta^2})/a^2} - D\cdot e^{-(x^2+\frac{y^2}{\zeta^2})/b^2}$$
1-dimensional inhibitory kernel	(5.20)	$$k(x) = \frac{K}{(Aa-Bb)\sqrt{\pi}}\cdot\left(Ae^{-x^2/a^2} - Be^{-x^2/b^2}\right)$$
Fourier transform of inhibitory kernel	(5.21)	$$\tilde{k}(\xi) = \frac{K}{(Aa-Bb)}\cdot\left(Aae^{-\xi^2a^2/4} - Bbe^{-\xi^2b^2/4}\right)$$
	(8.4)	$$\tilde{k}(\xi) = K\cdot\frac{1-\left(\frac{\xi^2}{2}\right)^\alpha}{\left(\frac{\xi}{\beta}\right)^4 + 2\left(\frac{\xi}{\gamma}\right)^2 + 1}$$
Point-spread	(5.22)	$$\tilde{P}(\xi) = e^{-\xi^2 s^2/4}$$

TABLE II

Parameter Values for the Hartline-Ratliff Model

Parameter	Description	Dimension	Preparation:*				
			2/22/77	5/26/77	7/26/78	7/31/78	8/2/78[§]
t_ℓ	mean bump latency	sec	0.023	0.023	0.038	0.023	0.038
t_d	latency dispersion time-constant	sec	0.0076	0.0091	0.0076	0.0061	0.0076
n_d	dispersion exponent		4	4	3	4	3
t_b	bump-shape time-constant	sec	0.017	0.019	0.017	0.016	0.017
n_b	bump-shape exponent		4	4	3	4	3
R	adaptation strength		0.96	0.89	0.75	0.75	0.75
t_a	adaptation time-constant	sec	0.013	0.020	0.030	0.030	0.030
p	low frequency adaptation exponent		0.25	0.25	0.25	0.25	0.25
κ	self-inhibitory strength		0.05	1.0	1.5	1.0	0.5
τ	self-inhibitory time-constant	sec	0.125	0.125	0.40	0.20	0.40
τ_1	lateral-inhibitory time-constant 1	sec	0.033	0.0415	0.036	0.030	0.050
τ_2	lateral-inhibitory time-constant 2	sec	0.050	0.0415	0.055	0.045	0.07
τ_3	lateral-inhibitory time-constant 3	sec	0.033	—[†]	0.036	0.030	0.05
τ_4	lateral-inhibitory time-constant 4	sec	0.017	0.010	0.019	0.015	0.03
C	lateral inhibition structure constant		0.1	0.	0.1	0.1	0.1
K	total lateral inhibitory strength		1.60	2.60	1.0	1.5	4.0
A	inhibitory strength (relative)	eye-widths	1.00	2.06	1.5	2.0	1.2
a	inhibitory space constant		0.182	0.17	0.125	0.17	0.12
B	crater strength (relative)	eye-widths	1.92	1.20	1.65	1.2	0.75
b	crater space constant		0.027	0.025	0.03	0.025	0.03
α	structure constants for	rad/eye-width			17.56	21.59	23.23
β	"rational expression" inhibitory	rad/eye-width			23.61	21.58	21.66
γ	kernel transform	rad/eye-width			24.83	14.81	27.62
s	point-spread space-constant	eye-width	0.016	0.0083	0.00951	0.00653	0.00951

Notes for Table II

† Time constant undefined when C=0.

§ Parameter set determined by comparison of observed
and predicted responses to moving pattern, with
parameters for preparation of 7/26/78 used as
starting point for parameter search. (See text.)

* These parameter sets correspond to experiments as follows:

2/22/77: Figures 4-1,4-2,4-3,4-4,4-5,4-6,6-8,6-10,6-15,6-16,C-3.

5/26/77: Figures 6-1,6-2,6-3,6-4,6-5,6-6,6-7,6-11,6-12,6-13,6-14.

7/26/78: Figures 8-2,8-3,8-4,8-5,8-6,8-10.

7/31/78: Figures 8-7,C-1.

8/2/78: Figures 8-8,8-9.

TABLE III

Summary of Formulas for Wiener-Hopf Treatment of the <u>Limulus</u> Retina

Description	Equation #	Equation
moving stimulus	(7.10)	$S(x,t) = S(x-vt)$
effective stimulus	(7.12)	$\tilde{P}(\omega) = \dfrac{1}{v} E(\omega)G(\omega)\tilde{P}(-\tfrac{\omega}{v})\tilde{S}(-\tfrac{\omega}{v})$
definition of solution operator	(7.3)	$\tilde{R}(x,\omega) = \tilde{P}(\omega)\cdot\tilde{\Phi}(x,\omega)$
effective dynamics of lateral inhibition	(7.24)	$S(\omega) = E(\omega)\cdot T_L(\omega)$
transform of inhibitory kernel	(7.26)	$\tilde{k}(\xi) = N(\xi^2)/D(\xi^2)$ (degree N < degree D = M; $D(\xi^2)$ monic)
factorization	(7.27)	$D(\xi^2) + S(\omega)N(\xi^2) = \displaystyle\prod_{\ell=1}^{M}(\xi^2-\mu_\ell^2(\omega))$ (Im$(\mu_\ell(\omega))>0$)
		$D(\xi^2) = \displaystyle\prod_{m=1}^{M}(\xi^2-\lambda_m)$ (Im$(\lambda_m)>0$)
solution operator, full eye	(7.5,7.36,7.40)	$\tilde{\Phi}(x,\omega)_{\text{full eye}} = \dfrac{e^{\,i(-\frac{\omega}{v})x}}{1+S(\omega)\tilde{k}(-\tfrac{\omega}{v})} = e^{\,i(-\frac{\omega}{v})x}\cdot\displaystyle\prod_{j}^{M}\dfrac{(-\tfrac{\omega}{v})^2-\lambda_j}{(-\tfrac{\omega}{v})^2-\mu_j^2(\omega)}$
solution operator, truncated retina, at the boundary	(7.35)	$\tilde{\Phi}(x{=}0,\omega)_{\text{truncated}} = \displaystyle\prod_{j}^{M}\dfrac{-\tfrac{\omega}{v}+\lambda_j}{-\tfrac{\omega}{v}+\mu_j(\omega)}$
solution operator, truncated retina, $x\geq 0$	(7.43)	$\tilde{\Phi}(x,\omega)_{\text{truncated}} = \tilde{\Phi}(x,\omega)_{\text{full eye}} + \tilde{\Phi}(x{=}0,\omega)_{\text{truncated}} \cdot \displaystyle\sum_{j}^{M}\dfrac{\prod_m(\mu_j(\omega)-\lambda_m)}{\prod_{\ell\neq j}(\mu_j(\omega)-\mu(\omega))}\cdot\dfrac{e^{\,i\mu_j(\omega)\check{x}}}{\mu_j(\omega)-(-\tfrac{\omega}{v})}\ .$

Appendix A: A Fiber-optic "Contact-Lens" for the Limulus Lateral Eye

The ommatidia of the Limulus lateral eye, which have an acceptance angle of less than 6°, diverge greatly, covering roughly a hemisphere of solid angle. A consequence of this geometry is that a stimulus consisting of parallel rays of incident light will excite only a small patch of ommatidia (corresponding to the pseudopupil seen from the direction from which the light comes). This has proved to be a scant impediment in studies involving only a few (or a few groups of), nearby ommatidia, where fiber-optic light guides less than a few millimeters in diameter have provided adequate stimuli. On the other hand, it has been very difficult to provide carefully controlled illumination to a large population of ommatidia. One approach to this problem (F. Dodge and E. Kaplan, personal communication) is to place a naked Limulus eye close to a display oscilloscope. While this method has the advantage of great simplicity, it is capable of illuminating only about one-third of the horizontal extent of the eye. The resolution of the "natural optics" is also somewhat limited. Much better resolution can be obtained by imaging a stimulus directly onto the Limulus cornea with a system of lenses. Unfortunately, this successfully illuminates only a small cluster of ommatidia. What is needed is an arrangement of light guides arranged along a curved surface resembling the Limulus cornea, whose optic axes converge in a manner corresponding to the

divergence of the ommatidial axes.

In order to approximate such an optical array, we have turned to the technology of fiber optic tapers. Such a taper consists of a frustum-like portion of a "coherent" lattice of glass fibers embedded in a glass matrix of lower refractive index, which has been heated and drawn into a conical shape. Ordinarily, the two end surfaces of such a taper are polished into parallel planes. The taper then maps each point of one surface to one point of the other surface, so that an image formed on one surface is reproduced on the other. Such tapers are routinely used as magnifiers or "condensers"(image-reducers) (see Fig. Ala) (Kapany, 1967). Unfortunately, if the narrow end of such a taper is simply ground to form a concave spherical surface conformable to the Limulus cornea, the optic axes of the fibers in the taper remain parallel to the axis of the cone, and to each other; they are thus poorly oriented to illuminate the divergent ommatidia in a Limulus eye.

Recently, we have obtained (courtesy of Walter P. Siegmund, Fiber-Optics Division, American Optical Corp., Southbridge, Mass.) fiber optic tapers with concave spherical small ends (and flat large ends) fabricated so that the optic fibers are approximately perpendicular to the polished spherical surface (Fig. Alb). While such an array of fibers diverges somewhat less than the array of Limulus ommatidia,

Figure A1. Schematic indication of the fiber orientation
in two kinds of fiber optic taper. (a) Standard magnifier/
condenser: fibers perpendicular to two flat surfaces.
(b) Fiber optic taper used for these studies. Note how
fibers are approximately normal to curved surface.

we have found that it satisfactorily illuminates virtually the entire Limulus eye. As these tapers provide the crucial link in the production of our visual stimulus, we describe them below in considerable detail.

The tapers (Fig. A2) are 2.8 cm in maximum diameter and 1.8 cm in height. The narrow ends are ground to spherical surfaces of different curvatures to accomodate eyes of various sizes. One taper was used for almost all the experiments, and is well suited to the eyes of most crabs of diameter 15-20 cm; it bears a spherical surface 1.2 cm wide and 0.25 cm deep, with a radius of curvature of about 0.85 cm. A second taper was used for a few crabs with large, flat eyes. Its spherical surface is 1.4 cm wide, .2 cm deep, with a radius of curvature of 1.3 cm. A third taper, designed for small eyes (spherical surface 1.0 cm wide, 0.3 cm deep, radius of curvature 0.57 cm), was not used.

The optical fibers of the tapers are roughly square in cross-section. At the flat surface of each taper, they are 10 μm square; on the spherical surface, they are roughly 5 μm square (Fig. A3). As each ommatidium presents a corneal aperture approximately 200 μm in diameter, it is clear that in no significant way do the discrete fibers of the fiber optic taper degrade the visual stimulus.

A more serious source of distortion stems from the geometric consequences of mapping a plane surface con- tinuously onto a portion of a sphere. In any such mapping,
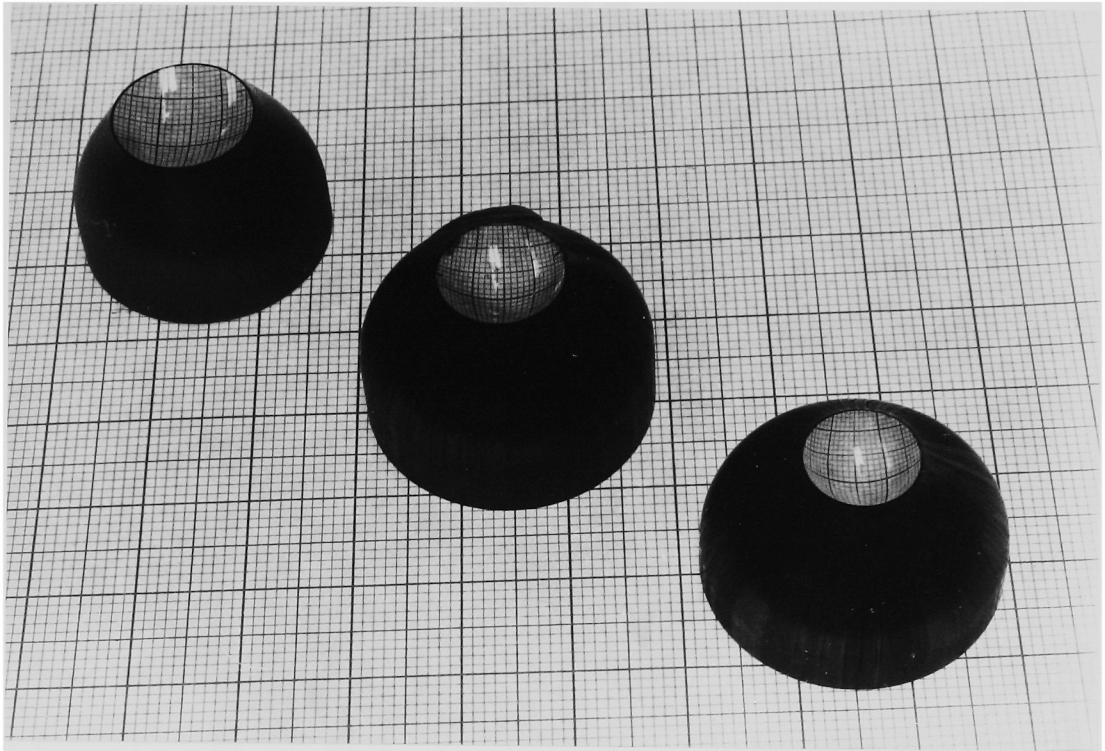
Figure A-2. Three fiber optic tapers obtained for this
study; from left to right for large, medium, and small eyes
respectively. The smallest subdivisions of the graph paper
on which the tapers rest are 1. mm squares.
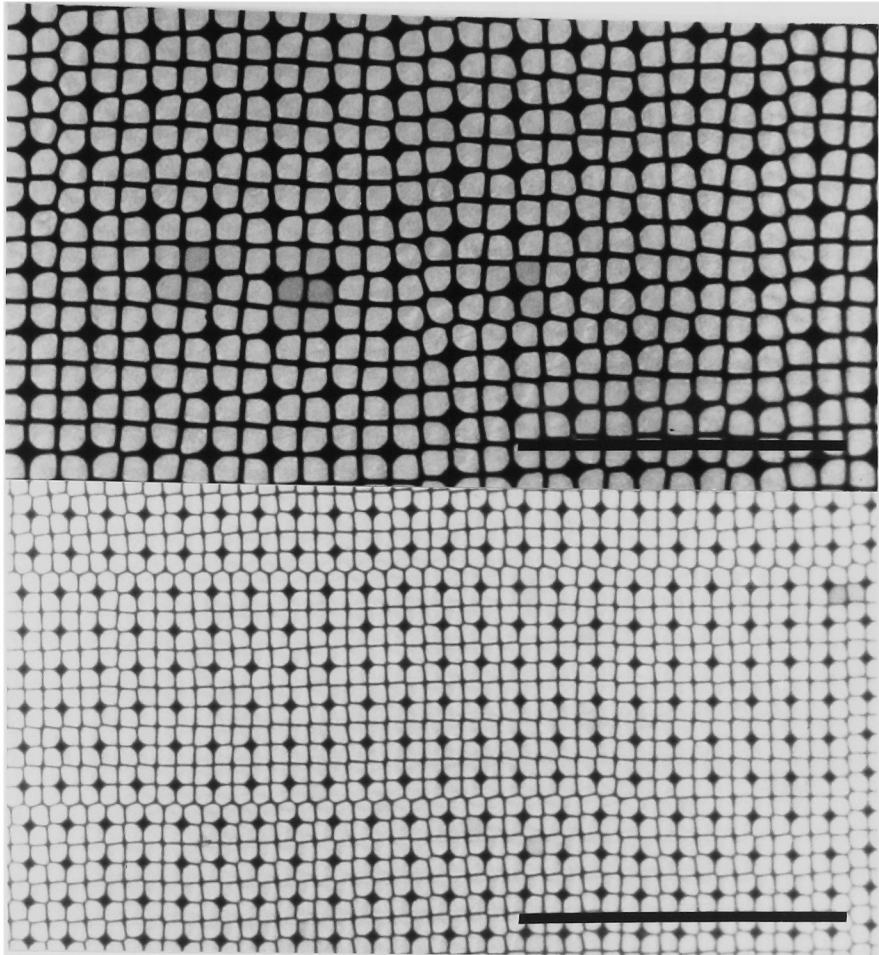
Figure A3. Top: Photomicrograph of the fiber array at the flat surface of fiber optic taper. The transmitting fibers are light, the matrix appears dark. Bottom: Photomicrograph of the fiber array at the spherical surface of fiber optic taper. Each fiber occupies roughly one-fourth of its previous area. Scale markers 100 µm.

some distortion is inevitable (Gauss, 1828). In our tapers, the distortion is modest and continuous (see Fig. A4), and was ignored in the experimental work, without apparent difficulty.[*]

The fiber optic tapers were coupled to the <u>Limulus</u> eyes, both optically and mechanically, by gluing them directly to the cornea with a quick-setting, transparent cyanoacrylate glue (Krazy Glue, Chicago, Ill.). This provided an extremely stable linkage, with excellent optical properties (see below). Before the dissection was performed, projecting ridges on the <u>Limulus</u> carapace were removed with a rapidly rotating burr, and the appropriate size fiber-optic taper was selected. After the dissection, two drops of glue were placed on the concave surface of the taper, which was then immediately applied to the cornea, and held there by hand for one minute. Once the taper was secured in this manner, the lattice of ommatidia was clearly visible on the flat surface of the cone (Fig. A5), and the neural response to test lamps was typically as vigorous as before the taper had been applied.

---

[*] If we regard as the linear system under study the fiber optic taper followed by the Limulus retina, it is clear that the optical distortion does not invalidate the linear synthesis of the response of one test-ommatidium (see chapter VIII). However, such distortion, if severe, could complicate the physiological interpretation of the measured transfer function. In the present study, we believe this effect to be unimportant.
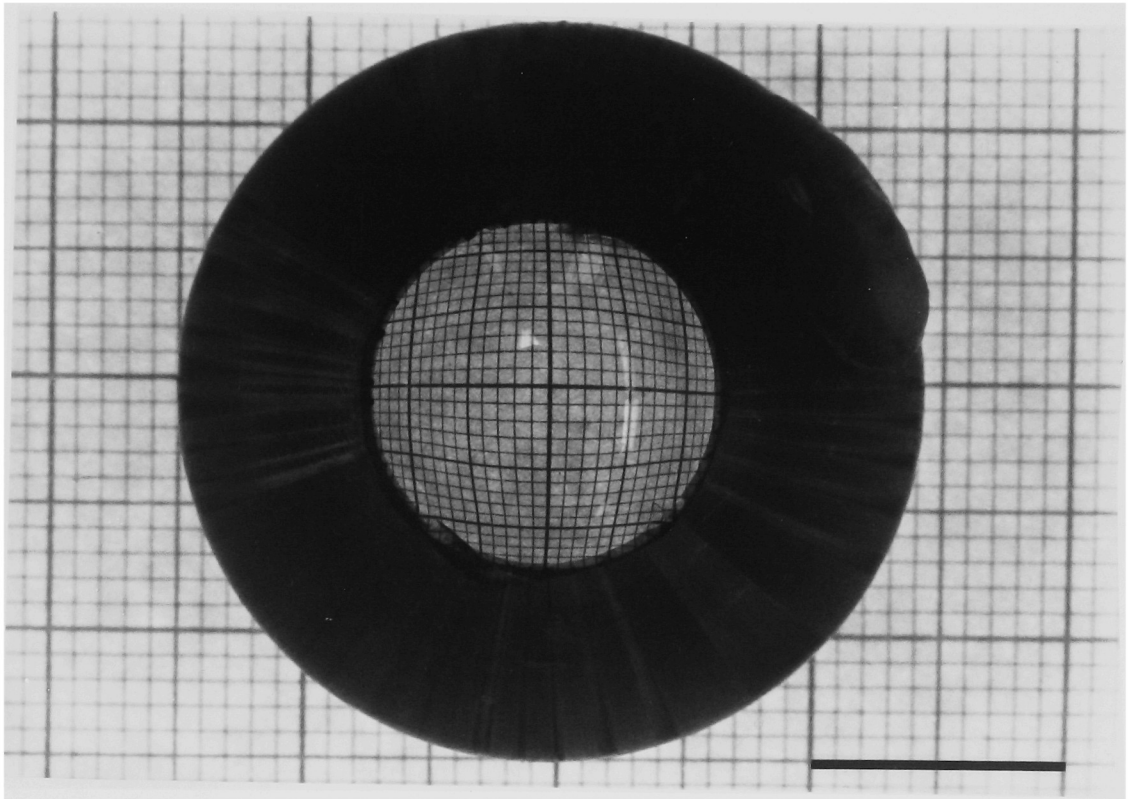
Figure A4. Continuous distortion produced by fiber optic taper mapping from flat surface to spherical surface. The medium-radius taper, used in most experiments, is seen from above, resting on uniform graph paper. The distortion at the edges of the cone is slightly exaggerated by photographic foreshortening of the spherical surface. Scale marker indicates 1.0 cm.
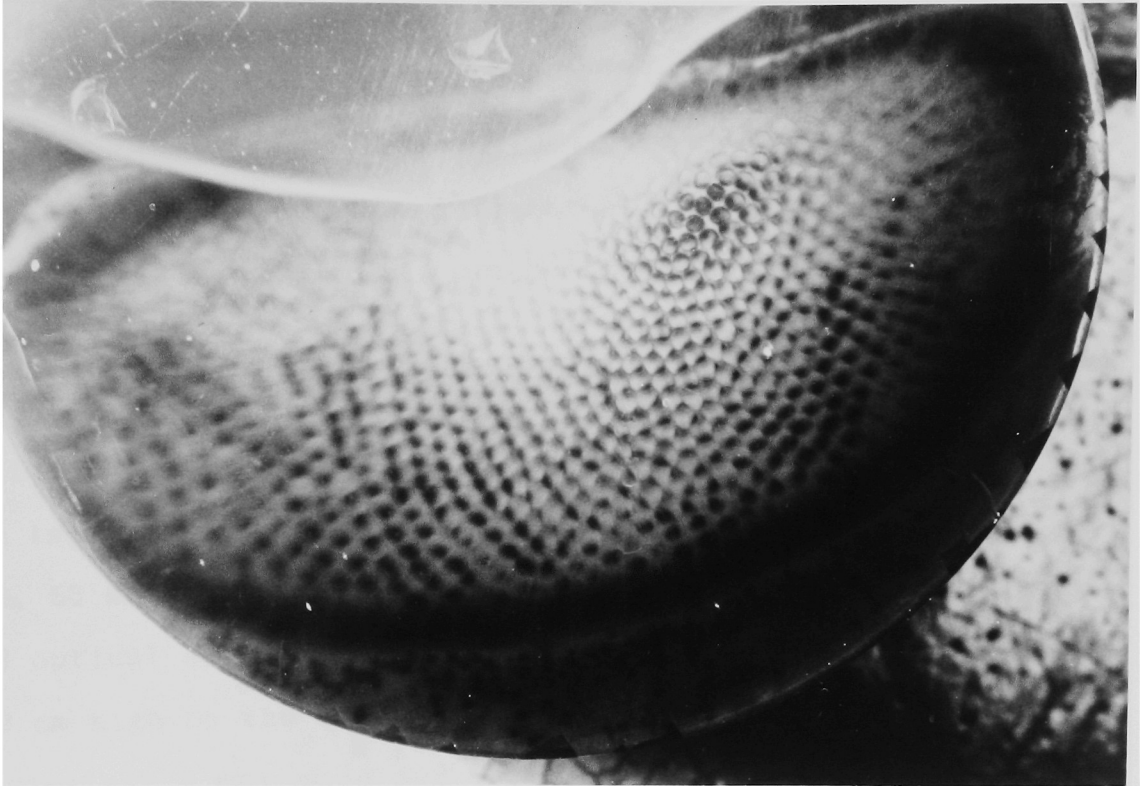
Figure A5. Lattice of ommatidia as seen through the
fiber optic taper. The meniscus at the top of the eye
is the upper limit of the glue which couples the taper
to the corneal surface. Except as described in chapter VIII,
test-ommatidia were selected only from the central
region of the eye, where the optical resolution was best.

Even though experimental test-ommatidia were generally chosen
from the central region of the eye, it was evident that the
fiber optic taper was easily able to stimulate even very
peripheral ommatidia, including those which ordinarily look
along the carapace. We are thus confident that our stimulus
effectively excited ommatidia across the entire width of the
eye.

The image of the pattern produced on the display
oscilloscope was focussed onto the flat surface of the fiber
optic taper by a suitably mounted camera lens (Nikon Nikkor,
f/1.2, 55 mm focal length). The overall effect of the com-
bined optical system was to convert a pattern 15 cm wide
and 2 cm high on the oscilloscope face to an image 1 eye-width
(approximately 1 cm) wide and 0.13 eye-widths high (approxi-
mately 5 ommatidial diameters, or $\frac{1}{4}$ of the height of the
eye) on the Limulus cornea.

In order to evaluate the optical performance of this
system, we examined its "point spread " characteristic,
that is, the size of the image of a point light source.
Of course, the ultimate performance of this system is limited
by the discrete nature of the Limulus eye: the image of a point
can be no smaller than a single ommatidium. To see if the image
was any larger, we employed two methods. One method con-
sisted of carefully removing the tissue behind the corneas
of excised Limulus eyes, exposing the array of crystalline

cones, and visually examining the image presented to the light-sensitive cells. The second method employed the comparison of transfer functions (light-to-impulse rate) for single ommatidia illuminated first by a small fiber optic light guide and then by the smallest spot obtainable with our oscilloscope-lens-fiber optic taper system. These experiments are described below.

To expose the crystalline cones, a <u>Limulus</u> eye was removed from the animal along with a rectangular section of the surrounding carapace, and placed in a vice. A rapidly-rotating burr was used to remove most of the hard materials behind the eye; the remaining covering was removed with forceps. The soft tissues behind the cornea were then wiped away with a cotton-tipped applicator, leaving the array of crystalline cones exposed. The eye was then glued to the fiber optic taper in the usual way, and studied from behind with a stereoscopic dissecting microscope.

The simplest way to describe the point spread characteristic is to observe the image of a point source. When such a source was positioned at the center of an ommatidium, that crystalline cone was observed to glow brightly. A faint glow was seen in the six nearest-neighbor crystalline cones, and in no others. Unfortunately, this pattern proved unsuitable for photography. A more dramatic illustration of this same effect can be seen by examining the image of an

edge; such an image is shown in Figure A6. Though inter-
pretation is hampered somewhat by the irregularity of the
ommatidial array, the figure clearly demonstrates that the
edge is spread over no more than one ommatidial diameter.
Figure A7 shows a <u>Limulus</u>-eye view of a sinusoidal grating
of approximately 4 cycles/eye. The physiological observation
that even peripheral ommatidia are well-illuminated is clearly
demonstrated. Figure A8 shows the image of a grating of
roughly 10 cycles/eye. It is well resolved by the ommatidial
array. Gratings at higher spatial frequencies were also
observed, and were resolved up to 16 or 20 cycles/eye.
These gratings were often difficult to see as static pat-
terns, but drifting or counterphase modulation readily demon-
strated their presence to the human observer. Beyond 20
cycles/eye, the Nyquist cutoff effect became prominent, and
drifting gratings began to "beat" against the ommatidial
lattice. (Recall that the eye is only 40 ommatidia wide.)
These observations confirm our claim that the optical
performance of this system is close to the limit imposed .
by the discrete nature of the eye itself.

Our second method of checking the point spread
of the optics was more physiological than the first. We
performed, in essence, a "small spot-large spot" experiment
(Ratliff et al., 1967), reasoning that if our optical system
significantly degraded the image of a point into a spot
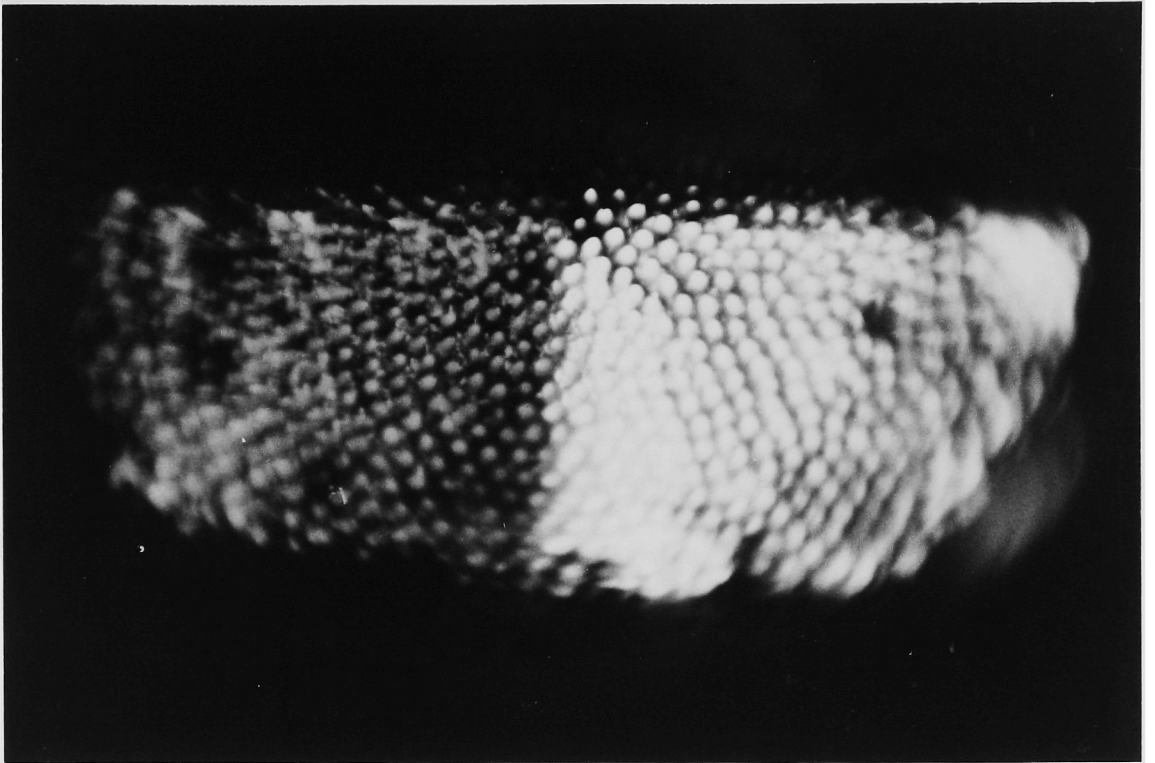
Figure A6. "Limulus-eye view" of an edge-stimulus. The photograph shows the interior surface of the array of crystalline cones, illuminated from the corneal surface by the optical system described in the text. The sharp edge is degraded by no more than the width of a single ommatidium. The entire eye is approximately 1 cm wide.
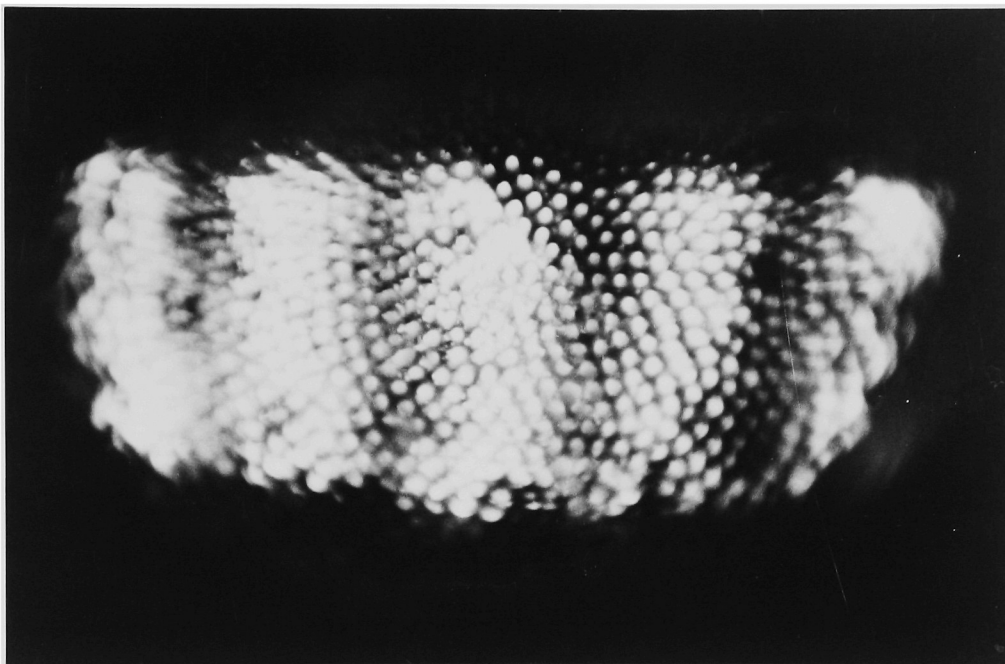
Figure A7. Crystalline cone image of sinusoidal grating,
4 cycles/eye-width.
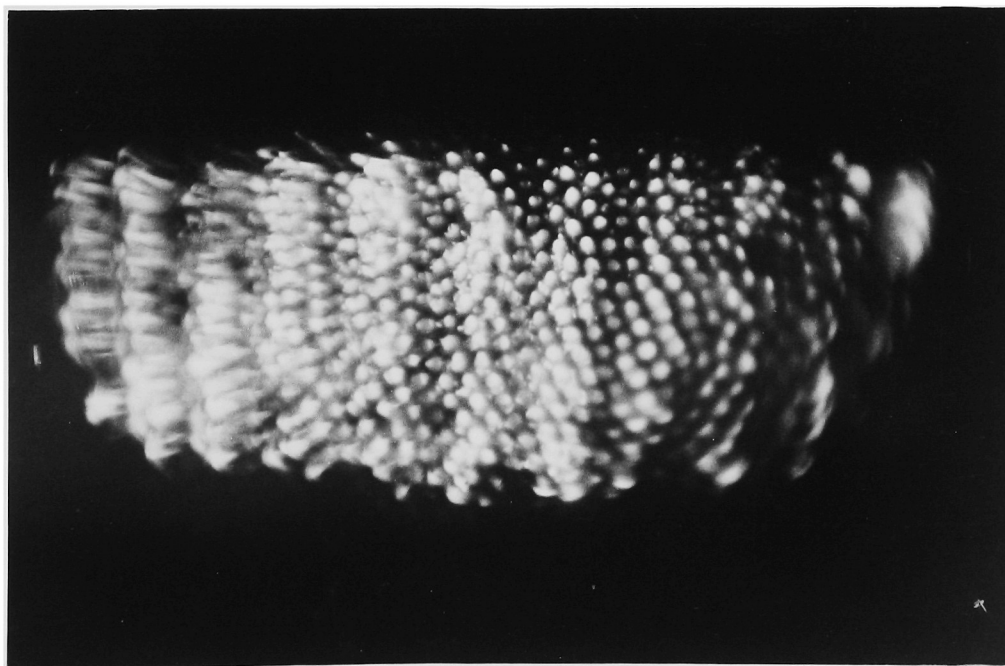
Figure A8. Crystalline cone image of sinusoidal grating,
10 cycles/eye-width.

illuminating the ommatidia surrounding the test-ommatidium,
then the light-to-impulse rate transfer function for this
optical system should show a "tuning" effect, as compared
to the transfer function produced by true point-source illum-
ination (Ratliff et al., 1969), as provided by a fiber optic
light-pipe (Barlow, 1967). We therefore measured the
transfer function of a test ommatidium illuminated by a
76 μm diameter light-pipe placed on the cornea. The light
source was a glow-modulator tube, operated as described else-
where (Knight et al., 1970), and driven by a computer-generated
sum-of-sinusoids signal. After this measurement, a fiber
optic taper was glued to the cornea. The same computer-
generated signal used above was used to drive the oscillo-
scope, and the transfer function of the same test-ommatidium,
now illuminated with our fiber-optic taper optical system
was measured. The f-stop diaphragm of the camera lens was
used to adjust the mean impulse rate to approximately equal that
obtained with light-pipe illumination.

Typical data are shown in Figure A9. The curves for
both amplitude and phase agree to well within the tolerance
required by the slight drift of the preparation over the
duration of the experiment (in this case, approximately $2\frac{1}{2}$
hours). We conclude that the fiber optic taper optical
system does not significantly degrade the point spread char-
acteristic of the intrinsic Limulus optics.

A more quantitative approach to the measurement of the
Limulus optical point spread characteristic is described in
chapter VI.

Figure A9. Comparison of light-to-impulse rate transfer functions: 76 μm diameter fiber optic light pipe <u>vs</u>. oscilloscope-lens-fiber optic taper optical system. The two transfer functions were obtained from the same test-ommatidium: O -light pipe, Δ -fiber optic taper. Mean impulse rates: light-pipe, 19.4 impulses/s; fiber optic taper, 17.0 impulses/s. The figures show Bode plots (log amplitude vs. log frequency; phase vs. log frequency) of relative fractional modulation of output, taken as mean impulse density (r(t)). Each curve is derived from pooled data from 12 presentations of the identical sum-of-sinusoids stimulus. (Frequencies were: .56, 1.00, 2.33, 5.15, 11.81, and 20.70 Hz.)
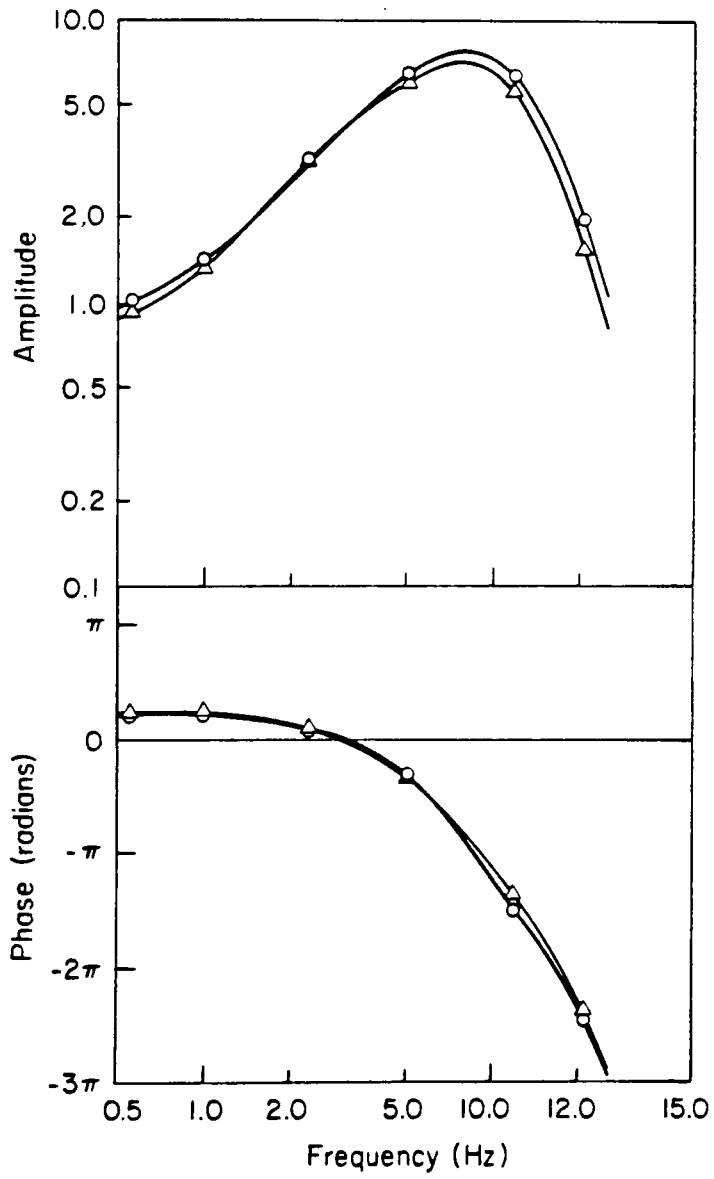
Figure A-9.

Appendix B: <u>Temperature dependence of the excitation processes</u>
<u>of the Limulus retina.</u>

The compound eye of the horseshoe crab, <u>Limulus</u>, like most
biological and biochemical systems, is markedly affected by the
temperature at which it operates. Previous studies of its temp-
erature-dependent properties have concentrated on excitatory and
inhibitory processes of the eye, as manifested by character-
istics of its steady-state response (Adolph, 1968,1973). In
this appendix, I report the results of studies on the temperature
dependence of dynamic properties of the <u>Limulus</u> eye. Similar
results in the eye of the fly have recently been obtained by
French and Järvilehto (1978).

The effect of temperature on the ommatidial dynamics may
be conveniently characterized by measuring transfer functions for
the light-to-impulse rate transduction, while varying the
temperature of the eye over the range of interest. Such measure-
ments are described below.

Methods.

In order to obtain the stability necessary for these
studies, an <u>in-situ</u> preparation similar to that described
in chapter III was used. The right optic nerve was

cut and introduced into a chamber mounted on the <u>Limulus</u>
carapace. The nerve was dissected until a fiber containing
a single active axon was obtained. The fiber was then laid
on a cotton wick electrode for recording. The stimulus was
produced by a glow-modulator tube, and conveyed to the eye
via a 76 μm diameter fiber-optic light pipe (Knight et al.,
1970). A digital computer controlled the fluctuations of the
light source, and recorded the intervals between nerve impulses
for later processing. The stimulus schedule consisted of 60s
periods of illumination, followed by 90s of darkness, to restore
the animal's state of light-adaptation. Data from the first
10 seconds of each experimental episode were discarded, to
avoid the effects of the initial on-transients.

For these experiments, six sinusoidal stimulus components
were used which spanned the frequency range of interest: 0.56,
1.00, 2.33, 5.15, 11.81, and 20.70 Hz. In order to optimize
the signal-to-noise ratio of the measurements and prevent phase
locking, these components were weighted according to the reciprocal
of the anticipated transfer function amplitudes (relative weights
were 153., 91.7, 45.8, 22.9, 45.8, and 91.7, respectively).
The transfer functions were computed from the nerve impulse data
by the least-squares algorithm described in Appendix C.

The temperature of the animal was controlled as follows: .
a 1:1 water-methanol solution was heated or cooled as needed,
and pumped through a thermal coupler placed on the dorsal
surface of the Limulus carapace. The coupler consisted of
an ordinary ice-bag fitted with a loop of copper tubing and
filled with the methanol solution. The animal's body temper-
ature was measured with a thermistor probe inserted under the
carapace, immediately adjacent to the left eye. This apparatus
was capable of producing body temperatures from 0°C to 35°C.
The transition between 15°C and 25°C took approximately two
hours.

Results.

The transfer functions from successive passes through
the same temperature range may be compared to rule out the
possible contamination of the temperature effects by deter-
ioration of the preparation over the hours of the experiment
(Fig. B-1). The agreement between successive transfer function
measurements indicates that drift is virtually absent in this
preparation. (The apparent disparity of the phases at 15°C
at high frequency reflects the inherent imprecision of phase
measurements for such severely attenuated responses.)

The graded dependence of the transfer function on temper-
ature over the range 15°C to 25°C is shown in Figure B-2. The
transfer function varies smoothly and directly with temperature

Figure **B-1** Comparison of transfer function measurements over duration of experiment. Bode plots (log amplitude vs log frequency; phase vs log frequency) of four measurements from the same ommatidium are shown. Temperature was varied from $15^{\circ}C$ to $25^{\circ}C$, back to $15^{\circ}C$, and back again to $25^{\circ}C$, over a period of 6 hours. Transfer functions at 15° (●) and 25° (◆) were each measured twice, the measurements separated by approximately 4 hours. Each curve is the average of several successive episodes, over which the temperature varied by less than $1^{\circ}C$. Except as indicated for the phase data at 15° C,

the uncertainty of each individual measurement is less than the extent of the dots in the figure. The amplitudes are expressed in terms of relative fractional modulation, the quotient of the observed modulation divided by the mean impulse rate. Mean impulse rates were 21.17 (top curve) and 20.11 (bottom curve) at $25^{\circ}C$, and 16.87 (top curve) and 16.76 (bottom curve) at $15^{\circ}C$ (Q_{10} = 1.23).
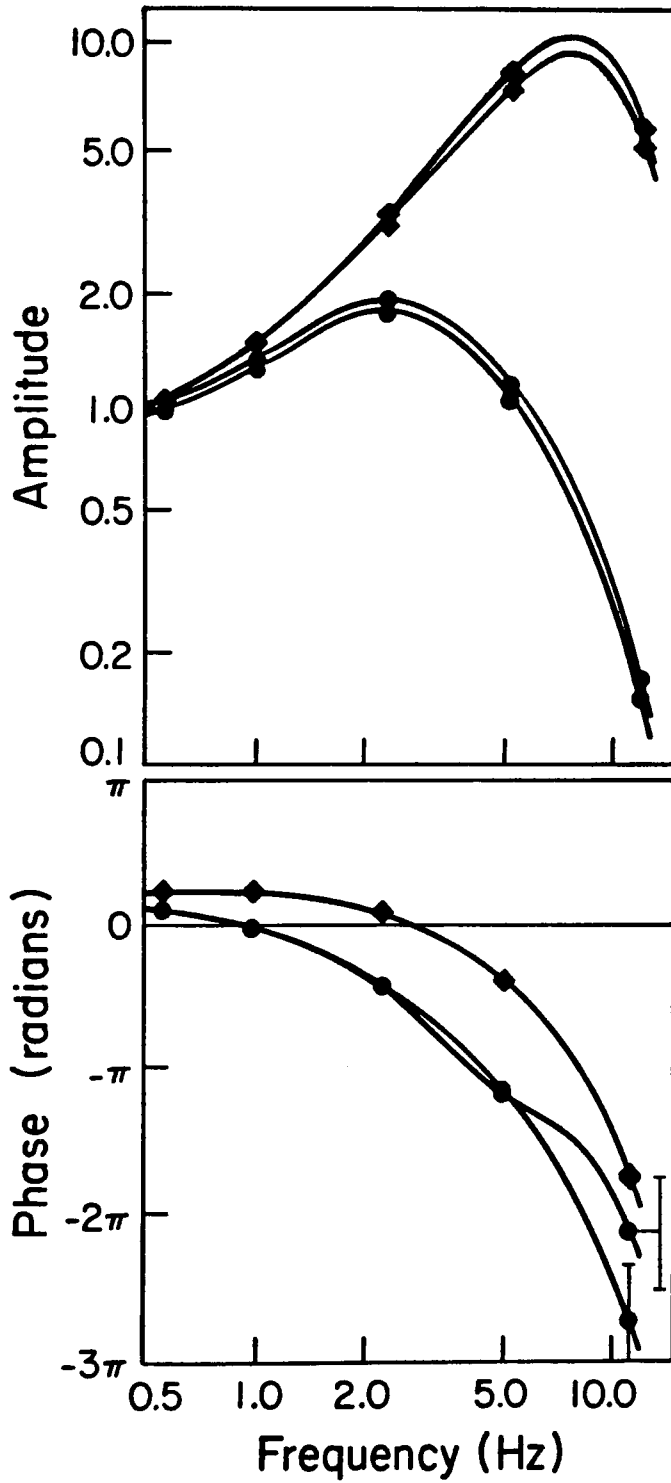
Figure B - 1

Figure B-2. Temperature dependence of transfer function. Bode plots, as in Figure B-1, of transfer functions measured during one sweep of temperature from $25^{\circ}C$ to $15^{\circ}C$; the data come from the same unit as in Figure B-1 . The curves correspond to temperature ranges of $25-25.3^{\circ}$ C ($\blacklozenge$), $22-23^{\circ}C$ ($\blacktriangle$), $20-21^{\circ}C$ ($\blacksquare$), $17-18^{\circ}C$ ($\blacktriangledown$), and $15-16^{\circ}C$ ($\bullet$). Mean impulse rates were 20.11, 21.20, 20.93, 19.00, and 16.87, respectively.
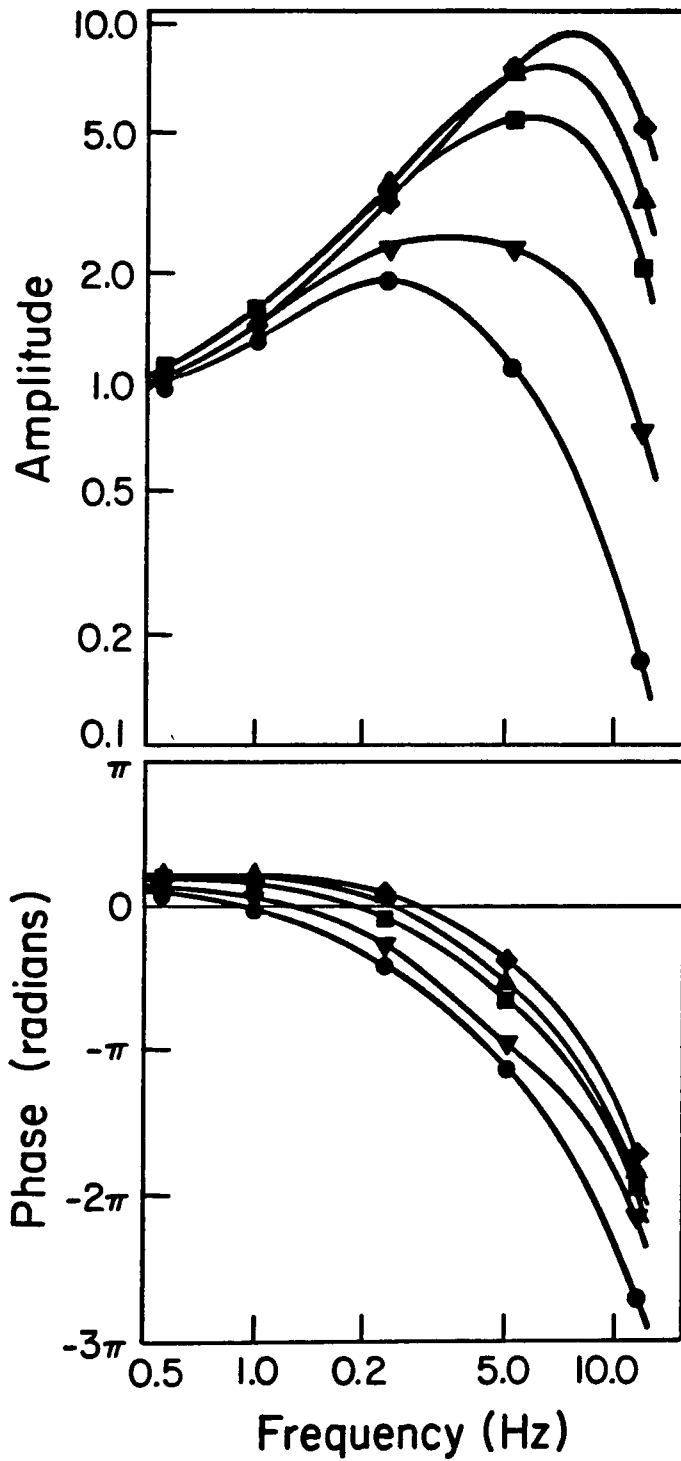
Figure B - 2

The frequency at which the eye is most sensitive to flickering light increases markedly with increasing temperature; the transfer function also becomes more sharply tuned to its peak frequency as the temperature rises. At the high end of the frequency range, the net effect of a ten-degree temperature increase is a fifty-fold increase in amplitude, and a decrease of π radians (180 degrees) in phase lag. Similar temperature dependence has been measured in a total of six Limulus specimens.

Discussion.

Though in principle these results may be consequences of temperature-dependent systemic changes in the physiology of the animal as a whole, they must ultimately be explained in terms of changes in the parameters of the visual tissues themselves. If we ignore the possible effect of screening pigment migration, which could explain only a small portion of the observed temperature dependence, we have left to consider the neural component of the Limulus excitatory visual transduction. This system may be separated into two successive linear processes: the formation of the "generator potential" and the encoding (with self-inhibition) of this slow potential into neural impulses. The measured transfer function of the combined process is accurately predicted by the product of the transfer functions of the component parts (Knight et al., 1970).

The temperature dependence of the generator potential

has been extensively studied in excised eyes by Adolph (1968)
and Wong (1977). Their data are well explained by an extension
of the "adapting-bump model" (Dodge, Knight and Toyoda, 1968;
Knight, 1973c). This model describes the generator potential
as the sum of many small brief depolarizations ("bumps")
which are triggered by incoming light. On the basis of a few
statistical and physiological assumptions, the model yields
the following expression for the generator potential transfer
function $G(\omega)$:

$$G(\omega) = e^{-it_\ell \omega} \cdot \left(\frac{1}{1+it_d\omega}\right)^{n_d} \cdot \left(\frac{1}{1+it_b\omega}\right)^{n_b} \cdot \left(1 - \frac{R}{1+it_a\omega}\right) \cdot \quad (B.1)$$

where ω is the modulation frequency.[*] The first factor rep-
resents a latency between the absorption of incident light and
the beginning of the resultant depolarization. The next factor
includes a stochastic dispersion of these latencies. The third
factor describes the effect on the transfer function of the
shape of the individual bumps, and the final factor describes
the "adaptation" of bump size in bright light.

Wong (1977) observed that the shapes of the individual
bumps change with temperature in such a way that equation (B.1)
correctly predicts the variation of the generator potential
transfer function with temperature. Such an effect is shown in
Figure B-3a, where the model parameters have been chosen so as

---

[*]   The Thorson low-frequency factor has been dropped here,
as the measurements do <u>not</u> extend to a sufficiently low frequency
for this factor to be significant.

.

Figure B-3. Transfer functions for component transductions. Bode plots of transfer functions at $15^{\circ}C$ (——) and $25^{\circ}C$ (---) for (a) generator potential, (b) encoder mechanism, including self-inhibition, and (c) overall light-to-impulse rate transduction (compare with Figure 1). Transfer functions for generator potential and encoder mechanism calculated from models described in text; light-to-impulse rate transfer function equals product of generator potential and encoder transfer functions.
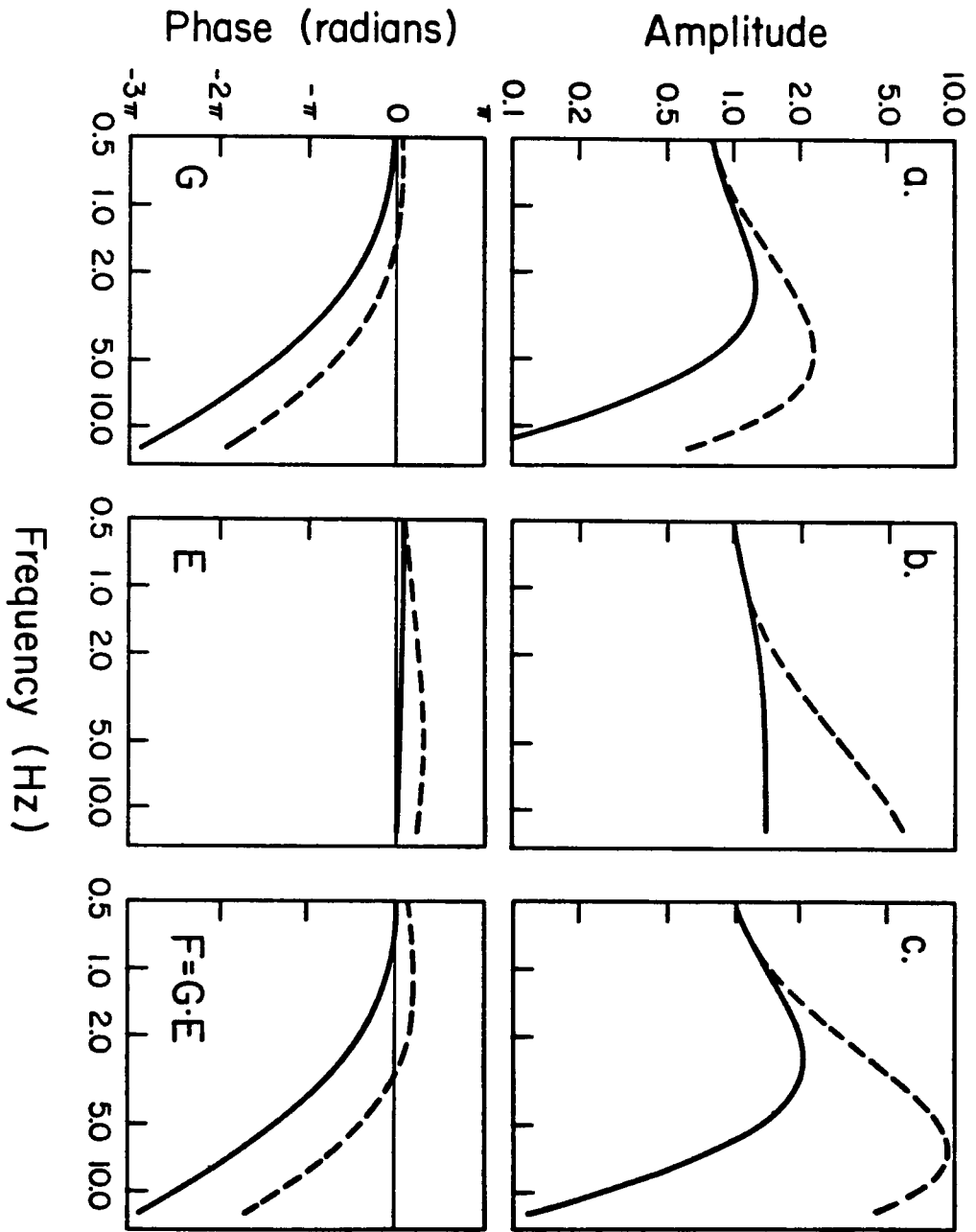
Figure B - 3

to be compatible with the data of Figure B-1 (see Table B1).
As temperature increases, the time constants decrease, though
direct comparison is complicated by the increase in the expon-
ents (which is necessary to account for the observed phase
data). The net effect is to reduce the effective bump time scale
by nearly a factor of two over a ten-degree increase in temper-
ature. There is no evidence concerning the effect of temper-
ature on the adaptation process. For the sake of simplicity, no
temperature dependence has been included for the adaptation
parameters.

The temperature dependence of the generator potential shown
in Figure B-3a, though representative of the temperature
effect observed in data from intracellular recordings from
excised eyes, is not sufficient to account for the temperature
dependence of the light-to-impulse rate transduction as shown in Fig-
ures B-1 and B-2. It is therefore reasonable to propose that
there is a similar temperature dependence in the "encoder"
transduction (from generator potential to neural impulses,
including self-inhibition). A model for this transduction
may be obtained by assuming that the encoder is an integrate-
and-fire device (Knight, 1972a), and by incorporating self-
inhibition as a simple feedback process (Stevens, 1964). This
yields the following expression for $E(\omega)$, the transfer function of

the encoder process:

$$E(\omega) = (1 + \kappa)\left(1- \frac{\kappa/(1+\kappa)}{1+i\frac{\tau}{1+\kappa}\omega}\right), \tag{B.2}$$

where κ describes the strength of the self-inhibitory process, and τ the time-constant of the self-inhibitory transient follow-ing each nerve impulse. It appears likely that, as the temper-ature increases, the strength of the self-inhibitory process increases; further, the self-inhibitory time constant is prob-ably reduced. Such a temperature effect on the encoder transfer function is illustrated in Figure B-3b.

The combined effect of temperature on the generator potential and encoder process is adequate to explain the temperature dependence of the overall light-to-impulse rate transduction. Figure B-3c shows the predicted transfer function $F(\omega) = G(\omega) \cdot E(\omega)$ obtained from the model calculations described above, and may be compared directly with Figure B-1.

The direct verification of the effect of temperature on the component transductions in the Limulus eye has not been possible, due to the difficulties in maintaining an intra-cellular electrode penetration over several hours in an in-situ Limulus preparation. Nevertheless, the parameters for the model calculations above are fixed by the overall light-to-impulse rate transfer function data with sufficient precision to imply that both the generator potential and encoder mechanisms

contribute significantly to the temperature dependence of the
complete visual transduction. The value $\kappa = 8$ given for the
self-inhibitory strength at 25° is much higher than the values
we have obtained from the complete analysis of spatiotemporal
transfer functions (chapter VI, Table II). Though the
temperature difference between 22.0^O and 25.0^O might account for
more than a factor of 2 in the discrepancy, this value for
the inhibitory strength should probably not be taken very
literally (see also Appendix E). It is quite plausible that even
a small temperature dependence of the adaptation parameter R
would allow a choice of κ closer in value to those of Table II
without compromising the agreement between the model and
experiment. In any event, the effect of temperature on the
dynamics of excitation in the Limulus visual system is far from
subtle. This observation should have significant implications
for the study of Limulus vision in the laboratory, and quite
likely in the animal's natural environment as well.

Table B-1

Parameters for <u>Limulus</u> Transfer Function

Parameter	Description	Dimension	Value 15°C	25°C
t_ℓ	bump latency	sec	0.050	0.012
t_d	latency dispersion time-constant	sec	0.020	0.008
n_d	dispersion exponent		2	4
t_b	bump shape time-constant	sec	0.037	0.015
n_b	bump shape exponent		3	4
t_a	adaptation time-constant	sec	0.013	0.013
R	adaptation strength		0.93	0.93
τ	self-inhibitory time-constant	sec	0.20	0.10
κ	self-inhibitory strength		0.5	8.

APPENDIX C - On the Choice of Output Variable for the
Analysis of Impulse Train Data

Output Variables

In the preceding exposition, we treated both the
stimulus $S(x,t)$ and the response $R(t)$ as functions of
the continuous real time variable t. This is a natural
way to describe a time-varying light stimulus, but is
somewhat problematical for the response, because the
output of a retinal neuron is a train of discrete nerve
impulses, rather than a continuous function of time.
Thus some algorithm for the conversion of a list of
impulse firing times to a continuous time function is
needed.

The traditional procedure for this purpose is the
construction of a nerve impulse histogram, synchronized
to the repetitions of the stimulus. Such a histogram
may be considered as an experimental estimate of the
"population firing rate" of the neuron, which is defined
below. (Here, the term "population" refers either to
a hypothetical population of identical, statistically
independent neurons, all exposed to the same stimulus,
or to an ensemble of statistically independent responses

of the same neuron to many repetitions of the same
stimulus.) To define the population rate, consider
the response of N elements drawn from the ensemble.
Over any brief time interval (t,t+dt), we can determine
the number of impulses, m_N(t,t+dt), produced by these
N elements. As N becomes large, we may expect to find
at least a few impulses over even very short time inter-
vals, at least in the absence of phase locking. We then
define the population rate r(t) as a normalized limit
of such impulse counts:

$$r(t)dt \equiv \lim_{N \to \infty} \frac{1}{N} m_N(t,t+dt) \ . \hspace{3cm} (C.1)$$

In general, the summed post synaptic effect of a
population of neurons on a given neuron will be related
very directly to this population rate variable (see
Knight, 1973b). Thus the population rate is the natural
description of the output of a neuron for use in quanti-
tative models such as those developed above.

Unfortunately, the response histogram is frequently
a very clumsy tool for the realization of the population

rate. In order to achieve good temporal resolution, the histogram must be constructed with bins considerably narrower than the shortest response feature of interest. But narrow bins, in turn, demand a very large ensemble of replicate experimental runs, in order to provide satisfactory statistical accuracy within each bin. In the laboratory, where the data are limited, the results are frequently disappointing, especially for neurons (such as those of the Limulus retina) whose population rate may vary greatly over the duration of a typical inter-impulse interval (Figure C-1).

To circumvent this problem, we have turned to an alternative output variable for the depiction of impulse train data, the "mean individual rate." To construct this variable, we first obtain an "individual firing rate" function s(t) for each impulse train in the response ensemble by assigning, to each time t, a rate estimate equal to the reciprocal of the duration of the inter-impulse interval into which the time t happens to fall (Hartline et al., 1956):

$$s(t) = \sum_n \chi_{(t_n, t_{n+1}]}(t) \cdot \frac{1}{t_{n+1} - t_n} \quad , \qquad (C.2)$$
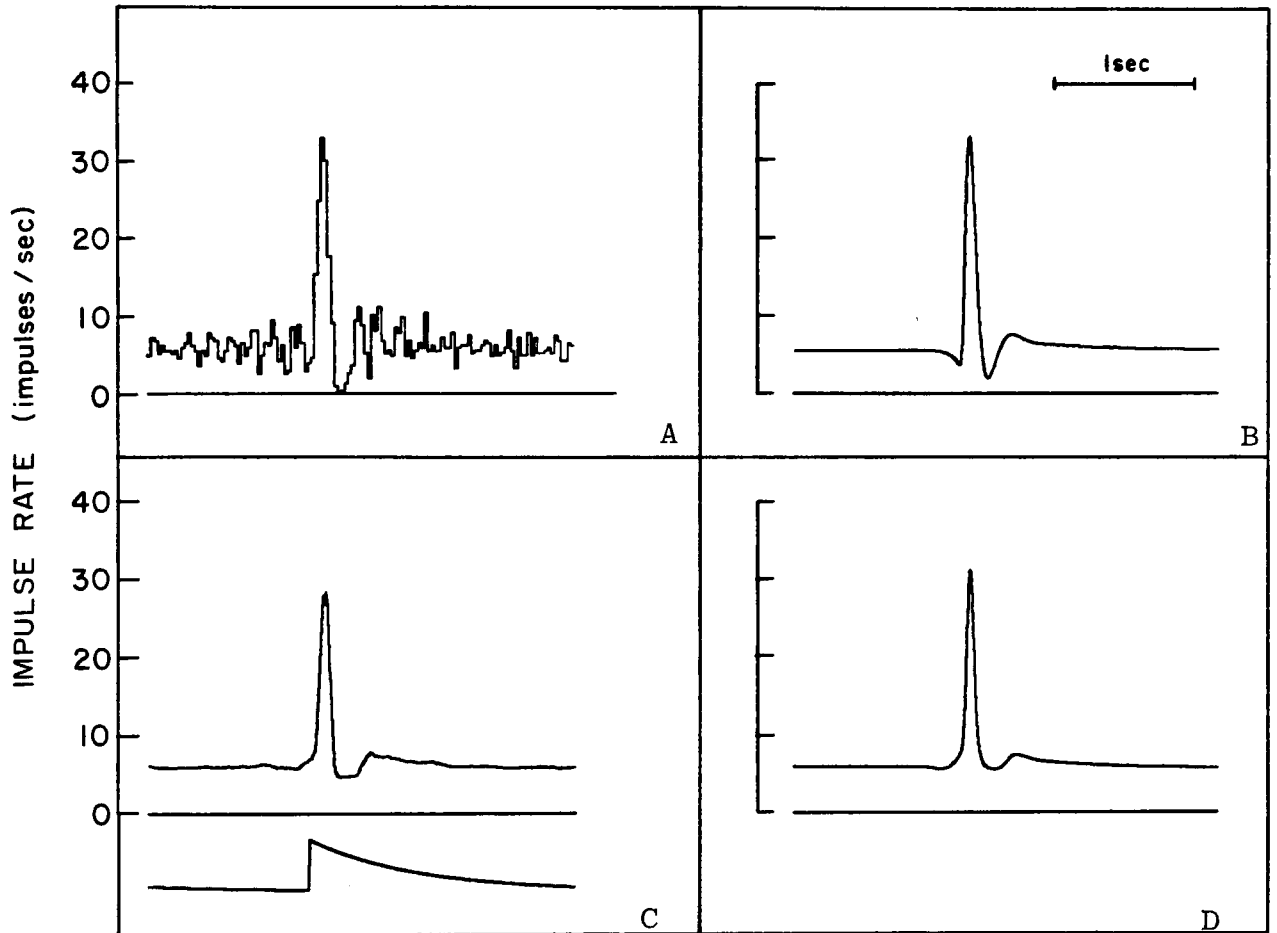
Figure C-1. Comparison of output variables. Experimental response records are shown at left, predicted response records at right. (a) Nerve impulse histogram, constructed from 128 presentations of moving stimulus (stimulus waveform shown at lower left), with bin width of 24 msec. (b) Predicted population rate response. (c) Mean individual rate response based on the same data as (a) above. (d) Predicted mean individual rate response, obtained from (b) by means of algorithm described in the text. (Data from experiment of Figure 8-7.)

where t_n is the time of occurence of the n'th
impulse, and the characteristic function $\chi_{(a,b]}(t)$
is 1 or 0 as t does or does not lie in the interval $a < t \leq b$.

Thus s(t) is a so-called step-function, with a
constant value on each inter-impulse interval. The mean
individual rate function $\sigma(t)$ is then defined as the
average, over the response ensemble, of the individual
rate functions:

$$\sigma(t) \equiv \langle s(t) \rangle = \frac{1}{N} \sum_{\ell=1}^{N} s_\ell(t) , \tag{C.3}$$

where $s_\ell(t)$ is the individual rate function for the
ℓ'th element of the response ensemble of N elements.

For a neuron, such as those of the <u>Limulus</u> retina,
whose inter-impulse intervals show only small stochastic
variation under uniform conditions, the mean individual
rate $\sigma(t)$ gives a much smoother description of the
neuron's output than does a response histogram constructed
from the same data (Figure C-1). In situations where
the population firing varies slowly relative to the typical
inter-impulse interval, the mean individual rate and the

population rate description of a neuron's output agree closely.
In general, however, this does not hold, and there are
significant differences between the two output variables.
Thus, in practice, it is necessary, in synthesis calculations,
to convert predictions obtained in terms of the population rate
into a form compatible with the mean individual rate records
obtained from laboratory measurements. A procedure for this
conversion is outlined below.

We suppose that, for an ensemble of responses of
a noise-free neuron, as described above, between any
two firings of a given member of the ensemble, every
other member of the ensemble will fire exactly once.*
Thus, in particular, if a neuron fires at time t, the
elapsed time $\tau(t)$ since its previous impulse satisfies

$$\int_{t-\tau(t)}^{t} r(t')dt' = 1 \ . \qquad\qquad (C.4)$$

---

* It is possible to contrive unrealistic neuron models
  for which this assumption fails, but it appears to be
  a safe assumption in practice.

Likewise, the interval $\theta(t)$ until the next impulse satisfies

$$\int_{t}^{t+\theta(t)} r(t')dt' = 1 \ . \tag{C.5}$$

It follows that the expectation (C.3) may be obtained
by averaging the reciprocal inter-impulse interval
$1/\tau(t')$ over all the inter-impulse intervals which
terminate between t and $t+\theta(t)$, according to the weight $r(t')$:

$$\sigma(t) = \int_{t}^{t+\theta(t)} \frac{r(t')}{\tau(t')} dt' \ . \tag{C.6}$$

In practice, the population rate $r(t)$ is available
only on a mesh of discrete time points separated by a
small time step dt. We thus implement equations (C.4,5,6)
at each mesh point by summing the quantity $r(t')dt'$
backwards in time until the running total
exceeds unity, and then interpolating to obtain $\tau(t')$
at that mesh point. Likewise, we sum forward from each
mesh point, and determine $\theta(t')$. Then $\sigma(t)$ may be

directly evaluated from (C.6) by simple numerical integration.[*]

The effects of such a program may be seen by comparison of

parts B and D of Figure C-1. Note that the Mach bands associated
with the excitatory transient are significantly attenu-

ated in the passage from the population rate variable

to the mean individual rate variable. This closely cor-

responds to the difference between the observed response

histogram and mean individual rate records (Fig. C-1,

A and C).

Under circumstances where the response may be treated

as a small perturbation from a constant output, the trans-

---

[*]   It is implicitly assumed in the derivation of this

       algorithm that the population rate r is never nega-

       tive. Thus, in order to apply this procedure to

       the predictions of linear models, which occasionally

       swing negative during vigorous off-transients, we

       have replaced all such negative population rates

       with the truncated value $r(t)=0$. This procedure

       may be considered a crude model for the truncation

       of off-transients seen in the actual experimental

       records.

duction from population rate to mean individual rate, which is in general nonlinear, may be satisfactorily approximated by a linear transduction. A simple formula for this transduction may be derived as follows. For a truly constant output r_o, we have

$$\tau_o = \theta_o = \frac{1}{\sigma_o} = \frac{1}{r_o} \; , \tag{C.7}$$

where the subscript o indicates the steady state. For a small perturbation about this steady state, we write

$$v(t) = v_o + \epsilon \, v_1(t) \; , \tag{C.8}$$

where v is any of r, σ, τ or θ , v_1/v_o is of order unity, and $\epsilon \ll 1$. If the relations (C.8) are substituted into (C.4, 5, 6) and the relations (C.7) subtracted, we obtain, to first order,

$$0 \doteq \theta_1(t) \cdot r_o + \int_t^{t+\theta_0} r_1(t')dt'$$

$$\dot{\theta} = \tau_1(t) \cdot r_o + \int_{t-\tau_0}^{t} r_1(t')dt' \qquad (C.9)$$

$$\sigma_1 = \theta_1(t) \cdot \frac{r_o}{\tau_o} + \int_t^{t+\theta_0} \left(\frac{r_1(t')}{\tau_0} - \frac{r_0}{\tau_0^2} \cdot \tau_1(t')\right)dt' \ .$$

If the first two of these equations are solved for θ_1 and τ_1, respectively, and substituted into the third, there results

$$\sigma_1(t) = \frac{1}{\tau_0^2} \int_t^{t+\tau_0} \int_{t'-\tau_0}^{t'} r_1(t'')dt'' \ dt' \ . \qquad (C.10)$$

This formula clearly displays the relation between r_1 and σ_1 as a linear transduction. The transfer function for this transduction may be obtained by setting $r_1(t)=e^{i\omega t}$ in (C.10). Elementary integrations yield the result

$$\frac{\sigma_1(t)}{r_1(t)} = \frac{(1-e^{-i\omega\tau_o})(e^{i\omega\tau_o}-1)}{(i\omega\tau_o)^2} = B(\omega,\tau_o) \cdot \overline{B(\omega,\tau_o)} \ , \quad (C.11)$$

where

$$B(\omega,\tau_o) \equiv \frac{1-e^{-i\omega\tau_o}}{i\omega\tau_o} \qquad \cdot \ ^*$$

An application of this analysis to a model calculation is shown in figure C-2. The mean individual rate records at the bottom of the figure were obtained by taking the inverse Fourier transform of the product of the transfer function (C.11) and the Fourier transform

---

*   The transfer function $B(\omega,\tau_o)$ may be shown to describe the transduction from the population rate to the "instantaneous frequency" of a neuron (Knight, 1972a). A more direct, though less general, deviation of (C.11), which makes use of this fact, may be found in Brodie et al. (1978a).
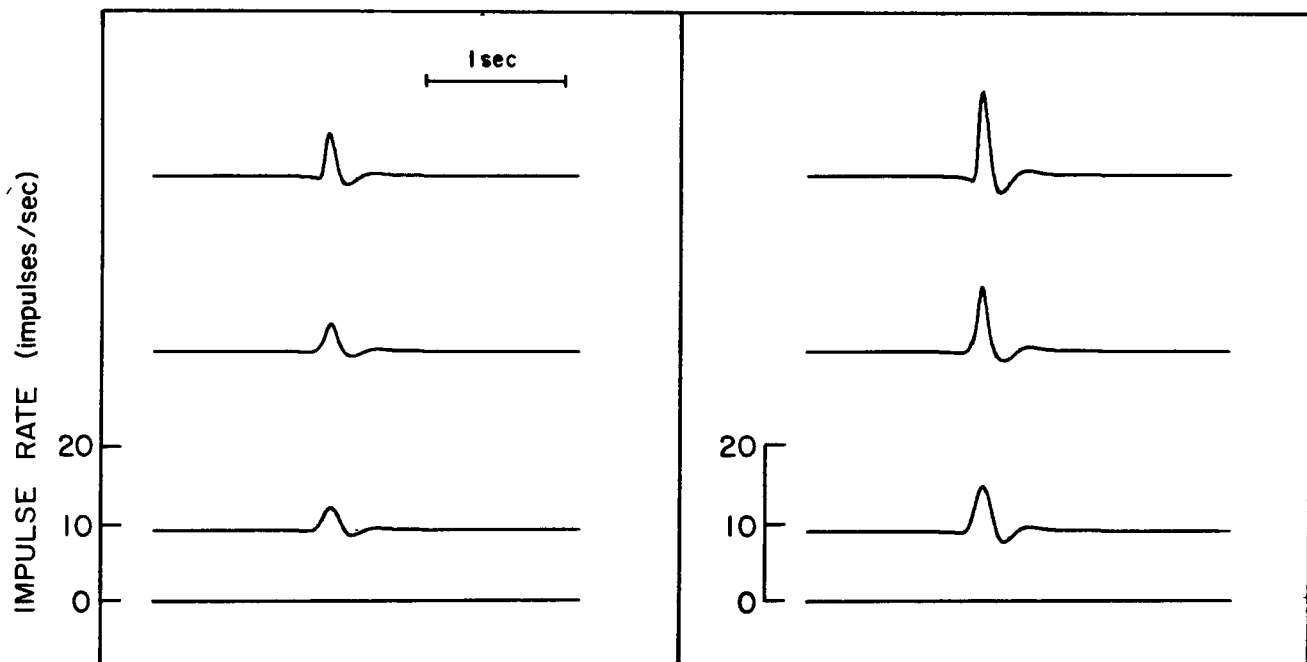
Figure C-2. Comparison of algorithms for conversion of population rate to mean individual rate. Top records: predicted population rate responses to low-contrast moving stimuli. Middle records: mean individual rate responses calculated from population rate by (exact) nonlinear algorithm based on equations (C.4,5,6). Bottom records: mean individual rate response calculated from population rate by means of linear transfer function of equation (C.11). Stimulus contrast for records at right is double the contrast for records at left.

of the population rate. There is good agreement between
the linear and nonlinear (exact) procedures for the "low
contrast" record at left. As the contrast increases,
the response can no longer be treated as a small perturba-
tion, and the two algorithms begin to produce divergent
results.

The two algorithms also agree closely for the case
of slowly moving stimuli, even at high contrast (Fig.
C-3). In this case, the impulse rate changes little
over the time scale of an inter-impulse interval, and
so both the linear and nonlinear procedures reduce to
the identity transduction.

For the initial studies of the Fourier synthesis
process described in chapters II-VI, the transfer func-
tion (C.11) was used to make the (generally trivial)
conversion from population rate to mean individual rate.
In the later studies described in chapters VII and VIII,
higher stimulus velocities were used in order to enhance
the dynamic edge effects. This necessitated the use of
the full nonlinear conversion algorithm based on equations
(C.4,5,6).

Figure C-3. Response records for slowly-moving stimulus.
From top to bottom, the records depict: predicted population
rate response; predicted mean individual rate response,
calculated by the linear perturbation algorithm; predicted
mean individual rate response, calculated by the nonlinear
algorithm based on equations (C.4,5,6); observed mean
individual rate response. (Data from experiment of
Figure 6-16.)
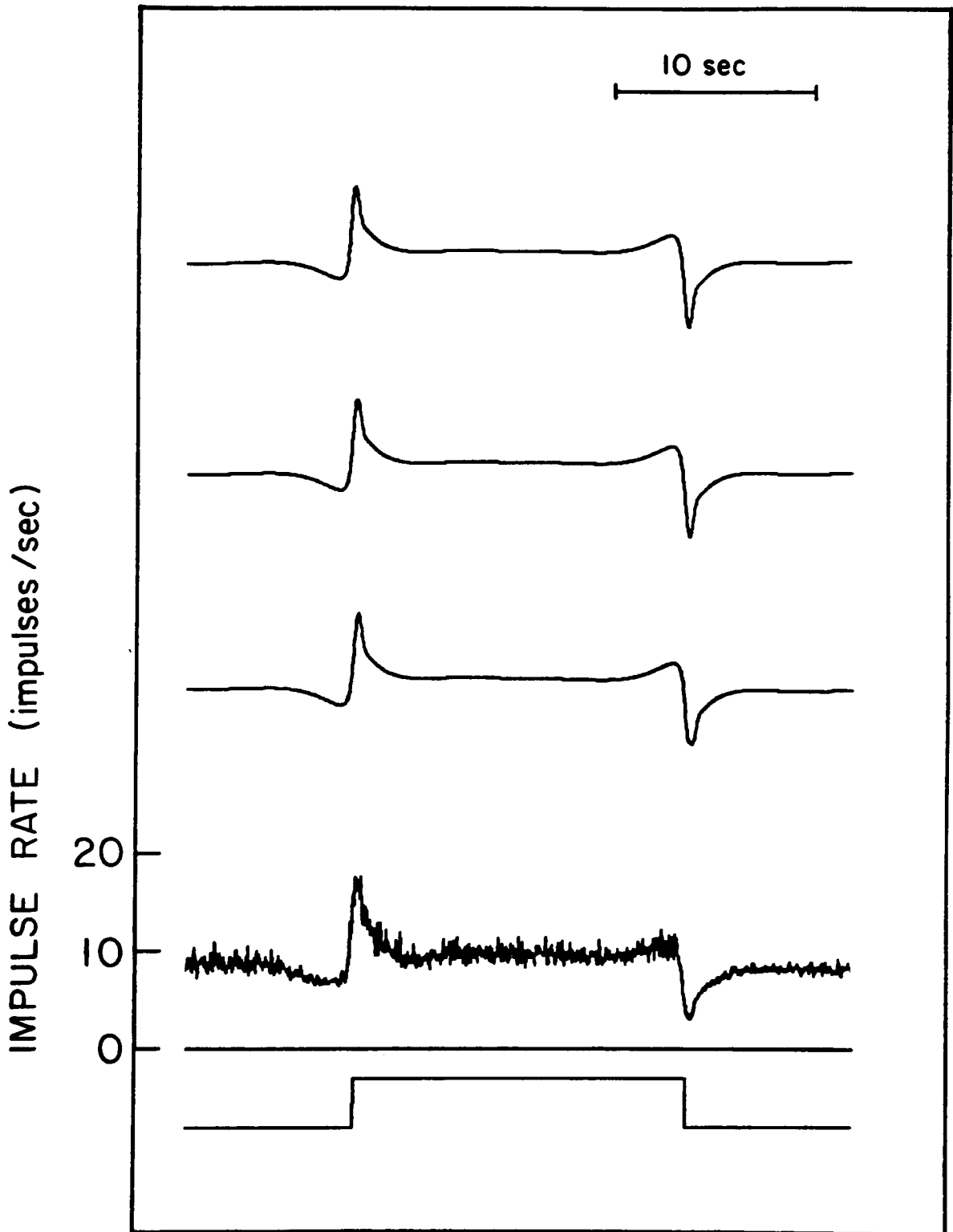
Figure C-3

Harmonic Analysis

The measurement of the harmonic content of various output variables has proved to be one of the most useful techniques for studying the dynamics of biological systems. When the output variable is a continuous function of time, such as muscle tension or an intracellular "slow potential," the application of these Fourier methods is straightforward. On the other hand, as discussed above, when the output is a train of neural impulses, the information carried by the signal is presumably contained in the impulse occurence times, and no function of continuous time is directly available for Fourier analysis. Several procedures for obtaining such a function have been proposed in the past (for example, French and Holden, 1971; Knight, 1972b; Fohlmeister et al., 1977a). We have recently adopted a procedure which determines the Fourier coefficients directly from the impulse occurrence times, without the intermediate calculation of a continuous time-function. The method is equivalent to the use of response histograms ("binning") with arbitrarily narrow bins. This procedure, its advantages, and its weaknesses, are discussed below.

In general, all calculations of Fourier coefficients may be interpreted as the result of a "least-squares"

best-fitting procedure. Such a procedure determines those coefficients c_n that minimize a quadratic error estimator of the form

$$\Delta = \int \{f(t) - \sum_n c_n f_n(t)\}^2 dt \ , \qquad (C.12)$$

where the f_n's are the functions with which we are attempting to approximate the data $f(t)$. (Here, for simplicity, we suppress the limits of integration and the corresponding division by the length of the interval of integration.) If the f_n's are sines and cosines, the c_n's are the usual Fourier coefficients, but other choices for f_n are equally suitable. In this context, the various procedures for Fourier analyzing impulse-train data amount to different explicit choices of the algorithm for obtaining $f(t)$, a function of a continuous variable, from the sequence of impulse occurence times.

Once such a choice has been made, one may readily differentiate equation (C.12) with respect to the c_n's; setting the partial derivatives $\partial \Delta / \partial c_m$ equal to zero yields a system of simultaneous equations for the c_n's:

$$\int f_m(t) \cdot f_m(t) dt = \sum_n c_n \cdot \int f_n(t) \cdot f_m(t) dt \ , \qquad m = 1, 2 \ \ldots \ \ .$$

$$(C.13)$$

If the f_n's are orthogonal (as are the sines and cosines, if integrated over an integral number of periods), the correlation matrix $\int f_n(t) \cdot f_m(t) dt$ reduces to $\delta_{n,m}$, and we retrieve the usual formula for the coefficients c_n.

The system of equations (C.13) makes perfectly good sense if we allow f(t) to be any suitably integrable function, even a sequence of Dirac delta-functions,

$$f(t) = \sum_k \delta(t-t_k) \ ,$$

where t_k is the time of occurence of the k'th impulse. For this choice of f, we obtain the form

$$\sum_k f_m(t_k) = \sum_n c_n \cdot \int f_n(t) \cdot f_m(t) dt \ , \qquad m = 1, 2, \ \ldots \ \ . \quad (C.14)$$

Unfortunately, such an f is not admissible in equation
(C.12), because the δ-function is not <u>square</u>-integrable.
Nonetheless, a careful limiting argument (in which one
approximates the δ-function by a sequence of increasingly
taller and narrower rectangular pulses) demonstrates that
(C.14) correctly calculates the spectral components
associated with that part of the structure of the impulse train
which is independent of impulse shape. Under the assumption
that only the impulse occurrence times convey information of
interest, this is no limitation. We will refer to the set of
Fourier components c_n obtained from equation (C.14) as the
"delta-function spectrum."

This calculation of the delta-function spectrum has
several computational advantages. First the correlation
matrix $\int f_n(t) f_m(t) dt$ can be calculated in advance; it
depends only on the functions f_n and the interval over
which data are collected. Second, the calculation is
linear in the data; thus, if data from several episodes
with identical stimuli are to be pooled, one may simply
add together the function values $f_m(t_k)$ from all episodes.
Third, the algorithm is well-suited to on-line data
acquisition: if tables of the functions f_n are stored in

memory, a pointer incremented in real time can provide
rapid access to the function value $f_n(t_k)$, so that when-
ever an impulse occurs, the current value is immediately
available for addition to a running total. The same
function table may even serve to provide a list of
successive stimulus values. Such a scheme has recently
been implemented with a microprocessor-driven device in
our laboratory (Milkman et al., 1978).

Because the delta function spectrum calculation is
linear, as described above, it follows immediately that,
as the number of pooled impulse trains grows large, the
equations (C.14) approach the continuous system (C.13),
if we make the choice $f(t) = r(t)$ (where $r(t)$ is the
population rate function as defined in equation C.1,
above). Thus, the delta-function spectrum serves as an
experimental estimate of the spectrum of the population
rate r, which is the natural variable for the theoretical
treatment of many neural networks (Knight, 1973b).

Another important feature of the formulation above
is the provision for non-orthogonal functions f_n. In
general, a "ramp" function $f_n(t) = t-t_0$ will not be
orthogonal to both a sine and cosine function over any

time interval. Similarly, sinusoids of incommensurate
periods fail to be orthogonal, as do commensurate sinusoids
except over carefully selected time intervals. The flexi-
bility of the system (C.14) in dealing with such functions
greatly facilitates the selection of episode lengths.

The various alternative choices for the function
f(t) generally fall into two classes. "Binning" methods
are particularly simple to apply. They divide the episode
into short successive equal time periods ("bins"), and
assign to each such period the number of impulses which
occur within it. "Instantaneous rate" methods, which
are often useful for impulse trains with few impulses,
assign function values equal to the reciprocals of the
time intervals between impulses. It is also possible
to combine these approaches. For impulse trains varying
slightly about a mean carrier rate, all of these functions
convey the same information and are simply related by
transfer functions, such as that calculated in equations
(C.11). Nonetheless, the delta-function procedure outline
above has several relative advantages in experimental
situations.

First, the delta function spectrum is highly insensi-
tive to discrimination errors, which may result in errone-

ously short intervals between impulses. These experi-
mental artifacts greatly distort calculations based on
reciprocal intervals, but scarcely perturb the running
sums from which the delta function spectrum is calculated.
Indeed, any number of spurious impulses uncorrelated
with the periodic stimulus have no systematic effect on
the computed spectrum. Second, unlike the results of
binning procedures, the delta function spectrum contains
no nulls due to the interaction of a modulation frequency
component with the bin width (a parameter which is entirely
external to the system under study). Finally, both binning
and reciprocal interval methods suffer from phase errors,
because the procedures which produce the function f(t)
somewhat distort the time at which an impulse is reflected
in the spectral estimation; in contrast, the delta function
procedure accurately reflects each impulse at the time
when it actually occurs.

In summary, the delta function spectrum, as determined
by the system of equations (C.14), provides an excellent
and easily computed characterization of the harmonic content
of impulse train data. The procedure is free from many of
the artifacts which affect other methods when applied to

laboratory data, and it imposes no arbitrary structure
of its own on the data.

Appendix D

Solution of Simultaneous Linear Equations.

In this appendix, we solve the system of equations (7.32),

$$\sum_{n=0}^{M-1} a_n (-\mu_\ell(\omega))^n = \frac{\prod_m (-\mu_\ell(\omega)+\lambda_m)}{i(\mu_\ell(\omega)+(\frac{-\omega}{v}))} \quad , \quad \ell = 1,2,\ldots M \ , \qquad (7.32)$$

for the leading coefficient $a_{M-1}(\omega)$, in terms of the roots $\mu_\ell(\omega)$ and λ_m.

The coefficient matrix

$$M_{\ell m} = (-\mu_\ell(\omega))^{m-1} \quad , \quad 1 \leq \ell, m \leq M \qquad (D.1)$$

is a so-called Vandermonde matrix. In order to obtain a_{M-1} , we need only determine the last row of M^{-1}. To this end, we invoke the formula for the determinant of a Vandermonde matrix, which yields, for the matrix of (D.1)

$$\det(M) = \prod_{q<p} (\mu_q(\omega) - \mu_p(\omega)) \ , \qquad (D.2)$$

where the product extends over all pairs of indices satisfying $1 \leq q < p \leq M$.[*]

---

*   This formula, which is crucial to the present calculation ,

seems to appear in textbooks only as an unproved exercise

(see for example Perlis, 1952, p.78).   A simple proof

goes as follows: We write $\det(x_1,x_2,\ldots,x_N)$ for the

determinant of the Vandermonde matrix X with entries

$(x_\ell)^{m-1}$, $1\leq\ell,m\leq N$.   We must show that

$$\det(x_1,x_2,\ldots,x_N) = \prod_{q<p} (x_p-x_q) \quad , \; 1\leq q<p\leq N \; .$$

For $N = 2$, this is trivial.   For $N>2$, we proceed by induction

on N.   Expanding   by cofactors of the last column, we

have

$$\det(x_1,x_2,\ldots,x_{N+1}) = \sum_{n=1}^{N+1}(-1)^{n+N+1}(x_n)^N \cdot \prod_{\substack{q<p \\ \neq n}} (x_p-x_q) \; .$$

On the other hand,

$$\prod_{1\leq q<p\leq N+1} (x_p-x_q) = \sum_{n=1}^{N+1}(-1)^{N+1-n}(x_n)^N \prod_{\substack{q<p \\ \neq n}} (x_p-x_q) + \ldots \; ,$$

where the unwritten terms are all of degree less than N

in all the x_n's. If we regard the left hand sides of
these two equations as polynomials in, say, x_{N+1} over
the polynomial ring $\mathbb{Z}[x_1, x_2, \ldots x_N]$, we may observe
that they have the same roots (namely the indeterminates
$x_1, \ldots, x_N$), and the same leading coefficient. They must
therefore be the same polynomial, QED.

(end of footnote)

Since the minor of each element in the last column of M is itself a Vandermonde matrix, it follows that the last column of the cofactor matrix C of M is given by

$$C_{\ell M} = (-1)^{\ell + M} \cdot \prod_{\substack{q < p \\ \neq \ell}} (\mu_q(\omega) - \mu_p(\omega)) , \qquad (D.3)$$

where the product extends over all pairs of indices $1 \leq q < p \leq M$ such that neither q nor p is equal to ℓ.

We can now compute the last row of M^{-1}, which is given by the quotient of the transpose of the cofactor matrix C and the determinant of M:

$$M^{-1}_{M\ell} = \frac{C_{\ell M}}{\det M} = \frac{(-1)^{\ell + M} \prod\limits_{\substack{q < p \\ \neq \ell}} (\mu_q - \mu_p)}{\prod\limits_{q < p} (\mu_q - \mu_p)} . \qquad (D.4)$$

In this expression, the product in the numerator cancels all of the factors in the demoninator except for the M-1 factors which contain the root μ_ℓ. Keeping track of the number of sign changes, we thus obtain

$$M^{-1}{}_{M\ell} = \frac{(-1)^{\ell+M} \cdot (-1)^{M-\ell}}{\prod_{q\neq\ell} (\mu_q - \mu_\ell)} = \frac{1}{\prod_{q\neq\ell} (\mu_q - \mu_\ell)} \quad . \tag{D.5}$$

The coefficient a_{M-1} may now be expressed as the inner product of (D.5) with the right side of (7.32):

$$a_{M-1} = \sum_{\ell=1}^{M} \frac{\prod_m (-\mu_\ell + \lambda_m)}{\prod_{q\neq\ell} (\mu_q - \mu_\ell)} \cdot \frac{1}{i(\mu_\ell + (\frac{-\omega}{v}))} \quad . \tag{D.6}$$

Now consider the formula

$$\tilde{\Phi}^-(\xi,\omega) = \frac{\tilde{\Phi}(x=0,\omega)}{i(\xi - (\frac{-\omega}{v}) - i\varepsilon)} \cdot \frac{\prod_m (\xi - \lambda_m)}{\prod_q (\xi - \mu_q(\omega))} \tag{7.34}$$

Since $\tilde{\Phi}(x=0,\omega) = \frac{1}{2\pi} \int e^{i\xi \cdot 0} \tilde{\Phi}^-(\xi,\omega) d\xi$, we have

$$1 = \frac{1}{2\pi i} \int \frac{\Pi_m(\xi - \lambda_m)d\xi}{\Pi_q(\xi - \mu_q(\omega))(\xi - (\frac{-\omega}{v}) - i\epsilon)} \quad . \tag{D.7}$$

Evaluation of this integral by contour integration in the upper half-plane gives

$$1 = \sum_{\ell=1}^{M} \frac{\Pi_m(\mu_\ell - \lambda_m)}{\Pi_{q \neq \ell}(\mu_\ell - \mu_q)} \frac{1}{(\mu_\ell - \zeta)} + \Pi_\ell \frac{(\zeta - \lambda_\ell)}{(\zeta - \mu_\ell)} \quad , \tag{D.8}$$

where ζ is an arbitrary real number (since v in $\frac{-\omega}{v}$ is arbitrary) Since the numerators in the first term of (D.8) have one more factor than the denominators, we have

$$1 = -\sum_{\ell=1}^{M} \frac{\Pi_m(-\mu_\ell + \lambda_m)}{\Pi_{q \neq \ell}(\mu_q - \mu_\ell)} \frac{1}{\mu_\ell + (\frac{-\omega}{v})} + \Pi_\ell \frac{\frac{-\omega}{v} + \lambda_\ell}{\frac{-\omega}{v} + \mu_\ell} \quad , \tag{D.9}$$

where we have set $\zeta = \frac{\omega}{v}$.[*]

---

[*]   This identity can also be obtained directly from a general polynomial interpolation formula (Sirovich, 1979).

Taken together, the relations (D.6) and (D.9) yield equation (7.35):

$$1 + ia_{M-1} = \prod_j \frac{-\frac{\omega}{v} + \lambda_j}{-\frac{\omega}{v} + \mu_j(\omega)} \quad ,$$

Q.E.D.

"In the early treatises on this subject, the mean value assigned to π will be found to be 40.000000. Later writers suspected that the decimal point had been accidentally shifted, and that the proper value was 400.00000; but, as the details of the process for obtaining it had been lost, no further progress was made in the subject till our own time, though several most ingenious methods were tried for solving the problem."

L. Carroll, 1874.

Appendix E: <u>Comparison of Transfer Function Parameters with</u> <u>Direct Measurement.</u>

Most of the parameters of the Hartline-Ratliff model correspond to quantities which can be determined directly, or at least inferred, from more invasive measurements of <u>Limulus</u> retinal physiology than were performed for this study. While those experiments, by their nature, effectively preclude the simultaneous determination of all the parameters for a single preparation, as was possible in this study, and have rarely been performed on the eye <u>in situ</u>, it is nevertheless instructive to compare our parameter values with those obtained by other methods.

The major systematic difference between our parameters and those obtained previously is that most of our time-constants are faster, often by a factor of 2 or more. This is most likely a consequence of the fact that our data were obtained from <u>in situ</u> eyes at a temperature of approximately $22^{\circ}C$. At such an elevated temperature, most processes within the eye appear to run faster than they do at lower temperatures (Appendix B). For example, our data show a peak response to flickering light at about 6 Hz, in contrast to values around 3 Hz previously reported in colder, excised eyes (Knight, 1973a).

We consider first the parameters for the generator potential. These describe properties of the discrete bumps which sum to form the observed potential.

The most complete measurements of these parameters, from intracellular voltage data, are those of Wong (1977). (Many other measurements of bump parameters have been made at much lower light levels than the present experiments. Such conditions facilitate the study of individual bumps, but they also obscure the adaptation effect and lengthen the latency between photon absorption and the consequent bump.) His parameter values (for excised eyes) were t_{ℓ} = 0.025s, 20°C, Q_{10} = 4; t_d = 0.016s, 20°C, Q_{10} = 4; n_d = 3; t_b = 0.03s, 20°C, Q_{10} = 2.5; n_b = 3; R = 0.59; t_a = 0.074s (temperature dependence not measured). Comparison with Table 2 shows reasonable agreement, though comparison of the time constants is somewhat complicated by the difference in the exponents n_d and n_b. Wong did not measure the temperature dependence of the adaptation parameters. Nonetheless, even if we assume that the time-constant t_a varies with temperature in a manner similar to the other time-constants, our data show an adaptation process considerably faster, and slightly stronger, than that described by his measurements.

It may also be noted that our value of eight for the number of factors of the form $1/(1+i\omega t)$ in our model for the generator potential is in good agreement with the original estimates of Fuortes and Hodgkin (1964). Under conditions of strong light-adaptation, their estimates of the number of

apparent "stages" of filtering in the generator potential ranged
from seven to thirteen, with a mean of 10.1. Indeed, as Wong
(1977) has pointed out, some of the stages of the Fuortes-Hodgkin
model seve principally to describe the latency between photon
absorption and the resultant bumps. These stages are thus
supplanted by the exponential mean latency factor in our model
transfer function.

The encoder parameters describe the strength and time-
scale of the self-inhibitory process. This process has been
studied in excised eyes (Stevens, 1964; Purple, 1964; Lange,
1965; Knight et. al., 1970; Fohlmeister et. al., 1977b) and
in in situ preparations (Biederman-Thorson and Thorson, 1971).
These numerous studies give self-inhibitory parameters which
vary widely: $\kappa = 1.$ to $\kappa = 6.$; $\tau = 0.250$ to $\tau = 1.0$ sec.
Our data (Table 2) are compatible with the faster and weaker
ends of this range. Our rapid time constant may be due to the
elevated temperature of our preparations. It should also
be noted that our treatment assigns an effective time-constant
only to the combined processes of self-inhibition and impulse
generation. It is possible that the impulse-generating
process (which is in fact better described by a "forgetful"
integrate-and-fire mechanism than by the simple model given
above) contributes a high-pass characteristic of its own to
the dynamic response of the eye. As "forgetting" time constants
for the Limulus eccentric cell have been reported ranging
from 0.04 sec to less than 0.01 sec (Barbi et. al., 1975;
Fohlmeister et. al., 1977b), our apparent time-constant for

the complete encoder might well be faster than the actual time
constant of the intracellular self-inhbitory hyperpolarization.
In any event, except for the slow component of light-
adaptation, self-inhibition is clearly the slowest process in
our model of the Limulus eye.

The parameters for the temporal dependence of lateral inhibition seldom have been measured directly. The impulse responses measured by Knight et. al. (1970) were approximated by them with the following (unpublished) parameter values: τ_1 = 0.1 sec, τ_2 = 0.15 sec, τ_3 = 0.1 sec, τ_4 = 0.05 sec, C = 0.1 . Our time constants (Table 2) are faster by a factor of 3, but are still reasonable. The vanishing of the constant C for one of our preparations is consistent with results observed in non-hyperpolarized cells. Clearly, most of the effective "delay" of the inhibitory transient is accounted for by the three low-pass filter stages.

Previous measurements of the inhibitory kernel have been made in excised eyes (using steady-state data) by Kirschfeld and Reichardt (1964); Barlow (1967,1969); and Johnston and Wachtel (1976), all, using very different methods. Kirschfeld and Reichardt measured steady-state Mach bands, and modeled their data with kernels given by the forms $K(x) = Ae^{-|x|/a}$ and $k(x) = Ae^{-x^2/a^2}$. They assumed a priori that the kernel decreased monotonically away from the origin. They were able to rule out the simple exponential kernel, and found that their data were adequately described by the Gaussian kernel, with a space-constant a = 0.22 eye-widths. This is in good agreement with our measured value. It should be noted, however, that the observed Mach band patterns are in fact rather insensitive to the details of the inhibitory kernel, especially as regards detection of a small crater in the inhibitory field (Barlow and Quarles, 1975).

Barlow directly measured the point-to-point inhibitory coupling of single units to small clusters of inhibiting ommatidia. He obtained a two-dimensional inhibitory field with a marked central crater. Johnston and Wachtel's measurements were performed on eyes with the cornea and crystalline cones removed. They obtained a monotonically decreasing inhibitory kernel extending to about 0.25 eye-widths from the test-ommatidium.

Dodge and Kaplan (1975, and personal communication) measured the inhibitory fields of the in-situ Limulus eye by measuring the response to flashing bars as viewed on a screen 10. cm from the eye by the Limulus using its natural optics in air. Their data were basically in agreement with previous investigators; they found a narrow crater in one-third of their preparations.

In order to compare our one-dimensional data with these various measurements, it is necessary to consider the relationship between the two-dimensional kernel and our one-dimensional treatment. If one illuminates the entire eye, and assumes that, for a centrally located ommatidium, the top and bottom edges of the eyes are (effectively) infinitely far away, then the two-dimensional Hartline-Ratliff equations (5.6) may be replaced by a one-dimensional analog in which the inhibitory kernel is simply related to its two-dimensional counterpart:

$$k(x) = \int_{-\infty}^{\infty} k(x,y)dy. \tag{E.1}$$

If the illumination pattern covers only a finite strip of the eye, the simple relation (A1) will no longer hold. Instead we have

$$k(x) = \int_{-Y}^{Y} k(x,y)g(y)dy/g(0),$$
(E.2)

where the illumination strip spans the region from $-Y$ to Y, and $g(y)$ is the steady-state response of an ommatidium at the distance y from the x-axis to the analysis stimulus consisting of a uniform bar of light ($\xi=0$). (We have not attempted to measure the weighting function $g(y)$, but the edge-effects measured elsewhere (Barlow and Quarles, 1975; Kirschfeld and Reichardt, 1964) suggest that taking g to be a constant function of y should be an adequate approximation.) When the two-dimensional kernel of equation (16) is inserted in equation (A2), we may observe several facts. First, the integral takes the form of a sum of two terms, each of which is a function of x times the integral of a function of y. This implies that the space-constants a and b determined for the one-dimensional kernel are the same as the space constants of the two-dimensional kernel. (This property is a consequence of our choice of Gaussian functions to describe the inhibitory kernel.) Second, the ratio B/A of the two components of the one-dimensional kernel is related to the analogous ratio (D in equation (5.16)) of the two-dimensional kernel by the relation

$$\frac{B}{A} = D \cdot \frac{\zeta b}{\eta a} \cdot \frac{erf(Y/\zeta b)}{erf(Y/\eta a)},$$
(E.3)

where $erf(u) \equiv \int_0^u e^{-v^2} dv$.

We distinguish two limiting cases: If Y is large (compared to ηa) then the error function quotient is approximately unity, and we see that the "apparent" crater strength B/A is less than the actual strength D by a factor of $\zeta b/\eta a$; in other words, the crater is "filled-in" by the integration over y. If Y is small (compared to ζb), then $erf(Y/\zeta b) \cong Y/\zeta b$ (and likewise for $erf(Y/\eta a)$), and the observed quotient B/A is equal to the true crater strength D. Our experiment falls between these two limits, with Y = 0.0666 eye-widths, ηa = 0.09 eye-widths and ζb = 0.02 eye-widths. This gives D = (B/A)·3.1 = 1.8 .

While this number, if taken at face value, suggests that the two-dimensional kernel actually takes on negative values, it must be remembered that this value for D results from the product of the observed ratio A/B and the square of the ratio ($\zeta b/\eta a$) of two very small and somewhat crudely estimated parameters. It is also to be noted that, for such small features of the inhibitory kernel as the crater, the continuous model of the Limulus retina breaks down, in that it tries to describe features whose scale is comparable to the size of a single ommatidium. Nonetheless, similar observations from several preparations allow us to conclude that the crater depth parameter D is approximately unity, a value compatible with Barlow's data.

Our value for the space constant, a, of the main feature in the inhibitory kernel in the horizontal direction is in good agreement with all the previous measurements, in which the kernel falls to zero at around 0.25 eye-widths from the test ommatidium. Our value for the space constant, b, of the crater corresponds to a feature about one-half as wide as that described by Barlow. Such a narrow feature would be difficult to detect with methods which produce a wider point-spread effect than our fiber-optic taper arrangement. In the vertical direction, our space constant, a, was about one-half of that in the horizontal direction, a ratio comparable to Barlow's measurements. Our value for the space-constant of the crater in the vertical direction was only slightly less than the value in the horizontal direction, though, as mentioned above, the width of the crater is one of our least well determined parameters These ratios must also be evaluated in light of the fact that they derive from measurements of different Limulus specimens.

The width of the stimulus stripe also enters into the comparison of our value for K with previous measurements. (Actually, the relevant parameter is the quotient $K/(1+\kappa)$, which is equivalent to the sum of the inhibitory coefficients in steady-state experiments.) We have

$$K = \int_{-\infty}^{\infty} k(x)dx = \int_{-\infty}^{\infty}\int_{-Y}^{Y} k(x,y)g(y)dydx/g(0). \qquad (E.4)$$

For our present purposes, we set g equal to a constant; further-
more, we may ignore the crater in this comparison, as it alters
the total inhibitory strength by only about two percent. With
these approximations, inserting our values for Y and ηa in equation
(A4) yields the conclusion that our value for $K/(1+\kappa)$ is
approximately 70% of the total steady-state inhibitory strength
of the whole eye.

Barlow (1967) stated that the sum of the coefficients
in his inhibitory kernel was 7, though this is a considerable
extrapolation which probably over-represents the ommatidia
with atypically strong inhibitory coupling. Lange (1965)
gave values as large as 2. In their subsequent paper Barlow
and Lange (1974) emphasized the dependence of the total

inhibitory strength on the level of excitation of the ommatidium
being inhibited. They reported values for this parameter
which varied (in different preparations) from 0.4 to 2.3, all
for an excitation of 25 impulses/sec; in one preparation, they
measured a total inhibition of 0.6 at an excitation of 5
impulses/sec, rising linearly to 1.7 at an excitation of 20
impulses/sec.

Our experimental design does not permit direct measure-
ment of the excitation level of our test ommatidium, but we
may estimate the excitation from the steady-state relation

$$r = e/(1 + \frac{K}{1+\kappa}) \ . \qquad \qquad \text{(E.5)}$$

Inserting the observed mean impulse rate r = 10 impulses/sec,
and inhibitory strength K/(1+κ) = 1.3, we recover the estimate
e = 23 impulses/sec. Thus, our corrected value for the
inhibitory strength of the entire eye, $\frac{K}{1+\kappa}$ (whole eye) = $\frac{1.3}{0.7}$ = 1.9,
is in excellent agreement with the measurements of Barlow and
Lange. Kirschfeld and Reichardt (1964) found a total inhibitory
strength of 1.111, at an excitation of over 30 impulses/sec.
Recently, Barlow and Fraioli(1978) have obtained values for
$\overline{K}/(1+\kappa)$ ranging from 1.5 to 3.7, for excitations comparable
to ours. They report that the strength of lateral inhibition
appears greatest in those animals in the best physiological condition.

Finally, though the effective point-spread characteristic
of our optical system has little consequence for the natural
optics of the Limulus eye, it compares favorably with the
point-spread functions measured for a Limulus ommatidium in air and
in water by Kirschfeld and Reichardt (1964) whose data
were summarized by Gaussian distributions with s-parameters
of approximately 0.019 eye-widths.

References

Adolph, A.R. (1966) Excitation and inhibition of electrical activity in the Limulus eye by neuropharmacological agents. In: Functional Organization of the Compound Eye, C. Berhard, ed., Pergamon Press, Inc., Elmsford, N.Y., 465-482.

Adolph, A.R. (1968) Thermal and spectral sensitivities of discrete slow potentials in Limulus eye. J. Gen. Physiol. 52, 584-599.

Adolph, A.R. (1971) Recording of optic nerve spikes underwater from freely-moving horseshoe crab. Vision Res. 11, 979-983.

Adolph, A.R. (1973) Thermal sensitivity of lateral inhibition in Limulus eye. J. Gen. Physiol. 62, 392-406.

Adolph, A.R. (1976) Putative synaptic mechanisms of inhibition in Limulus lateral eye. J. Gen. Physiol. 67, 417-431.

Adolph, A.R. and Tuan, F.J. (1972) Serotonin and inhibition in Limulus lateral eye. J. Gen. Physiol. 60, 679-697.

Barbi, M., Carelli, V., Frediani, C., and Petracchi, D. (1975) The self-inhibited leaky integrator: transfer functions and steady state relations. Biol. Cybern. 20, 51-59.

Barlow, R.B., Jr. (1967) Inhibitory fields in the Limulus lateral eye. Thesis, The Rockefeller University, New York.

Barlow, R.B., Jr. (1969) Inhibitory fields in the Limulus eye. J. Gen. Physiol. 54, 383-396.

Barlow, R.B., Jr. and Fraioli, A.J. (1978) Inhibition in the Limulus eye in situ. J. Gen. Physiol. 71, 699-720.

Barlow, R.B., Jr. and Lange, G.D. (1974) A nonlinearity in the inhibitory interactions in the lateral eye of Limulus. J. Gen. Physiol. 63, 579-589.

Barlow, R.B., Jr. and Quarles, D.A. (1975) Mach bands in the lateral eye of Limulus. Comparison of theory and experiment. J. Gen. Physiol. 65, 709-730.

Biederman-Thorson, M. and Thorson, J. (1971) Dynamics of excitation and inhibition in the light-adapted Limulus eye in situ. J. Gen. Physiol. 58, 1-19.

Brodie, S.E. (1979) Temperature dependence of the dynamic response of the Limulus retina. Vision Res. 19, 91-94.

Brodie, S.E., Knight, B.W., and Ratliff, F. (1978a) The response of the Limulus retina to moving stimuli: A prediction by Fourier synthesis. J. Gen. Physiol. 72, 129-166.

Brodie, S.E., Knight, B.W., and Ratliff, F. (1978b) The spatio-temporal transfer function of the Limulus lateral eye. J. Gen. Physiol. 72, 167-202.

Carroll, L. (1865) Alice's Adventures in Wonderland, Macmillan and Co., London.

Carroll, L. (1871) Through the Looking-Glass, and What Alice Found There. Macmillan and Co., London.

Carroll, L. (1874) The New Method of Evaluation as Applied to π. James Parker and Co., Oxford.

Carroll, L. (1876) The Hunting of the Snark. Macmillan and Co., London

Corning, W.C., Feinstein, D.A., and Haight, J.R. (1965)
Arthropod preparation for behavioral, electrophysiological,
and biochemical studies. Science 148, 394-395.

Dodge, F.A. (1969) Inhibition and excitation in the Limulus eye.
In: Processing of Optical Data by Organisms and by Machines.
Proceedings of the International School of Physics "Enrico Fermi
Course XLIII. W. Reichardt, ed., Academic Press, Inc. New York,
341-365.

Dodge, F.A. and Kaplan, E. (1975) Visual fields in the Limulus eye.
Biophys. J. 15, 172a, abstr.

Dodge, F.A., Knight, B.W., and Toyoda, J. (1968) Voltage noise in
Limulus visual cells. Science 160, 88-90.

Enroth-Cugell, C. and Robson, J.G. (1966) The contrast sensitivity
of retinal ganglion cells of the cat. J. Physiol. 187, 517-552.

Fohlmeister, J.F., Poppele, R.E., and Purple, R.L. (1977a)
Repetitive firing: A quantitative study of feedback in model
encoders. J. Gen. Physiol. 69, 815-848.

Fohlmeister, J.F., Poppele, R.E., and Purple, R.L. (1977b)
Repetitive firing: Quantitative analysis of encoder behavior
of slowly adapting stretch receptor of crayfish and eccentric
cell of Limulus. J. Gen. Physiol. 69, 849-877.

French, A.S. and Holden, A.V. (1971) Alias-free sampling of
neuronal spike trains. Kybernetik 8, 165-171.

French, A.S. and Järvilehto, M. (1978) The dynamic behavior of
photoreceptor cells in the fly in response to random (white
noise) stimulation at a range of temperature. J. Physiol. 274,
311-322.

Fuortes, M.G.F. (1959) Initiation of impulses in visual cells
    of Limulus. J. Physiol. 148, 14-28.

Fuortes, M.G.F. and Hodgin, A.L. (1964) Changes in time scale and
    sensitivity in the ommatidia of Limulus. J. Physiol.
    172, 239-263.

Gauss, C.F. (1828) Disquitiones generales circa superficies curvas.
    Commentat. Soc. R.Sci. Gott. Recent. 6, 99-146.

Graham, C.H. and Hartline, H.K. (1935) The response of single
    visual cells to lights of different wave lengths. J. Gen. Physiol.
    18, 917-931.

Graham, N. and Ratliff, F. (1974) Quantitative theories of the
    integrative action of the retina. In: Contemporay Developments
    in Mathematical Psychology. D.H. Krantz, R.C. Atkinson,
    R.D. Luce, and P. Suppes, eds., W.H. Freeman & Co., San Francisco,
    306-371.

Graham, N., Ratliff, F., and Hartline, H.K. (1973) Facilitation
    of inhibition in the compound lateral eye of Limulus.
    Proc. Nat. Acad. Sci., USA 70, 894-898.

Hartline, H.K. (1934) Intensity and duration in the excitation
    of single photoreceptor units. J. Cell.Comp. Physiol.,
    5, 229-247.

Hartline, H.K. and Graham, C.H. (1932) Nerve impulses from single
    receptors in the eye. J. Cell. Comp. Physiol. 1, 227-295.

Hartline, H.K. and McDonald, P.R. (1947) Light and dark adaptation
    of single photoreceptor elements in the eye of Limulus.
    J. Cell. Comp. Physiol. 30, 225-253.

Hartline, H.K. and Ratliff, F. (1957) Inhibitory interaction of
    receptor units in the eye of Limulus. J. Gen. Physiol. 40,
    357-376.

Hartline, H.K. and Ratliff, F. (1958) Spatial summation of inhibitory
    influences in the eye of Limulus, and the mutual interaction
    of receptor units. J. Gen. Physiol. 41, 1049-1066.

Hartline, H.K., Wagner, H.G., and Mac Nichol, E.F. (1952) The
    peripheral origin of nervous activity in the visual system.
    Cold Spring Harbor Symp. On Quant. Biol. XVII, 125-141.

Hartline, H.K., Wagner, H.G., and Ratliff, F. (1956) Inhibition
    in the eye of Limulus. J. Gen. Physiol. 39, 651-673.

Hempel, C.G. and Oppenheim, P. (1948) Studies in the logic of
    explanation. Philosophy of Science, XV, 135-175.

Hochstein, S. and Shapley, R.M. (1976) Quantitative analysis of
    retinal ganglion cell classifications. J. Physiol. 262,
    237-264.

Hughes, G.W. and Maffei, L. (1966) Retinal ganglion cell response
    to sinusoidal light stimulation. J. Neurophysiol. 29, 333-352.

Johnston, D. and Wachtel, H. (1976) Electrophysiological basis for
    the spatial dependence of the inhibitory coupling in the
    Limulus retina. J. Gen. Physiol. 67, 1-25.

Kapany, N.S. (1967) Fiber Optics: Principles and Applications.
    Academic Press, Inc. New York.

Kaplan, E. and Barlow, R.B., Jr. (1975) Properties of visual cells
    in the lateral eye of Limulus in situ. J. Gen. Physiol. 66,
    303-326.

Katznelson, Y. (1968) <u>An Introduction to Harmonic Analysis</u>.
John Wiley and Sons, Inc., New York.

Kirschfeld, K. and Reichardt, W. (1964) Die Verarbeitung stationärer
optischer Nachrichten im Komplexauge von <u>Limulus</u>. (Ommatidien-
Sehfeld und räumliche Verteilung der Inhibition). <u>Kybernetik</u> <u>2</u>,
43-61.

Knight, B.W. (1972a) Dynamics of encoding in a population of neurons
<u>J. Gen. Physiol</u>. <u>59</u>, 734-766.

Knight, B.W. (1972b) The relationship between the firing rate of
a single neuron and the level of activity in a population
of neurons. <u>J. Gen. Physiol</u>. <u>59</u>, 767-778.

Knight, B.W. (1973a) The horseshoe crab: A little nervous system
that is solvable. In: <u>Lectures on Mathematics in the Life</u>
<u>Sciences. Some Mathematical Questions in Biology, IV</u>,
J.B. Cowan, ed. The American Mathematical Society, Providence,
R.I., <u>5</u>, 113-144.

Knight, B.W. (1973b) Some questions concerning the encoding dynamics
of neuron populations. In: <u>Communication and Control Processes</u>
<u>in Biological Systems</u>. International Union for Pure and Applied
Biophysics, Academy of Sciences of the U.S.S.R., Symposial
Papers, 422-436.

Knight, B.W. (1973c) A stochastic problem in visual neurophysiology.
In: <u>Stochastic Differential Equations: Society for Industrial</u>
<u>and Applied Mathematics-American Mathematical Society Proceed</u>-
ings, J.B. Keller and H.P. McKean, eds., American Mathematical
Society, Providence, R.I., <u>6</u>, 1-19.

Knight, B.W., Brodie, S.E., and Sirovich, L. (1979) On the treatment of nerve impulse data for comparison with theory. Proc. Nat. Acad. Sci. USA, submitted.

Knight, B.W., Toyoda, J., and Dodge, F.A. (1970) A quantitative description of the dynamics of excitation and inhibition in they eye of Limulus. J. Gen. Physiol. 56, 421-437.

Lange, G.D. (1965) Dynamics of inhibitory interactions in the eye of Limulus: Experimental and Theoretical studies. Thesis. The Rockefeller University, New York.

Lange, D., Hartline, H.K., and Ratliff, F. (1966) Inhibitory interaction in the retina: Techniques of experimental and theoretical analysis. Ann. N.Y. Acad. Sci. 128, 955-971.

Lee, Y.W. and Schetzen, M. (1961) Measurement of the kernels of a non-linear system by crosscorrelation. Quart. Progr. Rept. no.60 M.I.T. Res. Lab. Electron.

Leung, L.S. and Freeman, W.J. (1977) The spatial temporal response of the Limulus eye neural set. J. Theor. Biol. 69. 41-56.

Mac Nichol, E.F. (1956) Visual receptors as biological transducers. In: Molecular Structure and Functional Activity of Nerve Cells, Amer. Inst. Biol. Sci., Pub. no.1, 34-53.

Mac Nichol, E.F. and Benolken, R. (1956) Blocking effect of ethyl alcohol on inhibitory synapses in the eye of Limulus. Science 124, 681-682.

Mac Nichol, E.F. and Jacobs, J.A.H. (1955) Electronic device for measuring reciprocal time intervals. Rev. Sci. Instrum. 26, 1176-1180.

Maffei, L. (1968) Inhibitory and facilitatory spatial interactions in retinal receptive fields. Vision Res. 8, 1187-1194.

Maffei, L. and Cervetto, L. (1968) Dynamic interactions in retinal receptive fields. Vision Res. 8, 1299-1303.

Maffei, L., Cervetto, L., and Fiorentini, A. (1970) Transfer characteristics of excitation and inhibition in cat retinal ganglion cells. J. Neurophysiol. 33, 276-284.

Marmarelis, P.Z. and Naka, K. (1972) White-noise analysis of a neuron chain: An application of the Wiener theory. Science 175, 1276-1278.

Marmarelis, P.Z. and Naka, K. (1973a) Nonlinear analysis and synthesis of receptive-field responses in the catfish retina. I. Horizontal cell→ganglion cell chain. J. Neurophysiol. 36, 605-618.

Marmarelis, P.Z. and Naka, K. (1973b) Nonlinear analysis and synthesis of receptive-field responses in the catfish retina. II. One-input white-noise analysis. J. Neurophysiol. 36, 619-633.

Marmarelis, P.Z. and Naka, K. (1973c) Nonlinear analysis and synthesis of receptive-field responses in the catfish retina. III. Two-input white-noise analysis. J. Neurophysiol. 36, 634-648

McCann, G.D. and Marmarelis, P.Z., eds. (1975) Proceedings of the First Symposium on Testing and Identification of Nonlinear Systems. California Institute of Technology, Pasadena.

Metz, W.D. (1978) Midwest computer architect struggles with speed of light. Science 199, 404-409.

Milkman, N., Shapley, R., and Schick, G. (1978) A microcomputer-based visual stimulator. <u>Behav. Res. Meth. and Instr.</u> <u>10</u>, 539-545.

Noble, B. (1958) <u>Methods Based on the Wiener-Hopf Technique for the Solution of Partial Differential Equations</u>. Pergamon Press, New York.

Perlis, S. (1952) <u>Theory of Matrices</u>. Addison-Wesley Pub. Co., Reading, Mass.

Piet Hein (1973) <u>Grooks 5</u>. Doubleday and Co., New York.

Pinter, R.B. (1966) Sinusoidal and delta function responses of visual cells of the <u>Limulus</u> eye. <u>J. Gen. Physiol.</u> <u>49</u>. 565-593.

Poggio, T. and Reichardt. W. (1976) Visual control of orientation behaviour in the fly. Part II. Towards the underlying neural interactions. <u>Quart. Rev. Biophys.</u> <u>9</u>, 377-438.

Purple, R.L. (1964) The integration of excitatory and inhibitory influences in the eccentric cell in the eye of <u>Limulus</u>. Thesis. The Rockefeller University, New York.

Purple, R.L. and Dodge, F.A. (1965) Interaction of excitation and inhibition in the eccentric cell in the eye of <u>Limulus</u>. <u>Cold Spring Harbor Symp. on Quant. Biol. XXX</u>, 529-537.

Ratliff, F. (1965) <u>Mach Bands: Quantitative Studies on Neural Networks in the Retina</u>. Holden-Day, Inc. San Francisco.

Ratliff, F., ed. (1974) <u>Studies on Excitation and Inhibition in the Retina</u>. The Rockefeller University Press, New York.

Ratliff, F., Knight, B.W., Dodge, F.A., and Hartline, H.K. (1974) Fourier analysis of dynamics of excitation and inhibition in the eye of _Limulus_: Amplitude, phase, and distance. _Vision Res._ 14, 1155-1168.

Ratliff, F., Knight, B.W., and Graham, N. (1969) On tuning and amplification by lateral inhibition. _Proc. Nat. Acad. Sci. USA_ 62, 733-740.

Ratliff, F., Knight, B.W., and Milkman, N. (1970) Superposition of excitatory and inhibitory influences in the retina of _Limulus_: Effect of delayed inhibition. _Proc. Nat. Acad. Sci. USA_ 67, 1558-1564.

Ratliff, F., Knight, B.W., Toyoda, J., and Hartline, H.K. (1967) Enhancement of flicker by lateral inhibition. _Science_ 158, 392-393.

Ratliff, F. and Sirovich, L. (1978) Equivalence classes of visual stimuli. _Vision Res._ 18, 845-851.

Reichardt, W. and Poggio, T. (1976) Visual control of orientation behaviour in the fly. Part I. A quantitative analysis. _Quart. Rev. Biophys._ 9, 311-375.

Rodieck, R.W. (1965) Quantitative analysis of cat retinal ganglion cell response to visual stimuli. _Vision Res._ 5, 583-601.

Rodieck, R.W. and Stone, J. (1965a) Response of cat retinal ganglion cells to moving visual patterns. _J. Neurophysiol._ 28, 819-832.

Rodieck, R.W. and Stone, J. (1965b) Analysis of receptive fields of cat retinal ganglion cells. _J. Neurophysiol._ 28, 833-849.

Rowe, M.H. and Stone, J. (1977) Naming of neurones. Classification and naming of cat retinal ganglion cells. Brain Behav. Evol. 14, 185-216.

Rudin, W. (1974) Real and Complex Analysis (2nd Edition). Mc Graw-Hill, Inc., New York.

Rushton, W.A.H. (1961) The intensity factor in vision. In: A Symposium on Light and Life, W.D. McElroy and B.Glass, eds., The Johns Hopkins Press, Baltimore. 706-723.

Shapley, R.M. (1971) Effects of lateral inhibition on fluctuations of the impulse rate. J. Gen. Physiol. 57, 557-575.

Shapley, R. and Rossetto, M. (1976) An electronic visual stimulator. Beh. Res. Meth. Instr. 8, 15-20.

Shapley, R.M. and Victor, J.D. (1978) The effect of contrast on the transfer properties of cat retinal ganglion cells. J. Physiol. 285, 275-298.

Sirovich, L. (1971) Techniques of Asymptotic Analysis. Springer-Verlag, New York.

Sirovich, L. (1979) Boundary effects in neural networks. SIAM J. Appl. Math., part C, submitted.

Sirovich, L., Brodie, S.E., and Knight, B.W. (1979) The effect of boundaries on the response of a neural network. Biophys. J., submitted.

Spekreijse, H. (1969) Rectification in the goldfish retina: Analysis by sinusoidal and auxilliary stimulation. Vision Res. 9, 1461-1472

Stevens, C.F. (1964) A quantitative theory of neural interactions: Theoretical and experimental investigations. Thesis, The Rockefeller University, New York.

Stevens, S.S. (1975) Psychophysics. John Wiley and Sons, New York.

Thorson, J. and Biederman-Thorson, M. (1974) Distributed relaxation processes in sensory adaptation. Science 183, 161-172.

Tomita, T. (1958) Mechanism of lateral inhibition in eye of Limulus. J. Neurophysiol. 21, 419-429.

Twain, M. (1883) Life on the Mississippi. Osgood and Co., Boston.

Victor, J.D. (1979a) The functional organization of the receptive fields of cat X and Y retinal ganglion cells. Thesis, The Rockefeller University, New York.

Victor, J.D. (1979b) Nonlinear systems analysis: Comparison of white noise and sum of sinusoids in a biological system. Proc. Nat. Acad. Sci. USA 76, 996-998.

Victor, J.D. and Knight, B.W. (1979) Nonlinear analysis with an arbitrary stimulus ensemble. Quart. Appl. Math. 37, in press.

Victor, J.D. and Shapley, R.M. (1979) A method of nonlinear analysis in the frequency domain. Biophys. J., submitted.

Victor, J.D., Shapley, R.M.,and Knight, B.W. (1977) Nonlinear analysis of cat retinal ganglion cells in the frequency domain. Proc. Nat. Acad. Sci. USA 74, 3068-3072.

Wiener, N. (1933) The Fourier Integral and Certain of its Applications Cambridge University Press, New York.

Wiener, N. (1958) <u>Nonlinear Problems in Random Theory</u>.
 M.I.T. Press, Cambridge, Mass.

Wiener, N. and Hopf, E. (1931) Über eine Klasse singulärer
 Integralgleichungen. <u>S.B. Preuss. Akad. Wiss</u>. 30, 696-706.

Wong, F. (1977) Mechanisms of the phototransduction process in
 invertebrate photoreceptors. Thesis, The Rockefeller University,
 New York.

Wong, F. and Knight, B.W. (1979) The adapting bump model for
 eccentric cells of <u>Limulus</u>. <u>J. Gen. Physiol</u>., in press.

Wong, F., Knight, B.W., and Dodge, F.A. (1979) Dispersion of
 latencies and the adapting bump model. <u>J. Gen. Physiol</u>., in press